An Experimental Study of the Effect of NaCl and Na_2SO_4 on Cu^{II} and Zn Adsorption onto Synthetic Goethite

Christopher G. Gunton

Department of Earth and Marine Science

September 2007

A thesis submitted for the degree of

Doctor of Philosophy of

The Australian National University

Declaration

The research and results within this thesis was undertaken at the Department of Earth and Marine Sciences, The Australian National University. Except where acknowledged, the content of this thesis is my own and has not been previously submitted to qualify for any other qualification or award.

Christopher G. Gunton

5 September 2007

Acknowledgements

Firstly, I would like to acknowledge that this research was supported and funded by the Co-operative Research Centre for Landscape, Environments and Mineral Exploration (CRC LEME) in conjunction with an Australian Postgraduate Award from the Australian Government.

Thanks must go to Dr Ying Chen from the Research School of Physical Sciences and Engineering at the Australian National University who conducted the N_2 BET analysis for surface area calculations, Dr Patrica Angus formerly from the Chemistry Department at the ANU for her valuable advice for setting up the experimental methodology and Linda McMorrow from the Department of Earth and Marine Science at the ANU for her patience and assistance with analysing samples. Thankyou to Dr Keith Scott form CRC LEME for your advice and insight on how to keep the project relevant to the 'real world'.

To anyone who has undertaken the mammoth task of completing a PhD, you can understand the time, effort and emotional highs and lows that accompany the task. I have been fortunate to have had the support of both my fellow students and staff at the Department of Earth and Marine Science who contributed to a stimulating research environment. To everyone in the department, my sincere thanks.

To my supervisors, Dr D.C. "Bear" McPhail and Dr Andrew Christy, without your support and guidance, this research certainly would not have developed this far and you always managed to give the right direction when it was most needed. Your advice, no matter how brutal at times, was always invaluable.

Finally, to the most important and influential people in my life, my family Angela and Chloe. I would never have completed this without your support and patience over the past 5 years. This is a journey and achievement we have made together.

Abstract

Metal mobility in natural environments may be controlled by the aqueous speciation of metals, dissolution/precipitation reactions or metal adsorption onto mineral and/or organic surfaces. Data from simple experimental systems has provided enough knowledge of adsorption reactions to examine more complex geochemical systems, such as those characteristic of natural environments.

This study examines Cu^{II} and Zn adsorption in 0.1-5 molal NaCl and 0.001-1 m Na_2SO_4 using batch experiments at 25°C and pH 2-9.5. Cu^{II} and Zn adsorption was greater in NaCl solutions when compared to SO_4^{2-} solutions at pH < 7.5. In 0.5 m NaCl and pH 6.5, all available Cu^{II} was removed from the aqueous phase and assumed to be adsorbed on goethite, while the concentration of adsorbed copper was approximately 20% lower in 0.01 m Na_2SO_4 at the same pH. In contrast, zinc adsorption was greater in sulfate solutions at pH < 7.5 than in NaCl solutions of the same pH. An adsorption maximum for Cu^{II} occurred at 2.0 molal NaCl, and at concentrations > 2.0 molal adsorption decreased. A similar effect was observed for Zn adsorption at 1.0 molal NaCl, where Zn adsorption decreased in NaCl concentrations >1 molal.

Surface complexation modelling using the Constant Capacitance Model (CCM) was used to infer the surface complexes responsible for adsorption and calculate equilibrium constants for the associated reactions. Results of the CCM imply that ternary metal surface

complexes, e.g. $SOCuCl^0$ and $SOZnCl_2^-$ (where SO represents the underlying goethite surface) are responsible for the enhanced adsorption of Cu^{II} and Zn in NaCl solutions. Adsorption was interpreted to decrease in NaCl concetrations >2.0 molal for Cu^{II} and 1.0 molal for Zn due to the formation of stable aqueous metal chloride species. In sulfate solutions, Cu^{II} and Zn was also interpreted to form ternary surface complexes e.g. $SOHCuSO_4$ and $SOZnSO_4$. The CCM implied that the formation of stable aqueous Cu^{II} and Zn sulfate complexes decreased adsorptin with increasing sulfate concentrations.

The predictive power of the model was established when results of a coexisting Cu^{II}, Zn and NaCl and Na_2SO_4 experiment were successfully replicated using the calculated equilibrium constants for Cu^{II} and Zn adsorption in NaCl and sulfate solutions. Finally, the model was used to assess Cu^{II} and Zn mobility in mixing waters in a natural environment based on measured data from Lake Tyrrell. This showed that mixing of a highly saline water with relatively fresh water would decrease Cu^{II} adsorption, thereby enhancing Cu^{II} mobility, while Zn adsorption increased with mixing.

Table of Contents

Chapter 1: Introduction

Adsorption is an important geochemical process that has the capability to control metal mobility in natural, low temperature, near surface environments (i.e. groundwater, laccustrine and marine environments). Adsorption is important to scientific disciplines such as soil science (e.g. Sposito, 1984; Barrow et al., 1982), mineral exploration (e.g. Rose and Biachi, 1993), hydrogeochemistry (e.g. Balistrieri and Murray, 1982), environmental geochemistry (including contaminated land, Swartz et al., 2004; and remediation), and minerals processing. However, due to the limited knowledge of adsorption reactions, most adsorption studies were conducted in simple experiments with low concentrations of inert electrolytes (e.g. $NaNO_3$, $NaClO_4$). These simple experimental conditions are not representative of natural systems, and yet understanding metal mobility in near surface environments is critical for solving many problems presently facing the global population.

1.1 The Role of Adsorption in Natural Environments

The purpose of this study was to examine the effect of NaCl and Na_2SO_4 on adsorption. This has implications in mineral exploration and environmental geochemistry, which are consistent with the objectives of the Co-operative Research Centre for Landscape, Environment and Mineral Exploration (CRC LEME). A brief description of the applications of this research is outlined below.

1.1.1 Applications of Adsorption in Environmental Geochemistry

The number of reported occurrences of groundwater contamination from anthropogenic and natural sources is rising (Koretsky, 2000), posing health risks to large populations of people who depend on these water resources. For example, arsenic contamination of groundwater used for drinking is a significant geohazard in countries such as India, Bangladesh (e.g. Swartz et al., 2004; Anawar et al., 2003; Pena et al. 2005), Vietnam, Chile and Switzerland (Pena et al., 2005; Pfeifer et al. 2004). This problem affects millions of people in Bangladesh alone, where it is estimated that >1 million people will suffer from arsenocosis (Yu et al., 2003; Swartz et al., 2004). Research has indicated that microbial activity has promoted the reduction of iron oxyhydroxides and mobilised arsenic (e.g., Pfeifer et al. 2004; Swartz et al. 2004). This hypothesis implies that mobility may have once been inhibited by arsenic adsorption onto iron oxyhydroxides (i.e. ferrihydrite, goethite, schwertmanite, mackinawite etc.) prior to reduction of the environment. Therefore understanding the effect of physical changes (i.e. changes in temperature) or chemical properties (i.e. salinity increases, pH changes, redox changes) on adsorption is a key to determining the cause and solving this harmful problem.

Acid sulfate soil is an increasing environmental problem in Australia, with an estimated 40,000 km^2 of coastal land affected. The impact of acid sulfate soils is felt by coastal communities and industries through the destruction of natural environments and eco-systems such as estuarine and coastal wet-lands; depletion of commercial resources (i.e. fisheries) and the destruction of community infrastructure (Sammut, 2000). The role of adsorption in these environments is not well known as yet. Metal mobility is predicted to

increase in acid sulfate soil environments due to the low pH of affected water and the formation of various metal-sulfate aqueous complexes which stabilize metal cations in solution. However, adsorption studies examining the role of aqueous sulfate on metal adsorption onto iron oxy-hydroxides (i.e. Swedlund and Webster, 2001; Balistrieri and Murray, 1982; Ali and Dzombak, 1996) have shown that sulfate may in fact enhance metal adsorption. This raises the question of whether adsorption may be a method of controlling, or possible remediation, of acid sulfate soil affected locations.

Understanding the role of adsorption on the retention or mobility of toxic metals in the environment is important if heavy metal contamination is to be controlled or remediated. However, the key controlling factors (i.e. aqueous speciation of solutions or mineral surface properties) must be understood before these major environmental problems can solved.

1.1.2 Applications of Adsorption in Mineral Exploration

Mineral exploration in Australia is becoming increasingly difficult because the majority of the large world class mineral deposits exposed at the surface (e.g. Broken Hill; de Caritat et al., 2005 and Mount Isa; Perkins, 1996) have been discovered. Therefore mineral explorers are forced to explore regions with a thick residual regolith (e.g. the goldfields of Western Australia) or covered by young transported sediments (e.g. Carpentaria Basin in NW Queensland and the Murray Basin in Victoria).

The discovery of large Proterozoic ore deposits underneath transported regolith (e.g. Olympic Dam in South Australia; Ernest Henry and Cannington in North-West

Queensland) have been made with geophysical methods such as magnetics and gravity surveys. However, not all styles of mineralisation may exhibit such strong geophysical responses, and other exploration tools, such as geochemical sampling of soils or groundwaters (c.f. de Caritat et al., 2005), may be useful for identifying areas with mineralisation. Given the enormous surface area of Australia covered by either a residual regolith or transported cover sediment, the potential for undiscovered world class orebodies to exist is high.

When considering geochemistry as a mineral exploration tool, it is important to understand the processes involved with enhancing metal concentrations in the regolith. Traditional exploration geochemistry models assume that mineralised host rocks are exposed at the surface, where physical and/or chemical weathering decomposes the rock, dissolving and transporting metals. However, other models for exploring in regions under cover need to be considered. de Caritat et al. (2005) proposed groundwater as a medium for sampling in regions with thick cover. Radford and Burton (1999) proposed the formation of geochemical anomalies in transported cover by the upward migration of metals caused by factors such as bioturbation and fluctuating groundwater levels. Both these strategies rely on adsorption/desorption processes to trap metals in the regolith and understanding the effect of groundwater chemistry, mineral and surface properties on these processes may lead to more effective sampling techniques. Chapter 5 will demonstrate how the adsorption data collected in this study can be used to predict the mobility of Cu^{II} and Zn in environments similar to those found in natural saline lakes.

1.2 Summary of Adsorption Research

It is difficult to distinguish between the adsorption of an ionic species on a solid surface and precipitation of a new mineral. The definition of adsorption used for this study is that of Koretsky (2000): "The term adsorption is used if species are taken up from the solution and are chemically bound in a monolayer at the mineral-water interface". This implies that adsorption occurs as a two-dimensional layer at the surface-water interface, while a precipitate is considered as a three-dimensional structure that extends in to the surrounding aqueous phase.

Surface – water interface geochemistry has been a topic of interest for a long period of time. The first observations of reactions between the surface – water interface were made during silicate dissolution experiments conducted in the early 1800's (Hochella and White, 1990). Significant advances in the knowledge of interface geochemistry did not occur until the late 1960's with the advent of better analytical methods (i.e. potentiometric titrations) which resulted in the development of surface complexation models (Dzombak and Morel, 1990). Interest in the mineral water interface was sustained until the early 1980's, when the number of published papers appeared to decrease. A resurgence of surface – water interface studies occurred in the early 1990's, which coincided with a rise in the number of metal/mineral combinations studied.

Adsorption research has ranged from experimental studies designed to quantify metal adsorption in carefully controlled environments (i.e. Balistrieri and Murray, 1982; Padmanabham, 1983a; Barrow et al., 1980), to the development of numerical models

designed to predict adsorption in specific conditions (i.e. Robertson and Leckie, 1997; Peacock and Sherman, 2004; Sahai and Sverjensky, 1990a; Criscenti and Sverjensky, 1996; Persson and Lovgren, 1996, Dyer et al. 2004). The recent availability of more sensitive and accurate analytical equipment (i.e. XAS, EXAFS and XANES), has allowed researchers to observe these reactions at the atomic level, providing information about the formation of specific complexes at the solid-solution interface (i.e. Trivedi et al. 2001; Peacock and Sherman, 2004; Waychunas et al. 2002; Waychunas et al. 2003).

Research has shown that adsorption onto mineral surfaces is controlled by stoichiometry and stability of the adsorbate species, surface properties of the adsorbing mineral and the properties of the host solution (i.e. pH and chemical speciation). It is well established that cation adsorption onto non-permanently charged surfaces (such as iron-oxyhydroxides) decreases with decreasing pH; caused by H^+ adsorption onto the mineral surface at low pH, which creates a net positive surface charge and repels other cations. The opposite occurs for negatively charged anions, such as metal-oxide complexes, where adsorption increases with decreasing pH (e.g. Dzombak and Morel, 1990). The adsorption edge, or the pH range where adsorption primarily occurs, has been shown to vary depending upon the metal species (e.g. increase in adsorption of Cu^{II} is greatest between pH 4.5-5.5 in $NaNO_3$ solutions, compared with that for Zn at pH 6-7; Dzombak and Morel, 1990).

A detailed description of the mineral surface is made by Davis and Kent (1990), therefore only a brief explanation is provided here. Two groups of mineral surfaces have been identified, permanent and with non-permanently charged surfaces, which reflect the major charge properties of the mineral. Non-permanently charged minerals possess proton bearing

functional groups and adsorption is strongly dependent on pH (Davis and Kent, 1990). Non-permanently charged include iron oxy-hydroxides (e.g., goethite, ferrihydrite), silicates and titanium oxides (Davis and Kent, 1990; Yates, 1975). These minerals are well characterized and have large volumes of data describing their morphology, surface area and adsorption site densities, while their relatively simple crystal structures and strong adsorbing properties make them ideal for studying adsorption reactions. Minerals with a permanent surface charge do not have proton bearing functional groups at the surface, and their permanent charge is attributed to cation exchange (e.g. Al^{3+} replacing Si^{4+} in kaolinite; Peacock and Sherman, 2005). Minerals used in adsorption studies examining metal adsorption onto permanently charged surfaces include kaolinite (Peacock and Sherman, 2005; Heidmann et al., 2005), montmorillonite (Catalano and Brown Jr, 2005; Brigatti et al., 2004), sepiolite (Vico, 2003) and vermiculite (Abate and Masini, 2005). Results of these studies suggest permanently charged surfaces are ideal adsorbates. However, separating the influence of cation exchange capacity from adsorption and precipitation reactions can be difficult (Catalano and Brown Jr, 2005).

The influence of solution chemistry, and in particular ligands, on the adsorption of metals has been a topic of recent interest (e.g. Criscenti and Sverjensky, 1999; Swedlund and Webster, 2001; Balistrieri and Murray, 1982; Ali and Dzombak, 1996) in an attempt to simulate natural environments. For example, sulfate is one of the more frequently anion species studied. It has been considered as an adsorbing anion itself (e.g. Persson and Lovgren, 2004; Rietra et al. 1999; Juang and Wu, 2005; Geelhoed et al., 1999) and as a complexing or competing ion, either suppressing or enhancing the adsorption of other cations (e.g. Ali and Dzombak, 1996; Balistrieri and Murray, 1982; Swedlund and Webster,

2001). The influence of solution speciation is not well understood, especially in conditions found in many natural environments. While the effect of anions on metal adsorption have been addressed previously (e.g. the effect of sulfate on metal adsorption), experimental conditions are usually kept simple and well constrained, in order to assist numerical modeling processes and eliminate complex issues (such as calculation of activity coefficients in high ionic strength solutions). As a result, no experimental adsorption data in solutions with high ionic strength is available and the adsorption behavior of metals in many natural environments is not known.

This study uses experiments to quantify oxidised copper (Cu^{II}) and zinc (Zn) adsorption onto synthetic goethite over a range of NaCl (0.1 – 5 molal) and Na_2SO_4 (0.001 – 1 molal) concentrations to represent saline (simulated by NaCl) and acid sulfate soil conditions (simulated by Na_2SO_4). No previous studies have not examined the effect of chloride at concentrations greater than sea water (0.56 molal, Balistrieri and Murray, 1982) or sulfate concentrations greater than 0.1 molal (Ali and Dzombak, 1996); and do not reflect some of the high concentrations of Cl^- and SO_4^{2-} associated with saline groundwater or acid sulfate soils. Furthermore, there are conflicting results for the effect of chloride and sulfate concentrations for Cu^{II} and Zn adsorption. Balistrieri and Murray (1982) concluded that NaCl had no effect on the adsorption of Cu^{II} and Zn onto goethite in simulated seawater conditions (NaCl = 0.56 molar), and Swallow et al. (1980) found that 0.5 molar NaCl did not affect Cu^{II} adsorption onto ferrihydrite. In contrast, Barrow et al. (1980) reported that the adsorption of copper increased when the NaCl concentration was increased from 0.0075 M to 0.075 M, which was in agreement with the conclusions of Padmanabham (1983b). Kanungo (1994) studied Zn adsorption in 0.5 molar NaCl in acidic solutions and found that

adsorption was enhanced slightly at low pH when compared with $NaNO_3$ experiments. To add to the confusion, an extensive literature review by Criscenti and Sverjensky (1999) examining the effect of anions on metal adsorption led them to believe that transition and heavy metal adsorption was suppressed with increasing NaCl.

1.3 Project Aims

The key aims of this project are:

1) Determine the effect of salinity (simulated by a range of NaCl concentrations) on the adsorption of Cu^{II} and Zn onto synthetic goethite under controlled experimental conditions.
2) Determine the effect of sulfate concentration on the adsorption of Cu^{II} and Zn onto synthetic goethite under controlled experimental conditions.
3) Use Cu^{II} and Zn to compare the effect of NaCl and Na_2SO_4 on base metal adsorption onto goethite.
4) Describe the impacts salinity and sulfate concentrations may have on the mobility of copper and zinc in the regolith.

To meet these objectives, experiments were used to collect Cu^{II} and Zn adsorption data in solutions 0.1 – 3.0 molal $NaNO_3$, 0.1 and 5.0 molal NaCl and 0.001, 0.01, 0.1 and 1.0 molal Na_2SO_4. This data was used in conjunction with surface complexation modelling to aid interpretation and calculate equilibrium constants for surface species. Synthetic goethite was selected for adsorption experiments because it is a common mineral in oxidized near

surface environments. Unlike ferrihydrite, goethite is relatively stable and unlikely to change in composition or morphology during experiments. Synthesizing goethite is a simple process, but more important surface properties such as morphology, surface area and site density remain consistent between synthesised batches, and it can be easily characterised (i.e. Kosmulski, 2003). Copper and zinc adsorption onto goethite in $NaNO_3$ solutions has been previously investigated (e.g. Balistrieri and Murray, 1982; Barrow et al., 1980; Padmanabham, 1983b; Kanungo, 1994b; Trivedi et al. 2001 ; Peacock and Sherman, 2005; Robertson and Leckie, 1997), so the results of this study can be compared with previous studies to determine the reliability of the experimental method. Furthermore, copper and zinc provide a contrast in their adsorption behaviour (since their acid-base properties and aqueous complexation are different), these metals frequently associated with one another and are relatively common in the oxidized, low temperature near surface environments that are considered in this study.

Cu^{II} and Zn were selected to examine the effect of NaCl and Na_2SO_4 concentration on to synthetic goethite because both metals are both economic commodities that are actively being explored for. Furthermore, both metals are common in natural oxidized near surface waters, but exhibit different aqueous speciation behaviour. These metals also demonstrate contrasting adsorption properties where Cu^{II} adsorption occurs in acidic conditions (e.g. between pH 4 and 6) while Zn adsorption occurs between pH 7 and 9, as shown in previous adsorption studies (e.g. Balistrieri and Murray, 1982; Trivedi et al., 2001; Dyer et al., 2004). Therefore, studying these two metals will determine how anion concentration may influence different metal species.

$NaNO_3$ was used in experiments to compare the results of this study with those of previous authors to determine the reproducibility of adsorption data from the experimental method used. Chloride and sulfate anions were used to simulate natural conditions. For example, NaCl was used to simulate saline water found in regions affected by dryland salinity, while Na_2SO_4 was used to simulate high sulfate concentrations found in areas with acid sulfate soils.

Chapter 2: Effect of NaCl on Cu^{II} Adsorption on Synthetic Goethite

2.1 Introduction

Understanding copper mobility in low-temperature waters, soils and more broadly, the regolith, is important for mineral exploration geochemistry, mineral processing, remediation of heavy metal contamination in waters and soils and the impact of copper as a micronutrient and/or toxin to biota (e.g., Bampton et al. 1977; Davis and Leckie, 1978; Padmanabham, 1983b; Barrow et al, 1982; Cairns et al. 2001). The mobility of copper depends on transport processes such as groundwater flow as well as geochemical processes such as the dissolution/precipitation of copper-bearing minerals and sorption onto inorganic and organic material. Microbiological processes may also be important (e.g., Gordon et al., 2000). Adsorption onto mineral surfaces is likely to be particularly important (Swallow et al., 1980; Balistrieri and Murray, 1982; Barrow et al., 1982; Padmanabham, 1983a; Padmanabham, 1983b; Dzombak and Morel, 1990; Rodda et al. 1993; Kooner, 1992; Rodda et al. 1996; Sen et al., 2000; Criscenti and Sverjensky; 1999, Bradl, 2004; Peacock and Sherman, 2004), but despite many published studies it is still not well understood, especially under the saline conditions found in regolith and other geological environments. This chapter the focuses on the effect of dissolved NaCl on the adsorption of Cu^{II} onto goethite, α-FeOOH. It aims to improve the understanding of copper adsorption in oxidised, weathered environments, where iron oxyhydroxide

minerals are likely to exert significant control on copper sorption and mobility (Kooner, 1992; Peacock and Sherman, 2004).

Metal adsorption onto mineral surfaces depends on the nature of the sorbate (i.e., aqueous geochemistry of the metal) and the nature of the sorbent (i.e., a mineral and its surface; e.g., Drever, 1997; Langmuir, 1997). The aqueous speciation of oxidised copper is affected by temperature, pressure, and the composition of the solution such as pH, redox and ligands such as Cl^- (cf., Brugger et al., 2001), SO_4^{2-} and organic compounds such as humic and fulvic acids (e.g., Weng et al., 2002). The specific surface area of goethite and density of active adsorption sites may affect adsorption and vary with both the crystalline habit of the goethite and other physical and chemical parameters of the system (e.g. Manceau et al., 2000). Many of these geochemical variables have already been studied for oxidised copper and iron oxyhydroxides such as goethite, ferrihydrite and lepidocrocite (e.g., Peacock and Sherman, 2004).

pH is perhaps the most important geochemical variable affecting adsorption of cations onto mineral surfaces and its effect on the adsorption of Cu^{II} onto goethite and other Fe oxides and oxyhydroxides and has been studied comprehensively. Table 2.1 summarises previous studies examining the adsorption of Cu^{II} onto goethite, with the results of these studies all showing that the adsorption of cations increases markedly as the pH of the solution increases.

The effects of temperature and pressure on sorption are likely to be small under the range of conditions typical of near surface environments. Rodda et al. (1993) studied the effect of temperature on copper sorption onto goethite, over a range between 10°C

and 80°C and found that sorption increased by only a few percent with increasing temperature.

Table 2.1: Summary of previous experimental studies of Cu^{II} adsorption onto goethite.

Author	*Electrolyte*	*Electrolyte Conc (M)*	*Goethite Conc (g/L)*	*Initial Cu Conc (μM)*	*pH Range*	*Reaction Time*
Ali & Dzombak (1996)	$NaNO_3$	0.01	1.6	2.3	3.4-6.5	24 hrs
	Na_2SO_4	0.1				
Balistrieri & Murray (1982)	$NaNO_3$	0.1	0.55	0.32	3.1-6.8	~12 hrs
	Simulated Seawater			1.80		
				31.0		
Barrow et al. (1982)	KNO_3	0.075	0.5	65.0	4.1-5.5	48 hrs
	NaCl	0.0075				
		0.075				
Kooner (1995)	$NaNO_3$	0.01	0.6	78.7	3.9-6.8	16-20 hrs
		0.1	5.5	78.7		
				157		
Padmanabham (1983)	NaCl	0.1	1.00×10^{-5}	10.0	3.3-6.5	16 hrs
Peacock & Sherman (2004)	$NaNO_3$	0.1	3.3	393	2.3-6.8	4 wks
Rodda et al. (1993)	KNO_3	0.01	0.2	100	3.0-11.0	20 mins

The compositions of waters and brines, especially the presence of complexing ligands, also have an effect on copper sorption. Electrolytes such as $NaNO_3$, KNO_3 and $NaClO_4$ are typically selected to study the effects of ionic strength on sorption due to their unreactive nature with mineral surfaces (Balistrieri and Murray, 1982) and weak complexing of metals with nitrate or perchlorate in aqueous solutions (Criscenti and Sverjensky, 1999). The role of ligands, such as Cl^- and SO_4^{2-}, on the adsorption of copper and other metals onto mineral surfaces has been examined, although over a

limited range of concentrations (Table 2.1). Results of these studies indicate that the presence of ligands influences adsorption of metals onto mineral surfaces, but the magnitude of the changes, and even whether they enhance or suppress sorption, is still poorly understood.

The effect of chloride concentration on the adsorption of Cu^{II} onto goethite is unclear. Balistrieri and Murray (1982) concluded that NaCl had no effect, based on their experimental study of Cu^{II} adsorption onto goethite under simulated seawater conditions. Swallow et al. (1980) studied the effect of NaCl on Cu^{II} adsorption onto hydrous ferric oxide, but they also concluded that NaCl had no effect on the adsorption of Cu^{II} after examining the adsorption of Cu^{II} and Pb^{II} onto hydrous ferric oxide in 0.1 M and 0.5 M $NaNO_3$ and 0.5 M NaCl solutions. Other studies, however, suggest that Cl^- enhances metal adsorption onto iron oxyhydroxides. Barrow et al. (1982) found that Cu^{II} adsorption onto 0.5 g/L synthetic goethite increased with increasing NaCl concentration (i.e., 0.0075 M and 0.075 M NaCl), and attributed this to the preferential adsorption of $CuCl^+$ aqueous complexes onto the goethite surface. Padmanabham (1983b) studied the adsorption of 1.0×10^{-5} M Cu^{II} onto synthetic goethite in 0.1 M NaCl and 0.1 M $NaNO_3$ solutions and found similar behaviour. In studies with other metals, e.g., Pb^{II} sorption onto goethite and alumina, increasing chloride concentrations enhances sorption (e.g., Gunneriusson et al., 1994; Bargar et al., 1998). In contrast, in an extensive review of adsorption literature and the effect of anions on metal sorption, Criscenti and Sverjensky (1999) concluded that transition and heavy metal adsorption decreased as the NaCl concentration increased.

In this chapter, the effect of pH, $NaNO_3$ and NaCl concentration on the adsorption of Cu^{II} onto synthetic goethite in an aqueous system is investigated experimentally. Adsorption data were collected for a range of $NaNO_3$ (0.1-3 molal) and NaCl concentrations (0.1-5 molal) to examine the changes in adsorption behaviour of Cu^{II} onto goethite as a function of NO_3^-, ionic strength and Cl^-. Surface complexation modelling was used to interpret the experimental data and fit thermodynamic equilibrium constants for surface reactions with Cu^{II} and Cl^-. The aim was to achieve a clearer understanding of how Cu^{II} adsorbs in near surface environments, settle the question of whether adsorption increases or decreases with NaCl, and obtain predictively useful thermodynamic properties that will allow more reliable geochemical and reactive transport models.

2.2 Materials and Methods

2.2.1 Goethite Synthesis and Characterisation

Goethite was synthesized according to the method outlined by Schwertmann and Cornell (1991) using reagent-grade chemicals. Briefly, 100 mL of 1.0 M aqueous $Fe(NO_3)_3$ solution was mixed with 180 mL of 5.0 M KOH in a 2 L polyethylene flask and diluted to 2 L with ultrapure water. The subsequent hydrolysis reaction produced a dark brown precipitate, which was sealed in the flask and placed in an oven at 70°C for 60 hours. The solution in the flask was decanted and the precipitate was rinsed a minimum of three times with double deionised water. The resulting material was analysed by X-Ray diffraction and the pattern was the same as that for goethite published by Schwertmann and Cornell (1991). Scanning electron microscopy showed

the goethite to be homogeneous, consisting only of acicular crystals up to approximately 2 μm long and 300 nm wide (Figure 2.1). The specific surface area was measured to be 36.05 ± 3.2 m^2/g using N_2 BET analysis. The site density was calculated using adsorption experiments and is described in detail later in Section *2.3.1.3*. Goethite was stored in ultrapure water at room temperature until required, and then filtered, dried and crushed in preparation for the adsorption experiments.

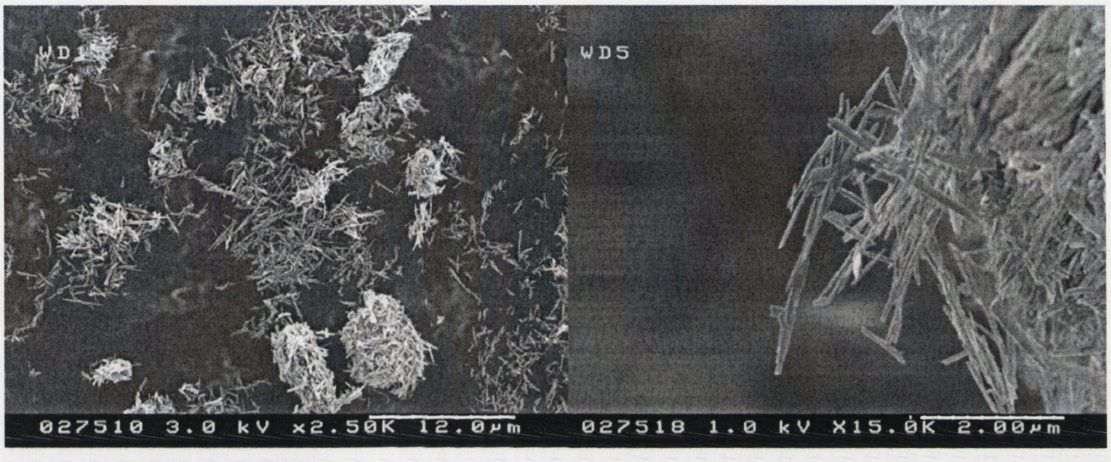

Figure 2.1: SEM images of synthetic goethite showing the morphology of the goethite crystals. The measured surface area of goethite was 36.05 nm^2/g.

2.2.2 Adsorption Experiments

Adsorption was measured in separate series of 11-12 individual experiments. For each experiment 0.075 g of dried goethite was placed in a 125 mL glass reaction vessel with 75 g of an electrolyte solution.

2.52×10^{-3} molal Cu^{II} stock solutions were prepared using $Cu(NO_3)_2.2^1/_2H_2O$ in a matrix consistent with the electrolyte used for each series. 5 g of the Cu^{II} stock solution was added to each reaction vessel such that the initial Cu^{II} concentration was 1.57×10^{-4}

molal for each experiment. The pH of each sample was adjusted using 0.1 M HNO_3 or 0.1 M NaOH and measured using a Thermo Orion 290A+ pH Meter and ROSS Sure Flow electrode with an uncertainty of ± 0.02 pH units. Reaction vessels were sealed with a Dreschel head and placed in a water bath at 25°C ± 0.1 to maintain constant temperature.

In order to minimise the effect of CO_2 adsorption onto goethite (i.e., Zeltner and Anderson, 1988), nitrogen gas was bubbled through a reaction vessel containing double deionised water to saturate the gas and minimise the effect of evaporation, before being passed through each reaction vessel in sequence to mix each solution and provide an inert atmosphere.

Kinetic experiments were conducted to measure the time for adsorption of Cu^{II} onto the goethite surface. 0.281 g of goethite was placed in a glass reaction vessel with 300 g of 0.1 molal $NaNO_3$ and 1.54×10^{-4} molal Cu^{II}. At specific time intervals, the pH of the experiment was recorded and 8 g of the goethite-bearing solution was withdrawn with a syringe and filtered through a 0.22 μm syringe filter before being analysed for dissolved copper. Kinetic experiments (Figure 2.2) show that steady state between goethite and Cu^{II} was achieved after 3-4 hours, but to ensure that equilibrium was achieved in each reaction vessel, all experimental series were run overnight for 16 hours. It is not clear whether equilibrium in these experiments and further data between 4 and 16 hours is necessary to conclusively show that equilibrium was achieved.

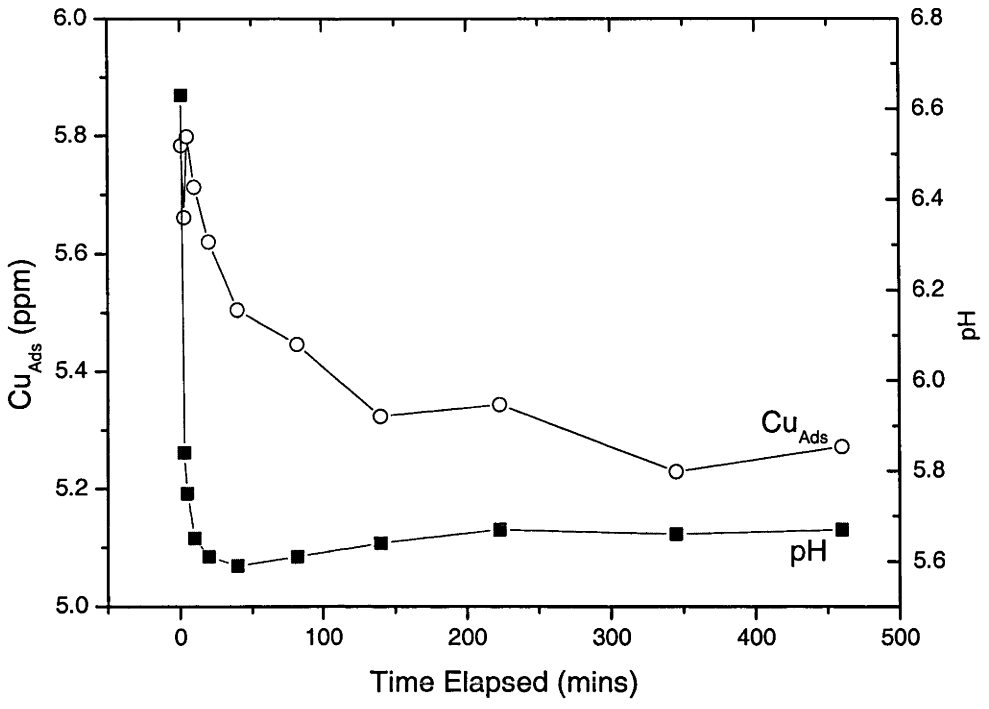

Figure 2.2: Concentration of adsorbed Cu^{II} and pH as a function of time at 25°C and 1 atmosphere. The total Cu^{II} concentration was 1.54×10^{-4} molal, in 0.1 molal $NaNO_3$ solution. Goethite concentration was 0.935 $g_{goethite}/kg_{solution}$.

At the conclusion of the equilibration period, the pH was measured and 30 mL of solution was extracted from each experiment and the goethite was filtered from each sample using a Millipore 0.22 μm filter. The supernatant solution was preserved by adding several drops of 10% HNO_3. Duplication of all experiments revealed an experimental uncertainty of approximately 5%.

Solutions were analysed for copper using a spectral line of 327.40 nm on a Varian Vista Pro Axial ICP-AES, with the matrix of blank and standard solutions matched to the NaCl concentration of experiments. The total adsorption of Cu^{II} was assumed to be the difference between the initial and final dissolved Cu concentration of each experiment.

Samples were also analysed for Fe; however, any Fe present in the solutions was below the ICP-AES detection limit of 0.05 mg/kg.

Selected goethite samples were dried and examined using SEM to determine whether any morphological changes occurred during the experiments. However, no noticeable changes could be detected and it was assumed no significant dissolution and/or precipitation occurred in our experiments.

2.2.3 Ionic Strength Effect Experiments

A 5 molal NaCl stock solution was prepared using reagent grade NaCl in a 2 litre poly propylene flask. The 5 molal solution was diluted to create 50mL aliquots of 4, 3, 2, 1, 0.5, 0.3 and 0.1 molal solutions. The pH of each solution was measured with a Thermo Orion 290A+ pH Meter and ROSS Sure Flow electrode with an uncertainty of ± 0.02 pH units, calibrated using unaltered commercial pH 3, 7 and 10 buffers.

The pH for each NaCl concentration listed above was calculated using the Pitzer Equation for determining activity coefficients in PHREEQC. The calculated pH was subtracted from the measured pH for each NaCl concentration to determine a pH difference. This pH difference for each NaCl concentration was added to the measured pH of adsorption experiments to calculate a pH adjustment for adsorption experiments.

2.3 Results

2.3.1 Cu^{II} Adsorption onto Goethite in $NaNO_3$ Solutions

Results for the adsorption of Cu^{II} onto goethite in $NaNO_3$ solutions (0.1 molal, 1.0 molal and 3.0 molal) are shown in Figure 2.3 and listed in Appendix A. The concentration units used to measure adsorption are moles of Cu^{II} adsorbed per gram of goethite (mol Cu^{II}/g goeth). These units provide a true measurement of the concentration of Cu^{II} on the mineral surface as opposed to referencing the concentration of CuII removed from solution (i.e. mol Cu_{ads}/L). The concentration of adsorbed copper increases with increasing pH, as is typical for the sorption of metals (e.g., Dzombak and Morel, 1990). The concentration of adsorbed copper decreases with increasing $NaNO_3$ concentration between 0.1 and 1 molal $NaNO_3$ and at pH greater than approximately 5, whereas between 1 and 3 molal $NaNO_3$ there is no discernible difference in the amount of copper adsorbed (Figure 2.3 and Figure 2.4). The precipitation of $Cu(OH)_2$(s) did not occur in any adsorption experiments. At pH 6, where $Cu(OH)_2$(s) precipitation is likely to occur, the concentration of dissolved Cu^{II} was less than the initial concentration of 1.102×10^{-4} due to Cu^{II} adsorption onto goethite at pH 6. To test this, $Cu(OH)_2$(s) was precipitated in a solution with 0.075 g goethite with an initial Cu^{II} concentration of 4.72×10^{-4} molal. When plotted the adsorption curve was did not behave in the same systematic way observed in adsorption experiments as all dissolved Cu^{II} was removed from solution at pH 6.2.

The results of the 0.1 molal $NaNO_3$ experiments were compared with those of Balistrieri and Murray (1982), Ali and Dzombak (1996) and Kooner (1992) and Peacock and Sherman (2004). To compare results between studies with different

goethite concentrations, surface area of goethite and dissolved Cu^{II} concentrations the distribution coefficient (K_d) was applied:

$$K_d = \frac{(Cu_{ads} \times W_{soln}) / (W_{goeth} \times A_s)}{Cu_{diss}} \qquad (2.1)$$

Cu_{ads} is the difference between the initial and final concentration of Cu^{II} in each experiment, W_{soln} is the total mass of solution (kg; excluding goethite), W_{goeth} is the mass of goethite in each experiment (kg), A_s is the measured surface area of goethite (m^2/kg) and Cu_{diss} is the measured concentration of dissolved copper (molal).

K_d values versus pH are illustrated in Figure 2.5. Most of the data fall within one order of magnitude at a given pH. The scatter is most likely due to variations in the characteristics of goethite, such as crystal morphology, surface area and site densities. For instance, the site density is different for different crystal faces of goethite (e.g., Lützenkirchen et al., 2002; 3.03 FeO sites/nm^2 on (101) and 7.19 sites on (100), Peacock and Sherman, 2004) so if the synthetic goethite in different studies had different morphologies the available sorption sites would be likely to differ. Unfortunately, morphologies and surface areas were not recorded for all studies, so the effect can not be established. In addition, the presence of atmospheric $CO_2(g)$ can inhibit metal adsorption on goethite (Zeltner and Anderson, 1988), but all of the datasets presented here had the atmosphere controlled so as to minimise the concentration of $CO_2(g)$.

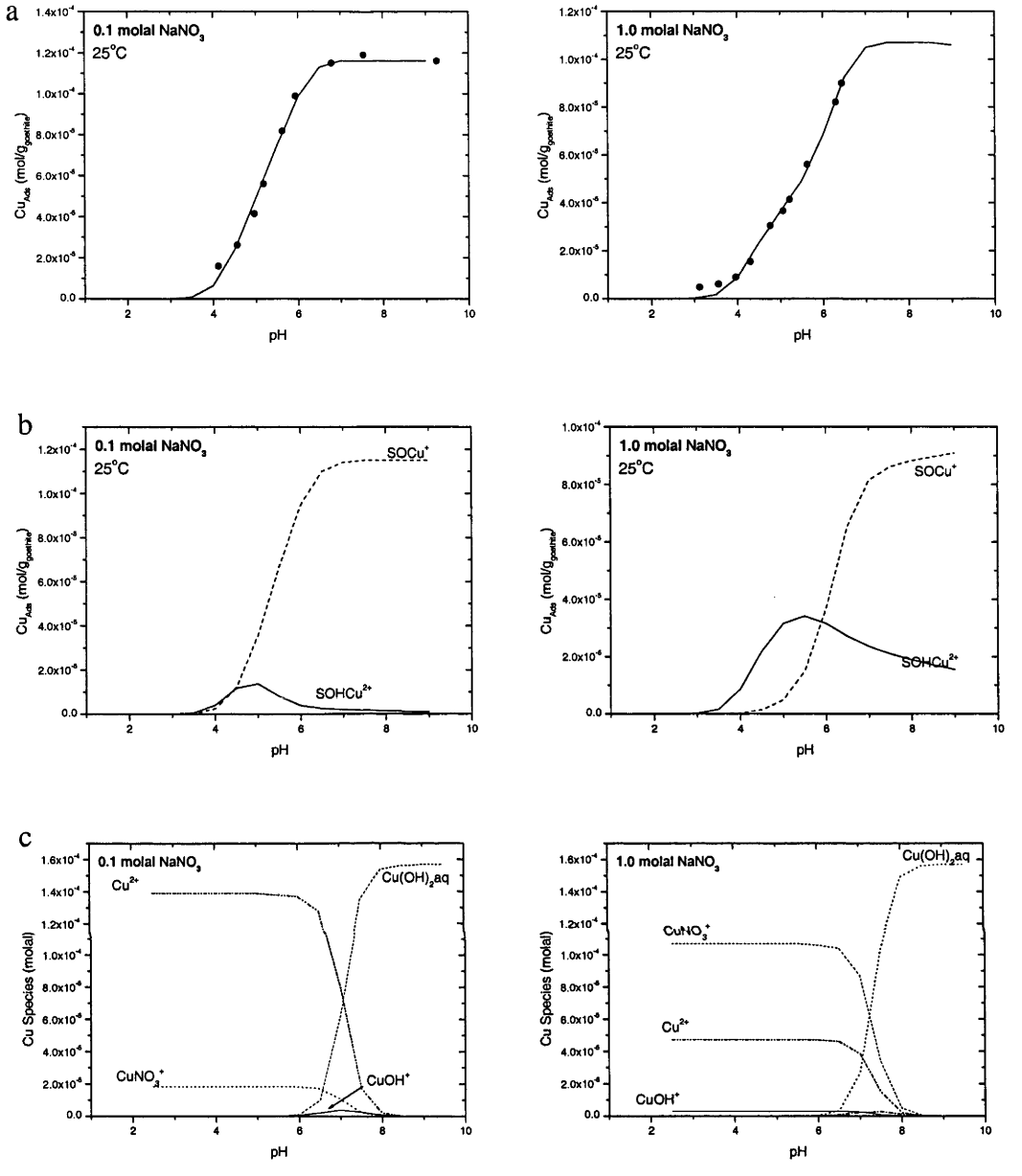

Figure 2.3: **(a)** Adsorption of Cu^{II} onto goethite at 25°C and 1 atmosphere as a function of pH for 0.1, and 1.0 molal $NaNO_3$. Initial Cu^{II} concentration was 1.102×10^{-4} molal and the goethite concentration was 0.935 g goethite per kg solution. Solid line is the CCM fit for each individual experiment at a fixed $NaNO_3$ concentration. **(b)** Calclated surface species using the CCM for 0.1 and 1.0 molal $NaNO_3$. **(c)** Calculated aqueous speciation of Cu^{II} in 0.1 and 1.0 molal $NaNO_3$. Activity coefficients were calculated with the Davies Equation. Values for the fitted log K with the CCM are shown in Table 2.3 and the assumptions made in the CCM are described in sections 2.3.1.1 to 2.3.1.4.

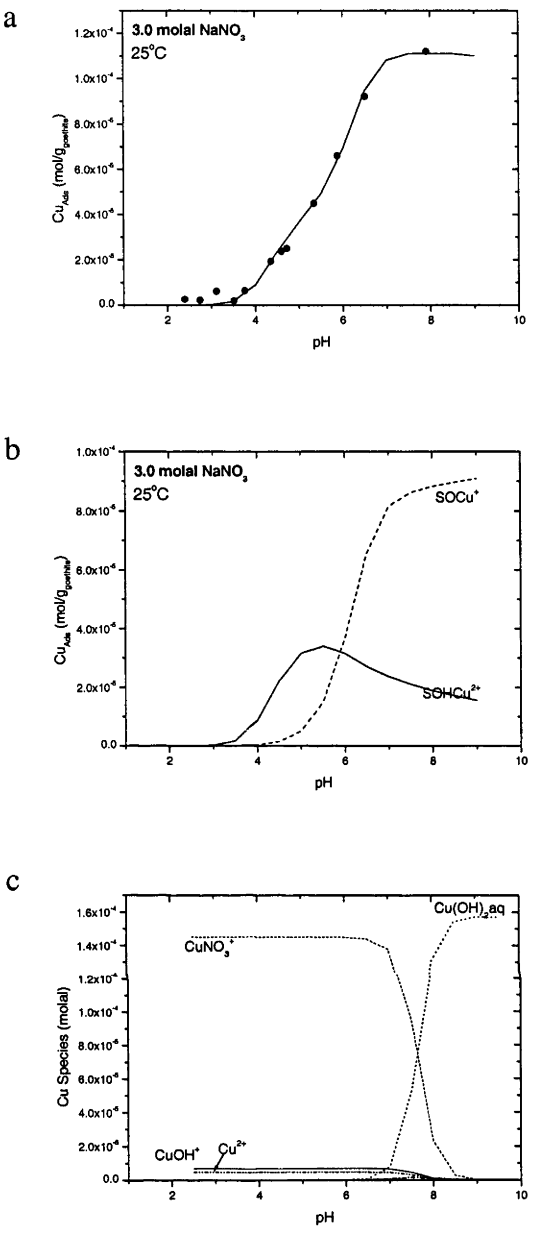

Figure 2.3 (continued): **(a)** Adsorption of Cu^{II} onto goethite at 25°C and 1 atmosphere as a function of pH for 3.0 molal $NaNO_3$. Initial Cu^{II} concentration was 1.102×10^{-4} molal and the goethite concentration was 0.935 g goethite per kg solution. Solid line is the CCM fit for each individual experiment at a fixed $NaNO_3$ concentration. **(b)** Calculated surface species using the CCM for 3.0 molal $NaNO_3$. **(c)** Calculated aqueous speciation of Cu^{II} in 0.1 and 1.0 molal $NaNO_3$. Activity coefficients were calculated with the Davies Equation. Values for the fitted log K with the CCM are shown in Table 2.3 and the assumptions made in the CCM are described in sections 2.3.1.1 to 2.3.1.4.

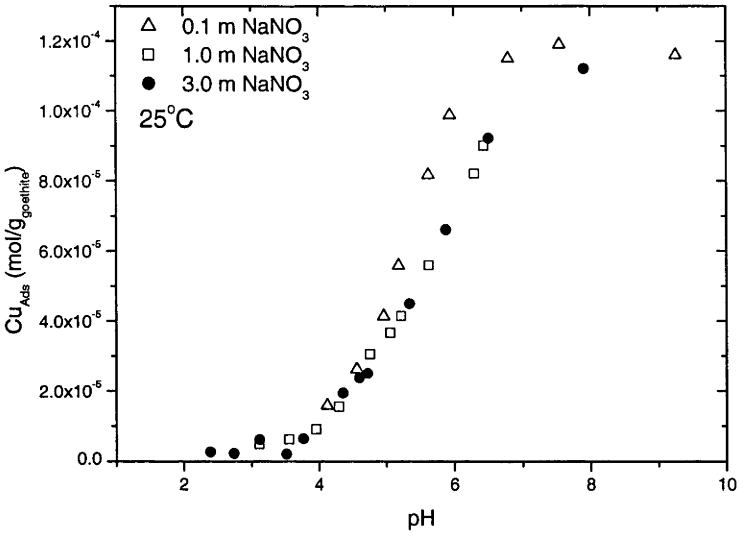

Figure 2.4: Adsorption of Cu^{II} in 0.1, 1 and 3.0 molal $NaNO_3$ onto goethite at 25°C and 1 atmosphere as a function of pH for 3.0 molal $NaNO_3$. Initial Cu^{II} concentration was 1.102×10^{-4} molal and the goethite concentration was 0.935 g goethite per kg solution.

Another important aspect of experimental design is the time necessary for equilibration. The experiments conducted by Peacock and Sherman (2004) were four weeks long, much longer than the 12-24 hour reaction times of our study and all the other comparable studies (Table 2.1; Figure 2.5), but did not present evidence for needing longer run durations. In this study it was demonstrated that a constant adsorbed copper concentration was reached within 3-4 hours (Figure 2.2) and all the experiments were run overnight for approximately 16 hours to ensure equilibrium was achieved. Peacock and Sherman (2004) measured higher concentrations of adsorbed Cu than found in the experiments of this study and it is possible that their solid materials were dissolving and re-precipitating, and therefore changing the surface area and/or site density, and/or that processes other than adsorption were operating in their experiments, such as copper diffusion into goethite (e.g., Manceau et al., 2000). In any case, there is not enough

information to assess what processes were operating in their experiments, or understand the differences in the results of the two studies.

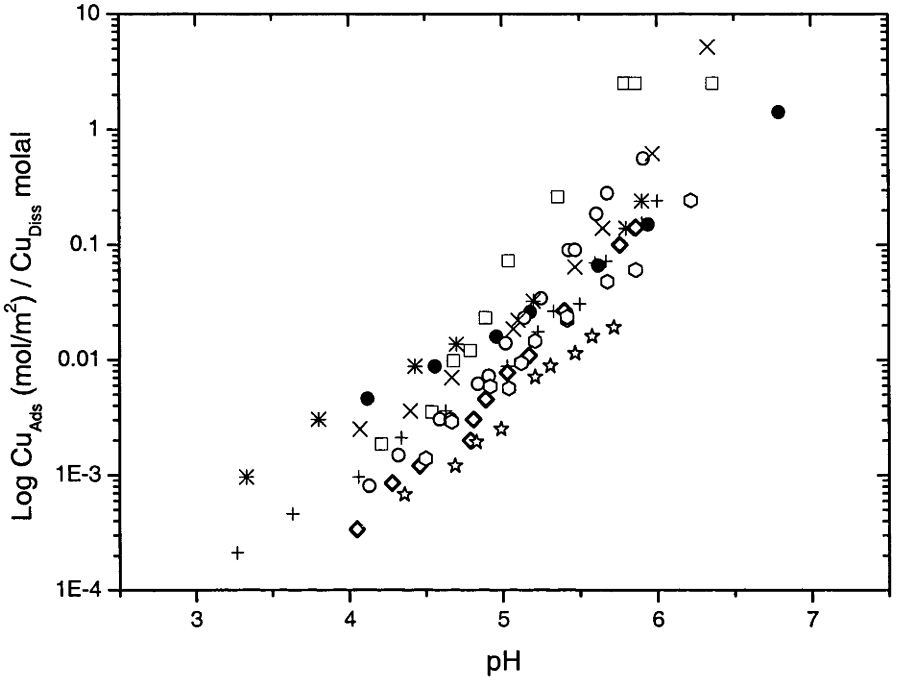

Figure 2.5: Comparison of Cu^{II} adsorption onto goethite at 25°C and 1 atmosphere in 0.1 M $NaNO_3$. Symbols represent the following studies: ■ Current study; □ Peacock and Sherman (2004) 3.3 g/L goethite, 393μM Cu^{II}; ○ Ali and Dzombak (1996) 1.6 g/L goethite, 2.3μM Cu^{II}; ☆ Kooner (1992) 0.6 g/L goethite, 157 μM Cu^{II}; ○ Kooner, (1992) 0.6 g/L goethite, 78 μM Cu^{II}; ◇ Kooner (1992) 5.5 g/L goethite, 78 μM Cu^{II}; + Balistrieri and Murray (1982) 0.55 g/L goethite, 0.32 μM Cu^{II}; × Balistrieri and Murray (1982) 0.55 g/L goethite, 1.8 μM Cu^{II}; ✳ Balistrieri and Murray (1982) 0.55 g/L goethite, 31 μ/L Cu^{II}.

2.3.1.1 Quantitative interpretation

Surface complexation modelling is commonly used to interpret adsorption experimental data and predict surface species (e.g., Sahai and Sverjensky, 1997a). In this section, the surface complexation model used for $NaNO_3$ experiments is described and how surface

complexes were selected. The process used to fit the model to the experimental data is also described.

In order to determine the reactions controlling copper adsorption in $NaNO_3$ solutions, the simplest likely surface complexes of copper, e.g., Peacock and Sherman (2004; Equations 10 and 11 in their Table 3) are shown in Equations 2.2 and 2.3.

$$\equiv SOH(ads) + Cu^{2+}(aq) = \equiv SOHCu^{2+}(ads) \quad (2.2)$$

$$\equiv SOH(ads) + Cu^{2+}(aq) = \equiv SOCu^{+}(ads) + H^{+}(aq) \quad (2.3)$$

and their associated equilibrium constants are:

$$K = \frac{a_{\equiv SOHCu^{2+}}}{a_{\equiv SOH} a_{Cu^{2+}}} \quad (2.4)$$

$$K = \frac{a_{\equiv SOCu^{+}} a_{H^{+}}}{a_{\equiv SOH} a_{Cu^{2+}}} \quad (2.5)$$

"≡S" in these equations is a cation at a surface adsorption site. By plotting $\log[Cu]_{Ads} - \log[Cu]_{Diss}$ versus pH, where $[Cu]_{Ads}$ is the total concentration of adsorbed Cu^{II}, $[Cu]_{Diss}$ is the total concentration of dissolved Cu^{II} and for the purpose of this analysis it is assumed that ≡SOH is the total number of available adsorption sites. Note that Equation 2.2 is independent of pH and that we assume no activity coefficient effects at this stage. The effect of pH in these experiments is shown in Figure 2.6, where best-fit lines show slopes of 0.94 for 0.1 molal $NaNO_3$, 0.56 for 1.0 molal $NaNO_3$ and 0.76 for 3.0 molal $NaNO_3$. The slopes between 0 and 1 indicate that both reactions were operating in the experiments. Other surface complexes are possible, e.g., $\equiv SOCuOH^{\circ}$ and $\equiv SOHCuOH^{+}$

(cf., Peacock and Sherman, 2004), although it cannot be determined if they were present from the calculated slopes in Figure 2.6 alone; however these and other species are considered in the following section on fitting equilibrium constants to the experimental data.

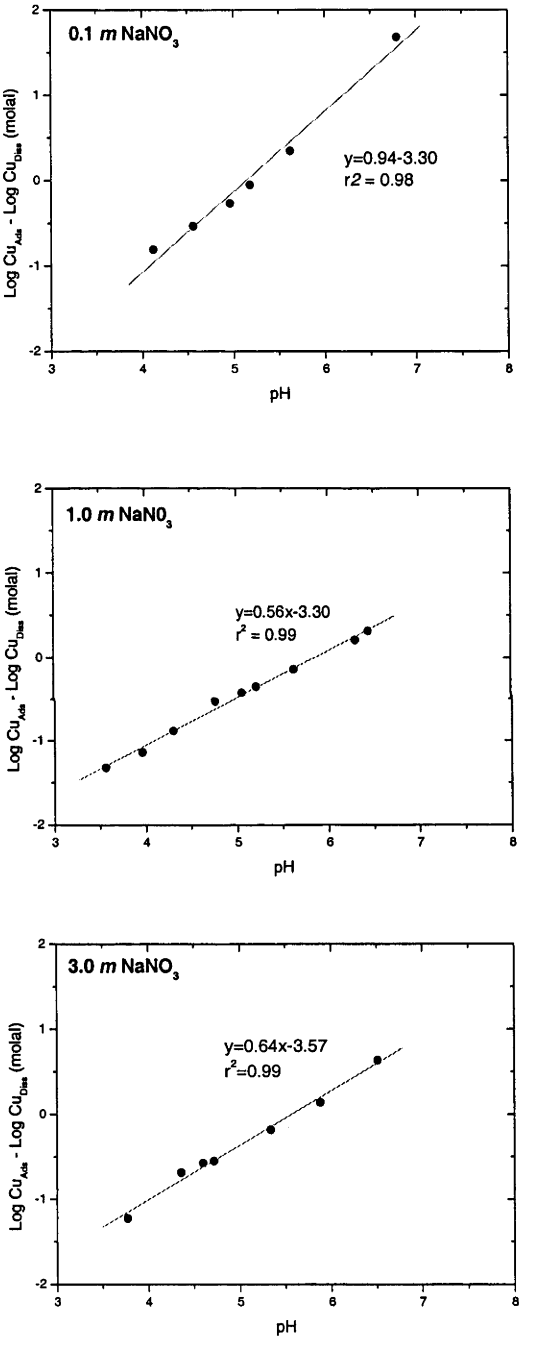

Figure 2.6: $Log[Cu]_{Ads} - log[Cu]_{Diss}$ versus pH showing Cu^{II} adsorption onto goethite in different concentrations of $NaNO_3$. Experimental data are listed in Appendix A. The slopes of the linear regression lines indicate the stoichiometry of dominant adsorption reactions and corresponding copper surface complexes.

2.3.1.2 Surface Complexation Modelling

In a heterogeneous multicomponent system, any thermochemical interpretation requires the identification of the dissolved and surface species that are present. The minimum number of reactions that need be considered include protonation and deprotonation reactions at the surface attachment sites and reactions describing the formation of each dissolved or adsorbed species. Equilibrium constants need to be known or determined for all of these reactions. The molal units (moles of solute per kilogram of H_2O), typically used to describe concentrations in the liquid, can also be used to express concentrations of surface species if the number of surface attachment sites per mass of $H_2O(l)$ is known. In order to determine this, it requires knowledge of the mass of solid per mass of $H_2O(l)$, the specific surface area of the solid, and the density of attachment sites on the solid surface.

Several physical models have been used to describe the changes in the structure of the liquid near the solid surface, and have implications for the total surface charge, the charge distribution and electrostatic potential in the liquid, and hence the activity coefficients of charged species in the vicinity of the surface (Dzombak and Morel, 1990). The interfacial structure models commonly applied to adsorption data include the constant capacitance model (CCM), diffuse layer model (DLM) and triple layer model (TLM) (Sposito, 1984; Davis and Kent, 1990; Dzombak and Morel 1990; Gunneriusson et al, 1994; Lumsdon and Evans, 1994; Ali and Dzombak, 1996; Sahai and Sverjensky 1997a; Peacock and Sherman, 2004). Each of these models is a progressively more complex description of the electrostatic behaviour near the mineral surface, and we briefly review each of these models and assumptions here. For more detailed

descriptions, refer to Sposito (1984), Davis and Kent (1990) and Dzombak and Morel (1990).

The CCM, DLM and TLM are all based on the assumptions that the surface is effectively flat, infinite, and has an electrical charge that is a product of adsorption reactions (Dzombak and Morel, 1990). Positive and negative species in the solution experience an electric field due to the surface, and are accordingly attracted and repelled so as to balance the surface charge. This produces a "diffuse layer" in the liquid adjacent to the surface in which the electrical potential of the surface falls away to zero. The three models differ in how they describe the decrease of the potential with distance away from the surface.

The simplest model, the CCM, assumes linear variation of potential with distance away from the surface (cf., Davis and Kent, 1990). In other words, it assumes that there is effectively a constant capacitance in the boundary layer of the solution. This capacitance value is a fittable parameter. The "surface" is assumed to include strongly bound adsorbed species. In the DLM, the differential equation relating electric field and potential through the diffuse layer is solved, assuming that the local charge imbalance between positive and negative species obeys Boltzmann statistics (cf., Davis and Kent, 1990) and capacitance is no longer an independently fittable parameter. At the limit of low surface charge and low potential, the DLM behaves like a CCM. A more complex version of the DLM is the Stern model, in which the thin layer of strongly chemisorbed species is separated as a distinct constant capacitance layer between the surface proper and the diffuse layer. The TLM generalises this approach, and has two constant capacitance layers, not necessarily thin, between the surface and the diffuse layer. The

TLM is more complex than the other models because it includes an additional surface layer to account for the weaker adsorption of large ionic species such as alkali earth cations (e.g., Langmuir, 1997). In this case, there are two capacitances that can be fit to experimental data, although in practice the capacitance of the outer layer is typically set to a constant value (e.g., Yates, 1975; Sahai and Sverjensky, 1997).

The Constant Capacitance Model was chosen because it was found to be the simplest model that could be fit to most of the data. Furthermore, the CCM is appropriate where the mineral surface has a low surface charge or the solution is of high ionic strength and the diffuse layer is compressed close to the mineral surface (Barrow et al., 1982; Davis and Kent, 1990) such as the conditions of our experiments. Details of the reactions and fit parameters necessary in the CCM are described below.

The formation of charged surface sites provides the sites for metal sorption and they are represented by the following reactions:

$$\equiv SOH(ads) + H^{+}(aq) = \equiv SOH_2^{+}(ads) \qquad (2.6)$$

$$\equiv SO^{-}(ads) + H^{+}(aq) = \equiv SOH(ads) \qquad (2.7)$$

Their apparent equilibrium constants expressed as concentrations are:

$$K_1^{app} = \frac{a_{\equiv SOH_2^+}}{a_{\equiv SOH} a_{H^+}} \qquad (2.8)$$

$$K_2^{app} = \frac{a_{\equiv SOH}}{a_{\equiv SO^-} a_{H^+}} \qquad (2.9)$$

The activity of H^+ is assumed to change as a function of distance from the mineral surface, due to the effect of the surface charge (Dzombak and Morel, 1990). Therefore, the addition of a coulombic "correction factor" is introduced for the activity of each adsorbed species of charge z and is multiplied by $\exp(-zF\psi_o/RT)$:

$$K_1^{int} = \frac{a_{\equiv SOH_2^+}}{a_{\equiv SOH} a_{H^+}} \exp\left(\frac{-zF\psi_0}{RT}\right) \qquad (2.10)$$

$$K_2^{int} = \frac{a_{\equiv SOH}}{a_{\equiv SO^-} a_{H^+}} \exp\left(\frac{-zF\psi_0}{RT}\right) \qquad (2.11)$$

where ψ_o is the electrical potential (V) at the surface, F is the Faraday constant (96487 C/mol), R is the universal gas constant (8.314 J K^{-1}/mol) and T is temperature in Kelvin. The chosen standard state is a hypothetical 1 molal for the adsorbed species and zero surface potential (i.e. Sahai and Sverjensky, 1997).

In the CCM the electrical potential is calculated assuming a constant capacitance:

$$\psi_o = \frac{\sigma_o}{C} \qquad (2.12)$$

Where σ_o is the charge of the solid surface (Coulombs) and C is the constant capacitance (F/m^2; Davis and Kent, 1990). The reactions and associated equilibrium constants for the metal complexes are treated in the same way, and the specific equations are given below.

2.3.1.3 Surface Site Density

Surface site density is a necessary parameter in surface complexation models for determining the concentration of ≡SOH (Equations 2 to 9), but it is difficult to estimate accurately. The difficulty results from uncertainty in the nature of these sites with a number of different types of sites (e.g., singly, doubly and possibly triply coordinated oxygens for protonation/deprotonation reactions on various crystal planes; Peacock and Sherman, 2004), the nature of the surface (e.g., surface roughness and surface edges (Boily et al., 2000; Gaboriaud and Ehrhardt, 2003), the dependence on ionic strength, the type of electrolytes and the methods used to measure site densities (cf., Lützenkirchen et al., 2002; Peacock and Sherman, 2004). Another complicating factor is that site densities for goethite are different for different crystal planes, e.g., 3.03 FeO sites/nm^2 on (101) and 7.19 sites on (100); Peacock and Sherman, 2004), which implies that different morphologies of goethite will have different average site densities. It is also possible that the nature and number of sites available are different for cations or anions of different properties, such as the very small hydrogen ion. Existing estimates for goethite site density show more than an order of magnitude difference (Table 2.2). Potentiometric titration methods have resulted in values between 1.7 and 2.7 sites/nm^2 (Table 2.2), whereas tritium exchange measurements resulted in 16.4 site/nm^2 (Yates, 1975). Molecular statics calculations are close to the latter measurement, where they indicate a value between 15 and 16 sites/nm^2 (Rustad, 1996). Potentiometric methods are likely to underestimate the site density because they are susceptible to interferences from CO_2 (which adsorbs strongly to goethite surfaces, and limits the sites available for acid-base reactions during titration; Zeltner and Anderson, 1988) and they are done at high or low pH values depending on the type of mineral surface titrated, e.g., pH < 3 for

goethite to ensure proton saturation (Lützenkirchen et al., 2002), which can result in large errors because the acidity of the solutions implies that the titrations are measuring small changes in big numbers (Dzombak and Morel, 1990; Lützenkirchen et al., 2002).

Table 2. 2: Published surface areas, site densities and protonation (K_1^{int}) and deprotonation (K_2^{int}) reactions for goethite.

Author	*Calculation Method*	*Surface Area* (m^2/g)	*Surface Site Density* ($sites/nm^2$)	*Log* K_1^{int}	*Log* K_2^{int}
Ali and Dzombak (1996)	Titration	79.4	1.4	7.68	-8.32
Gao and Mucci (2001)	Titration	27.7	1.8	7.45	-9.6
Lövgren et al. (1993)	Titration	39.9	1.7	7.47	-9.51
Lumsdon and Evans (1994)	Titration	86	2.74	7.52	-10.63
Missana et al. (2003)	Titration	35	2.2	7.2	-10.0
Peacock and Sherman (2004)	Titration	32.7	6.02	7.5	-9.5
Rustad (1996)	Molecular Statics	-	15-16	-	-
Van Geen et al. (1994)	Titration	45	2.3	7.91	-10.02
Yates (1975)	Tritium Exchange	-	16.4	4.2	-10.8

Given the uncertainty in the site density estimates, the adsorption of copper on our synthetic goethite was measured by varying the goethite/solution ratio in a series of 5 experiments at pH = 5.5 (Figure 2.7) in an attempt to measure the maximum copper adsorption. Results show that copper occupies 14 sites/nm^2. This estimate is likely to be a minimum value as the maximum concentration of adsorbed copper in our experiments may not have been achieved. Our value is in good agreement with the results of the tritium exchange experiments of Yates (1975) and the molecular statics calculations of Rustad (1996), so we choose the site density of 16.4 sites/nm^2 estimated by Yates (1975). Sahai and Sverjensky (1997a) made the same choice; however, in contrast, Peacock and Sherman (2004) chose a value of 7.5 sites/nm^2 as proposed by Venema et al. (1998). In any case, choosing different values of site density did not affect the conclusions about the nature of surface complexation and the reactions present in the experiments.

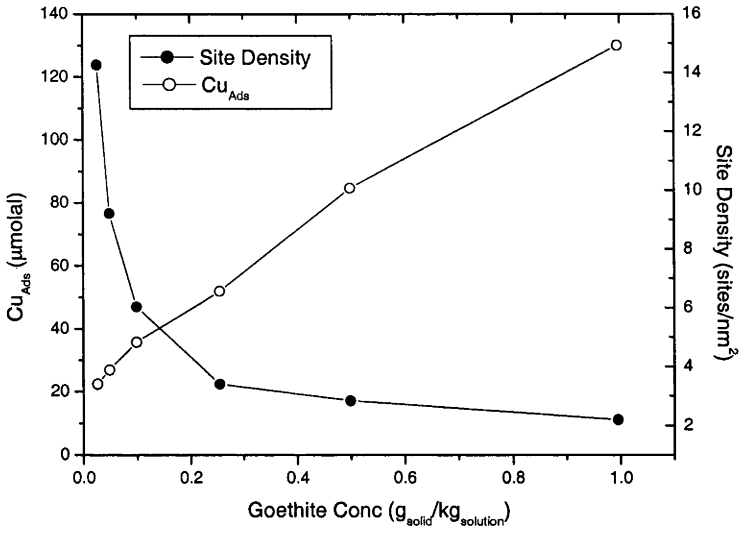

Figure 2.7: Concentration of Cu^{II} adsorbed as a function of goethite concentration and calculated density of occupied sites by Cu^{II} per nm^2.

2.3.1.4 Fitting equilibrium constants

In this section the results of fitting the equilibrium constants for the protonation and deprotonation and copper adsorption reactions in Equations 2.2 to 2.9 are shown. FITEQL 4.0 (Herbelin and Westall, 1999) was used to fit the equilibrium constants, using the assumptions and measurements discussed above. FITEQL 4.0 is a computer program that uses a non-linear least squares method to optimise equilibrium constants for adsorption reactions (e.g., Dzombak and Morel, 1990; Herbelin and Westall, 1999). In FITEQL, the quality of the fit is indicated by the variance v_y, which is the weighted sum of squares of residuals (*SOS*) divided by the degrees of freedom (*DF*; Herbelin and Westall, 1999):

$$V_y = \frac{SOS}{DF} = \Sigma \frac{(y_r / s_r)^2}{n_p n_r - n_u} \qquad (2.13)$$

where y_r is the difference between predicted and measured adsorbed concentration for each experiment, and s_r is the estimated experimental error for each experiment. n_p is the number of data points, n_r is the number of components with known total concentration and n_u is the number of adjustable parameters. v_y values between 0.1 and 20 are considered to represent a "reasonably good" fit (e.g., Herbelin and Westall, 1999).

The amphoteric treatment of single sites is a surface representation used for the convenience of modelling and does not reflect the true nature of surface reactions (Rustad et al., 1996). For example, the formation of $\equiv SOHCu^{2+}$ and $\equiv SOCu^{+}$ are unlikely to be true representations of the surface species on goethite, because they are the simplest reactions for describing metal adsorption over a wide range of pH vales. This is substantiated by the study of Peacock and Sherman (2004) who used EXAFS to identify a series of complex bidentate-mononuclear and polynuclear copper surface complexes. However, they were unable to fit their model with these reactions alone and found that they required the reactions in Equations 2.2 and 2.3 to successfully fit their model over the entire pH range studied. Therefore, for modelling purposes these are the considered in this study.

Equilibrium constants for all reactions involving surface complexes were fitted to each series of experiments, i.e., for 0.1, 1 and 3 molal $NaNO_3$ concentrations. Two copper surface complexes were included, based on the slopes of 0 to 1 of adsorbed copper versus pH (Figure 2.6) and because preliminary fits with a single copper surface complexes did not fit the experimental data over the entire pH range. The aqueous speciation of Cu^{II} was calculated with FITEQL 4.0, using mass balance constraints on

total Na, NO_3^- and Cu, pH, mass action equations for appropriate aqueous and mineral species (e.g., OH^-, Cu hydroxide and aqueous nitrate complexes; Table 2.3) and assuming an activity of $H_2O(l)$ = 1. The standard state for aqueous species was the hypothetical 1 molal solution to infinite dilution. Activity coefficients were estimated in FITEQL 4.0 using the Davies equation:

$$\log \gamma = Az^2 \left(\frac{I^{1/2}}{1 + I^{1/2}} - 0.3I \right) \qquad (2.14)$$

where I is the stoichiometric ionic strength (Davies, 1962) and A = 0.509 (Herbelin and Westall, 1999). Applying the Davies equation to the $NaNO_3$ adsorption data allows a direct comparison with previous studies, and draw comparisons between studies. Aqueous copper nitrate complexes were included all calculations using the thermodynamic properties in the NIST database (Smith and Martel, 2004). The impact of different choices of aqueous and surface complexes is discussed and the potential uncertainty in activity coefficient estimates below. The value of 0.83 F/m^2 for capacitance provided the closest fit of the model to the experimental data as indicated by the variance (v_y). This value is close to the capacitance of 1.28 F/m^2 optimised by Lövgren et al. (1996) who determined this value based on the acid-base surface reactions of goethite in 0.1 M $NaNO_3$. The capacitance was fitted for each $NaNO_3$ concentration, but the optimised capacitance value only varied by 0.05 F/m^2.

The CCM and surface speciation was fitted to the data using the copper surface complexes in Equations 2.2 and 2.3, the protonation and deprotonation reactions in Equations 2.6 and 2.7 and each of the four following sets of assumptions: (a) exclude aqueous copper nitrate complexes (i.e., $CuNO_3^+(aq)$ and $Cu(NO_3)_2(aq)$) and a surface

nitrate complex (i.e., $\equiv SOH_2NO_3$); (b) include aqueous copper nitrate complexes but no surface nitrate complex; (c) include the surface nitrate complex but no aqueous copper nitrate complexes and (d) include both the surface complex $\equiv SOH_2NO_3$ and copper nitrate aqueous complexes. Note that the copper surface complexes $\equiv SOCuOH$ and $\equiv SOHCuOH^+$ was considered, as suggested by Barrow et al. (1982), but found they did not fit the experimental data. Peacock and Sherman (2004) also found these complexes unnecessary. No poly-metallic surface complexes as suggested by Peacock and Sherman (2004) or multiple adsorption sites (i.e. $\equiv SO_2Cu^0$) were invoked as they were not necessary to successfully fit the experimental data.

Table 2.3: Equilibrium constants for species used to model Cu^{II} adsorption onto goethite for each concentration of $NaNO_3$. Equilibrium constants describe the formation reactions of species. Other surface complexes included in our model are $\equiv SO^-$, $\equiv SOH_2$ with log K values for taken from Richter et al. (2005). Activity coefficients are calculated using the Davies Equation.

Species	**Log K ($NaNO_3$ Concentration)**		
	0.1	***1.0***	***3.0***
$\equiv SOHCu^{2+}$	-1.85	-1.86	-2.15
$\equiv SOCu^+$	5.28	6.52	6.34
V_y	2.84	2.68	0.95

The log K values of Richter et al. (2005; Table 2) were used for the protonation and deprotonation reactions; where $\log K_1^{int} = 6.36 \pm 0.38$ (2σ) and $\log K_2^{int} = -10.44 \pm 0.38$ (2σ). Richter et al. (2005) calculated these by averaging the log K values for the reactions described in Equations 2.6 and 2.7 from 15 independent studies. Fitted equilibrium constants are shown in Table 2.3. The reaction for $\equiv SOHCu^{2+}$ (Equation 2.2) varied by 0.30 log K units between the 0.1 and 3.0 molal $NaNO_3$ experimental data and 1.24 log K units for the reaction $\equiv SOCu^+$ (Equation 2.3). The surface complex

$\equiv SOH_2NO_3$ was tried, similar to Peacock and Sherman (2004) and Criscenti and Sverjensky (2002), but fitted equilibrium constants for reactions in Equations 2.2 and 2.3 did not improve the fit with the experimental data between each $NaNO_3$ series. Because there is no unequivocal evidence for the existence of the nitrate surface complex, and no improvement with the fit of the model to the experimental data the complex was excluded from the model. A fit using all the experimental data from 0.1 – 3.0 molal $NaNO_3$ was attempted; however the model could be converged.

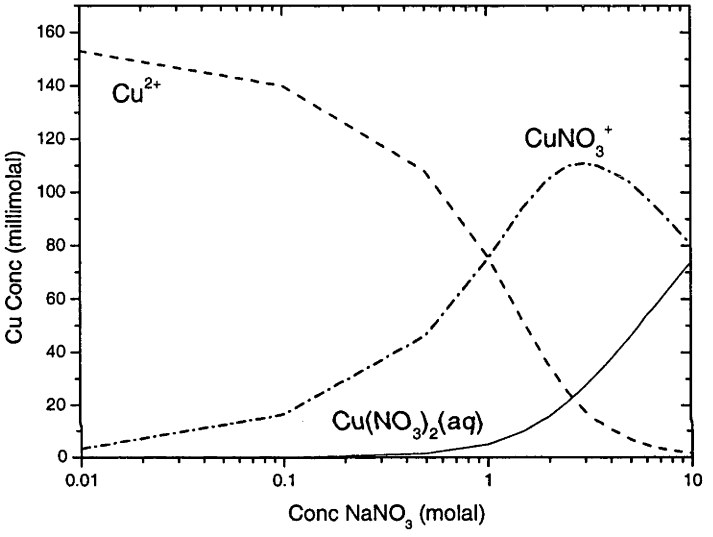

Figure 2.7: Aqueous Cu^{II} nitrate complexes calculated at 25°C and 1 bar as a function of $NaNO_3$ concentration at pH 5.0 Equilibrium constants are from NIST (Smith and Martell, 2004) and activity coefficients were calculated with the Davies equation.

Adsorption decreased by up to 30% in the 1.0 and 3.0 molal $NaNO_3$ series at pH greater than 5.0 (Figure 2.7). The lower adsorption in 1.0 and 3.0 molal $NaNO_3$ coincides with the predominance of $CuNO_3^+$ in solution and may be the cause of the apparent suppression of adsorption (Figures 2.8 and 2.3). A further possible cause for the lower adsorption in 1.0 and 3.0 molal $NaNO_3$ at pH > 5.0 is the effect of high ionic strength on pH. Wiesner et al. (2006) studied the effect of ionic strength on measured pH in

adsorption experiments. They concluded that the measured pH changed with increasing ionic strength, but they did not quantify this effect. The effect could not be quantified successfully in this study either, but it may be important and further investigation into this is required for future studies. It is possible that more Cu^{II} was adsorbed onto the reaction vessel in the 1.0 and 3.0 $NaNO_3$ solutions. However the effect that this may have on results could not be investigated due to limited time and resources to conduct further experiments.

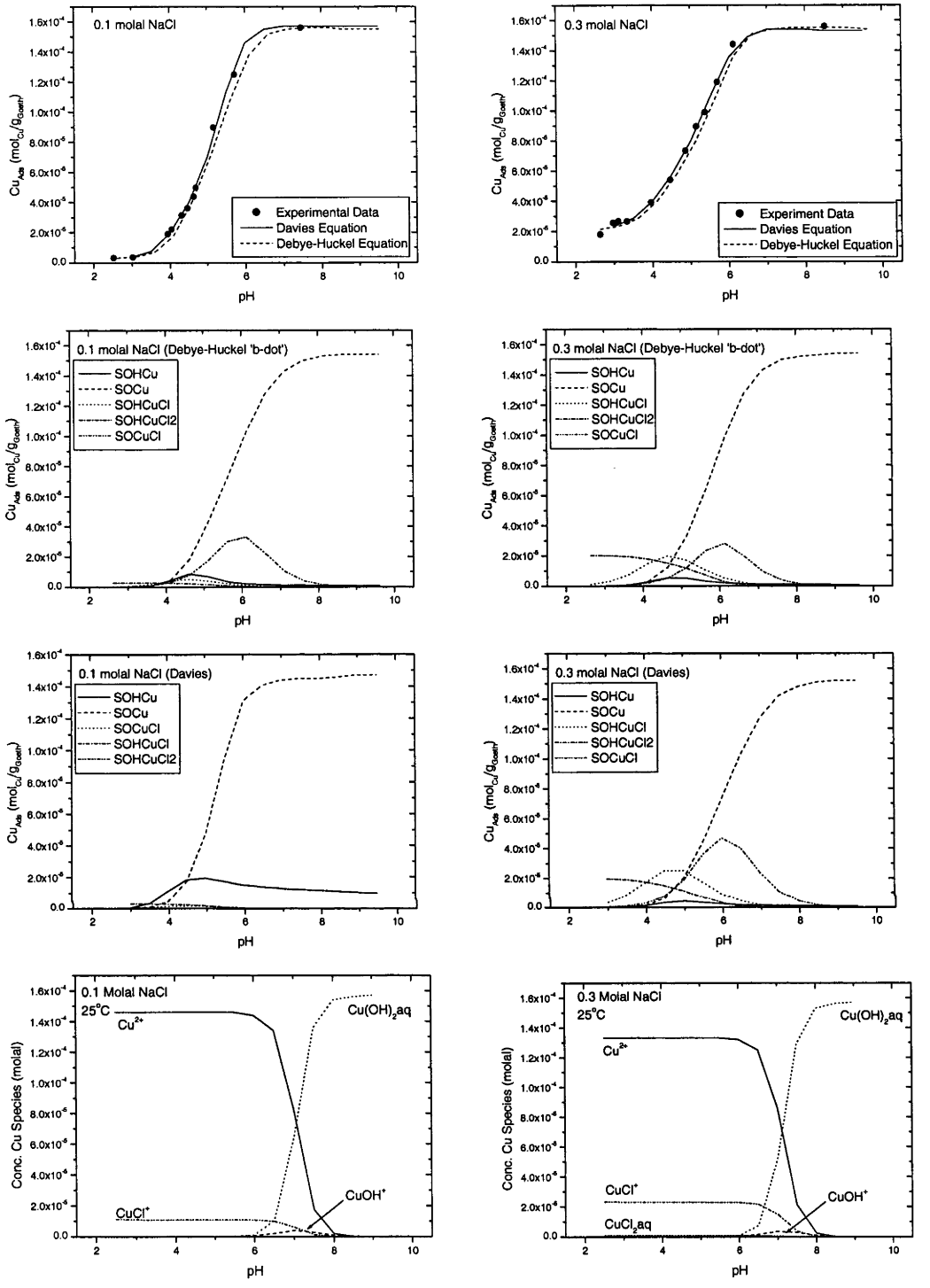

Figure 2.9a: Adsorption of Cu^{II} onto goethite as a function of pH in 0.1 and 0.3 molal NaCl solutions, with predicted surface species calculated using fitted equilibrium constants from each series of experimental data with the CCM using the Debye-Hückel b-dot Equation and the Davies Equation. Goethite concentration = 0.937 g/L, $Cu^{II} = 1.54 \times 10^{-4}$ molal, site density 16.4 sites/nm2, capacitance = 0.87 F/m^2. Optimised equilibrium constants shown in Tables 2.4 and 2.5. Aqueous speciation shows the predominant Cu^{II} species for 0.1 molal and 0.3 molal NaCl calculated with the Debye-Hückel b-dot Equation where the standard state is the hypothetical 1 molal solution to infinite dilution. Other aqueous Cu^{II} species included but not shown due to their low concentrations are $Cu_2(OH)_2^{2+}$, $CuNO_3^+$ and $Cu(NO_3)_2(aq)$.

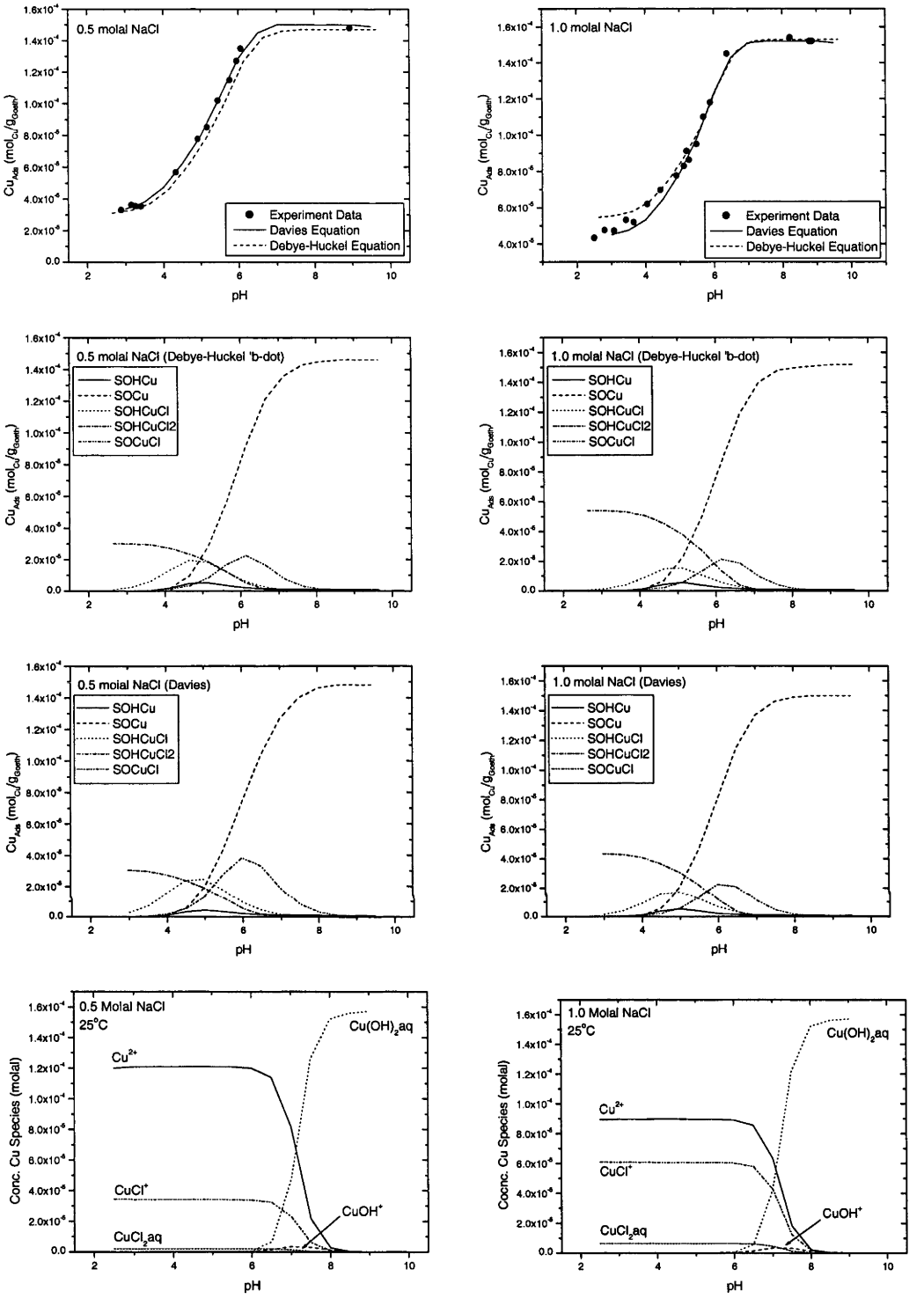

Figure 2.9b: Adsorption of Cu^{II} onto goethite as a function of pH in 0.5 and 1.0 molal NaCl solutions, with predicted surface species calculated using fitted equilibrium constants from each series of experimental data with the CCM using the Debye-Hückel b-dot Equation and the Davies Equation. Goethite concentration = 0.937 g/L, $Cu^{II} = 1.54\times10^{-4}$ molal, site density 16.4 sites/nm2, capacitance = 0.87 F/m^2. Optimised equilibrium constants shown in Tables 2.4 and 2.5. Aqueous speciation shows the predominant Cu^{II} species for 0.1 molal and 0.3 molal NaCl calculated with the Debye-Hückel b-dot Equation. Other aqueous Cu^{II} species included but not shown due to their low concentrations are $Cu_2(OH)_2^{2+}$, $CuNO_3^+$ and $Cu(NO_3)_2(aq)$.

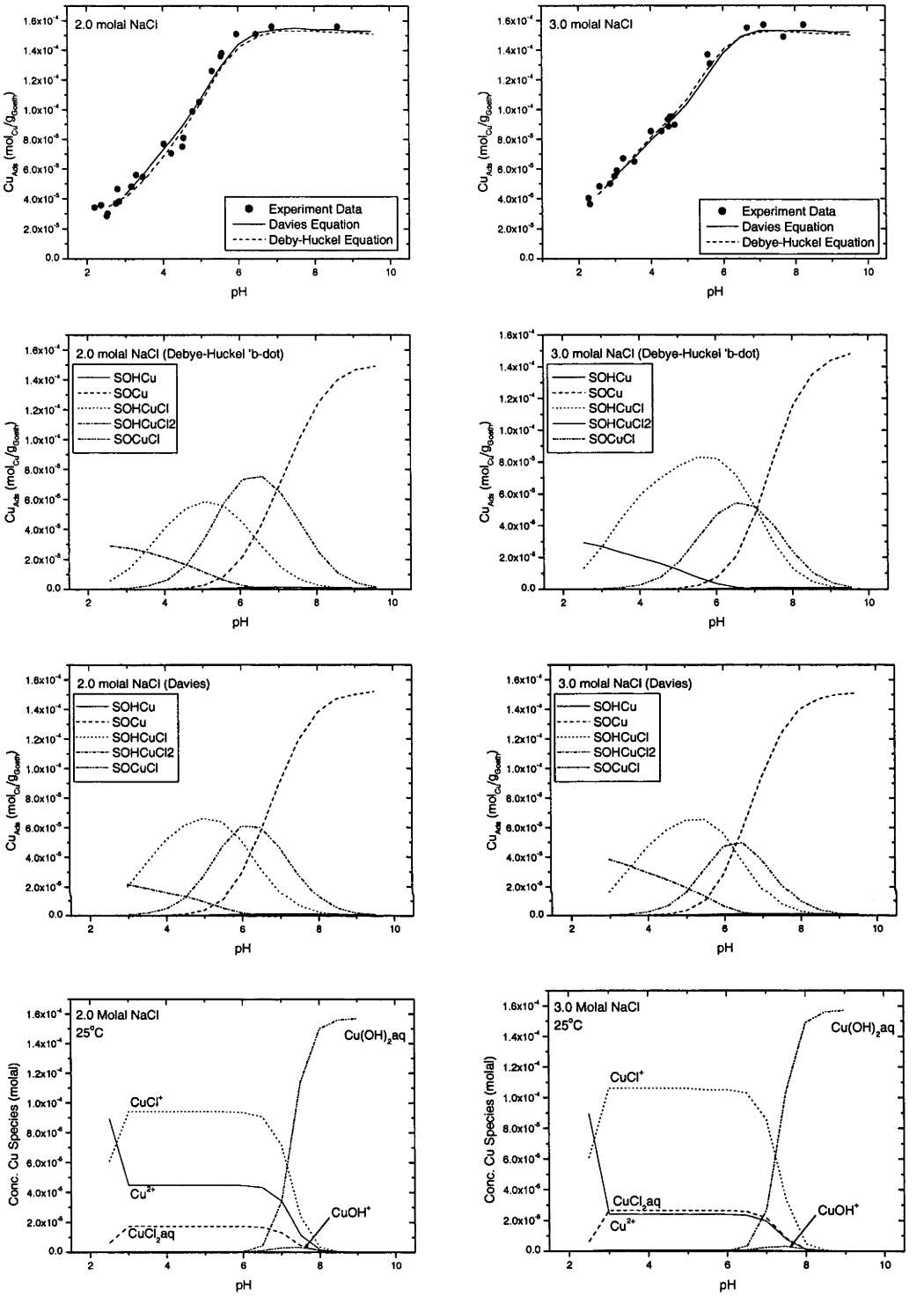

Figure 2.9c: Adsorption of Cu^{II} onto goethite as a function of pH in 1.0 and 3.0 molal NaCl solutions, with predicted surface species calculated using fitted equilibrium constants from each series of experimental data with the CCM using the Debye-Hückel b-dot Equation and the Davies Equation. Goethite concentration = 0.937 g/L, $Cu^{II} = 1.54 \times 10^{-4}$ molal, site density 16.4 sites/nm2, capacitance = 0.87 F/m^2. Optimised equilibrium constants shown in Tables 2.4 and 2.5. Aqueous speciation shows the predominant Cu^{II} species for 0.1 molal and 0.3 molal NaCl calculated with the Debye-Hückel b-dot Equation. Other aqueous Cu^{II} species included but not shown due to their low concentrations are $Cu_2(OH)_2^{2+}$, $CuNO_3^+$ and $Cu(NO_3)_2(aq)$.

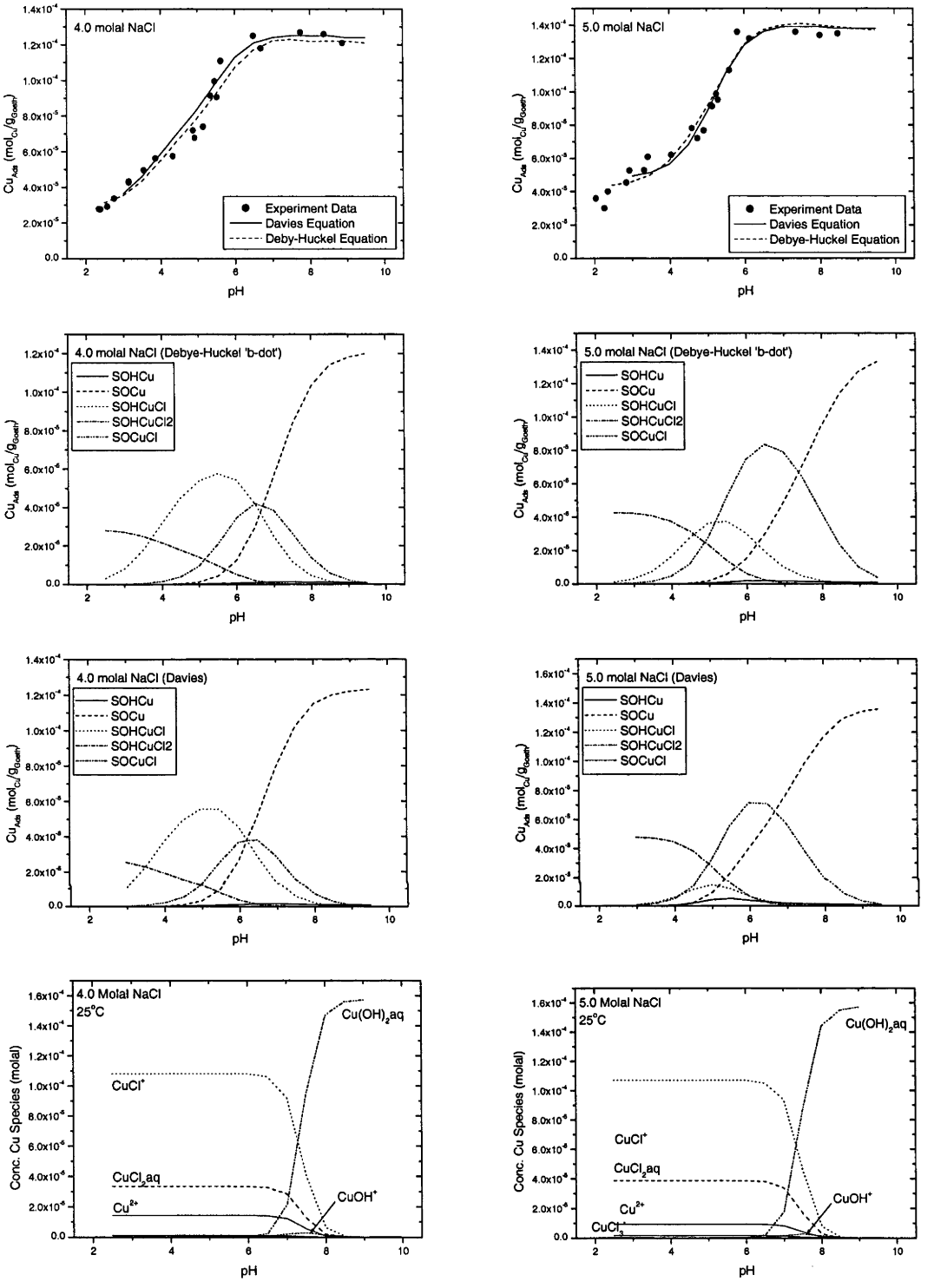

Figure 2.9d: Adsorption of Cu^{II} onto goethite as a function of pH in 1.0 and 3.0 molal NaCl solutions, with predicted surface species calculated using fitted equilibrium constants from each series of experimental data with the CCM using the Debye-Hückel b-dot Equation and the Davies Equation. Goethite concentration = 0.937 g/L, Cu^{II} = 1.54×10^{-4} molal, site density 16.4 sites/nm^2, capacitance = 0.87 F/m^2. Optimised equilibrium constants shown in Tables 2.4 and 2.5. Aqueous speciation shows the predominant Cu^{II} species for 0.1 molal and 0.3 molal NaCl calculated with the Debye-Hückel b-dot Equation. Other aqueous Cu^{II} species included but not shown due to their low concentrations are $Cu_2(OH)_2^{2+}$, $CuNO_3^+$ and $Cu(NO_3)_2(aq)$.

2.3.2 Cu^{II} Adsorption onto Goethite in NaCl solutions

Results for Cu^{II} adsorption onto goethite in NaCl solutions are presented in Figure 2.9a-d and Appendix A. The concentration of Cu^{II} adsorbed increased with increasing pH, as observed with the $NaNO_3$ solutions. Adsorption also increased with increasing NaCl concentrations between 0.1 molal NaCl and 2.0 molal NaCl and at pH less than 5.0 (Figure 2.9). At pH >5.0, no discernible difference to Cu^{II} adsorption between $NaNO_3$ and NaCl was observed. The enhanced Cu^{II} adsorption in NaCl observed in this study is consistent with the findings of Barrow et al. (1982) and Padmanabham (1983b), but contradicts the conclusions of Balistrieri and Murray (1982) and Criscenti and Sverjensky (1999).

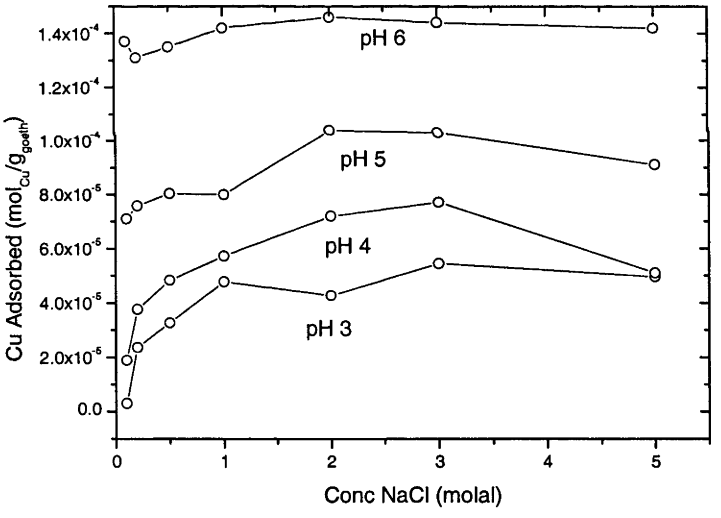

Figure 2.10: Adsorption of Cu^{II} onto goethite as a function of NaCl concentration and pH between 0.1 and 5 molal NaCl. Experimental conditions are the same as those reported in Figure 2.7.

An attempt to isolate the effect of NaCl on CuII adsorption was made by plotting $Log[Cu_{Ads}] - log[Cu_{Diss}] - pH$ versus log[NaCl] to identify possible surface complexes and reactions occurring in experiments. The result of this is shown in Figure 2.11,

where NaCl has the greatest influence at pH 3.0 in NaCl concentrations less than 0.5 molal, and the line of best fit slope was 1.83. When the NaCl concentration was greater than 0.5 molal and at pH 3, the slope of the line decreased to 0.11. At higher pH, i.e., 4.0 and 5.1, the slopes of the lines are near zero: 0.06 and 0.07, respectively (Figure 2.11).

When NaCl concentrations >0.5 molal and pH <5.5, adsorption was nearly independent of NaCl (Figure 2.11) and is interpreted to be due aqueous copper chloride complexes being dominant in solution, e.g.:

$$\equiv SOH + CuCl^{+} = \equiv SOCuCl^{0} + H^{+} \qquad (2.20)$$

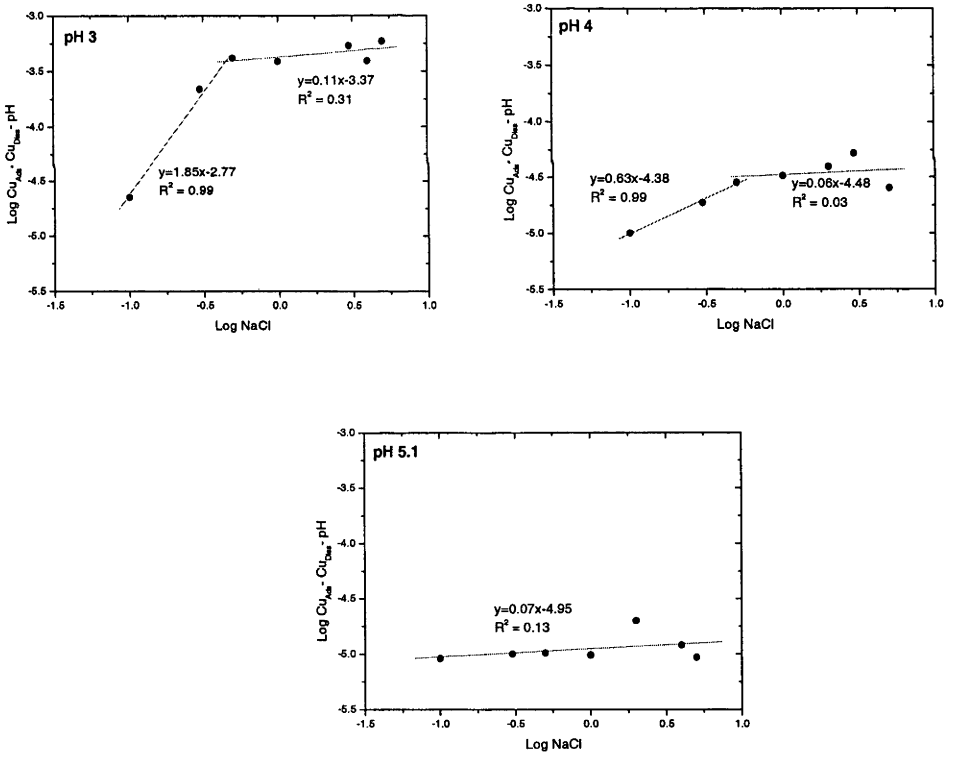

Figure 2.11: $Log[Cu]_{Ads} - log[Cu]_{Diss} - pH$ versus log[NaCl] showing the adsorption of Cu^{II} onto goethite in NaCl solutions at different pH. The slope of the regression lines for the data points indicates the controlling reactions for the formation of copper surface complexes.

The same method of data treatment for assessing pH dependence as that used in $NaNO_3$ solutions was used. The effect of pH is shown in Figure 2.12, where one line of best fit with a slope of 0.8 at 0.1 molal NaCl could be fitted. The pH dependence decreases when the NaCl concentration is >0.5 molal, as demonstrated by the increase of the best-fit line slopes in Figure 2.12. The change of slope may be caused by a change in the dominant reaction from a pH-independent (e.g., Equation 2.2) to pH-dependent reaction (e.g., Equation 2.3).

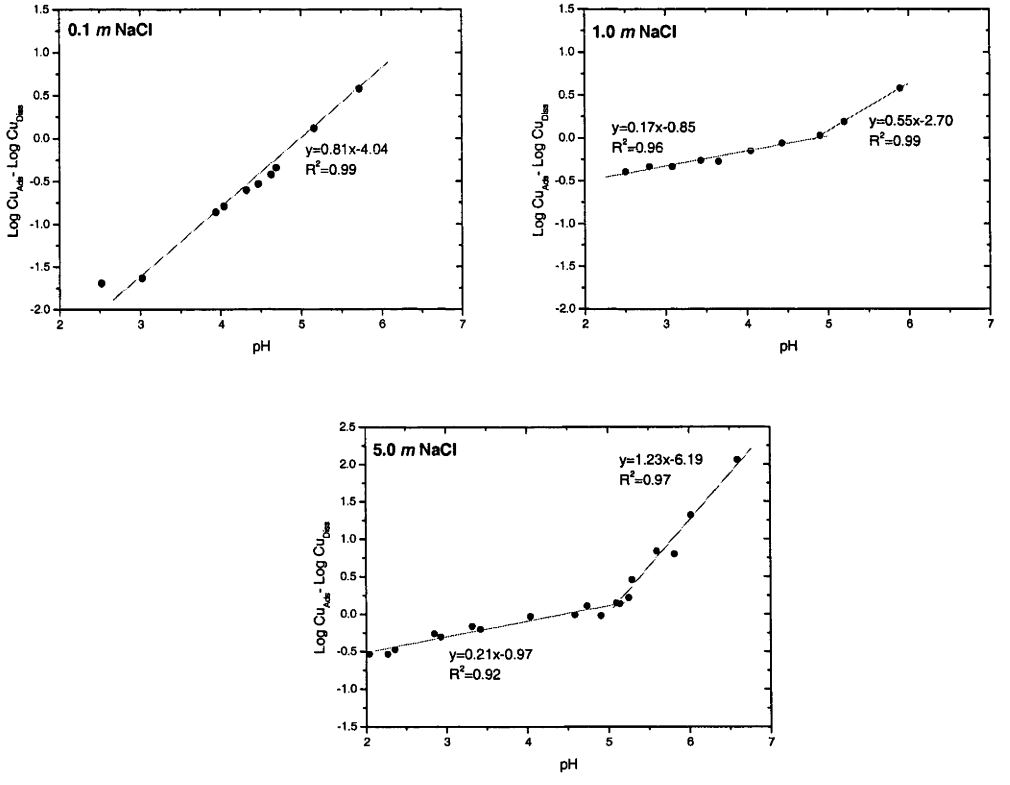

Figure 2.12: Log[Cu_{Ads}] – log[Cu_{Diss}] versus pH showing the adsorption of Cu^{II} onto goethite in 0.1, 0.5, 1.0 and 5.0 molal NaCl solutions. The slope of the regression lines for the data points indicates the pH dependence of the controlling reactions for Cu^{II} adsorption.

Based on the results shown in Figures 2.11 and 2.12, the reactions in Equations 2.17 to 2.19 could be added to Equations 2.2 and 2.3 to describe the adsorption of Cu^{II} onto

goethite. This is explored further in the following section for fitting equilibrium constants.

$$\equiv SOH + Cu^{2+} + Cl^- = \equiv SOHCuCl^+ \qquad (2.17)$$

$$\equiv SOH + Cu^{2+} + Cl^- = \equiv SOCuCl^0 + H^+ \qquad (2.18)$$

$$\equiv SOH + Cu^{2+} + 2Cl^- = \equiv SOHCuCl_2^0 \qquad (2.19)$$

2.3.2.1 Fitting Equilibrium Constants

This section describes the method for fitting equilibrium constants for formation reactions of Cu^{II} surface complexes in NaCl solutions of varying concentrations. Because a wide range of ionic strengths were used in experiments, consideration for the effects on measured pH and care with the choice of model for activity coefficients is required despite some uncertainty as to which activity coefficient model is most appropriate for the range of NaCl concentrations used in experiments. Previous adsorption studies used low ionic strength (i.e. >0.5 molal) solutions and as a result thermodynamic optimisation programs such as FITEQL 4.0 use the Davies Equation (Equation 2.14) to calculate activity coefficients. However, the Debye-Hückel b-dot Equation is believed to be a better method of calculating activity coefficients in solutions with >0.5 molal NaCl (e.g. Helgeson and Kirkham; 1974):

$$Log(\gamma) = \frac{-A_\gamma z_i^2 \sqrt{I}}{1 + B_\gamma a_i \sqrt{I}} + b^\bullet I \qquad (2.21)$$

The Pitzer Equation is probably the most appropriate method of calculating activity coefficients for high ionic strength solutions (i.e. >1.0 molal). However, the parameters for the Pitzer Equation are limited to the major ion species and no information for trace elements such as Cu^{II} are available. Because no Pitzer Equation parameters are available, and it is beyond the scope of this study to calculate these, the Davies Equation and the Debye-Hückel b-dot Equation are used in the adsorption models.

FITEQL 4.0 uses the Davies Equation as the default method for activity coefficient calculations; however, fitting of the data using the Debye-Hückel "b-dot" equation required activity coefficients to be calculated externally and integrated into the FITEQL 4.0 input file. PHREEQCi v2.12.5 was used to calculate the activity coefficient for each experimental condition (i.e. for the specific pH of each solution) and concentrations of total Cu, Na, Cl and nitrate. The calculated activity coefficients for each species in solution (listed in Table 2.3) was entered into the input file of FITEQL 4.0 and used in the distribution of species calculation to fit the experimental data. An example of the input file which used the Debye-Hückel "b-dot" equation is shown in Appendix E.

Log K values for the formation reactions of the aqueous species are shown in Table 2.3. Copper chloride aqueous complexes were taken from Brugger et al. (2002) and the NaCl(*aq*) ion pair was included using the formation reaction from Smith and Martell (1997). The predicted aqueous speciation of Cu^{II} in 0.1 – 5.0 molal NaCl calculated with the Debye-Hückel "b-dot" model and Davies Equation as a function of pH are shown in Figure 2.9a-d. The two activity models are compared as a function of NaCl concentration is shown in Figure 2.13.

The predicted speciation between the two models differed by less than 5% at NaCl concentrations less than 1 molal, which suggests that the method of calculating activity coefficients is not going to change the fit of the model significantly with NaCl concentrations <1.0 molal. However, at higher NaCl concentrations, the Davies equation predicted approximately 30% less Cu^{2+}.

Table 2.3: Reactions and equilibrium constants for aqueous species used to model Cu^{II} adsorption onto goethite in $NaNO_3$ solutions. Equilibrium constants describe the formation reactions of species.

Species	Mass Action Reaction	Log K	Source
OH^-	$OH^- + H^+ = H_2O$	13.98	a
$CuOH^+$	$Cu^{2+} + H_2O = CuOH^+ + H^+$	-8.00	a
$Cu(OH)_2$	$Cu^{2+} + 2H_2O = Cu(OH)_2 + 2H^+$	-13.68	b
$Cu_2(OH)_2^{2+}$	$2Cu^{2+} + 2H_2O = Cu_2(OH)_2^{2+} + 2H^+$	-17.50	b
$CuNO_3^+$	$Cu^{2+} + NO_3^- = CuNO_3^+$	0.50	a
$Cu(NO_3)_2$	$Cu^{2+} + 2NO_3^- = Cu(NO_3)_2$	-0.40	a
$NaNO_3(aq)$	$Na^+ + NO_3^- = NaNO_3(aq)$	-0.55	a
NaCl(aq)	$Na^+ + Cl^- = NaCl(aq)$	-0.3	a
$CuCl^+$	$Cu^{2+} + Cl^- = CuCl^+$	0.30	c
$CuCl_2$	$Cu^{2+} + 2Cl^- = CuCl_2$	-0.26	c
$CuCl_3^-$	$Cu^{2+} + 3Cl^- = CuCl_3^-$	-2.29	c

[a] Smith and Martel (1997)

[b] Peacock and Sherman (2004)

[c] Brugger et al. (2002)

Therefore at NaCl concentrations <1.0 molal, it made no discernable difference as to which activity model was used. However at NaCl concentrations >1.0 molal, it is not clear which model is most suitable and is discussed further when fitting the adsorption data.

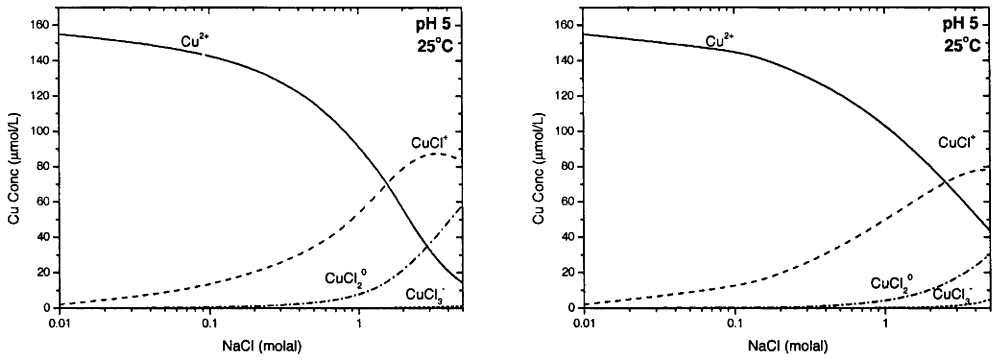

Figure 2.13: Predicted speciation of Cu^{II} complexes as a function on NaCl concentration at pH 5.0. (a) activity coefficients calculated with the Davies equation in FITEQL 4.0 (Herbelin and Westall, 1999). (b) activity coefficients calculated with the b-dot model in Geochemists Workbench (Bethke, 2002).

Equilibrium constants for adsorption reactions were fitted individually for each NaCl concentration series using a number of different scenarios. Initially, the the only surface complexes used were those defined in Equations 2.2 and 2.3 with the fitted equilibrium constant from $NaNO_3$ experimental data. Other scenarios modelled included: (a) different single copper chloride surface complexes; (b) different combinations of two copper chloride surface complexes; and (c) three copper chloride complexes. Each scenario included to the surface complexes defined in Equations 2.2 and 2.3.

When the reactions in Equations 2.2 and 2.3 were used to model Cu^{II} adsorption in NaCl solutions, convergence of the model could not be achieved when the NaCl concentration was > 0.3 molal. When there was 0.3 molal or less NaCl, the best fit equilibrium constants were an order of magnitude greater for the $\equiv SOCu^{+}$ surface species and 3 orders of magnitude greater for the $\equiv SOHCu^{2+}$ in the 0.3 molal NaCl when compared to solutions with 0.1 molal NaCl. Because the model was unable to fit the experimental data with these two surface species, it suggests that the formation of copper chloride ternary surface species may be an important process in experiments.

The surface species shown in Equations 2.17 to 2.20 were added as single copper chloride surface complexes to the model. However none of these fit the data, evident by the high variance values (i.e. $v_y > 25$) and the poor fit of the modelled adsorption curves with the measured ones. Furthermore, fitted log K values changed by more than 1.4 units over the entire range of NaCl concentrations. Combinations of two surface complexes from Equations 2.17 to 2.20 where then used and no combination of two copper chloride surface complexes could fit the data over the entire range of NaCl concentrations. For example, the combination of the ≡SOCuCl and ≡$SOHCuCl_2$ surface species best fit the 0.3 and 0.5 molal NaCl series, but the ≡SOCuCl and ≡$SOHCuCl^+$ surface species provided the best fit for NaCl concentrations between 2 and 5 molal.

Table 2.4: Fitted equilibrium constants for formation from SOH, Cu^{2+} and Cl^- for species used to model Cu^{II} adsorption onto goethite for each concentration of NaCl. Other surface complexes included in our model are ≡SO^-,≡SOH_2^+, ≡$SOCu^+$ and ≡$SOHCu^{2+}$. Log K values for ≡SO^- and ≡SOH_2^+ are from Richter et al. (2005), while ≡$SOHCu^{2+}$ and ≡$SOCu^+$ were calculated in this study from experiments in $NaNO_3$. Activity coefficients are calculated using the Davies Equation.

Species	**Log K (NaCl Concentration)**								
	0.1	***0.3***	***0.5***	***1***	***2***	***3***	***4***	***5***	***0.1-3.0***
≡SOCuCl	-1.85	-1.86	-2.15	-2.70	-1.96	-2.05	-2.23	-1.87	-1.96
≡$SOHCuCl^+$	5.28	6.52	6.34	5.91	7.01	7.38	6.79	5.69	5.35
≡$SOHCuCl_2$	3.43	3.50	3.39	3.15	2.48	2.97	2.45	2.71	3.37
V_y	2.84	2.68	0.95	8.92	8.52	5.11	7.68	17.80	11.89

Table 2.5: Fitted equilibrium constants for formation from ≡SOH, Cu^{2+} and Cl^- for species used to model Cu^{II} adsorption onto goethite for each concentration of NaCl. Equilibrium constants describe the formation reactions of species. Other surface complexes included in our model are SO^-, SOH_2^+, ≡$SOCu^+$ and ≡$SOHCu^{2+}$. Log K values for SO^- and SOH_2^+ are from Richter et al. (2005), while ≡$SOHCu^{2+}$ and ≡$SOCu^+$ were calculated in this study from experiments in $NaNO_3$. Activity coefficients are calculated using the Debye-Hückel "b-dot" Equation.

Species	**Log K (NaCl Concentration)**								
	0.1	***0.3***	***0.5***	***1***	***2***	***3***	***4***	***5***	***0.1-3.0***
≡SOCuCl	-2.01	-2.54	-2.76	-2.95	-1.67	-1.74	-1.84	-1.28	-2.49
≡$SOHCuCl^+$	5.71	5.99	5.89	5.65	6.98	7.63	7.2	6.80	6.04
≡$SOHCuCl_2$	2.84	2.87	2.82	2.83	2.67	2.85	3.04	3.32	2.82
v_y	4.51	2.12	0.84	7.24	10.58	4.93	12.09	21.83	3.99

The combination of three copper chloride surface complexes best described the shape of the measured adsorption curves (Figure 2.9) over the entire range of NaCl concentrations. Fitted equilibrium constants describing Cu^{II} adsorption onto goethite for each NaCl concentration with the Davies Equation are listed in Table 2.4, while results with the Debye-Hückel "b-dot" equation are listed in Table 2.5. Figure 2.14 plots the change of equilibrium constants as a function of NaCl concentration. Ideally, equilibrium constants vary with changing pressure and temperature, but should be independent on NaCl concentration. There are too many parameters within the CCM to identify the cause of the changing equilibrium constants. However, a likely cause is associated with the calculation of activity coefficients for both aqueous and surface species.

An attempt was made to fit equilibrium constants for all the experimental data between 0.1 and 5.0 molal NaCl using the Davies Equation (Table 2.4) and Debye-Hückel "b-dot" equation, (Table 2.5) and calculate a single log K for each Cu^{II} adsorbed species.

Convergence for both models could only be obtained for concentrations between 0.1 and 3.0 molal, therefore the results for 0.1 – 3.0 molal NaCl are presented.

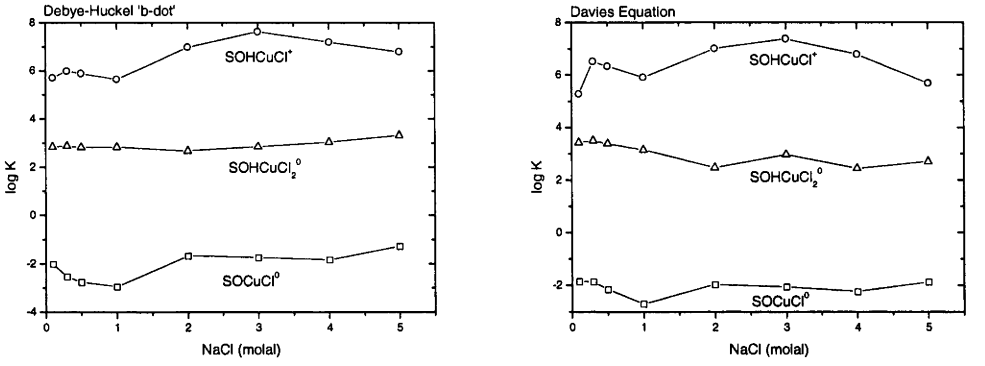

Figure 2.14: Changes to equilibrium constants as a function of NaCl for log K values calculated using the Debye-Hückel "b-dot" equation and Davies equation for determining activity coefficients. True equilibrium constants are independent of NaCl concentration and should plot as a straight line.

Results with the Debye-Hückel "b-dot" equation were closer to the experimental data for NaCl concentrations between 0.1 and 0.5 molal than the Davies equation. At NaCl concentrations >1.0 molal, the Debye-Hückel "b-dot" equation underestimated the total adsorption, while the Davies equation overestimated the total adsorption for the same concentration range. At 0.1 molal NaCl, the results suggest NaCl does not influence Cu^{II} adsorption as $\equiv SOHCu^{2+}$ and $\equiv SOCu^{+}$ are the dominant surface complexes. However, when the NaCl concentration was increased to 0.3 molal and pH values <4.5, the predominant surface complexes were $\equiv SOHCuCl_2$ and $\equiv SOHCuCl$. This is reflected by the change in the shape of the adsorption edge below pH 4.5 with increasing chloride concentration in experimental data (Figure 2.15 and 2.16). In solutions with 0.5 – 5.0 molal NaCl and at pH less than 4.5, the formation of copper chloride surface complexes such as $\equiv SOHCuCl^{+}$, $\equiv SOHCuCl_2^{0}$ and $\equiv SOCuCl^{0}$ account for the enhanced adsorption onto goethite. The $\equiv SOHCuCl_2$ is the predominant surface complex which describes the

initial Cu^{II} adsorption at pH less than 2.5, while between pH 3.5 and 5.5 at NaCl = 2 molal, ≡SOHCuCl becomes the predominant surface complex. In all of the NaCl concentrations examined, the effect of NaCl is prominent in solutions where the pH is less than or equal to 6 and at pH values >6, $\equiv SOCu^{+}$ accounts for the majority of adsorbed Cu^{II}.

The results of this study compare well with the studies of Barrow et al.(1982) and Padmanabham (1983a). Padmanabham (1983a) assumed that $\equiv SOHCuCl^{0}$ was the predominant surface species in his study, which is consistent with the results presented earlier at low pH and intermediate NaCl concentrations. Barrow et al. (1982) did not specify a surface complex, but calculated an equilibrium constant for the adsorption of $CuCl^{+}(aq)$ (log K = 6.6). If the reaction in their experiments was:

$$\equiv SOH + CuCl^{+} = \equiv SOHCuCl^{+} \qquad (2.22)$$

which is reasonable for the conditions of their study, the log K from this study is 6.19, only 0.4 log K units lower than their value. Compared with those two studies, two additional copper chloride surface complexes were required because a much wider range of NaCl concentration was examined.

Comparisons between calculated concentrations of Cu^{II} adsorbed with the Davies Equation and Debye-Hückel "b-dot" Equation at low concentrations show that both activity coefficients models return similar results at NaCl concentrations <2 molal. At NaCl concentrations >2.0 molal, the Davies Equation and Debye-Hückel "b-dot" Equation differ by up to 20% and it is still unclear which activity model is correct.

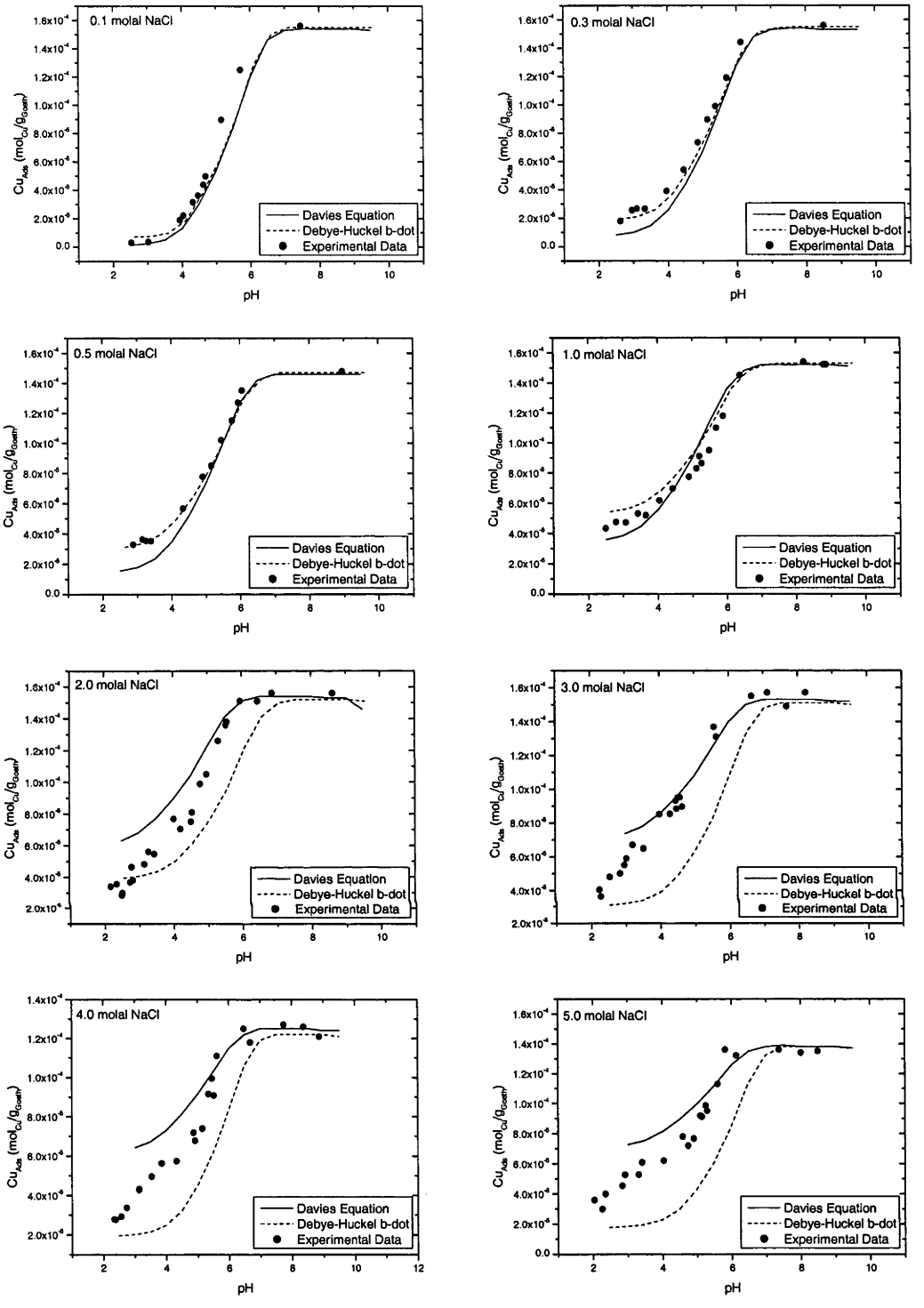

Figure 2.15: Adsorption of Cu^{II} onto goethite as a function of pH in 0.1 to 5.0 molal NaCl solutions showing results of surface complexation modelling using the Davies equation and Debye-Hückel "b-dot" equation for calculating activity coefficients. Equilibrium constants for copper chloride surface reactions were calculated from 0.1-3.0 molal NaCl experimental data using the Debye-Hückel "b-dot" equation and 0.1-3.0 molal NaCl experimental data using the Davies equation and extrapolated over the entire range of NaCl concentrations.

2.4 Conclusions

The results of this study show that Cu^{II} adsorption onto goethite is influenced by the concentration of nitrate and chloride in solution and the aqueous speciation of Cu^{II}. Copper adsorption was suppressed by up to 30% as $NaNO_3$ concentration increases from 0.1 to 1.0 molal at pH > 4.5. The copper surface complexes inferred in $NaNO_3$ experiments are $\equiv SOHCu^{2+}$ and $\equiv SOCu^{+}$. The cause of the suppression is not known, but may be caused by the formation of copper nitrate aqueous complexes ($Cu(NO_3)^{+}$ and $Cu(NO_3)_2(aq)$) and the absence of copper nitrate surface complexes. Another possible cause was the adsorption of CuII onto the reaction vessel, however limited time and resources prevented further investigation of this. Ionic strength effects are not clear and while these were examined, there is not enough information from this study to imply the influence or magnitude of these on Cu^{II} adsorption.

Cu^{II} adsorption increases with increasing NaCl concentration, but the magnitude of this effect depends on pH and NaCl concentration. The greatest increase of Cu^{II} adsorption was in acidic conditions, i.e., 20 to 30 times increase at pH 3 between 0.1 and 1 molal NaCl. At higher NaCl concentrations and this pH, the effect is smaller. Under less acidic conditions, e.g., pH > 5, there is no enhancement, even up to 5 molal NaCl. This is due to the competition between surface complexes and copper chloride aqueous complexes. At lower NaCl concentrations (< 2 molal), the large increase in Cu adsorption with increasing NaCl at acidic pH is due to the predominance of $\equiv SOHCuCl^{+}$ and $Cu^{2+}(aq)$, whereas at higher pH there is little to no increase in adsorption because $\equiv SOCu^{+}$ and Cu^{2+} predominate to higher NaCl concentrations. At higher NaCl concentrations (>3 molal), $\equiv SOHCuCl_2^{0}$ and $CuCl_2(aq)$ are predicted to

predominate at acidic pH (<4) , resulting in no change in copper adsorption, whereas at higher pH, $\equiv SOHCuCl^+$ and $CuCl_2(aq)$ predominate and there is likely to be a suppression of Cu adsorption. Due to time and resource constraints, the effect of different metal to sorbate ratios was not thoroughly examined during this study. This work is recommended to better understand the influence of copper chloride complexes on adsorption, especially if fewer adsorption sites are available.

The results of this study show that the mobility of Cu^{II}, and potentially other metals, may be limited by increasing chloride concentration under some conditions, assuming adsorption is the controlling process. This is in contrast to more conventional understanding that metal chloride aqueous complexes enhance the mobility of metals in aqueous and hydrothermal environments because the solubility of metal-bearing minerals increases with increasing chloride concentration. There is a clear need to understand if adsorption, mineral solubility and/or other processes are controlling the mobility of copper and other metals in complex natural environments, which requires knowledge of aqueous speciation, surface speciation and the presence and reactivity of different minerals and their surfaces.

Future studies designed to understand role of adsorption in the transport of metals in natural environments still need to be conducted. This study highlights the importance of the mineralogical component of an environment and has shown that the transport of oxidised copper in highly saline and acidic water (similar to the conditions in the Lake Tyrrell district described by Lyons et al., 1992) could be limited due to the enhanced adsorption of copper chloride complexes onto goethite. It is still not clear how

adsorption and groundwater chemistry (i.e. salinity) may affect the transport of copper through natural regolith environments.

Chapter 3: The Effect of NaCl on the Adsorption of Zn onto Synthetic Goethite

3.1 Introduction

Previously, the concentration of NaCl in a solution was shown to enhance the adsorption of Cu^{II} onto goethite in acidic solutions. In natural environments, this has the potential to decrease the mobility of dissolved copper in highly saline groundwater. The focus of this chapter continues the theme of the effect of NaCl concentrations on the adsorption of dissolved metals onto goethite between pH values 3 and 10. Zn is used to examine how adsorption varies with different metal species likely to be present in the regolith in highly saline solutions and look for similarities and contrasts in metal behaviour.

Understanding zinc mobility in the regolith and low-temperature near-surface waters is important for mineral exploration, minerals processing and its bio-availability in soils (Uygur and Rimmer, 2000). Zn mobility is affected by transport processes such as groundwater flow, dissolution/precipitation of zinc-bearing minerals (eg. Smithsonite) and adsorption onto organic and inorganic materials. Zn adsorption onto iron (oxy)hydroxide phases is likely to be an important process in the regolith (Balistrieri and Murray, 1982; Kooner, 1992; Rose Bianci-Mosquera, 1992; Kanungo, 1994; Swedlund and Webster, 2001; Trivedi et al., 2001; Dyer et al.,2004), but it is still not well understood, especially in saline conditions. The focus of this chapter is the effect of dissolved NaCl on the adsorption of Zn onto goethite in oxidised conditions, where iron

oxy-hydroxide minerals are likely influence the mobility and adsorption of zinc in the regolith.

The adsorption of metals onto mineral surfaces is dependent on the aqueous geochemistry of the metal and surface properties of the adsorbate (Drever, 1997). The aqueous speciation of zinc is affected by the concentration of zinc, temperature, pressure, and composition of the surrounding solution, which includes pH, redox and concentration of ligands such as Cl^-, SO_4^{2-}, CO_3^{2-} and organic compounds i.e. fulvic and humic acids (e.g. Duker et al. 1995) The specific surface area, density of active adsorption sites and net surface charge affect the adsorption of metals onto goethite and vary depending on the crystal habit and chemical composition of the goethite (Manceau et al., 2000).

pH is probably the most important and well studied geochemical variable that influences the adsorption of zinc (and other cations) onto iron oxy-hydroxide minerals such as goethite. Table 3.1 summarises previous studies examining the adsorption of zinc onto goethite, with the results of these studies all showing that the concentration of adsorbed zinc increases as the pH of the solution increases.

The effect of pressure and temperature on the adsorption of zinc onto goethite is likely to be small under the range of conditions typical of near surface environments. Rodda et al. (1993) examined the effect of temperature on zinc adsorption onto goethite between 10°C and 80°C and found that adsorption was only enhanced by a few percent with increasing temperature.

Table 3.1: Summary of experimental studies examining Zn adsorption onto goethite.

Author	*Electrolyte*	*Electrolyte Conc (M)*	*Goethite Conc (g/L)*	*Initial Zn Conc (μM)*	*pH Range*	*Reaction Time*
Rose & Bianchi Mosquera (1993)	NaCl	0-4	8	7.65	5-9	1 hr
Balistrieri & Murray (1982)	$NaNO_3$	0.1	0.55	0.56	4.9-7.5	~12 hrs
	Simulated Seawater			2.9		
				29.0		
Trivedi et al. (2001)	$NaNO_3$	0.001	1	5	4-8	2-4 hrs
		0.01		1		
Kooner (1993)	$NaNO_3$	0.01	0.6	76	3.9-6.8	16-20 hrs
		0.1	5.5			
Barrow et al. (1982)	NaCl	0.1	2	50-1200	3.8-10	48 hrs
Rodda et al. (1993)	KNO_3	0.01	0.2	100	3.0-11.0	20 mins

The solution composition of complexing ligands has an effect on the adsorption of zinc onto goethite. Electrolytes such as $NaNO_3$, KNO_3 and $NaClO_4$ are commonly selected to study the adsorption of metals onto goethite due to their non-reactive nature with mineral surfaces (Balistrieri and Murray, 1982) and their weak complexing of nitrate and perchlorate with metals in aqueous solutions (Criscenti and Sverjensky, 1999). The number of studies examining the effect of NaCl on zinc adsorption onto iron hydroxides and oxyhydroxides are limited to Kanungo (1994) and Balistrieri and Murray (1982), while the range of concentrations are restricted to 0.5 M and less (Table 3.1). Results of these studies indicate that the presence of NaCl has either a small or no effect on the adsorption of zinc onto goethite. Balistrieri and Murray (1982) concluded that NaCl had no effect on the adsorption of zinc in 0.53 M NaCl between pH 5.5 and 8 when compared to solutions with 0.1 M $NaNO_3$. However, in 0.5 M NaCl, Kanungo (1994) found that zinc adsorption increased in slightly more acidic conditions and concluded

that NaCl did not inhibit adsorption. Kanungo (1994) suggested that zinc adsorption in more acidic solutions was caused by the stronger bonding of zinc chloride complexes with the surface of hydrous ferric oxide than uncomplexed zinc ions.

The role of NaCl on the adsorption of zinc onto goethite is still not clear, although the number of studies that address this issue are limited. In this study, the role of pH, $NaNO_3$ and NaCl concentrations on the adsorption of zinc onto synthetic goethite in aqueous systems is investigated. Adsorption data was collected for a range of $NaNO_3$ (0.1 – 1.0 molal) and NaCl concentrations (0.1 – 5 molal) to examine the changes in zinc adsorption behaviour as a function of NO_3^-, Cl^-, ionic strength and pH. The aim of this chapter is to achieve a clearer understanding of how zinc adsorbs in near surface environments, determine whether NaCl affects the adsorption of zinc onto goethite in aqueous environments, and calculate reliable thermodynamic properties that may be useful for predictive geochemical and reactive transport models. Finally the results obtained from studying Zn adsorption in NaCl are compared to the results of Cu^{II} adsorption in similar systems presented in Chapter 2.

3.2 Materials and Methods

3.2.1 Goethite Synthesis and Characterization

Goethite was synthesized according to the method outlined by Schwertmann and Cornell (1991). A detailed description is provided in the preceding chapter.

3.2.2 Adsorption Experiments

Adsorption was measured in series of 11-12 individual experiments. Each experiment contained 0.075 g goethite in a glass reaction vessel with 80 g of $NaNO_3$ or NaCl with between 1.53×10^{-4} and 1.07×10^{-4} molal Zn prepared from $Zn(NO_3)_2.6H_2O$. The pH of each experiment was adjusted using 0.1 M HNO_3 or 0.1 M NaOH and was measured using a Thermo Orion 290A+ pH Meter and Ross Sure Flow electrode calibrated using Sigma-Aldrich 4, 7 and 10 buffers with an uncertainty of ± 0.02 pH units. Samples were sealed with a Dreschel head and placed in a water bath at 25.0°C ± 0.1 to maintain a constant temperature. Nitrogen gas was passed through a reaction vessel containing ultrapure water to minimize the effect of evaporation, before being passed through each reaction vessel to provide an inert atmosphere to minimize the effect of CO_2 and mix the solution.

Samples were allowed to equilibrate for 16 hours before being removed and the final pH measured. In the previous chapter, kinetic data showed copper adsorption reached steady state after three hours. The reaction time for zinc adsorption is not expected to be

significantly different. This is consistent with the results of Trivedi et al. (2001) who observed that zinc adsorption did not change experiments between 2 and 4 hours. To ensure that equilibrium was achieved in each reaction vessel, all experiments were run overnight for 16 hours.

The goethite was filtered from each experiment using a 0.45 μm filter. The supernatant solution was preserved by adding several drops of 10% HNO_3. Each experiment was duplicated to test the reproducibility of the results. Solutions were analysed for Zn using a Varian Vista Pro Axial ICP-AES to measure Zn concentrations with the 213.857 nm wavelength line. The concentration of adsorbed Zn was assumed to be the difference between the initial and final concentrations of zinc. Samples were also analysed for Fe with the 238.204 nm wavelength; however any Fe present in solution was below the ICP-AES detection limit (Ca. 0.1 mg/kg in the undiluted solution).

3.3 Results

3.3.1 Zn Adsorption onto Goethite in $NaNO_3$ Solutions

Results for the adsorption of Zn onto goethite in 0.1 and 1.0 molal $NaNO_3$ are shown in Figure 3.1 and listed in the Appendix B. The concentration of Zn adsorbed onto goethite increased with increasing pH, as is typical for most divalent metals (ie. Dzombak and Morel, 1990). No difference between the adsorption of Zn in 0.1 molal $NaNO_3$ and 1.0 molal $NaNO_3$ was observed, and therefore assume that ionic strength has no discernable effect on the adsorption of Zn onto goethite (Figure 3.1).

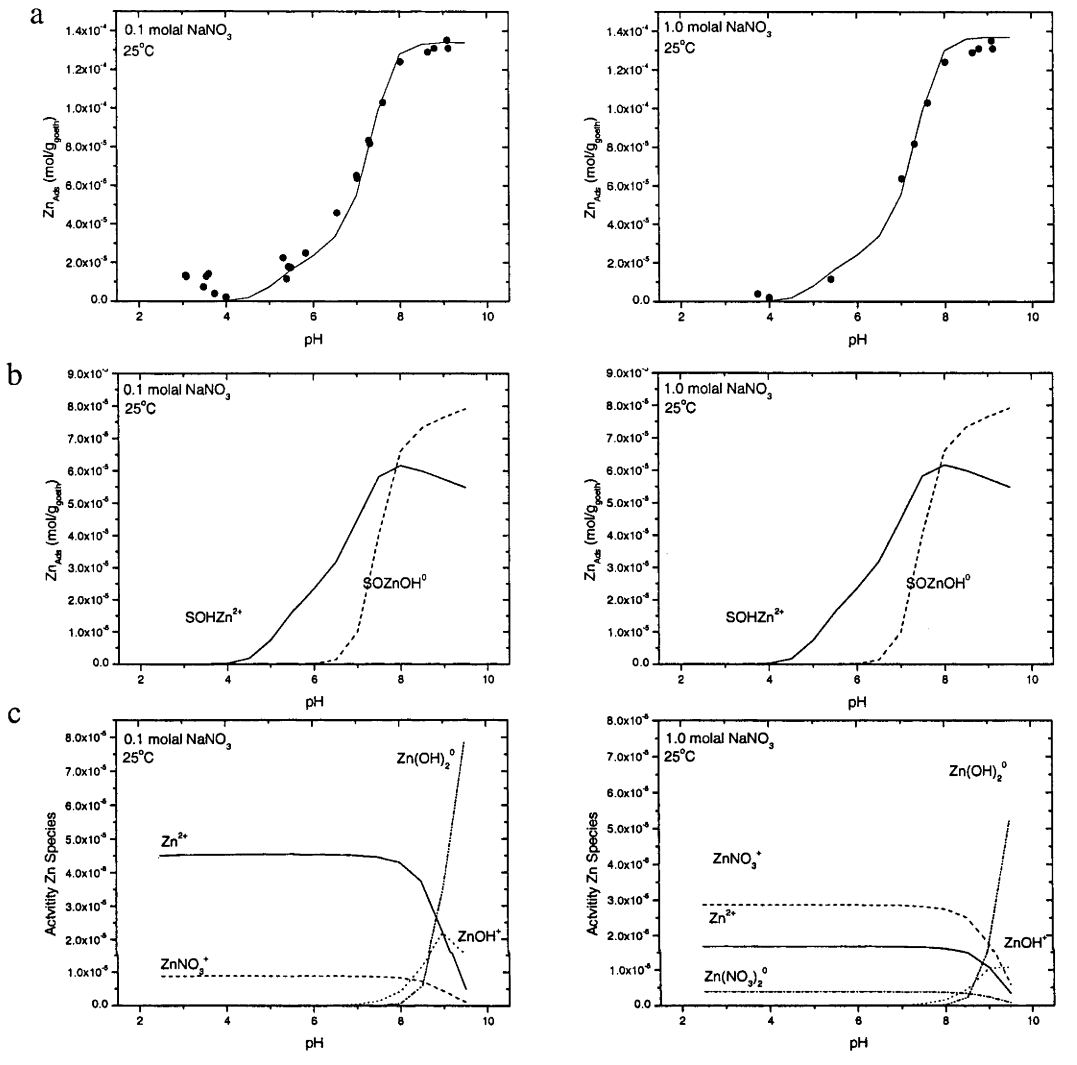

Figure 3.1: **(a)** Experimental results of Zn adsorption onto goethite in 0.1 and 1.0 molal $NaNO_3$. Temperature 25°C, pressure = 1 atmosphere; Total Zn concentration = 1.54×10^{-4} molal; Goethite concentration = 0.93 g/L; surface area = 36.05 m^2/g and site density 16 sites/nm^2. Solid line shows the results of the CCM modelled for each individual experimental series. **(b)** Predicted surface speciation of Zn onto goethite using the CCM. **(c)** Predicted aqueous speciation of Zn in 0.1 and 1.0 molal $NaNO_3$ calculated using PHREEQC.

Experimental and analytical error in the 0.1 molal $NaNO_3$ experimental data at pH <6 is approximately 10%, while the error observed at pH >6 is slightly less at 5%. The 10% error in more acidic solutions has a higher analytical error associated with it. This is because the more acidic solutions contained high concentrations of dissolved zinc (i.e. >

1.0×10^{-4} molal), from which small changes in concentration from adsorption are being measured (i.e. changes of 1.0×10^{-6} molal Zn). This explains the higher level of scatter observed in solutions with pH <6.

The results from the 0.1 molal $NaNO_3$ experimental data are compared with those of Balistrieri and Murray (1982), Kooner (1993), Rose and Bianchi-Mosquera (1993) and Trivedi et al. (2001) using a modified distribution coefficient (K_d). The data are normalised against the initial concentration of Zn, goethite concentration and surface area to account for differences between the various studies, by calculating a distribution coefficient, K_d:

$$K_{d(Zn)} = \frac{(Zn_{ads} \times M_{sol})/(M_{goethite} \times A_s)}{Zn_{diss}} \qquad (3.1)$$

Zn_{ads} is the concentration of Zn adsorbed (M), M_{sol} is the mass of solution (kg), $M_{goethite}$ is the mass of goethite (kg) in an experiment and A_s is the calculated surface area of goethite (m^2/g) using BET analysis; Zn_{diss} is the concentration of dissolved Zn (M).

Results of the normalised data are shown in Figure 3.2. Two separate trends are observed in the data with the data consistent with the results of Trivedi et al. (2001) and most of the data points falling on the same line with a consistent slope. However, the data of Kooner (1993) Balistrieri and Murray (1982) and Rose and Bianchi-Mosquera (1993) show separate trends with a variable slope and a higher degree of scatter amongst the data. These differences may be attributed to variations in goethite characteristics between studies. For example, site density may change with different

crystallographic faces (i.e. Lützenkirchen et al., 2002; 3.03 FeO sites/nm^2 on (101) and 7.19 sites on (100), Peacock and Sherman, 2004), therefore if the morphologies of synthetic goethite were different between studies, then the available adsorption sites would also differ. Unfortunately morphologies were not recorded in the all of the studies listed in Table 3.1, making it difficult to establish the effect of morphology. Dissolved $CO_2(g)$ may also inhibit the adsorption of metals onto goethite (Zeltner and Anderson, 1988) competing for adsorption sites on the mineral surface. The influence of $CO_2(g)$ is well known and the experimental method used in these other studies were controlled to minimise this effect.

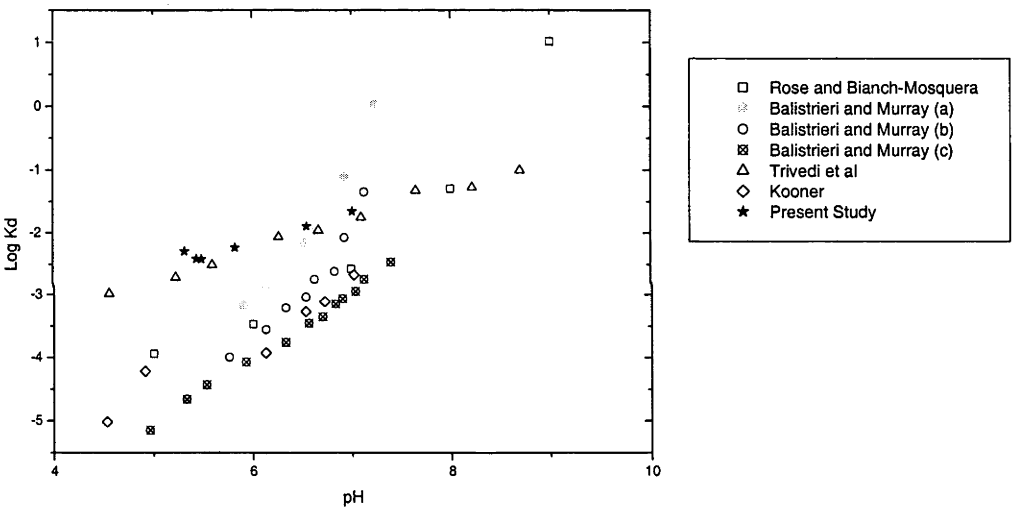

Figure 3.2: K_d plot showing the comparison of Zn onto goethite in 0.1 M $NaNO_3$ between the results of this study and those of Rose and Bianch-Mosquera (1993), Balistrieri and Murray (1982), Trivedi et al. (2001) and Kooner (1993).

The number of studies that use goethite as the mineral phase in experiments is limited as described previously. However, unlike copper, a wide range of minerals have been used in adsorption studies including ferrihydrite (Dyer et al., 2004), montmorillonite, kaolinite (Ikhsan et al., 2005) and sepiolite (Vico, 2003). This provides an opportunity to examine the effect of the mineral species on Zn adsorption and compare Zn

adsorption onto other minerals and goethite by plotting the K_d (Equation 3.1) value for each mineral in $NaNO_3$, KNO_3 or $NaClO_4$ solutions. The results of the calculated K_d values for Zn adsorption onto ferrihydrite, montmorillonite, kaolinite and sepiolite are shown in Figure 3.3. From the data presented in Figure 3.3, the line of best fit for ferrihydrite was calculated to be 1.24 compared to 1.05 and 1.02 for sepiolite and kaolinite and 0.87 for montmorillonite. The slope of the best fit lines for these minerals were all greater than the calculated slope of best fit line for synthetic goethite in this study which was 0.47. Different surface properties, i.e. surface area, mineral morphology, presence of a permanent or non-permanent surface charge and crystal structure are likely to influence Zn adsorption. Surface area may change in the same mineral species. To test the sensitivity of the K_d with changing surface area of the mineral, firstly the concentration of each mineral for each data set in Figure 3.3 was increased by 20%, followed by the surface area of each mineral (also increased by 20%) and the K_d values recalculated for each change. Increasing the mineral concentration decreased the log K_d value by approximately 0.08 log units at a constant pH, while increasing the surface area of each had a similar effect with log K_d decreasing by 0.09 log units. When altering either the mineral concentration or the surface area of the mineral, the slope of the line of best fit did not change. Therefore the slope of the best fit lines for the K_d value appears to be controlled by the mineral species and not the concentration and surface area. Therefore, it may be possible that the different slopes for synthetic goethite used by Balistrieri and Murray and Kooner (which had steeper lines of best fit for the plotted K_d) may have contained traces of ferrihydrite.

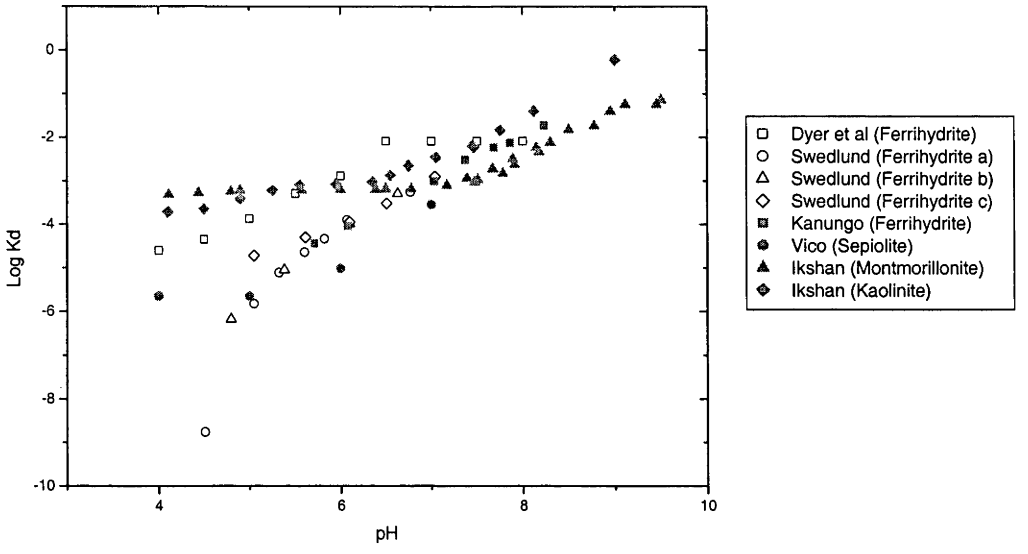

Figure 3.3: K_d plot of Zn adsorption onto ferrihydrite (Dyer et al. 2004), kaolinite, montmorillonite (Ikhsan et al. 2005) and sepiolite (Vico, 2003) in 0.1 M $NaNO_3$.

3.3.1.1 Quantitative Interpretation

Surface complexation modelling was used to interpret experimental data and predict likely surface species. In this section, the surface complexation modelling process is described and the surface reactions applied to the model are discussed.

Firstly, the simplest reactions that may control Zn adsorption onto goethite in $NaNO_3$ were considered:

$$\equiv SOH + Zn^{2+} \leftrightarrow \equiv SOHZn^{2+} \qquad (3.2)$$

$$\equiv SOH + Zn^{2+} \leftrightarrow \equiv SOZn^{+} + H^{+} \qquad (3.3)$$

$$\equiv SOH + Zn^{2+} + H_2O \leftrightarrow \equiv SOZnOH + 2H^{+} \qquad (3.4)$$

with the equilibrium constants:

$$K = \frac{a_{SOHZn^{2+}}}{a_{SOH}\, a_{Zn^{2+}}} \qquad (3.5)$$

$$K = \frac{a_{SOZn^{2+}}\, a_{H^+}}{a_{SOH}\, a_{Zn^{2+}}} \qquad (3.6)$$

$$K = \frac{a_{SOZnOH^+}\, a_{H^+}^{\,2}}{a_{SOH}\, a_{Zn^{2+}}\, a_{H_2O}} \qquad (3.7)$$

"≡S" in the above reactions represents the underlying mineral phase. By plotting log $[Zn_{ads}]$ – log $[Zn_{diss}]$ versus pH, the effect of pH on Zn adsorption and the predominant reactions in the experiments is assessed. Two linear trends in the data are inferred (Figure 3.4), indicating a change of the predominant reactions. In 0.1 molal $NaNO_3$, the best fit line had a slope of 0.53 at pH values <7.5, which suggests that the reactions for $\equiv SOHZn^{2+}$ and $\equiv SOZn^{+}$ (Equations 3.2 and 3.3) may be present in experiments. At pH values greater than 7.5, the best fit line had a slope of 1.47, which may be caused by a change in the predominant reactions to equations (3.3) and (3.4). In 1.0 molal $NaNO_3$, the best fit line slope was 0.27 at pH values >7, which increased to 1.75 at pH values <7. The formation of other surface complexes is possible (e.g. $(SO)_2Zn^0$; cf. Dyer et al., 2004), but it can not be determined if they were present from the calculated slopes in Figure 3.4. These species are considered later when fitting equilibrium constants to the experimental data.

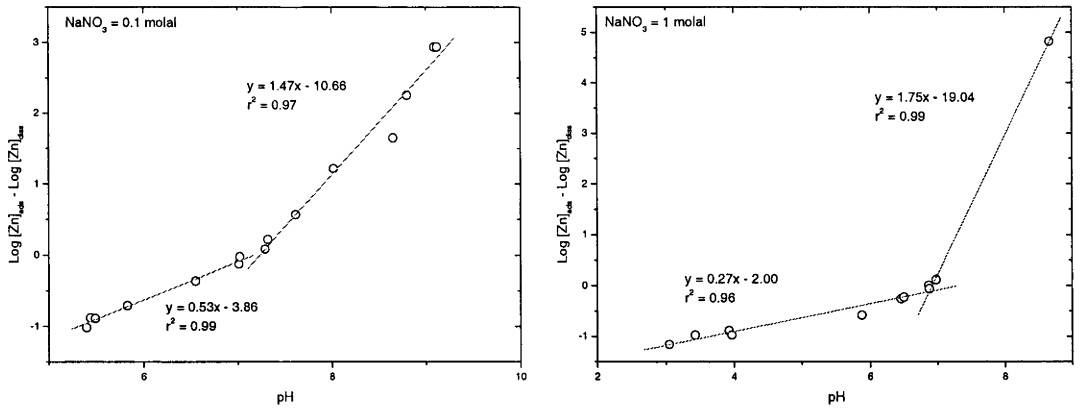

Figure 3.4: $Log[Zn]_{Ads} - log[Zn]_{Diss}$ versus pH showing Zn adsorption onto goethite in different concentrations of $NaNO_3$. Experimental data is listed in the Appendix B. The slopes of the linear regression lines indicate the stoichiometry of dominant adsorption reactions and corresponding zinc surface complexes.

3.3.1.2 Surface Complexation Modelling

A brief overview of surface complexation modelling methods and the common reactions required to describe adsorption is in Chapter 2 (e.g. Equation 2.1 and 2.2). Furthermore, the choice of surface complex model used to interpret experimental data and the parameters used (i.e. capacitance values) are discussed. The reader is referred to Section 2.4.3 in Chapter 2 for a description of the surface complexation model used.

3.3.1.3 Surface Site Density

The importance of surface site densities in adsorption calculations is discussed in detail in Section 2.3.1.3. Results of experiments aimed to estimate Zn adsorption densities for calculating adsorption are described below.

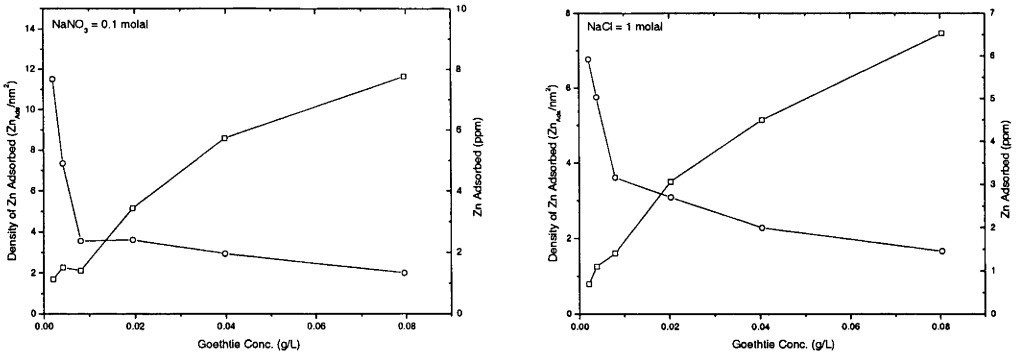

Figure 3.5: Calculated density of adsorbed Zn per nm^2 on the goethite surface and concentration of Zn adsorbed as a function of goethite concentration in 0.1 molal $NaNO_3$ and 1.0 molal NaCl.

Due to the uncertainty associated with calculated site densities, the density of Zn adsorption was measured in 6 experiments with varying zinc to goethite ratios. Changes in site density between $NaNO_3$ and NaCl solutions were also considered using two series of experiments. The first used 0.1 molal $NaNO_3$ and the second 1.0 molal NaCl at pH 7.5. The results of both experiments are presented in Figure 3.5. Results in the $NaNO_3$ experiments indicated that the adsorption density of Zn onto goethite in 0.1 molal $NaNO_3$ was 11.5 sites/nm^2. This is considered to be a minimum estimate as the maximum concentration of adsorbed Zn in our experiments was probably not reached. Despite this, the estimate is similar to the 16.4 sites/nm^2 measured with tritium exchange by Yates (1975). Rustad et al. (1996) estimated a site density of between 15 and 16 sites/nm^2 for goethite with molecular statics, which is also similar to estimated density determined in this study and the measured density of Yates (1975). As with the Cu^{II} experiments presented in Chapter 2, a site density of 16.4 sites/nm^2 was applied based on the estimate of Yates (1975; which was also used by Sahai and Sverjensky (1997)). In contrast, Peacock and Sherman (2004) estimated a site density of 6.0 sites/nm^2 based on crystallographic considerations made by Hiemstra and Van Riemsdijk (1996) for the goethite surface. Venema et al. (1998) and Boily et al. (2001)

considered the effect of crystal face geometry and used potentiometric titrations to measure site densities of 3.1 sites/nm^2 and 2.1 sites/nm^2 respectively. Other potentiometric titration estimates by Ali and Dzombak (1996) and Lumsdon and Evans (1994) assumed a homogeneous surface and calculated site densities of 1.4 sites/m^2 and 2.7 sites/nm^2 respectively. Choosing other values for the site density did not affect the conclusions regarding the nature of surface complexes. However the fitted equilibrium constants of experiments did change as discussed below.

In the 1.0 molal NaCl experiments, the density of Zn adsorption was estimated to be 6.5 sites/nm^2. The lower site density is assumed to be caused by the adsorption of different aqueous Zn complexes such as $ZnCl_2^0$ to form surface complexes such as $SOZnCl_2^-$. Unfortunately it is not possible to determine the actual cause of the decreased surface site densities with the data from this study. However it is suggested that aqueous Zn speciation may influence site density, and in this case, the larger Zn chloride complexes may decrease the density of adsorbed Zn, although further experiments are required to determine this.

3.3.1.4 Fitting equilibrium constants

In this section the results of fitting equilibrium constants to the zinc adsorption are shown. FITEQL 4.0 was used for fitting equilibrium constants using the previously discussed measurements and assumptions for surface site density. FITEQL 4.0 is a computer program that uses a non-linear least-squares method to optimise equilibrium constants for adsorption reactions (e.g. Dzombak and Morel, 1990; Herbelin and Westall, 1999). In FITEQL 4.0 the quality of the fit is primarily measured by the

variance, v_y, which is the weighted sum of squares of residuals divided by the degrees of freedom (Herbelin and Westall, 1999) and is represented by the equation:

$$V_y = \frac{SOS}{DF} = \Sigma \frac{(y_r / s_r)^2}{n_p n_r - n_u} \qquad (3.8)$$

Where y_r is the difference between the predicted and measured concentration for each experiment and s_r is the estimated experimental error for each experiment. n_p is the number of data points, nr is the number of components with known total concentration and n_u is the number of adjustable parameters. Value of v_y between 0.1 and 20 are considered to represent a "reasonably good" fit (Herbelin and Westall, 1999). Other measurements of fit success included directly comparing the results of the predicted adsorption using FITEQL 4.0 with the results measured in experimental data.

Fitted equilibrium constants are listed in Table 3.3. Equilibrium constants were fitted individually for experimental data from 0.1 and 1.0 molal $NaNO_3$ series. Fitting for a single reaction from Equations 3.2-3.4 was attempted. However, finding a single Zn surface complex to fit the experimental data was unsuccessful, and combinations of two Zn surface complexes were considered. The aqueous speciation of zinc was calculated with FITEQL 4.0 with mass balance constraints on Na^+, NO_3^-, Zn^{2+} and pH. The mass action equations for aqueous and mineral phases are listed in Table 3.3, all of which assumed the activity of $H_2O(l)$ = 1. The standard state for aqueous species was the hypothetical 1 molal solution to infinite dilution. Activity coefficients were calculated with the Davies equation:

$$\log\gamma = Az^2\left(\frac{I^{1/2}}{1+I^{1/2}} - 0.3I\right) \qquad (3.9)$$

Where I is the stoichiometric ionic strength (Davies, 1962) and A = 0.509 (Herbelin and Westall, 1999). The aqueous nitrate complexes, $ZnNO_3^+$ and $NaNO_3(aq)$ were used in the calculations. The effect of these complexes, plus the uncertainty associated with activity coefficient estimates (particularly in the NaCl series of experiments) is discussed below. A capacitance value of 0.83 F/m^2 was used in the CCM based on best fit results of Cu^{II} adsorption onto goethite.

Equilibrium constants calculated by fitting the Constant Capacitance Model to experimental data are listed in Table 4.3. As described in the previous chapter for Cu^{II} adsorption, log K values for the protonation and deprotonation reactions used were from Richter et al. (2005; $\log K_1^{int} = 6.36 \pm 0.38$ (2σ); $\log K_2^{int} = -10.44 \pm 0.38$ (2σ))

Table 3.3: Fitted Equilibrium constants for Zn surface species onto goethite in 0.1 and 1.0 molal $NaNO_3$. Equilibrium constants describe formation reactions of species. Activity coefficients were calculated with the Davies Equation.

Species	**Log K ($NaNO_3$ Concentration (molal))**	
	0.1	***1***
$\equiv SOHZn^{2+}$	7.36	7.60
$\equiv SOZnOH^{\circ}$	-11.76	-11.63
v_y	11.5	32.3

While the experimental data was fitted using the reactions in Equations 3.2-3.4, the more complex surface reactions proposed by Palmqvist et al. (1997) who investigated zinc adsorption onto goethite with voltametric in-situ measurements was tried:

$$2{\equiv}SOH + Zn = ({\equiv}SOH)_2Zn^{2+} \qquad (3.10)$$

$${\equiv}SOH + Zn^{2+} + 2H_2O = {\equiv}SOZn(OH)_2 + 3H^+ \qquad (3.11)$$

The combination of the $\equiv SOHZn^{2+}$ and $\equiv SOZn(OH)_2$ (similar to the reactions used by Palmqvist et al. 1997) fit the experimental data closely, (log K = 8.70 ±0.04 and -21.49 ±0.26 respectively in 1.0 molal $NaNO_3$ (ν_y = 13.55) and log K = 7.89 ±0.03 and -19.47 ±0.07 (ν_y = 37.01) in 0.1 molal $NaNO_3$), but the $\equiv SOHZn^{2+}$ and $\equiv SOZnOH$ surface species were used in the model. This combination of reactions provided a slightly better fit in both 0.1 and 1 molal $NaNO_3$, but this combination of reactions provided better results over the entire range of NaCl concentrations, which will be discussed below.

Differences between the invoked surface species used by Palmqvist et al. (1997) and those used to fit the experimental data of this study could be due to the different methods of measuring the total adsorption of Zn onto goethite. Palmqvist et al. (1997) used voltametric techniques to measure in-situ ion concentrations, compared with the more traditional method of measuring the supernatant solution with ICP-AES used in this study. Other causes may be associated with the model parameters such as the protonation and deprotonation equilibrium constants (Palmqvist et al. used $\equiv SOH_2^+$ = 7.47 and $\equiv SO^-$ = -9.51), surface site density (i.e. 1.7 sites/nm^2), capacitance values (i.e. C = 1.28 F/m^2) and experimental conditions including the concentration of goethite (0.9 g/L) and the initial dissolved zinc concentration (2.7×10^{-6} m).

3.3.2 Zn Adsorption onto Goethite in NaCl solutions

The results of Zn adsorption onto goethite in NaCl solutions are shown in Figure 3.6 and Appendix B. Also plotted in Figure 3.6 are the results of the optimised equilibrium constants calculated with the CCM. As observed in $NaNO_3$ experiments, Zn adsorption onto goethite increased with increasing pH. In addition, adsorption increased with increasing NaCl concentrations between 0.1 molal NaCl and 1 molal NaCl at pH less than 8 (Figure 3.7), although the slope of the adsorption edge curve decreased for NaCl concentrations greater than 0.3 molal. At NaCl concentrations greater than 1 molal, zinc adsorption decreased with increasing NaCl over the entire pH range studied.

The increase in Zn adsorption with increasing NaCl for solutions with < 1.0 molal NaCl is consistent with the findings of Kanungo (1994), however the magnitude of enhancement in our experiments is higher than reported by that author. In contrast, enhancement of zinc adsorption in 0.1 – 0.3 molal NaCl contradicts the findings of Balistrieri and Murray (1982) who concluded that Cl^- had no effect on zinc adsorption.

To interpret the effect of NaCl on the adsorption of Zn onto goethite, $\log[Zn_{Ads}] - \log[Zn_{Diss}]$ – pH versus log[NaCl] was plotted and try to infer the reactions and surface complexes occurring in the experiments (Figure 3.8). A strong NaCl dependence is observed at concentrations of less than 0.5 molal NaCl at pH 5.0, suggested by a slope of 1.15 for the line of best fit although this changed when the NaCl concentration increased to greater than 0.5 molal, the slope decreased to -2.06, suggesting that Cl^- was released from the goethite surface. Plots for pH equal to 6.5 and 8.0, indicate that the slope of the best fit line is near zero (slope of 0.13 and -0.05 respectively) when the

NaCl concentration is less than 0.5 molal. This suggests that there is no net change in Cl^- between the solution and the mineral surface. In NaCl concentrations greater than 0.5 molal, the slopes increase to -0.63 and -0.58. The changes of slope observed in Figure 3.8 indicate the dependence of Cl^- where a positive slope indicates Cl^- uptake on the goethite surface, while a negative slope suggests Cl^- being removed.

The effect of pH is examined in Figure 3.9 by plotting $\log[Zn_{Diss}] - \log[Zn_{Ads}]$ versus pH. A greater pH dependence is observed in 0.1 molal NaCl and pH greater than 7.5, where the slope of line of best fit is 1.43. The pH dependence decreased in the 1 molal and 5 molal NaCl solutions where the slopes of the line of best fit were 0.69 and 0.97 respectively.

Using the information from Figure 3.8 and 3.9 the reactions in Equations 3.12 – 3.14 are inferred. The low number of data points in Figure 3.8 (especially for pH = 5) makes it difficult to apply a best fit line. However, this data is used as an indicator for NaCl dependence in experiments. A best fit line with a slope of 1 (i.e. pH = 5 in Figure 3.8) suggests that the reaction is dependent on Cl^-. Because the best fit line for pH 5 in Figure 3.8 is > 1, it is inferred that both zinc chloride and zinc di-chloride surface complexes could be present. Therefore the reactions in Equations 3.12 - 3.14 are considered when fitting the experimental data.

$$\equiv SOH + Zn^{2+} + Cl^- = \equiv SOZnCl + H^+ \qquad (3.12)$$

$$\equiv SOH + Zn^{2+} + 2Cl^- = \equiv SOHZnCl_2 \qquad (3.13)$$

$$\equiv SOH + Zn^{2+} + 2Cl^- = \equiv SOZnCl_2 + H^+ \qquad (3.14)$$

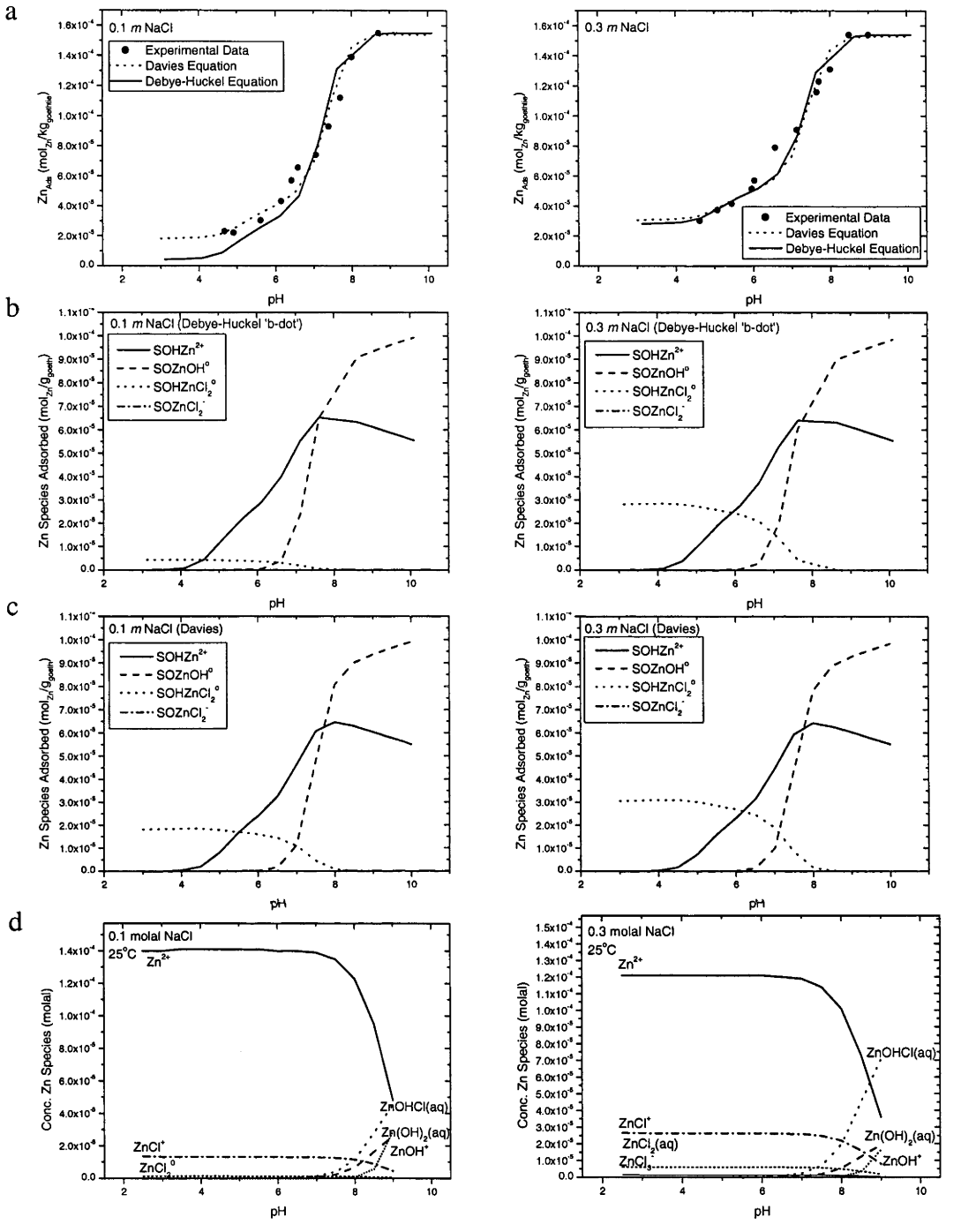

Figure 3.6: **(a)** Adsorption of Zn onto goethite as a function of pH in 0.1 to 0.3 molal NaCl solutions. Symbols represent experimental data and solid lines show the optimised results of the CCM for individual experiments using the Davies Equation and Debye Hückel Equation. Goethite concentration = 0.937 g/L, surface area = 36.05 m^2/g. **(b)** Predicted surface species calculated using the Debye Hückel Equation. **(c)** Predicted surface species calculated using the Davies Equation. **(d)** Calculated aqueous speciation of Zn in NaCl solutions using the Debye Hückel Equation.

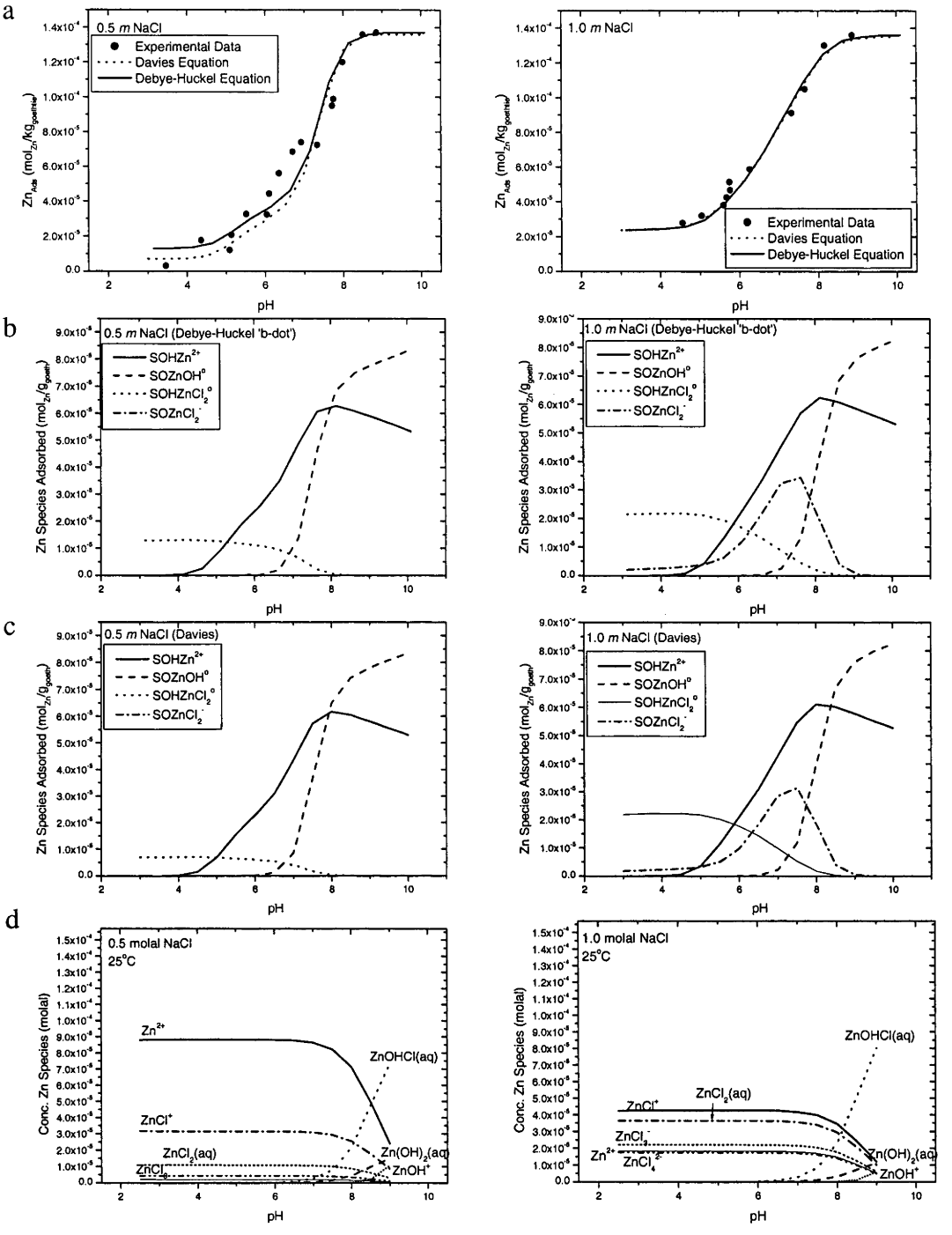

Figure 3.6: **(a)** Adsorption of Zn onto goethite as a function of pH in 0.5 to 1.0 molal NaCl solutions. Symbols represent experimental data and solid lines show the optimised results of the CCM for individual experiments using the Davies Equation and Debye Hückel Equation. Goethite concentration = 0.937 g/L, surface area = 36.05 m^2/g. **(b)** Predicted surface species calculated using the Debye Hückel Equation. **(c)** Predicted surface species calculated using the Davies Equation. **(d)** Calculated aqueous speciation of Zn in NaCl solutions using the Debye Hückel Equation.

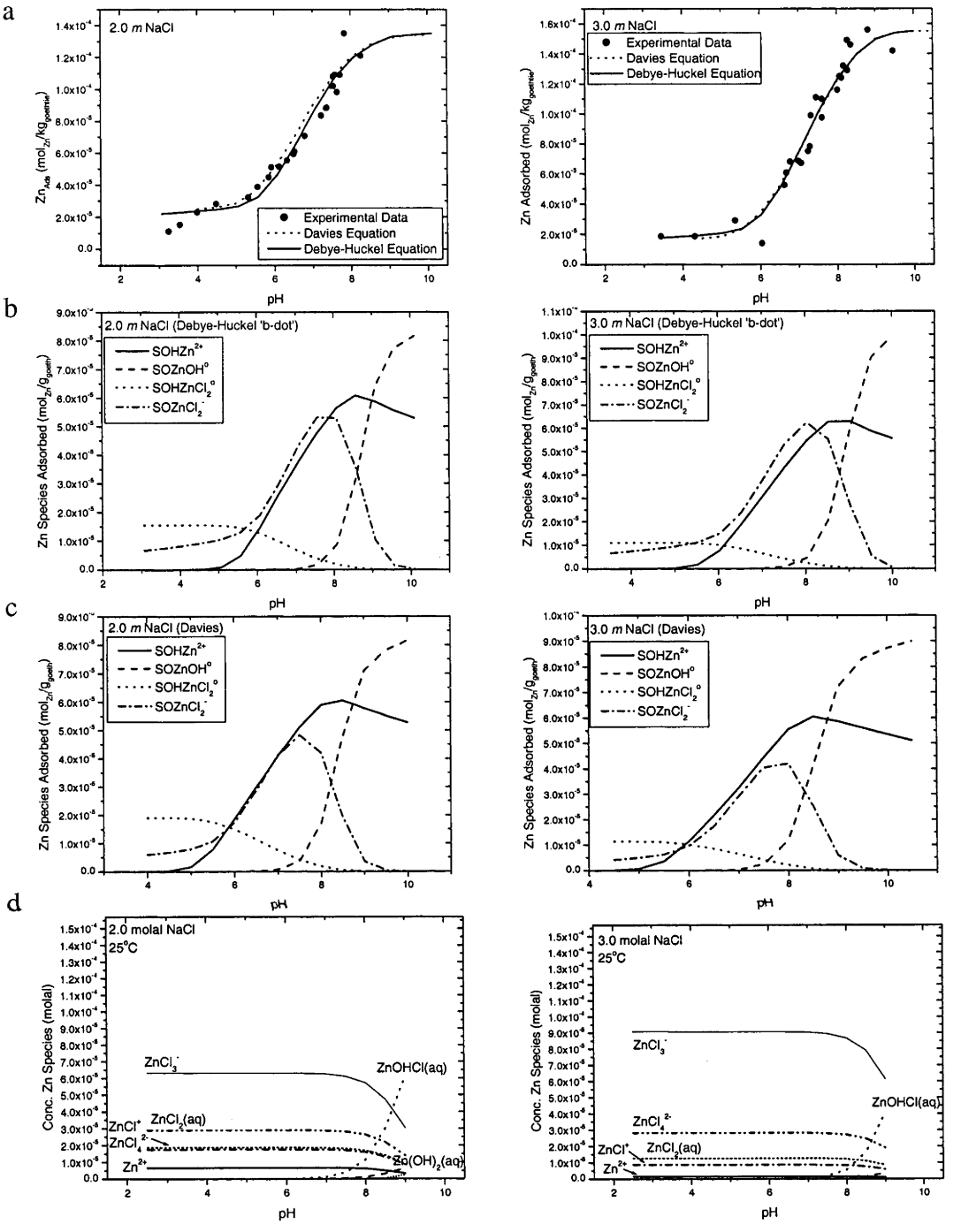

Figure 3.6: **(a)** Adsorption of Zn onto goethite as a function of pH in 2.0 to 3.0 molal NaCl solutions. Symbols represent experimental data and solid lines show the optimised results of the CCM for individual experiments using the Davies Equation and Debye Hückel Equation. Goethite concentration = 0.937 g/L, surface area = 36.05 m^2/g. **(b)** Predicted surface species calculated using the Debye Hückel Equation. **(c)** Predicted surface species calculated using the Davies Equation. **(d)** Calculated aqueous speciation of Zn in NaCl solutions using the Debye Hückel Equation.

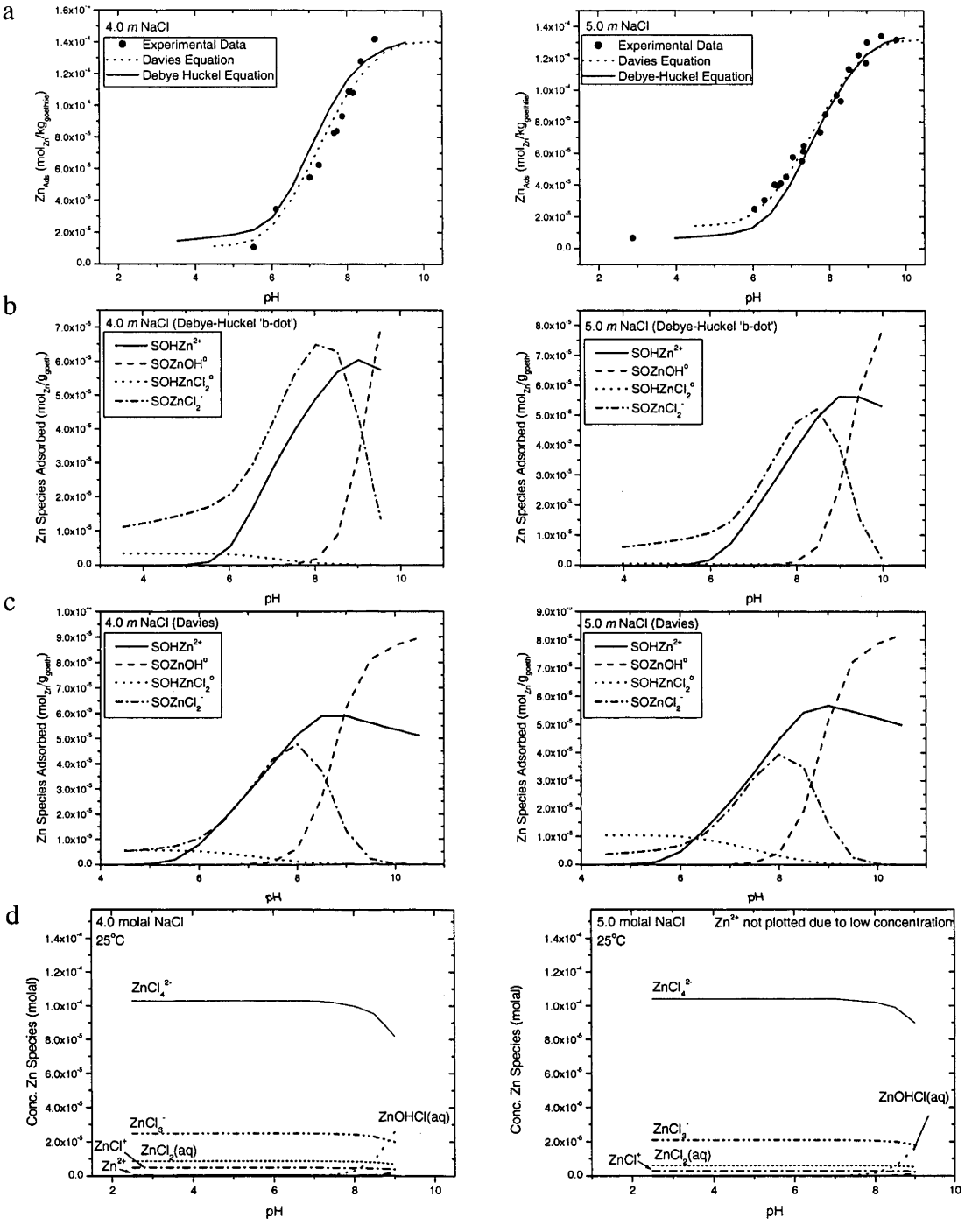

Figure 3.6: **(a)** Adsorption of Zn onto goethite as a function of pH in 0.1 to 0.3 molal NaCl solutions. Symbols represent experimental data and solid lines show the optimised results of the CCM for individual experiments using the Davies Equation and Debye Hückel Equation. Goethite concentration = 0.937 g/L, surface area = 36.05 m^2/g. **(b)** Predicted surface species calculated using the Debye Hückel Equation. **(c)** Predicted surface species calculated using the Davies Equation. **(d)** Calculated aqueous speciation of Zn in NaCl solutions using the Debye Hückel Equation.

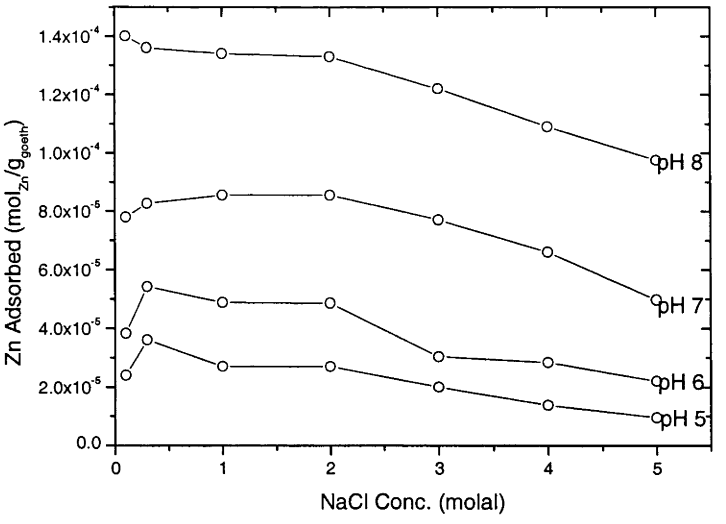

Figure 3.7: Adsorption of Zn onto goethite as a function of NaCl concentration at constant pH of 5, 6, 7 and 8. Adsorption experiments contained 1.40×10^{-4} molal Zn at 25°C and 1 atmosphere.

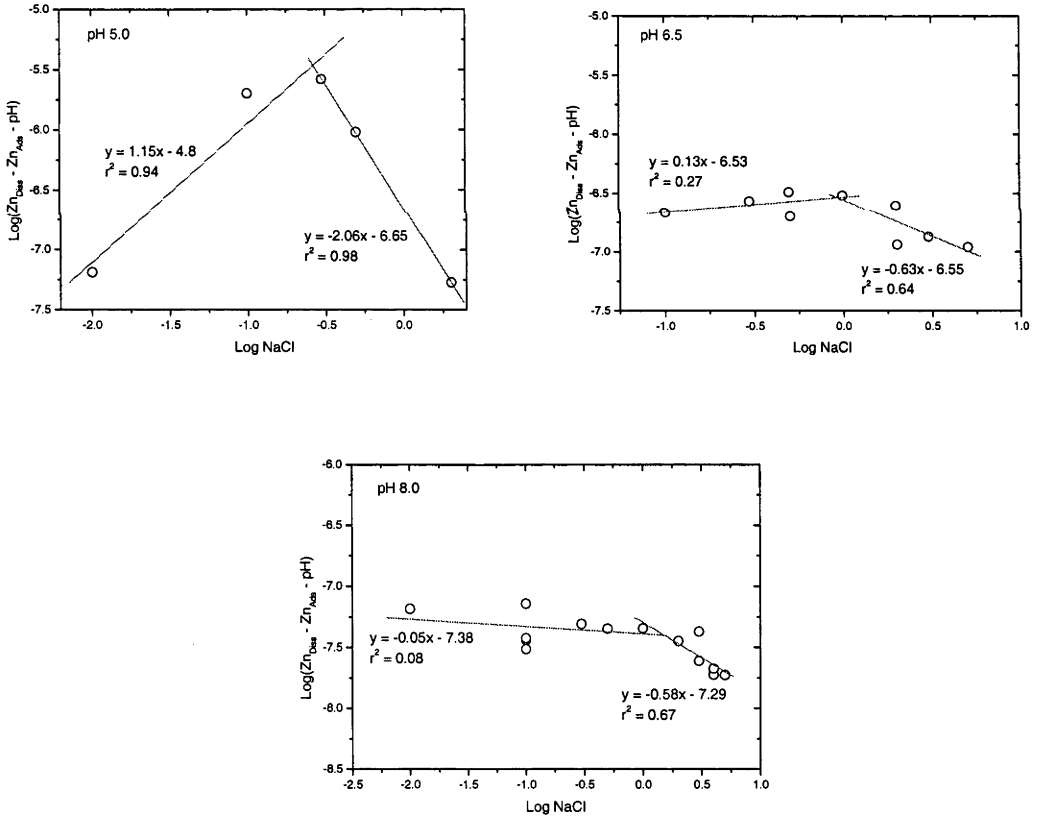

Figure 3.8: Log [Zn_{Ads}] – log[Zn_{Diss}] – pH versus log[NaCl] showing the adsorption of Zn onto goethite as a function of NaCl at pH 5, 6.5 and 8. The slope of the regression line indicates the NaCl dependence of the controlling reactions for the formation of Zn surface complexes.

At pH greater than 5.0, and less than 1 molal NaCl, the best fit line is near 0, indicating that zinc adsorption is independent of NaCl (Figure 3.8). Several possible reactions can describe this trend including the adsorption of zinc-chloride aqueous complexes (i.e. Equation 3.15) or the formation of no ZnCl surface complexes (i.e. Equations 3.3 and 3.4).

$$\equiv SOH + ZnCl^{+} = \equiv SOZnCl + H^{+} \qquad (3.15)$$

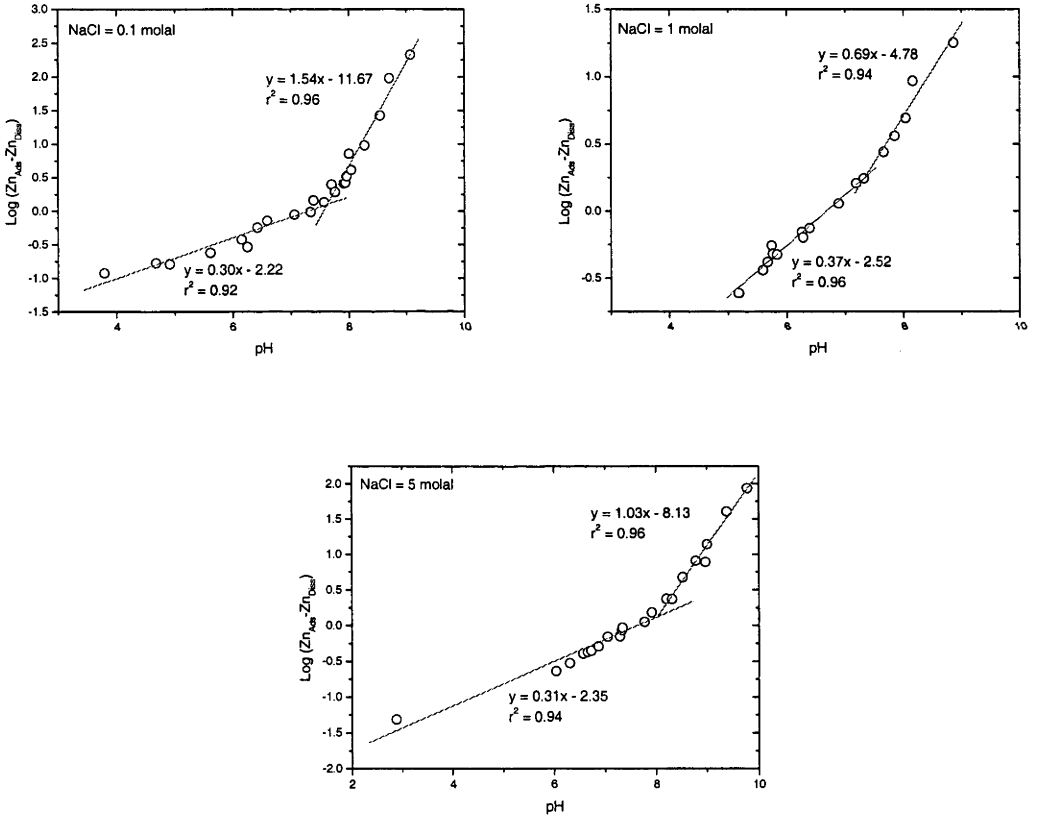

Figure 3.9: Log[Zn_{Ads}] – log[Zn_{Diss}] versus pH showing the adsorption of Zn onto goethite in 0.1, 1 and 5 molal NaCl. Slopes of the regression lines indicate the pH dependence of controlling reactions for the formation of zinc surface complexes.

Simarly, a negative slope of the best fit lines for NaCl concentrations greater than 1 molal is likely to be caused by Cl^- detaching from the mineral surface may be induced by one of the following reactions:

$$\equiv SOZnCl^0 = \equiv SOZn^+ + Cl^- \qquad (3.16)$$

$$\equiv SOHZnCl_2^0 = \equiv SOZn^+ + 2Cl^- + H^+ \qquad (3.17)$$

The reactions described in Equations 3.16 would have an expected best fit line slope of -1, while the reaction in Equation 3.17 would result in a slope of -2, which is observed in experimental data at pH 5.0 and greater than 0.5 molal NaCl (Figure 3.9).

3.3.2.1 Fitting Equilibrium Constants

In this section, the results are shown of fitting equilibrium constants for the formation reaction of zinc surface complexes in increasing concentrations of NaCl. Firstly, the aqueous speciation of Zn in chloride solutions is described. The log K values for the formation reactions of zinc-chloride complexes were taken from the MINTEQ database (Allison et al., 1991) and are listed in Table 3.3. The formation reaction for NaCl(aq) of log K = -0.3 (Table 3.3; Smith and Martell, 1997) was included in the calculation.

In Chapter 2, the uncertainty regarding the appropriate activity model for calculating Cu^{II} speciation in the range of NaCl concentrations was discussed and the same uncertainties apply when calculating Zn speciation in the same range of NaCl

concentrations. Therefore, both the Davies Equation and the Debye-Hückel b-dot Equation are used for calculating activity coefficients for aqueous species.

The predicted aqueous speciation for zinc in 0.1-5.0 molal NaCl was calculated with the Davies Equation (Equation 3.9) using FITEQL 4.0, while the Debye-Hückel b-dot Equation (Equation 3.18) was calculated using Geochemists Workbench 6.0 (Bethke, 2005). Results are shown for pH 6 in Figure 3.10.

$$Log(\gamma) = \frac{-A_\gamma z_i^2 \sqrt{I}}{1 + B_\gamma a_i \sqrt{I}} + b^\bullet I \qquad (3.18)$$

Up to a 20% difference between like zinc species over the 0.1-5 molal NaCl concentrations occurs between the Davies Equation and the Debye-Hückel "b-dot" Equation. Less Zn^{2+} is predicted at NaCl concentrations less than 1 molal by the Davies Equation, but higher concentrations of $ZnCl^+$ are predicted when NaCl is less than 4 molal.

Equilibrium constants for adsorption reactions were fit using the Davies Equation and Debye-Hückel "b-dot" Equation. The default activity coefficient model in FITEQL 4.0 is the Davies Equation, but to use the Debye-Hückel "b-dot" Equation activity coefficients were calculated externally with PHREEQCi v2.12.5 and manually input into the adsorption models in FITEQL 4.0.

Table 3.3: Reactions and equilibrium constants used to model aqueous and surface species for Zn adsorption onto goethite. Equilibrium constants describe formation reactions.

Species	Mass Action Reaction	Log K	Source
Aqueous Species			
OH^-	$OH + H = H_2O$	*-13.98*	*a*
$ZnNO_3^+$	$Zn^{2+} + NO_3^- = ZnNO_3^+$	*0.40*	*b*
$ZnOH^-$	$Zn^{2+} + H_2O = ZnOH^+ + H^+$	*-8.96*	*b*
$Zn(OH)_2$	$Zn^{2+} + 2H_2O = Zn(OH)_2 + 2H^+$	*-16.90*	*b*
$NaNO_3(aq)$	$Na^+ + NO_3^- = NaNO_3(aq)$	*-0.55*	*a*
NaCl(aq)	$Na^+ + Cl- = NaCl(aq)$	*0.30*	*a*
$ZnCl^+$	$Zn^{2+} + Cl^- = ZnCl^+$	*-0.40*	*b*
$ZnCl_2(aq)$	$Zn^{2+} + 2Cl^- = ZnCl_2(aq)$	*0.45*	*b*
$ZnCl_3^-$	$Zn^{2+} + 3Cl^- = ZnCl_3^-$	*0.50*	*b*
$ZnCl_4^{2-}$	$Zn^{2+} + 4Cl^- = ZnCl_4^{2-}$	*0.20*	*b*
ZnOHCl	$Zn^{2+} + H_2O + Cl^- = ZnOHCl + H^+$	*-7.480*	*b*

[a] *Smith and Martel (1997)*

[b] *Allison et al. (1991)*

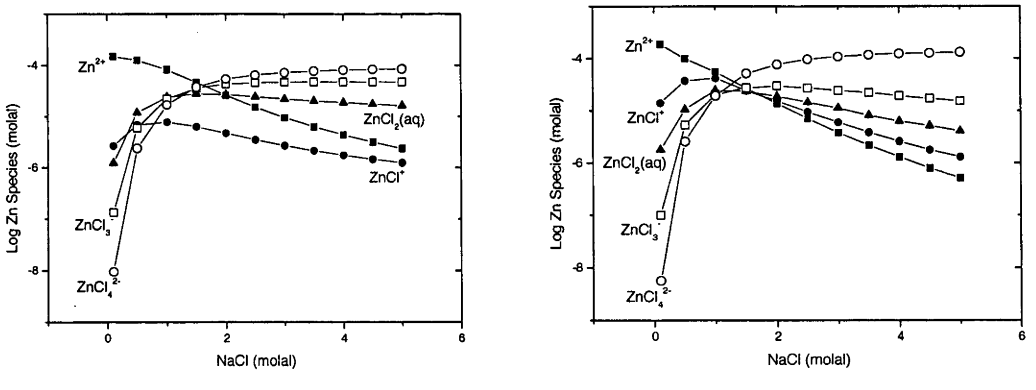

Figure 3.10: Predicted aqueous speciation of Zn as a function of NaCl at pH 6 (a) using activity coefficients calculated with the Davies equation in FITEQL v4.0 (Herbelin and Westall, 1999) and (b) using activity coefficients calculated with the "b-dot" equation in Geochemists Workbench (Bethke, 2005).

Equilibrium constants were fitted separately for each data series of NaCl concentrations (0.1-5 molal), based on several scenarios. Starting with the surface complexes calculated for Zn adsorption in $NaNO_3$ solutions (Equations 3.2 and 3.4), the experimental data was fitted for (a) different single zinc chloride surface complexes; (b) different combinations of two zinc chloride surface complexes; (c) three zinc chloride surface complexes (shown in Equations 19-21). A fit with three zinc surface complexes was tried, but there was no discernible improvement of the fit. It was deduced that a third species was absent, or if it was present that its concentration correlated too strongly with another species to fit separately. Therefore only two species are used in the fit.

It is possible that the adsorption larger zinc chloride surface complexes could decrease the number of adsorption sites on goethite. To test whether a lower site density would influence the fit of the CCM with the experiments, the site density for goethite was changed from 16.4 sites/nm^2 to 6 sites/nm^2. Results showed that the concentration of adsorbed zinc over the entire range of NaCl concentrations of experiments does not change, indicating that saturation of the goethite surface by zinc was not approached in experiments.

Fitting the experimental data with a single zinc chloride surface complex was unsuccessful. The closest fit was with $\equiv SOZnCl_2^0$ in NaCl concentrations greater than 4. At lower NaCl concentrations, the variance values were high ($V_y > 40$) and the curves of the predicted adsorption did not match the experimental data.

Table 3.4: Equilibrium constants for species used to model Zn adsorption onto goethite for each concentration of NaCl. Equilibrium constants describe formation reactions of species. Log K values for $\equiv SOH_2^+$, $\equiv SO^-$, $\equiv SOHZn^{2+}$ and $\equiv SOZnOH^0$ were calculated from $NaNO_3$ experiments. Activity coefficients were calculated with the Davies Equation.

Species	**Log K (NaCl Concentration)**								
	0.1	***0.3***	***0.5***	***1***	***2***	***3***	***4***	***5***	***0.1-2.0***
$\equiv SOHZnCl_2$	4.22	3.57	2.92	2.89	2.99	3.02	2.94	3.43	3.19
$\equiv SOZnCl_2$	-5.57	-5.57	-5.57	-5.57	-5.00	-4.92	-4.60	-4.53	-4.17
V_y	22.5	9.2	27.2	4.0	11.6	22.4	20.0	6.4	418.5

Table 3.5: Equilibrium constants for species used to model Zn adsorption onto goethite for each concentration of NaCl. Equilibrium constants describe formation reactions of species. Log K values for $\equiv SOH_2^+$, $\equiv SO^-$, $\equiv SOHZn^{2+}$ and $\equiv SOZnOH^0$ were calculated from $NaNO_3$ experiments. Activity coefficients were calculated with the Debye-Hückel "b-dot" Equation.

Species	**Log K (NaCl Concentration)**								
	0.1	***0.3***	***0.5***	***1***	***2***	***3***	***4***	***5***	***0.1-2.0***
$\equiv SOHZnCl_2$	4.29	2.97	2.41	2.81	3.24	3.45	3.13	4.38	2.72
$\equiv SOZnCl_2$	-5.56	-5.56	-5.56	-5.56	-4.46	-4.15	-3.73	-3.6	-5.5
V_y	14.8	19.9	24.9	4.3	11.2	12.7	11.3	2.8	88.8

The combination of two zinc-chloride surface complexes best described the shape of the adsorption curve over the entire range of NaCl concentrations. Results of predicted Zn adsorption onto goethite in NaCl solutions are shown in Figure 3.6 and fitted equilibrium constants using the Davies Equation are listed in Table 3.4 and the Debye-Hückel "b-dot" Equation in Table 3.5.

Fitting with all the experimental data (i.e. all data between 0.1 – 5.0 molal NaCl) proved unsuccessful as FITEQL 4.0 was unable to converge the model. The largest range of data that was able to be successfully modelled was for NaCl concentrations between 0.1 and 2.0 molal for both the Davies Equation and the Debye-Hückel "b-dot" Equation.

The fit of the experimental data was considered very poor as the result did not reflect the experimental data variance values were very large (Table 3.3 and 3.4). Because equilibrium constants are values that represent the product of chemical reaction, they should remain constant over all NaCl concentrations. However, the fitted equilibrium constants in Table 3.4 and 3.5 decrease with increasing NaCl concentrations (Figure 3.11), highlighting a possible problem with the calculated activity coefficients for aqueous species over the range of NaCl concentrations. A more appropriate method of calculating aqueous activity coefficients may be required, but as briefly described earlier, the Pitzer Equation is limited to solutions with major ion species only. Another potential source for error is associated with the coulombic correction used in the CCM. This is effectively an activity coefficient for the surface species (Dzombak and Morel, 1990) and if incorrect may change the equilibrium constant with increasing NaCl concentration. The effect of the coulombic correction on equilibrium constant was not undertaken in this study as the scope of work to investigate this problem is large, but it should be considered in the future.

Figure 3.12 shows a comparison between the Davies Equation and Debye-Hückel "b-dot" equation. The Debye-Hückel "b-dot" equation fits the experimental data better in < 1molal NaCl, but in > 2 molal NaCl the predicted adsorption was seriously underestimated. Results of the Davies Equation were erratic, over predicting adsorption in 0.3, 0.5, 2 and 3 molal NaCl, while it under predicted adsorption in 1, 4 and 5 molal NaCl. In NaCl concentrations > 1 molal, neither model was able to fit the data, emphasising the inability for the current activity coefficient models to predict surface species over the range of NaCl concentrations studied.

At pH 4, a 20 times increase of zinc adsorption in NaCl concentrations between 0.1 and 1 molal was observed. Zinc adsorption was enhanced by the presence of $\equiv SOHZnCl_2$ and $\equiv SOZnCl_2$ surface complexes (Figure 3.12). $\equiv SOHZnCl_2$ is predicted to predominate in acidic solutions (pH < 4.5 between 0.3 and 1 molal NaCl and pH 6.5 between 1 and 3 molal NaCl) and is responsible for the increased adsorption of zinc at NaCl concentrations less than 3.0 molal. At 0.5 molal NaCl, adsorption was approximately 1 order of magnitude higher than in 0.1 molal NaCl, but decreased with increasing NaCl concentrations in solutions with > 1.0 molal (Figure 3.12).

The predominant zinc surface complexes as a function of pH and NaCl are shown in Figure 3.6 using the equilibrium constant calculated using a combined 0.1 – 3 molal NaCl experimental data in Table 3.4. The decrease in adsorbed zinc coincides with the predominance of $ZnCl_3^-$ and $ZnCl_4^{2-}$ aqueous complexes (Figure 3.10). The decreased concentration of adsorbed zinc may be caused by the formation of these stable aqueous zinc complexes, which prevents the formation of zinc surface complexes. The predicted surface speciation of Zn adsorption is shown in Figure 3.6. Both activity models calculate similar predominant surface species, although there is some variation between the concentrations of each species. For example, in 0.1 molal NaCl, the Davies Equations predicts that at pH <4, Zn adsorption is three times higher than predicted by Debye-Hückel "b-dot" Equation due to the formation of $\equiv SOHZnCl_2^0$.

Initial increase in Zn adsorption in 0.3 molal NaCl coincides with the formation of $\equiv SOHZnCl_2^0$, which is predominate surface species up to pH 5.5. In NaCl concentrations greater than 0.3 molal, $\equiv SOHZnCl_2^0$ only predominates in solutions with pH less than 5 molal, where a change in surface speciation from zinc chloride to zinc

hydroxide surface species occurs. This change in surface species is consistent with the negative slope trend observed in the $\log[Zn_{Ads}] - \log[Zn_{Diss}] - pH$ versus logNaCl plots in Figure 3.8.

Suppression of adsorbed Zn in NaCl concentrations > 1 molal is shown to be caused by a preference of Zn to remain in solution, presumably complexed with Cl^- to form $ZnCl_3^-$ and $ZnCl_4^-$ which are the predominant aqueous Zn species in solutions with more than 1 molal NaCl (refer to Figure 3.10).

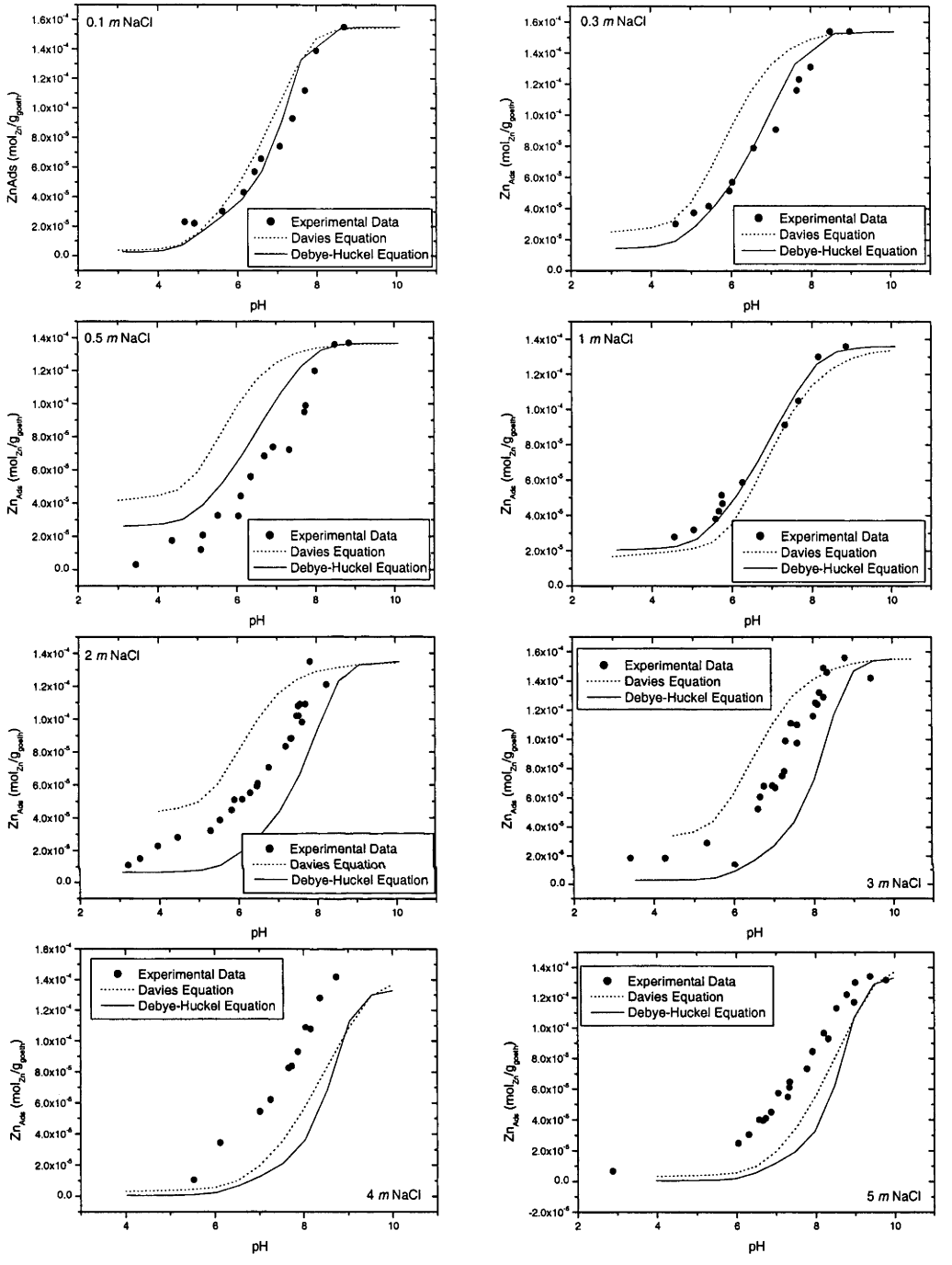

Figure 3.11: Zn adsorption onto goethite as a function of pH in 0.1-5.0 molal NaCl solutions showing the results of surface complexation modelling with the Davies Equation and Debye-Hückel "b-dot" Equation for determining activity coefficients. A single equilibrium constant calculated with 0.1-2.0 molal data for both models was applied over the entire range of NaCl concentrations.

3.4 Conclusions

The results of this Chapter show that dissolved $NaNO_3$ does not influence the adsorption of zinc onto goethite. No discernable change in zinc adsorption onto goethite between 0.1 and 1.0 molal $NaNO_3$ could be detected. $\equiv SOHZn^{2+}$ and $\equiv SOZnOH^0$ are predicted to be the predominant surface reactions occurring in the experiments.

In NaCl solutions, zinc adsorption onto goethite is influenced by the presence of dissolved NaCl and the presence of aqueous zinc and surface complexes. In solutions with between 0.1 and 1 molal NaCl, a 20 times increase in zinc adsorption onto goethite was noted in acidic conditions (pH 4). However, in higher NaCl concentrations (NaCl >1), zinc adsorption decreases with increasing NaCl. The change in the adsorption behaviour with increasing NaCl concentration are caused by the formation of $\equiv SOHZnCl_2^0$ surface complexes at lower concentrations of NaCl (<1 molal NaCl) at acidic pH. At higher concentrations of NaCl and acidic pH, the decrease in zinc adsorption is caused by the predominance of $ZnCl_3^-$ and $ZnCl_4^{2-}$ aqueous complexes, while the predominant zinc surface complex was $\equiv SOHZn^{2+}$. At high pH, (i.e. pH >7.5), $\equiv SOHZn^{2+}$ and $\equiv SOZnOH^0$ are the predominant surface complexes.

The results show that Zn adsorption is enhanced in NaCl solutions at less than 1 molal, and suppressed in NaCl concentrations greater than 1 molal. The results of this study are in contrast to the findings of Balistrieri and Murray (1982) and Kanungo (1994c). From the results of their studies, they concluded that the presence of Cl^- in solution had no effect on Zn adsorption. Kanungo noted a small increase in adsorption, but this was not large enough to conclude that Cl^- enhanced zinc adsorption.

The results of our study show that zinc mobility may be limited in saline conditions (i.e. near seawater concentrations of NaCl) in acidic conditions, assuming that adsorption is a controlling process. However, in either highly saline or near fresh water environments, zinc mobility is enhanced due to the formation of zinc hydroxy and/or chloro complexes. This highlights the importance of understanding processes such as adsorption and/or mineral solubility and how they may influence metal mobility. Therefore knowledge of processes such as aqueous speciation, adsorption and mineral reactivity is required if more reliable geochemical speciation and reactive transport models are to be used as predictive tools.

Chapter 4: Effect of Sulfate on Zn^{II} and Cu^{II} Adsorption onto Synthetic Goethite

4.1 Introduction

Previously, the effect NaCl concentrations on the adsorption of Cu^{II} and Zn were investigated, which showed that both Cu^{II} and Zn adsorption was enhanced with increasing NaCl concentration. An adsorption maximum was reached at 2.0 molal NaCl for Cu^{II} and 1 molal NaCl for Zn, and was attributed to the formation of metal-chloride surface complexes on goethite. When the concentration of NaCl was >2.0 molal, adsorption was suppressed due to the predominance of higher order metal chloride aqueous species (i.e. $CuCl_2(aq)$ and $ZnCl_4^{2-}$). This chapter examines the effect of dissolved Na_2SO_4 on Cu^{II} and Zn adsorption onto synthetic goethite and compares the results with those from NaCl experiments.

Anion adsorption (e.g. PO_4^{2-}, SO_4^{2-}) onto mineral surfaces in low temperature waters, soils and the regolith is likely to be an important process when considering environments such as acid mine drainage, acid sulfate soils, groundwater contamination (including heavy metal remediation from soils and groundwater) and mineral exploration (c.f Persson and Lövgren, 1996; Elzinga et al., 2001; Swedlund and Webster, 2001), and adsorption onto inorganic and organic surfaces may be a major contributor to sulfate bioavailability (Geelhoed et al., 1997). Sulfate adsorption onto iron oxy-hydroxides has been extensively studied (e.g., Balistrieri and Murray, 1982; Dzombak and Morel, 1990; Ali and Dzombak, 1996;

Geelhoed et al., 1997; Collins et al., 1999; Rietra et al., 1999; Elzinga et al.2001; Swedlund and Webster, 2001); however, the concentration of sulfate and metal ions used in these experimental systems was low (Table 4.1).

Table 4.1: Previous studies examining sulfate and metal adsorption onto goethite in SO_4^{2-} solutions.

Author	*Metal*	*Metal Conc*	*Sulfate Conc (M)*	*Mineral Conc (g/L)*	*pH Range*	*Reaction Time*
Ali & Dzombak	Cu	2.3 μM	0.01	1.6	3.4 – 6.5	24 hrs
Collins et al.	Cd	354 μM	2×10^{-5}	36	~5.5	24 hrs
Balistrieri & Murray	Cu, Pb, Zn, Cd	0.32 – 31 μM	0.028	0.55	3.1 – 9	~12 hrs
Rietra et al.	-	-	0.033	12-15	5.5 – 8	20 hrs
Geelhoed et al.	-	-	0.1	4-16	2 – 10	24 hrs
Persson & Lövgren	-	-	2×10^{-4}	11	3 – 8	24 hrs
Elzinga et al.	Pb	5 – 1000 μM	0.1	2.5 mg	4.5 – 6	3 hrs

Dissolved metal and sulfate concentrations in natural environments may exceed those listed in Table 4.1. For example, Smith and Melville (2004) measured up to 0.02 M SO_4^{2-} in acid sulfate soils at Tweed Heads in Australia, and Edraki et al. (2005) measured between 0.09 – 0.59 M SO_4^{2-} in acid mine drainage waters at the Mount Morgan mine in Queensland, Australia. Dissolved copper and zinc concentrations at Mount Morgan also exceed those in adsorption experiments, with between 2 – 81 mg/L Cu^{II} and 0.1 – 8 mg/L Zn measured (Edraki et al., 2005). In this study, high metal (up to 10 mg/kg) and sulfate (up to 1 molal) concentrations were used, similar to those measured in natural environments.

The adsorption of metals and anions such as sulfate onto iron oxy-hydroxides is dependent on the aqueous geochemistry of the solution and the properties of the mineral surface.

Aqueous speciation of copper, zinc and sulfate is dependent upon their concentration, temperature and pressure and the chemistry of the surrounding solution, including pH, redox, ionic strength, concentration of ligands (i.e., Cl^-, PO_4^{2-} CO_3^{2-}) and the presence of organic compounds such as fulvic and humic acids (e.g., Duker et al. 1995). Surface properties such as surface area, density of adsorption sites and net surface charge also influence the adsorption of metals and anions. These properties are dependent upon the crystal morphology and chemical composition of goethite (Manceau et al., 2002).

pH has a strong effect on metal and anion adsorption onto goethite (e.g., Persson and Lövgren, 1996; Geelhoed et al., 1997; Rietra et al., 1999). The highest concentrations of adsorbed sulfate occur at low pH (i.e. <4), while metal adsorption, such as Cu^{II} and Zn^{II}, occurs in more alkaline solutions (e.g., Peacock and Sherman, 2004; Ali and Dzombak, 1996). Geelhoed et al. (1997) also noted that sulfate adsorption may be ionic strength dependent, where sulfate adsorption decreases with increasing ionic strength.

The effect of temperature and pressure is expected to be small in the range of conditions found in near surface environments. Rodda et al. (1996) examined the effect of temperature on copper and zinc adsorption between 10 and 80°C and found that adsorption was enhanced by only a few percent at 80°C.

Studies have shown that the presence of anions can increase metal adsorption by the formation of ternary surface complexes. For example, in Chapter 2 it was demonstrated that Cu^{II} adsorption was enhanced by the formation of copper-chloride surface complexes in

acidic pH between 0.3 and 5 molal NaCl. Furthermore, anions may change the electrostatic properties of the mineral surface by changing the net surface charge and thereby promoting metal adsorption (e.g. Collins et al., 1999). However, anions may also inhibit the adsorption of metals onto surfaces by forming aqueous metal species which may reduce the concentration of dissolved metal available for adsorption.

The importance of sulfate on metal adsorption is reflected by the number of studies examining these effects (e.g., Elzinga et al., 2001; Ali and Dzombak, 1996; Swedlund and Webster, 2001; Geelhoed et al., 1997; Persson and Lövgren, 1996; Rietra et al., 1999; Balistrieri and Murray, 1982). Persson and Lövgren (1996) and Rietra et al. (1999), who both studied the adsorption of sulfate onto goethite, concluded that the highest concentrations of sulfate adsorption occurred at acidic pH (pH <3.5). Other studies examined the effect of sulfate on metal adsorption. Ali and Dzombak (1996) observed an up to a 10 times increase in the concentration of adsorbed copper between pH 3.5 and 5.5 in experiments with up to 1 mM SO_4^{2-} and 9.8×10^{-5} M copper. They explained their results with the formation of $\equiv FeOHCuSO_4$ ternary surface complexes over the entire pH range, with this species predominating at pH < 4.7 and $\equiv FeOCu^+$ predominant at pH > 4.7. Swedlund and Webster (2001) came to the same conclusion based on experiments with up to 2.47 molal copper and 0.02 molal SO_4^{2-} in the presence of 11 g/L ferrihydrite and schwertmannite. They modeled their experimental data using the ternary surface complexes $\equiv FeOHCuSO_4$ and $\equiv FeOHZnSO_4$. Swedlund and Webster (2001) noted up to a 25% increase in copper adsorption in experiments with a higher mineral concentration (Fe/metal

ratios of 0.00167:1, where Fe represents the concentration of Fe in ferrihydrite), but adsorption increased by <5% in solutions with lower Fe/metal ratios (0.0264:1).

The effect of low sulfate concentrations in solution (i.e. <0.02 molal SO_4^{2-}) on copper and zinc adsorption had been studied, but the effect of high sulfate concentrations (i.e., >0.02 molal), is not well understood. In this chapter, the role of pH and Na_2SO_4 concentrations on the adsorption of copper and zinc onto synthetic goethite are examined. Adsorption data for each metal was collected for a range of Na_2SO_4 concentrations between 0.001 and 1 molal over the pH range 4-8 for copper and 5-9 for zinc. The aim of this chapter is to better understand the effect of high SO_4^{2-} concentrations on copper and zinc adsorption in near surface environments and calculate reliable thermodynamic properties that may be used in predictive geochemical and reactive transport models.

4.2 Materials and Methods

The synthesis of goethite (which used the method Schwertmann and Cornell (1991) and the materials and method used to conduct adsorption experiments are described in detail in Section 2 of Chapter 2.

4.2.1 Adsorption Experiments

Adsorption was measured with series containing 12 individual experiments. For each experiment, 0.075 g goethite was added to a 125 mL glass reaction vessel with 80 mL of 0.001, 0.01, 0.1 and 1 molal Na_2SO_4 and 1.57×10^{-4} molal dissolved Cu^{II} or Zn. Solutions

were prepared using either $Cu(NO_3)_2.2^1/_2H_2O$ or $Zn(NO_3)_2.6H_2O$. The pH of each experiment was adjusted with either 0.1 M HNO_3 or 0.1 M NaOH and was measured with a Thermo Orion 290A+ pH Meter and Ross Sure Flow electrode calibrated with Sigma-Aldrich 4.01, 7.00 and 10.00 buffers with an uncertainty of ± 0.01 pH units. Reaction vessels were sealed with a Dreschel head and placed in a water bath at 25°C ± 0.1 to maintain a constant temperature. When preparing the 1 molal Na_2SO_4 solution, a magnetic stirrer was used to dissolve the Na_2SO_4(s), and no precipitates were visually identified. The solubility of mirabilite ($Na_2SO_4.10H_2O$; saturation index (SI) = -0.04) and thenardite (Na_2SO_4; SI = -0.78) was calculated with PHREEQCi, of which neither mineral was predicted to precipitate, although mirabilite was predicted to be near saturation.

To minimize the effect of CO_2 adsorption onto goethite (i.e., Zeltner and Anderson, 1988) nitrogen gas was bubbled through each reaction vessel. N_2 was firstly passed through ultrapure water to saturate the gas and minimize the effect of evaporation, before being passed through each reaction vessel in sequence to mix the solutions and provide an inert atmosphere.

Samples were allowed to equilibrate for 16 hours before being removed and the final pH measured. Results from kinetic experiments (Refer to Chapter 2) indicated that metal adsorption onto goethite achieved a steady state after approximately 3-4 hours. To ensure that equilibrium was achieved in all reaction vessels, experiments were run overnight for approximately 16 hours.

After pH was measured for each sample, 30 mL of solution was extracted from each experiment and the goethite was removed from the sample using a Millipore 0.45 μm filter. The supernatant solution was preserved by adding several drops of 10% HNO_3.

Solutions were analysed for sulfur, copper and zinc using a Varian Vista Pro Axial ICP-AES. Total S can be measured with the ICP-AES however it can not identify the oxidation state of sulfur, therefore given the tendency of sulfur to oxidize to SO_4^{2-} in the conditions of the experiments it is assumed that SO_4^{2-} was only sulfur species present. Based on this assumption, the sulfate concentration is a ratio of the total sulfur concentrations and can be calculated using Equation 4.1. This method of determining SO_4^{2-} concentrations is described by Reisman et al., (2007), and it should be noted that this indirect method of determining SO_4^{2-} concentrations is only successful when a single sulfur species is likely to be in solution (i.e. sulfides and sulfites are not present).

$$\left[SO_4^{2-}\right]_{tot} = [S]_{tot} \times \left(\frac{\mu^{SO_4^{2-}}}{\mu^S}\right) \qquad (4.1)$$

Where $[SO_4^{2-}]_{tot}$ is the calculated concentration of sulfate (molal); $[S]_{tot}$ is the measured concentration of S (molal); μ^S is the molar mass of S (32.060 g)and $\mu^{SO_4^{2-}}$ is the molar mass of SO_4^{2-} (96.056 g).

The total adsorbed concentration of sulfur and metal was assumed to be the difference between the initial and final concentrations of each experiment. Samples were also

analysed for Fe, but the concentration of Fe in solutions was below the ICP-AES detection limit of 9.0×10^{-7} molal.

4.3 Sulfate Adsorption onto Synthetic Goethite

Sulfate adsorption in the presence of Cu^{II} and Zn was calculated to assess the interaction of sulfate with the goethite surface. The studies of Ali and Dzombak (1996), Persson and Lövgren (1996), Geelhoed et al. (1997) and Rietra et al. (1999) presented measured sulfate adsorption without other metals in solution. The aim of measuring sulfate adsorption here was to determine how dissolved metals (i.e., Cu^{II} and Zn) in solution may influence the concentration of sulfate adsorbed. Experiments with SO_4^{2-} only were not conducted and no direct comparisons with the data of of Ali and Dzombak, Persson and Lövgren, Geelhoed et al. and Rietra et al. could be made.

SO_4^{2-} adsorption onto synthetic goethite in 0.001 and 0.01 molal Na_2SO_4 with 1.57×10^{-4} molal Cu^{II} and 1.54×10^{-4} molal Zn was measured and the results are shown in Figure 4.1 and 4.2.

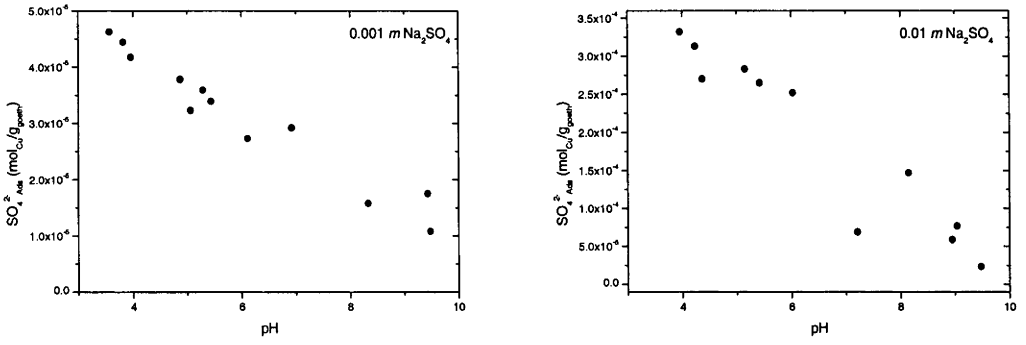

Figure 4.1: Sulfate adsorption in the presence of 1.57×10^{-4} molal Cu^{II} onto 0.9375 g/L goethite in 0.001 and 0.01 molal Na_2SO_4 at pH 4 – 9.5 at 25°C and 1 atmosphere.

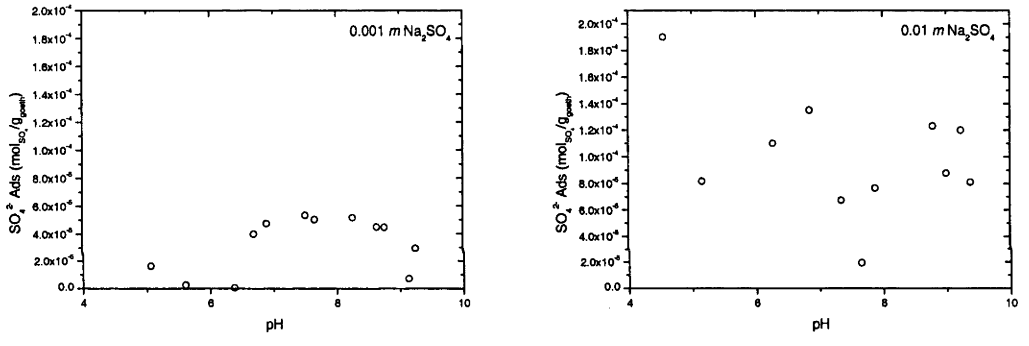

Figure 4.2: Sulfate adsorption in the presence of 1.54×10^{-4} molal Zn onto 0.9375 g/L goethite in 0.001 and 0.01 molal Na_2SO_4 at pH 4 – 9.5 at 25°C and 1 atmosphere.

The results of SO_4^{2-} adsorption in Cu^{II} solutions shows that the highest measured concentration of adsorbed SO_4^{2-} occurs at pH 3.5, and decreases with increasing pH, which is consistent with the studies of Ali and Dzombak (1996), Persson and Lövgren (1996), Geelhoed et al. (1997) and Rietra et al. (1999). In contrast the results for SO_4^{2-} adsorption in the Zn solutions did not show any systematic trend and no interpretation of the Zn data is made. Therefore only the effect of Cu^{II} on SO_4^{2-} adsorption is discussed below.

The results of this study did not show a maximum adsorption as a function of pH in sulfate concentrations of 0.001 or 0.01 molal, but this is probably due to the experimental data being limited to pH values > 3.5, whereas the previous studies reported the maximum SO_4^{2-} adsorption at pH 3.0. The adsorption of sulfate as a function of pH onto goethite in the absence of metals has a steep positive slope (i.e., Ali and Dzombak, 1996; Persson and Lövgren, 1996; Geelhoed et al. 1997); however the slope for adsorption for in this study is much lower. The difference between the slopes in this study and those of Ali and Dzombak, Persson and Lövgren, Geelhoed et al. and Rietra et al. could be caused by the adsorption of copper sulfate ternary surface complexes. This is consistent with the calculated surface speciation of Cu^{II} in 0.001 and 0.01 molal Na_2SO_4 up to pH 7, where the $SOHCuSO_4^0$ surface species is predicted (refer to section 4.4.2.2). However, at pH > 7, no copper sulfate surface complexes are predicted and the cause of further SO_4^{2-}adsorption is unknown as the previous studies of Ali and Dzombak (1996), Persson and Lövgren (1996), Geelhoed et al. (1997) and Rietra et al. (1999) all show that SO_4^{2-} adsorption onto goethite reaches a minimum between pH 7 and 8 for concentrations similar to those used in this study. The analytical and experimental error for adsorption is estimated to be $\pm 5.0 \times 10^{-6}$ moles/g for SO_4^{2-}, which may account for some apparent SO_4^{2-} adsorption at pH >7. However it is not possible to determine the cause of the adsorbed SO_4^{2-} at high pH from the available data. Other analytical methods such as EXAFS may be required to identify any metal sulfate solutions on the goethite surface and identify the structure of such metal sulfate ternary surface complexes.

4.4 Cu^{II} Adsorption onto Goethite in Na_2SO_4

Results for the adsorption of Cu^{II} in 0.001, 0.01 0.1 and 1 molal Na_2SO_4 as a function of Na_2SO_4 concentration are shown in Figure 4.3 and as a function of pH in Figure 4.4 and Appendix 3. Cu^{II} adsorption onto goethite increased with increasing pH, as was the case with copper adsorption in NaCl and $NaNO_3$. The total Cu^{II} concentration in solution was up to 8.73×10^{-5} molal lower the 0.1 and 1.0 molal Na_2SO_4 experiments than in the 0.001 and 0.01 molal Na_2SO_4 solutions. To compare each Na_2SO_4 concentration and determine the effect of sulfate on copper adsorption, the percentage of adsorbed copper is shown in Figure 4.3. A small decrease in Cu^{II} adsorption between 0.01 and 0.1 molal Na_2SO_4 between pH 4 and 6 was observed. This decrease is exaggerated when adsorption is plotted as a function of Na_2SO_4 concentration due to the differences between the total Cu^{II} concentrations. The effect of Na_2SO_4 observed in the experimental data differs from the results of Balistrieri and Murray (1982) and Ali and Dzombak (1996), who both concluded that Na_2SO_4 increased copper adsorption.

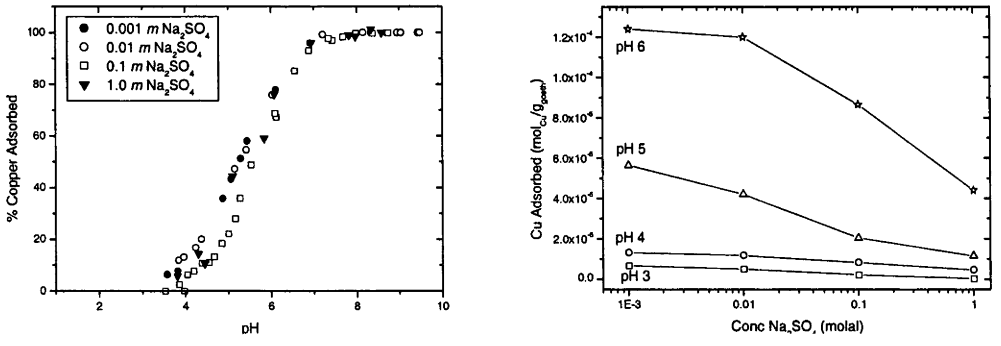

Figure 4.3: Percent of adsorbed copper as a function of pH (goethite concentration = 0.938 g/L, total Cu^{II} concentrations 1.54×10^{-4} in 0.001 molal Na_2SO_4; 1.38×10^{-4} in 0.01 molal Na_2SO_4; 1.11×10^{-4} in 0.1 molal Na_2SO_4 and 6.27×10^{-5} in 1 molal Na_2SO_4); and concentration of adsorbed Cu^{II} as a function of Na_2SO_4 concentration (0.001 – 1.0 molal) at fixed pH of 3, 4, 5 and 6.

The results of this study are compared with those of Balistrieri and Murray (1982) and Ali and Dzombak (1997) using the K_d described in Chapter 2 and is shown in Figure 4.6. The data is separated by up to two orders of magnitude at a given pH, although the slope of the best fit lines is similar between the three studies, with a slope of 0.8 calculated from the data of this study, 1.3 from the data of Ali and Dzombak and 1.0 from the data of Balistrieri and Murray. As discussed in Chapter 3, changing parameters such as goethite concentration and surface area moves the data along the K_d axis without changing the slope. Therefore the separation of the three data sets is likely to be caused by variations in the goethite characteristics such as crystal morphology, surface area or adsorption site densities. These effects are described in detail in Chapter 2; Section 2.3.1.

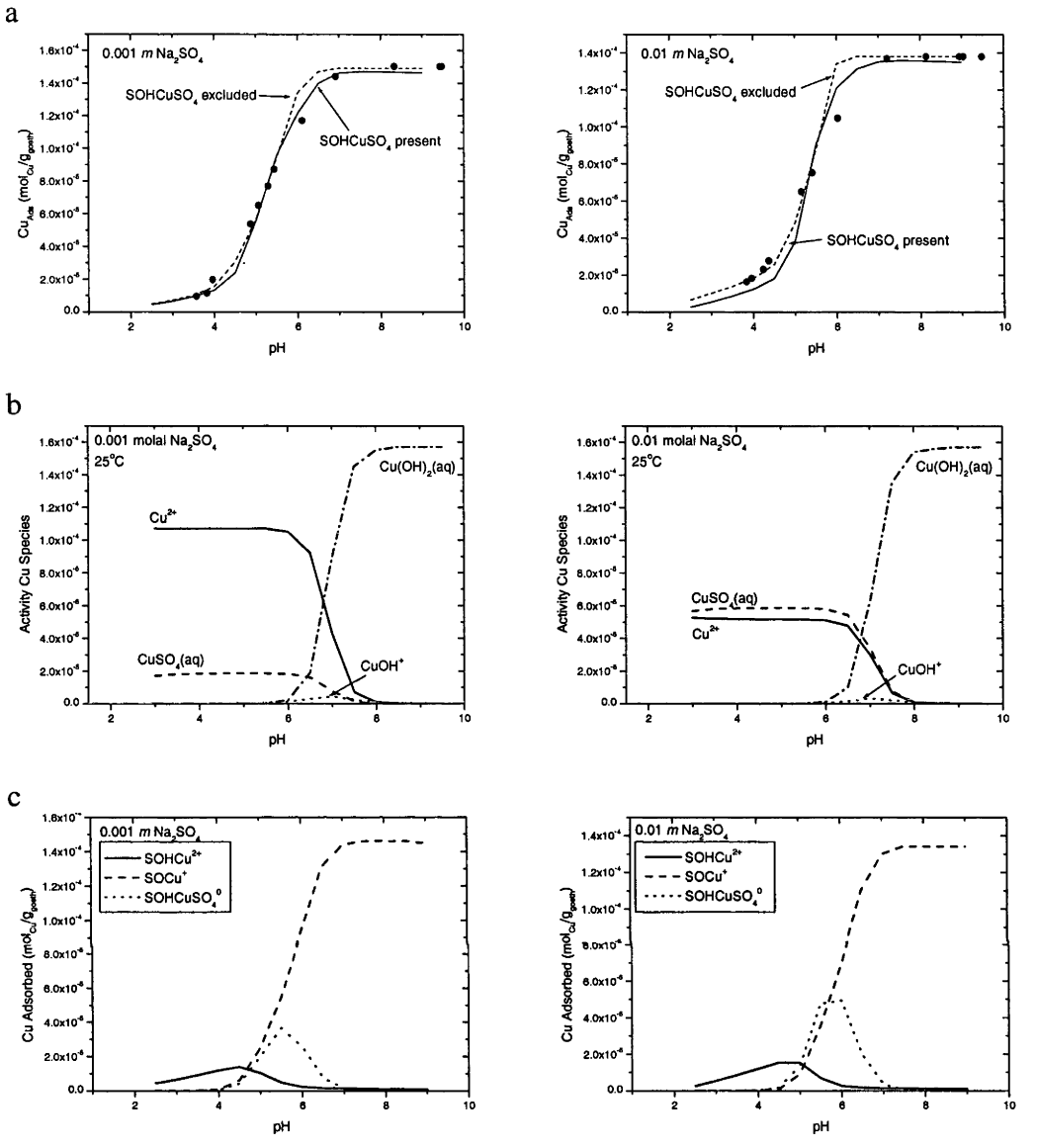

Figure 4.4: **(a)** Adsorption Cu^{II} onto goethite in 0.001 and 0.01 molal Na_2SO_4 between pH 3.5 -9 at 25°C and 1 atmosphere. Initial Cu^{II} concentrations are 1.50×10^{-4} molal in 0.001 molal Na_2SO_4 and 1.38×10^{-4} in 0.01 molal Na_2SO_4. Solid lines represent the predicted Cu^{II} adsorbed calculated with the Constant Capacitance Model. **(b)** Aqueous copper speciation as a function of pH for 0.001 and 0.01 molal Na_2SO_4; total Cu^{II} concentrations are 1.50×10^{-4} molal in 0.001 molal Na_2SO_4 and 1.38×10^{-4} in 0.01 molal Na_2SO_4. **(c)** Predicted surface speciation of Cu^{II} on goethite in 0.001 and 0.01 molal Na_2SO_4.

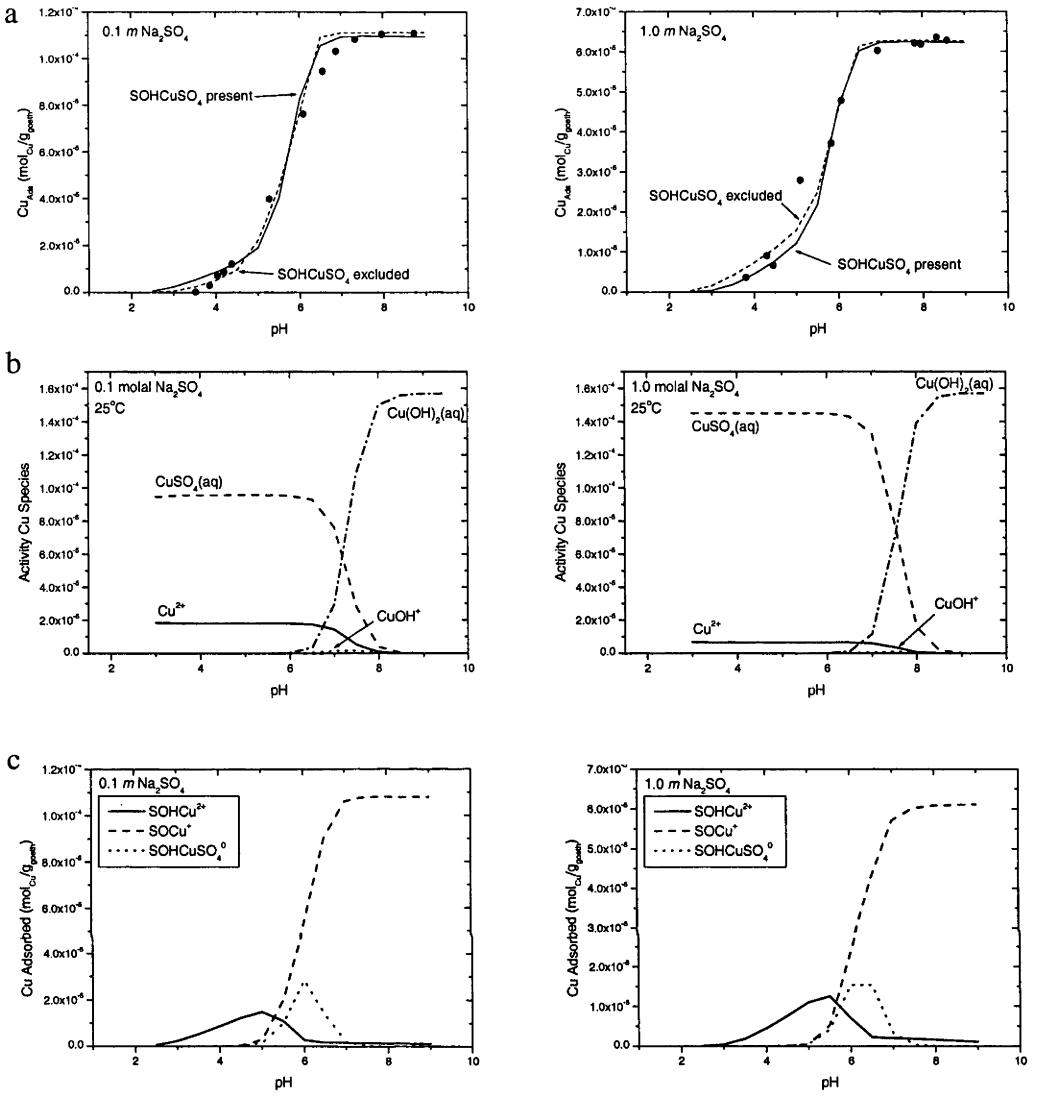

Figure 4.4: **(a)** Adsorption Cu^{II} onto goethite in 0.1 and 1.0 molal Na_2SO_4 between pH 3.5 -9 at 25°C and 1 atmosphere. Initial Cu^{II} concentrations are 1.11×10^{-4} molal in 0.1 molal Na_2SO_4 and 6.27×10^{-5} molal in 1.0 molal Na_2SO_4. Solid lines represent the predicted Cu^{II} adsorbed calculated with the Constant Capacitance Model. **(b)** Aqueous copper speciation as a function of pH for 0.1 and 1.0 molal Na_2SO_4; total Cu^{II} concentrations are 1.11×10^{-4} molal in 0.1 molal Na_2SO_4 and 6.27×10^{-5} in 1.0 molal Na_2SO_4. **(c)** Predicted surface speciation of Cu^{II} on goethite in 0.1 and 1.0 molal Na_2SO_4.

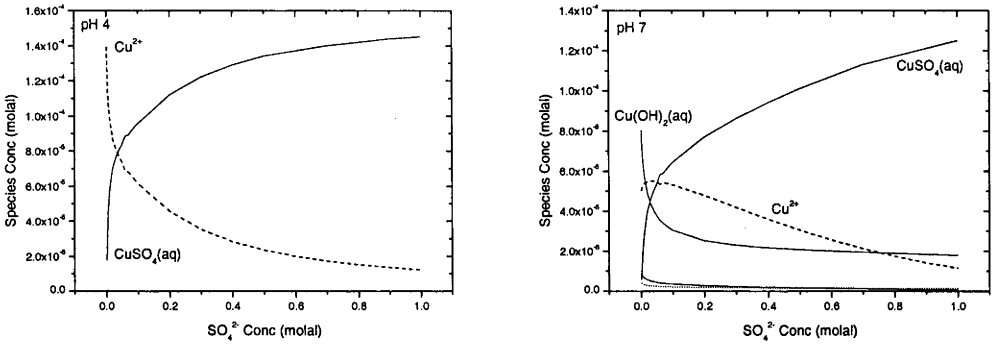

Figure 4.5: Predicted aqueous speciation of Cu^{II} as a function of sulfate concentration at pH 4 and 7 at 25°C and 1 atmosphere. Species calculated but not included in the plot include $CuNO_3^+$, $Cu(NO_3)_2(aq)$, $Cu_2(OH)_2^{2+}$.

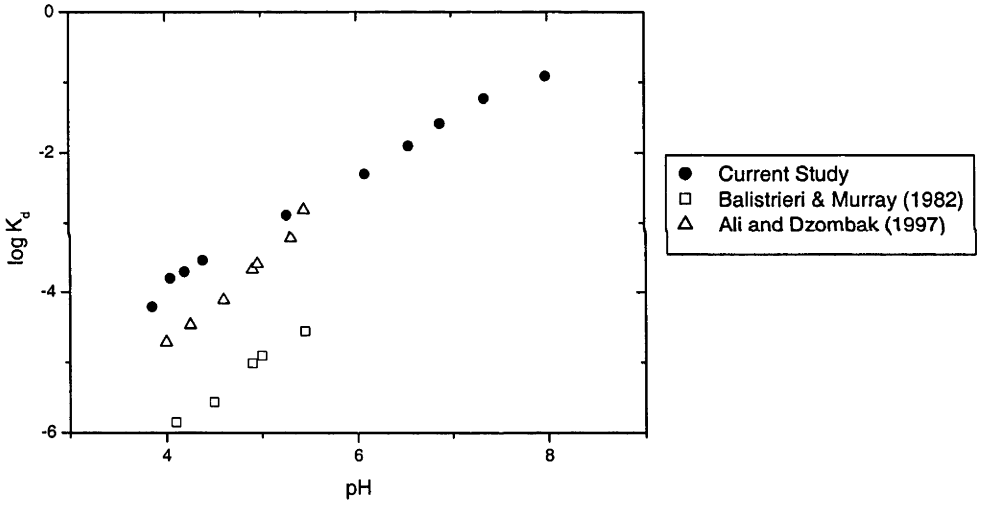

Figure 4.6: Log K_d plot comparing Cu^{II} adsorption between the current study (goethite = 0.9375 g/L; goethite surface area = 36.05 m^2/g; initial Cu^{II} = 1.13 × 10^{-4} molal; Na_2SO_4 = 0.001 molal) and those of Balistrieri and Murray (goethite = 28.5 g/L; goethite surface area = 51.8 m^2/g; initial Cu^{II} = 2.5 × 10^{-6} molal; Na_2SO_4 = 0.028 molal); Ali and Dzombak (goethite = 1.6 g/L; goethite surface area = 79.4 m^2/g; initial Cu^{II} = 9.8 × 10^{-5} molal; Na_2SO_4 = 0.001 molal).

4.4.1 Quantitative Interpretation

In this section, the reactions selected for surface complexation modeling are inferred. The reactions shown in Equations 4.2 and 4.3 are used based on the copper adsorption results in $NaNO_3$ solutions and are the simplest surface reactions. Fitting of these reactions to experimental data for $NaNO_3$ solutions is described in Chapter 2; Section 2.3.1.1.

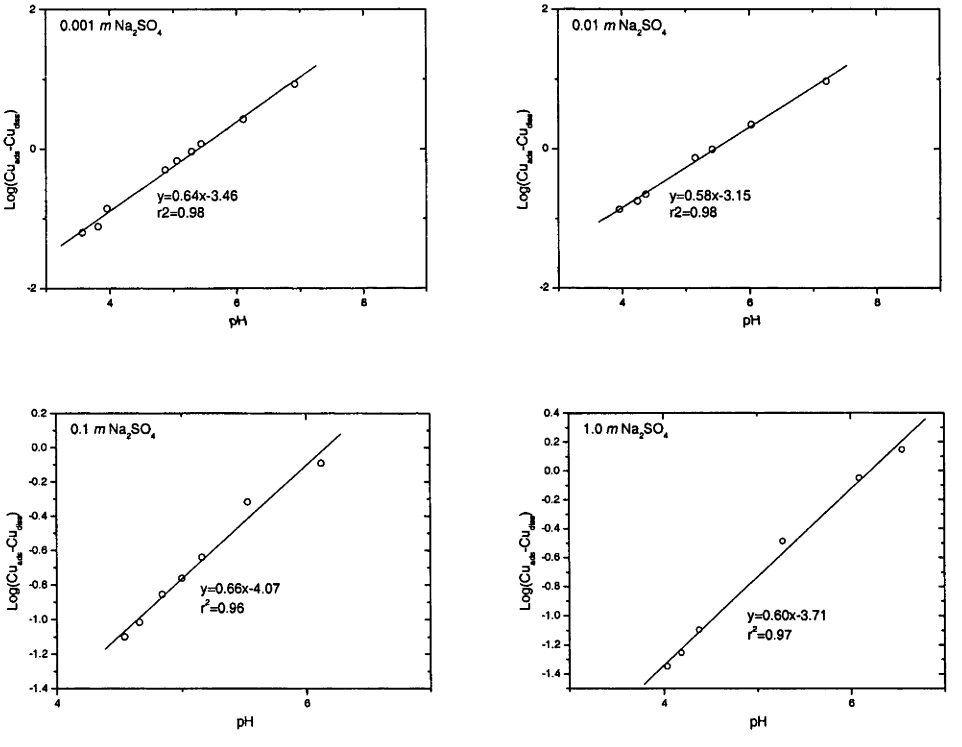

Figure 4.7: Log[Cu_{Ads}] – log[Cu_{Diss}] versus pH showing Cu^{II} adsorption onto goethite in 0.001, 0.01, 0.1 and 1.0 molal Na_2SO_4. The slopes of the linear regression lines indicate the stoichiometry of dominant adsorption reactions and corresponding copper surface complexes.

To isolate the effect of pH on copper adsorption in 0.001, 0.01, 0.1 and 1.0 molal Na_2SO_4, $\log[Cu_{Ads}] - \log[Cu_{Diss}]$ versus pH is plotted (Figure 4.7). The data in Figure 4.7 remains linear with a the slope of the line of best fit remaining fairly constant for 0.001, 0.01, 0.1 and 1.0 molal Na_2SO_4 (the minimum slope was 0.58 in 0.01 molal Na_2SO_4 and the maximum slope was 0.66 in 0.1 molal Na_2SO_4). The slopes of the best fit lines imply that a combination of pH dependent, and pH independent reactions occur in the experiments. Reactions that fit the $\log[Cu_{Ads}] - \log[Cu_{Diss}]$ versus pH data include the those shown in Equations 4.2 and 4.3 below. Other pH dependent copper sulfate surface complexes may be possible although it can not be determined if these are present from the data in Figure 4.7.

The effect of sulfate concentration is shown in Figure 4.8 by plotting $Log[Cu_{Ads}]$-$Log[Cu_{Diss}]$-pH versus SO_4^{2-} for pH 4, 5, 6 and 7. The small number of different sulfate concentrations used in experiments makes it difficult to accurately fit a trend to the data. However, plotting a best fit line through the data as an indication for any trend shows a negative slope between -0.2 and -0.3 over the entire range of pH values.

$$\equiv SOH + Cu^{2+} = \equiv SOHCu^{2+} \qquad (4.2)$$

$$\equiv SOH + Cu^{2+} = \equiv SOCu^{+} + H^{+} \qquad (4.3)$$

$$\equiv SOH + Cu^{2+} + SO_4^{2-} = \equiv SOHCuSO_4^{0} \qquad (4.4)$$

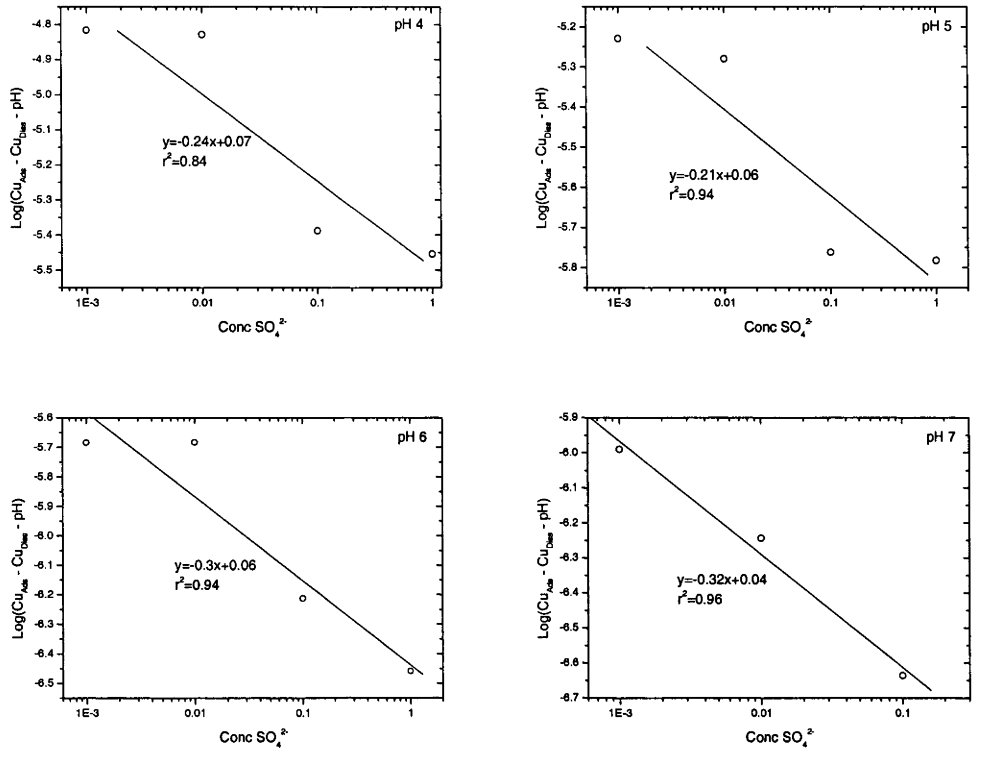

Figure 4.8: Log[Cu_{Ads}]-Log[Cu_{Diss}]-pH versus SO_4^{2-} showing Cu^{II} adsorption for pH 4, 5, 6 and 7. Due to the low total concentration of Cu^{II} in the 1.0 molal Na_2SO_4 experiment, the data point for 1 molal Na_2SO_4 at pH 7 of -4.22 has been omitted.

The formation of copper-sulfate ternary surface complexes e.g., Equation 4.4 as proposed by Ali and Dzombak (1996), in the experiments is possible. However, due to the limited amount of data quantify any sulfate dependence is difficult. The formation of $SOHCuSO_4^0$ is considered below when fitting equilibrium constants to the experimental data.

4.4.2 Surface Complexation Modelling

As described in Chapters 2 and 3, the Constant Capacitance surface complexation model was used to predict the formation of Cu^{II} surface complexes on the goethite surface. A detailed description of the model is given in Chapter 2, as are the parameters and assumptions used to calculate speciation of dissolved and surface complexes. The result of fitting the CCM to the copper experimental data of this chapter are given below.

4.4.2.1 Summary of Model Parameters

The parameters required to describe copper adsorption onto goethite with the CCM were: goethite concentration in each experiment (individual experiments contained 0.935 g/L); goethite surface area (measured to be 36.05 m^2/g using BET analysis) and capacitance. A capacitance value of 0.83 F/m^2 was used for all Na_2SO_4 concentrations. This was the fitted value for Cu^{II} adsorption in $NaNO_3$ solutions. A brief comparison of this value with those from previous studies (i.e., Lövgren et al., 1996) is made in Chapter 2 (Section 2.3.1.4). Reactions and equilibrium constants for protonation and deprotonation reactions are shown in Equations 4.5 and 4.6:

$$\equiv SOH(ads) + H^+(aq) = \equiv SOH_2^+(ads) \qquad (4.5)$$

$$\equiv SO^-(ads) + H^+(aq) = \equiv SOH(ads) \qquad (4.6)$$

with the equilibrium constants:

$$K_1^{int} = \frac{a_{SOH_2^+}}{a_{SOH}a_{H^+}} \exp\left(\frac{-zF\psi_o}{RT}\right) \quad (4.7)$$

$$K_2^{int} = \frac{a_{SO^-}a_{H^+}}{a_{SOH}} \exp\left(\frac{-zF\psi_o}{RT}\right) \quad (4.8)$$

Where ψ_o is the electrical potential (V) at the surface, F is the Faraday constant (96487 C/mol), R is the universal gas constant (8.314 J K^{-1}/mol) and T is temperature in Kelvin. The log K values: log K_1^{int} = 6.36 ± 0.38 (2σ) log K_2^{int} = -10.44 ± 0.38 (2σ) were taken from Richter et al. (2005).

Persson and Lövgren (1996) used the reactions in Equation 4.9 and 4.10 to describe the formation of sulfate surface complexes.

$$\equiv SOH + H^+ + SO_4^{2-} = \equiv SOH_2SO_4^{2-} \quad (4.9)$$

$$\equiv SOH + 2H^+ + SO_4^{2-} = \equiv SOH_2HSO_4^0 \quad (4.10)$$

Both reactions were tried in fits for Zn and Cu although the reaction in Equation 15 best fit the experimental data of this study. Fitting with only the $SOH_2SO_4^-$ surface complex resulted with a poor fit with the experimental data, supported by the high v_y values when fitting for zinc and copper surface complexes (see below). When Equations 15 and 16 were used simultaneously, no distinguishable improvement of the model fit to the experimental

data could be determined. Therefore the $SOH_2HSO_4^0$ surface complex was chosen for describing the sulfate adsorption, using the log K of 13.5 described by Persson and Lövgren (1996). It is recognised that the log K value of Persson and Lövgren (1996) is only true for their experiments (i.e. for the goethite used in their experiments), but due to time and resource constraints it was not possible to undertake the experiments required to determine the equilibrium constant for Equation 4.10. The log K value of Persson and Lövgren (1996) did improve the fit of the CCM in this study and it is a reaction that is likely to be occurring in the experiments. By calculating a new equilibrium constant for this reaction, it is likely that the model fits would be slightly better.

4.4.2.2 Fitting Equilibrium Constants

In this section, equilibrium constants for the formation reactions of copper surface complexes in 0.001, 0.01, 0.1 and 1 molal Na_2SO_4 solutions are fitted. Unlike fitting equilibrium constants in NaCl solutions, the choice of activity coefficient model is clearer when considering solutions with Na_2SO_4.

The Debye-Hückel b-dot Equation was used for calculating activity coefficients for NaCl solutions because the $b^{\bullet}$ parameter was calibrated specifically for these solutions (Helgesson and Kirkham, 1974; although it may also be applied to solutions with different monovalent anions). However, the presence of the SO_4^{2-} anion in solution may result in an unreliable activity coefficient calculation because the $b^{\bullet}$ parameter was not calculated for solutions with divalent anions (i.e., SO_4^{2-}). Therefore the Davies Equation was used to

calculate activity coefficients for Na_2SO_4 solutions, and the Debye-Hückel b-dot Equation was not considered.

The experimental data were individually fit for each Na_2SO_4 concentration (i.e., for 0.001, 0.01, 0.1 and 1 molal) using several scenarios. The scenarios used were: (a) fitting log K values only with the two copper surface complexes described in Equations 4.2 and 4.3; (b) including the $SOHCuSO_4^0$ surface complex (Equation 4.4) and leaving log K values for $\equiv SOHCu^{2+}$ and $\equiv SOCu^{+}$ constants in Table 2.3; and (c) optimizing the log K values for all three copper surface complexes. The aqueous speciation for Cu^{II} was calculated with FITEQL 4.0 for the species listed in Table 4.2, using mass balance constraints on total Na, Cu, SO_4, NO_3 and pH, assuming an activity for $H_2O(l)$ = 1. Activity coefficients were estimated using the Davies Equation in FITEQL 4.0:

$$\log \gamma = Az^2 \left(\frac{I^{1/2}}{1 + I^{1/2}} - 0.3I \right) \qquad (4.11)$$

where I is the stoichiometric ionic strength, (Davies, 1962) and A = 0.509 (Herbelin and Westall, 1999). The adsorption of sulfate onto goethite was included in the CCM using the SOH_2HSO_4 surface complex (log K = 13.5) proposed by Persson and Lövgren (1996).

Results of fitting the copper surface complexes of Equations 4.2 and 4.3 for each Na_2SO_4 concentration is shown in Figure 4.4, and log K values are shown in Table 4.3. The low v_y values, which range between 5.0 and 11.1, indicate that the copper surface complexes $SOHCu^{2+}$ and $SOCu^{+}$ fit the experimental data closely. However, when plotted, the slope of

the predicted adsorption curve was greater than the slope of the experimental data and predicted approximately 30% more adsorption between pH 5.5 and 6.5. The fitted log K value for $\equiv SOHCu^{2+}$ changed by more than two orders of magnitude between different data sets, while the log K for $\equiv SOCu^{+}$ was consistently greater than those calculated in $NaNO_3$ solutions. This indicates that a parameter such as an additional surface complex, could be missing from the model.

Table 4.2: Formation reactions and equilibrium constants used to calculate Cu^{II} adsorption onto goethite in 0.001, 0.01, 0.1 and 1.0 molal Na_2SO_4 solutions.

Species	Mass Action Reaction	Log K	Source
OH-	$OH + H = H_2O$	*13.98*	*a*
NaOH(aq)	$Na^+ + OH^- = NaOH(aq)$	*0.1*	*b*
$CuNO_3^+$	$Cu^{2+} + NO_3^- = CuNO_3^+$	*0.50*	*b*
$Cu(NO_3)_2(aq)$	$Cu^{2+} + 2NO_3^- = Cu(NO_3)_2(aq)$	*-0.40*	*a*
$CuOH^+$	$Cu^{2+} + H_2O = CuOH^+ + H^+$	*-8.00*	*b*
$Cu(OH)_2$	$Cu^{2+} + 2H_2O = Cu(OH)_2 + 2H^+$	*-13.68*	*b*
$Cu_2(OH)_2^{2+}$	$2Cu^{2+} + 2H_2O = Cu_2(OH)_2^{2+} + 2H^+$	*-17.5*	*b*
$NaNO_3(aq)$	$Na^+ + NO_3^- = NaNO_3(aq)$	*-0.55*	*a*
$CuSO_4(aq)$	$Cu_2^+ + SO_4^{2-} = CuSO_4(aq)$	*-2.34*	*b*
$NaSO_4^-$	$Na^+ + SO_4^{2-} = NaSO4^-$	*-0.72*	*b*
HSO_4^-	$H^+ + SO_4^{2-} = HSO_4^-$	*-1.99*	*b*

[a] *Smith and Martel (1997)*

[b] *Allison et al. (1991)*

Table 4.3: Equilibrium constants for species used to model copper adsorption onto goethite for each concentration of Na_2SO_4. Equilibrium constants describe formation reactions and the activity coefficient for aqueous species was calculated with the Davies Equation in FITEQL 4.0. Other surface complexes used in the model include SOH_2^+ (log K = 6.36) SO^- (log K = -10.44) from Richter et al. (2005); $SOH_2HSO_4^0$ (log K = 13.5) from Persson and Lövgren (1996).

Species	Log K (Na_2SO_4 Concentration)			
	0.001	***0.01***	***0.1***	***1***
$\equiv SOHCu^{2+}$	8.52	9.68	7.46	9.29
$\equiv SOCu^+$	1.56	2.31	1.42	1.66
Vy	6.4	11.1	5.0	5.6

The $SOHCuSO_4^0$ surface complex was added to the model as suggested by the results of Ali and Dzombak (1996). The log K values for the $\equiv SOHCu^{2+}$ (log K = 8.43) and $\equiv SOCu^+$ (log K = 0.85) surface complexes were fixed using the results of copper adsorption in $NaNO_3$ solutions. The results are shown in Figure 4.4 and the log K values are listed in Table 4.4. The v_y values of the model with the $\equiv SOHCuCSO_4^0$ are slightly higher than those of the model without the copper sulfate surface complex. However, when plotted, the slope of the predicted adsorption curve has a closer fit with the experimental data in 0.001 and 0.01 molal Na_2SO_4. In the solutions with 0.1 and 1.0 molal Na_2SO_4, no significant difference between the two models can be identified. Despite the improved fit with the $\equiv SOHCuSO_4^0$ surface complex, the predicted adsorption does not match the experimental data. Optimising for three copper surface complexes (i.e., $\equiv SOHCu^{2+}$, $\equiv SOCu^+$ and $\equiv SOHCuSO_4^0$) was attempted, but convergence of the model could only be obtained for the experimental data in 0.001 molal Na_2SO_4. The fitted log K values for the 0.001 molal Na_2SO_4 solution were similar to the log K values in Table 4.5: $\equiv SOHCu^{2+}$ = 8.72; $\equiv SOCu^+$ = 0.73; and $\equiv SOHCuSO_4^0$ = 6.18 (v_y = 4.08). Fitting for a fourth surface species was also

tried i.e., $SOCuSO_4^-$, however the model would not converge when this species was included.

The model consisting of three copper surface complexes, $\equiv SOHCu^{2+}$, $\equiv SOCu^{+}$ and $\equiv SOHCuSO_4^0$ and the equilibrium constants in Table 4.4 appears to fit the experimental data closest. Furthermore, the log K values for $\equiv SOHCu^{2+}$ and $\equiv SOCu^{+}$ were used to fit copper adsorption in $NaNO_3$ and NaCl solutions, and the results of optimizing the three copper surface complexes in 0.001 molal Na_2SO_4 are within half an order of magnitude of the log K values in Table 4.4.

Table 4.4: Equilibrium constants for species used to model copper adsorption onto goethite for each concentration of Na_2SO_4. Equilibrium constants describe formation reactions and the activity coefficient for aqueous species was calculated with the Davies Equation in FITEQL 4.0. Other surface complexes used in the model include $\equiv SOH_2^+$ (log K = 6.36) $\equiv SO^-$ (log K = -10.44) from Richter et al. (2005); $\equiv SOHCu^{2+}$ and $\equiv SOCu^{+}$ (calculated in Chapter 2); $\equiv SOH_2HSO_4^0$ (log K = 13.5) from Persson and Lövgren (1996).

Species	**Log K (Concentration of Na_2SO_4)**				
	0.001	***0.01***	***0.1***	***1***	***0.001-1***
$\equiv SOHCuSO_4^0$	6.12	5.71	4.71	4.55	6
Vy	6.3	13.4	7.6	7.1	188.4

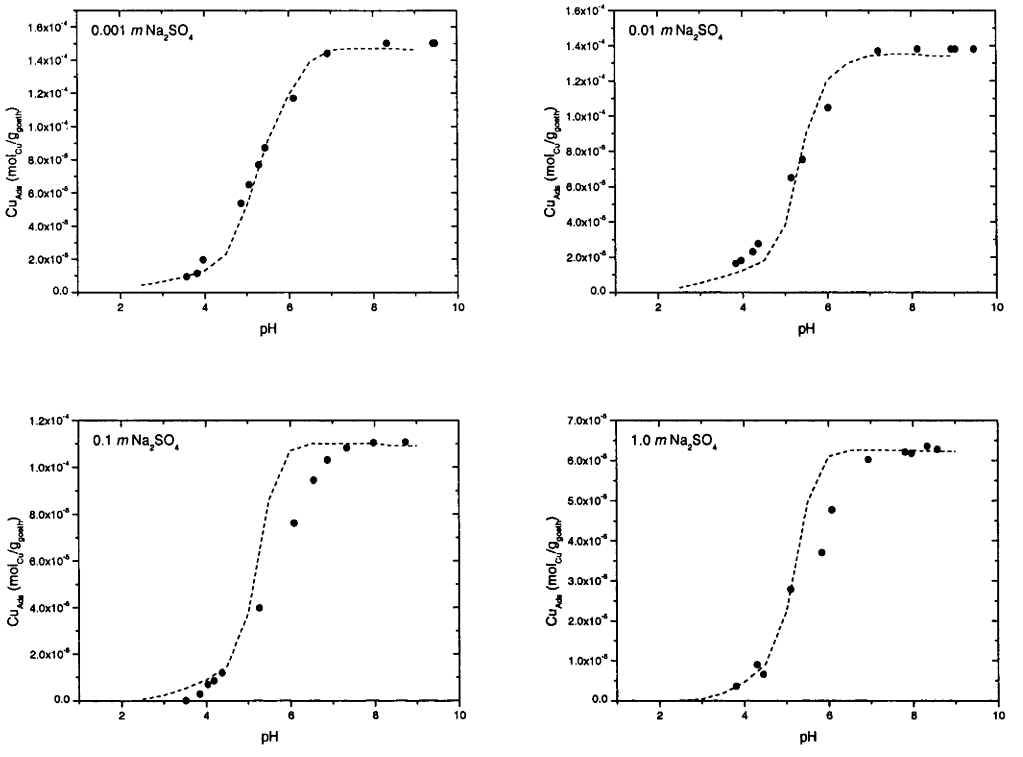

Figure 4.9: Adsorption of Cu^{II} onto goethite as a function of pH in 0.001, 0.01, 0.1 and 1.0 molal Na_2SO_4. The equilibrium constant for $\equiv SOHCuSO_4^0$ surface complex was fitted to experimental data from 0.001 – 1.0 molal Na_2SO_4. Log K values of $\equiv SOHCu^{2+}$ = 8.43 and $\equiv SOCu^{+}$ = 0.85.

An attempt to fit an equilibrium constant for all of the experimental data (i.e., experimental data from 0.001, 0.01, 0.1 and 1.0 molal Na_2SO_4) was made (Table 4.4). The value for v_y of 188.4 indicates the CCM did not fit the experimental data, which is confirmed in Figure 4.9 which shows that the model overestimated copper adsorption in the solutions with > 0.01 molal Na_2SO_4 and pH > 4.5.

Surface speciation for Cu^{II} adsorption onto goethite using the Log K values for individual Na_2SO_4 concentrations is shown in Figure 4.4. $\equiv SOHCu^{2+}$ is the dominant surface species

in acidic conditions (i.e. pH < 4.5) over the entire range of Na_2SO_4 concentrations. At pH greater than 4.5 the dominant surface complex changed to $\equiv SOCu^+$, which accounts for most of the adsorbed copper at pH 7.5 and above. The formation of $\equiv SOHCuSO_4^0$ increases copper adsorption in the pH range between 4.5 and 6, but it never becomes the dominant surface species. The aqueous speciation of copper as a function of Na_2SO_4 concentration at pH 4 and 7 is shown in Figure 4.8. The $CuSO_4$(aq) complex is predicted to predominate at sulfate concentrations greater than 0.2 molal. However, the total adsorption and hence the concentration of the $\equiv SOHCuSO_4^0$ surface complex decreases with increasing Na_2SO_4 concentration and is not predicted to exceed 5.0×10^{-5} mol_{Cu}/g_{goeth}.

4.5 Zn Adsorption onto Goethite in Na_2SO_4

Results for the adsorption of Zn onto goethite in 0.001, 0.01, 0.1 and 1 molal Na_2SO_4 are shown in Figure 4.10 and Appendix 3. The concentration of adsorbed zinc increased with increasing pH, as observed with Zn adsorption in NaCl and $NaNO_3$ solutions. Figure 4.11 shows that Zn adsorption also increased with increasing Na_2SO_4 concentration between 0.001 and 0.01 molal for pH 4, 5 and 6, but decreased when the Na_2SO_4 concentration was >0.01 molal. At pH 7, zinc adsorption decreased over the entire range of Na_2SO_4 concentrations. This result differs from that of Swedlund and Webster who concluded that sulfate increased zinc adsorption over the entire Na_2SO_4 concentration range they studied.

The results this study are compared with those of Balistrieri and Murray (1982) using the K_d described in Chapter 2 and the results are shown in Figure 4.12. Balistrieri and Murray was the only other study that examined the effect of sulfate on Zn adsorption onto goethite.

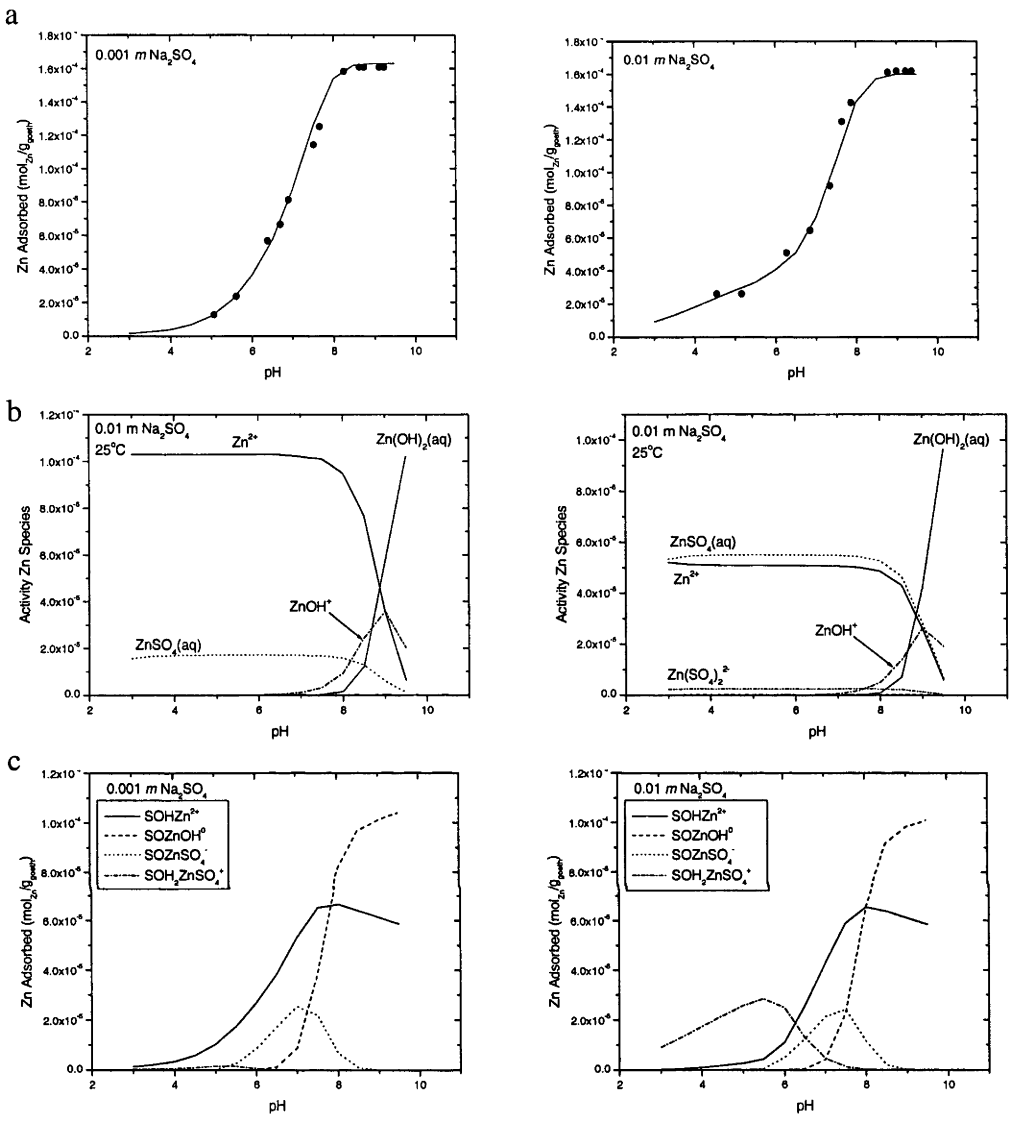

Figure 4.10: **(a)** Adsorption Zn onto goethite in 0.001 and 0.01 molal Na_2SO_4 between pH 3.5-9 at 25°C and 1 atmosphere. Initial Zn concentrations were 1.60×10^{-4} molal in 0.001 molal Na_2SO_4 and 1.62×10^{-4} molal in 0.01 molal Na_2SO_4. Solid lines represent the predicted Zn adsorbed calculated with the Constant Capacitance Model. **(b)** Aqueous copper speciation as a function of pH for 0.001 and 0.01 molal Na_2SO_4; total Zn concentrations are 1.60×10^{-4} molal in 0.001 molal Na_2SO_4 and 1.62×10^{-4} molal in 0.01 molal Na_2SO_4. **(c)** Predicted surface speciation of Zn on goethite in 0.001 and 0.01 molal Na_2SO_4.

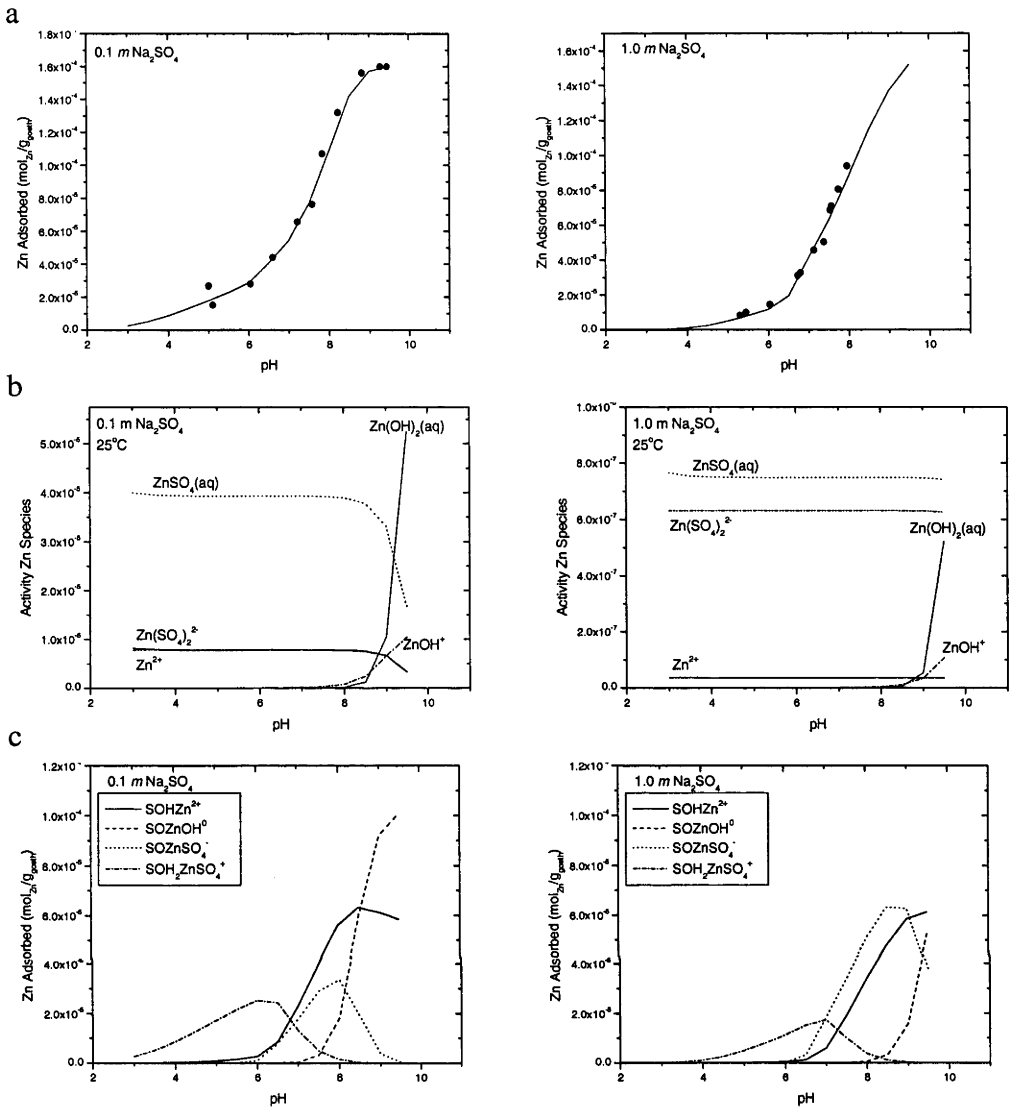

Figure 4.10: **(a)** Adsorption Zn onto goethite in 0.1 and 1.0 molal Na_2SO_4 between pH 3.5-9 at 25°C and 1 atmosphere. Initial Zn concentrations were 1.60×10^{-4} molal in 0.1 molal Na_2SO_4 and 1.59×10^{-4} molal in 1.0 molal Na_2SO_4. Solid lines represent the predicted Zn adsorbed calculated with the Constant Capacitance Model. **(b)** Aqueous copper speciation as a function of pH for 0.1 and 1.0 molal Na_2SO_4; total Zn concentrations are 1.60×10^{-4} molal in 0.1 molal Na_2SO_4 and 1.59×10^{-4} molal in 1.0 molal Na_2SO_4. **(c)** Predicted surface speciation of Zn on goethite in 0.1 and 1.0 molal Na_2SO_4.

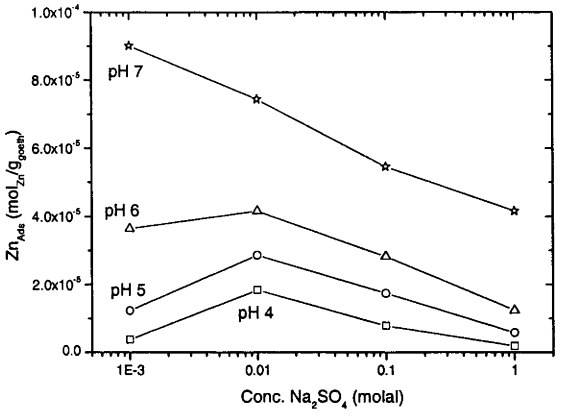

Figure 4.11: Concentration of adsorbed Zn^{II} as a function of Na_2SO_4 concentration at fixed pH of 4 – 7.

Figure 4.12 shows that the K_d varies by up to 1.5 orders of magnitude between the the data of Balistrieri and Murray (1982) and the results of this study at a given pH. However, the difference is smaller when comparing different experimental conditions by the same authors, for instance, the K_d difference observed in data from Balistrieri and Murray between different goethite concentrations is approximately 0.3 log units, while this study shows a difference of 0.5 order of magnitude between sulfate concentrations. As discussed in Chapter 3, changing the parameters of the mineral (i.e., surface area or goethite concentration) moves the data along the K_d axis without altering the slope of the data. Therefore the difference in K_d between the two studies may be due to variations in crystal morphology (e.g. Lützenkirchen et al., 2002; Kosmoulski, 2004; Peacock and Sherman, 2004; refer to Chapter 2, Section 2.3.1 for discussion on goethite crystal morphology) or adsorption site densities. The slopes of best fit lines through each data set were calculated, with the data of Balistrieri and Murray showing slopes of 0.72 and 0.78, compared to slopes of 0.50 and 0.62 from this study. As discussed in Chapter 3, the slope of the K_d data

may be controlled by the mineral species (i.e., ferrihydrite has a steeper slope than goethite, refer to Section 3.3.1). Balistrieri and Murray used the goethite synthesis method of Atkinson et al. (1967), with a measured surface area of 51.8 m^2/g. Balistrieri and Murray do not describe the morphology or purity of their synthetic goethite and it is possible that it contained traces of ferrihydrite, which would explain the different slope and K_d to the data of this study.

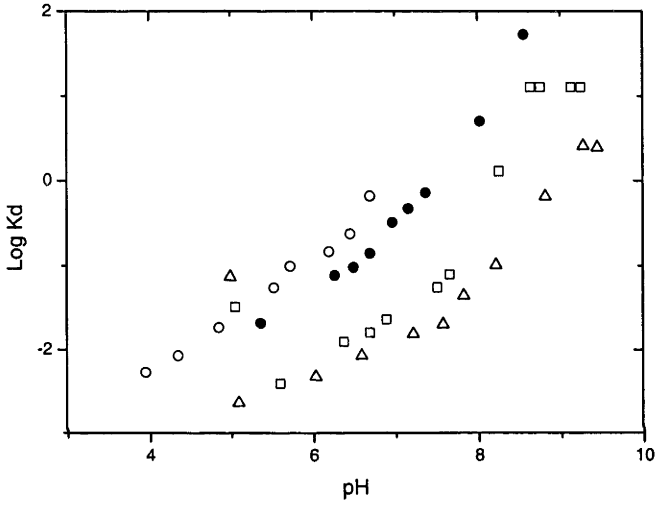

Figure 4.12: Log K_d plot comparing Zn^{II} adsorption onto goethite between studies by Balistrieri and Murray (1982) in 0.1 molal Na_2SO_4 and 0.6 g/L goethite (•) and 8.6 g/L goethite (○); and the current study with 0.94 g/L goethite in 0.001 molal Na_2SO_4 (□) and 0.1 molal Na_2SO_4 (Δ).

4.5.1 Quantitative Interpretation

In this section, inferred reactions used for surface complexation modeling are described. To isolate the effect of pH on Zn adsorption in 0.001, 0.01, 0.1 and 1.0 molal Na_2SO_4, $\log[Zn_{Ads}]$-$\log[Zn_{Diss}]$ versus pH is plotted in Figure 4.13. In 0.001, 0.01 and 0.1 molal Na_2SO_4 solutions, two data sub-sets can be distinguished, identified by a change in slope of the line of best fit. However, the number of data points in each data sub-set is small, thereby reducing the confidence of the slope value and the pH where the slope change occurs. In 1.0 molal Na_2SO_4 the slope of the best fit line is constant at 0.5.

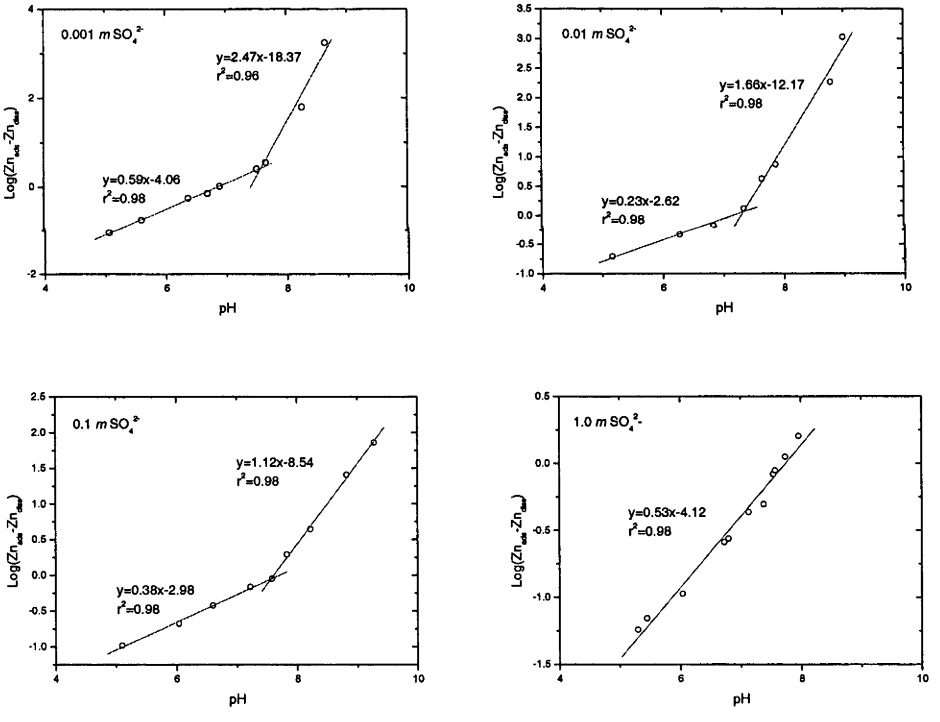

Figure 4.13: $Log[Zn]_{Ads}$ – $log[Zn]_{Diss}$ versus pH showing Zn^{II} adsorption onto goethite in different concentrations of Na_2SO_4. The slopes of the linear regression lines indicate the stoichiometry of dominant adsorption reactions and corresponding zinc surface complexes.

The slopes for the best fit lines in 0.001, 0.01 and 0.1 molal Na_2SO_4, which range between 0.2 and 0.6 show that Zn adsorption is pH dependent over the entire pH range studied. At approximately pH 7.5, the slope of the best fit lines increased to between 1.1 and 2.5, which shows an increase in pH dependence for Zn adsorption reactions. Based on the data in Figure 4.13, the following reactions may be inferred (excluding any sulfate dependence):

$$\equiv SOH + Zn^{2+} = \equiv SOHZn^{2+} \qquad (4.12)$$

$$\equiv SOH + Zn^{2+} + H_2O = \equiv SOZnOH^0 + 2H^+ \qquad (4.13)$$

The reaction shown in Equation 4.12 is independent of pH (e.g., slope of $Log[Zn]_{Ads}$ – $log[Zn]_{Diss}$ versus pH = 0), while the reaction in Equation 4.13 shows a strong pH dependence (i.e., slope = 2). However, the coexistence of these reactions in a single experiment would alter the slope of a $log[Zn]_{Ads} - log[Zn]_{Diss}$ versus pH plot. For example, if Equation 4.12 was the predominant reaction controlling Zn adsorption, with less adsorption from the reaction Equation 4.13, then the net slope of the $log[Zn]_{Ads}$ – $log[Zn]_{Diss}$ versus pH will be between 0 and 1 (e.g., as observed at pH < 7.5 for all Na_2SO_4 concentrations). Similarly, at pH > 7.5, the reaction in Equation 4.13 is predicted to be the predominant reaction and the net slope of the $log[Zn]_{Ads} - log[Zn]_{Diss}$ versus pH will be > 1 (e.g., as observed at pH > 7.5 for 0.001 molal Na_2SO_4). Other zinc sulfate surface complexes may also be pH dependent (i.e., Equation 4.14 and 4.15), although it is not possible to determine if these are present from the data in Figure 4.13.

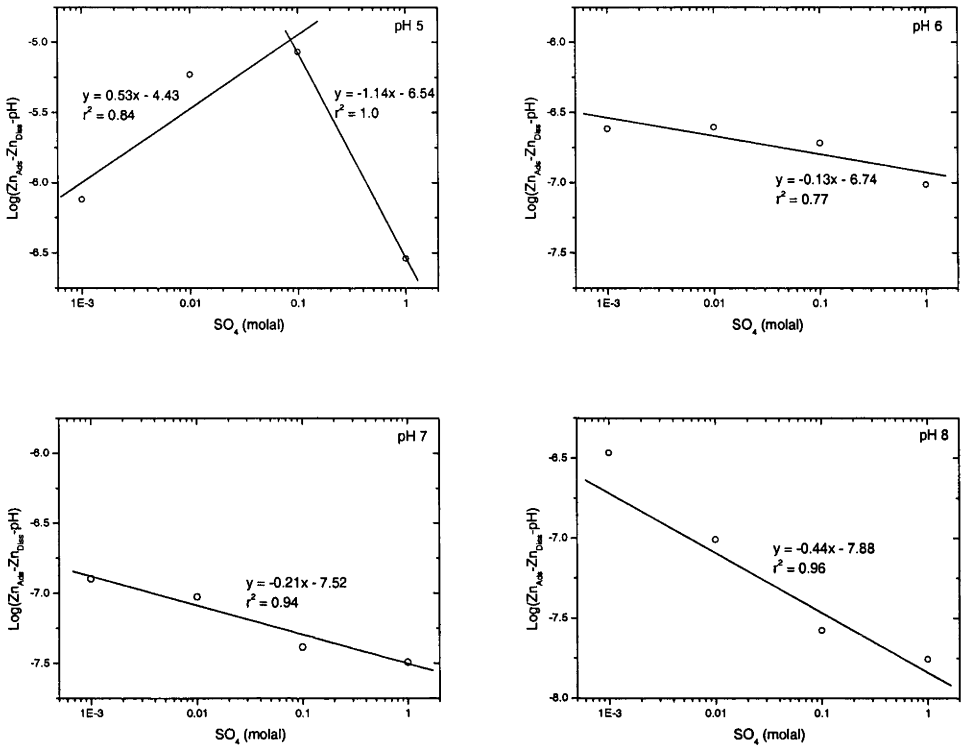

Figure 4.14: Log$[Zn]_{Ads}$ – log$[Zn]_{Diss}$ – pH versus Log SO_4^{2-} showing Zn adsorption onto goethite in over the entire range of Na_2SO_4 used in experiments for pH 5, 6, 7 and 8. The small number of data points makes it difficult to comment on the stoichiometry of dominant adsorption reactions and corresponding zinc surface complexes, however, these are plotted to indicate the possible influence of SO_4^{2-}.

The effect of sulfate on Zn adsorption is shown in Figure 4.14 by plotting log$[Zn_{Ads}]$-log$[Zn_{Diss}]$-pH versus Log $[SO_4^{2-}]$ to isolate the effect of SO_4^{2-} for pH 5, 6, 7 and 8. The low number of sulfate concentrations used in experiments makes it difficult to infer the effect of SO_4^{2-} confidently. However, the best fit lines are plotted in Figure 4.14 as an indicator for possible SO_4^{2-} effects. Figure 4.4 shows that sulfate has the greatest influence at pH 5, between SO_4^{2-} concentrations 0.001 and 0.1 molal where the slope of the best fit line is 0.5.

However, at pH > 5 the slopes of the best fit line range between -0.13 and -0.44, suggesting that there is no or little dependence on sulfate. Reactions that may describe the trends of the best fit lines are presented in Equations 4.14 – 4.17

$$\equiv SOH + Zn^{2+} + SO_4^{2-} = \equiv SOZnSO_4^- + H^+ \qquad (4.14)$$

$$\equiv SOH + Zn^{2+} + SO_4^{2-} + H_2O = \equiv SOH_2ZnSO_4 + OH^- \qquad (4.15)$$

$$\equiv SOH + Zn^{2+} + SO_4^{2-} = \equiv SOHZnSO_4 \qquad (4.16)$$

$$\equiv SOH + ZnSO_4 + H_2O = \equiv SOZnOH^0 + SO_4^{2-} + 2H^+ \qquad (4.17)$$

Reactions in Equations 4.14 - 4.16 show sulfate dependence, and have a slope of 1 when plotted as $\log[Zn_{Ads}]$-$\log[Zn_{Diss}]$-pH versus Log $[SO_4^{2-}]$. The positive slope calculated at pH 5 in Figure 4.14 occurred between 0.001 and 0.1 molal SO_4^{2-}. It is possible that the slope of 0.5 indicates that one or more of these reactions are present in experiments, in conjunction with other sulfate independent reactions (i.e., Equations 4.12 and 4.13). The negative slope of the best fit lines at pH 6, 7 and 8 with increasing sulfate concentration may be due to the reaction in Equation 4.17. In Chapter 3, it was shown that the formation of the $\equiv SOZnOH^0$ surface complex was predicted to predominate in $NaNO_3$ and NaCl (upto 1.0 molal NaCl) in solutions between pH 7 and 8, therefore the reaction in Equation 4.17 is plausible.

The reactions described in Equations 4.14 – 4.17 derived from Figures 4.13 and 4.14 are inferred. These were used identify likely zinc surface complexes for fitting the

experimental data with the CCM, where the predicted surface complexes to describe the experimental data were fitted.

4.5.2 Surface Complexation Modelling

As described in Section 4.2.1, the CCM model was used to predict the formation of Zn surface complexes on goethite. A detailed description of the CCM is made in Chapter 2, while the parameter and assumptions made in the model used for modeling Zn adsorption are made in Section 4.4.2.1.

4.5.2.1 Fitting Equilibrium Constants

In this section, equilibrium constants for the formation reactions of zinc surface complexes in 0.001, 0.01, 0.1 and 1.0 molal Na_2SO_4 are fitted to experimental data. Results of the fitted log K values are shown in Figure 4.10.

The experimental data was fitted for each individual Na_2SO_4 concentration (i.e., 0.001, 0.01, 0.1 and 1.0 molal Na_2SO_4) using the scenarios: (a) fitting with the zinc surface reactions in Equations 4.12 and 4.13 based on fitted surface complexes in $NaNO_3$ solutions (refer to Chapter 3; Section 3.3.1); (b) adding a single zinc sulfate ternary complex ($\equiv SOZnSO4^{-1}$ and $\equiv SOH_2ZnSO_4^{+}$); and (c) combing two zinc sulfate ternary complexes. The aqueous speciation for Zn was calculated with FITEQL 4.0 for the aqueous species in Table 6, using the Davies Equation for calculating activity coefficients and mass balance constraints on total Na, NO_3, Zn, SO_4 and pH, and assuming an activity of $H_2O(l) = 1$. The

reason for calculating activity coefficients with the Davies Equation is described in Section 4.4.2.2.

Equilibrium constants were fitted to each data series for Na_2SO_4 (i.e. concentrations of 0.001 - 1.0 molal Na_2SO_4) only using the reactions in Equations 4.12 and 4.13. The fit of the predicted zinc adsorption with the experimental data was poor. Although the model fit the experimental data 0.001 molal Na_2SO_4, it was unable to replicate the shape of the adsorption curve for experiments in 0.01, 0.1 and 1.0 molal Na_2SO_4. This was supported by the high value for v_y (i.e., $\geq$ 38.55 for solutions 0.01, 0.1 and 1.0 molal Na_2SO_4) and and inconsistent log K values, which varied by up to 4 log units for $\equiv SOZnOH^0$ between 0.001 and 1 molal Na_2SO_4.

A single zinc sulfate ternary surface was added to the model. The surface complex proposed by Swedlund and Webster (1996) for zinc adsorption onto ferrihydrite (Equation 4.14) was used first. The fit for the predicted zinc adsorption was closer in 0.001, 0.01 and 0.1 molal Na_2SO_4, although less adsorption was predicted at pH >6 between 0.01 and 1 molal Na_2SO_4 than in experiments. The fitted equilibrium constant for the $\equiv SOZnSO_4^-$ surface complex was similar for 0.001, 0.01 and 0.1 molal Na_2SO_4, but 1.5 log K units lower in 1 molal Na_2SO_4 value for 0.001 molal Na_2SO_4. When the $\equiv SOH_2ZnSO_4$ surface complex was applied to the model, the predicted zinc adsorption did not match the experiments. Values for v_y ranged between 19.9 in 0.01 molal Na_2SO_4 and 85.6 in 1.0 molal Na_2SO_4 and the equilibrium constants varied by up to 2 orders of magnitude.

The two zinc sulfate ternary complexes were combined and fit the shape of the experimental data closely over the entire pH range in all Na_2SO_4 concentrations. The predicted adsorption is compared to the experimental data in Figure 4.10, and fitted log K values are shown in Table 4.7.

Table 4.6: Formation reactions and equilibrium constants used to calculate Zn adsorption onto goethite in 0.001-0.1 molal Na_2SO_4 solutions.

Species	Mass Action Reaction	Log K	Source
OH-	$OH + H = H_2O$	*13.98*	*a*
NaOH(aq)	$Na^+ + OH^- = NaOH(aq)$	*0.1*	*b*
$ZnNO_3^+$	$Zn^{2+} + NO_3^- = ZnNO_3^+$	*-0.40*	*b*
$Zn(NO_3)_2(aq)$	$Zn^{2+} + 2NO_3^- = Zn(NO_3)_2(aq)$	*0.30*	*b*
$ZnOH^+$	$Zn^{2+} + H_2O = ZnOH^+ + H^+$	*9.00*	*b*
$Zn(OH)_2(aq)$	$Zn^{2+} + 2H_2O = Zn(OH)_2(aq) + 2H^+$	*16.89*	*b*
$NaNO_3(aq)$	$Na^+ + NO_3^- = NaNO_3(aq)$	*-0.55*	*a*
$NaSO_4^-$	$Na^+ + SO_4^{2-} = NaSO_4^-$	*-0.74*	*b*
$ZnSO_4(aq)$	$Zn^{2+} + SO_4^{2-} = ZnSO_4(aq)$	*-2.34*	*b*
$Zn(SO_4)_2^{2-}$	$Zn^{2+} + 2SO_4^{2-} = Zn(SO_4)_2^{2-}$	*-3.28*	*b*
HSO_4^-	$H^+ + SO_4^{2-} = HSO_4^-$	*-1.99*	*b*

[a] *Smith and Martel (1997)*

[b] *Allison et al. (1991)*

An attempt to fit an equilibrium constant for each zinc surface species using all of the experimental data (i.e., experimental data from 0.001, 0.01, 0.1 and 1.0 molal Na_2SO_4) was made. The results are shown in Figure 4.15 and Table 4.7, which shows a poor fit for the predicted Zn adsorption with experiments and is also reflected in the v_y value of 223.4. The closest fit of the predicted zinc adsorption and experimental data was in 0.001 molal Na_2SO_4, where adsorption was over estimated by approximately 20% for pH < 8 and 1.0

molal Na_2SO_4 which underestimated by approximately 20% at pH < 8. In 0.01 and 0.1 molal Na_2SO_4 up to 2 times more Zn is predicted to be adsorbed between pH 5 and 9 than shown in experiments.

Table 4.3: Equilibrium constants for species used to model Zn^{II} adsorption onto goethite for each concentration of Na_2SO_4. Equilibrium constants describe formation reactions of species and activity coefficients for aqueous species were calculated with the Davies Equation in FITEQL 4.0. Other surface complexes used in the model include $\equiv SOH_2^+$ (log K = 6.36); SO^- (log K = -10.44) from Richter et al. (2005); $\equiv SOHZn^{2+}$ and $\equiv SOZnOH^0$ (calculated in Chapter 3); $\equiv SOH_2HSO_4^0$ (log K = 13.5) from Persson and Lövgren (1996).

Species	**Log K (Concentration of Na_2SO_4)**				
	0.001	***0.01***	***0.1***	***1***	***0.001-1***
$\equiv SOZnSO_4^-$	-3.42	-4.06	-3.78	-2.41	-2.88
$\equiv SOH_2ZnSO_4^+$	12.35	13.36	13.44	13.73	13.64
Vy	2.91	2.46	4.7	3.15	223.4

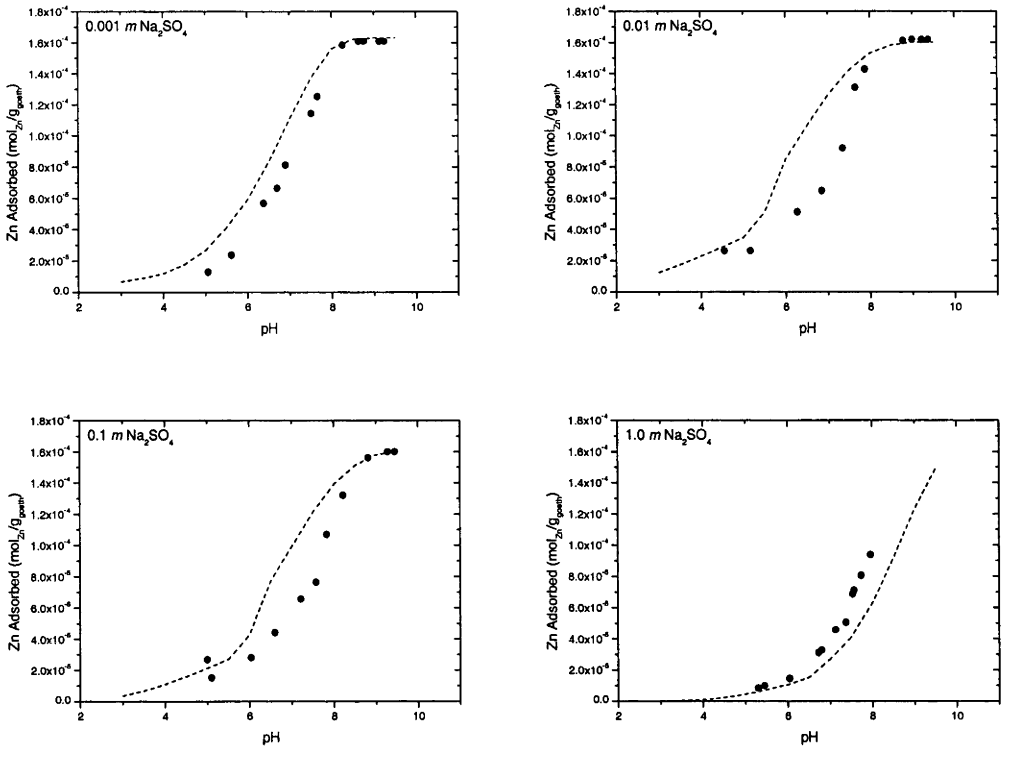

Figure 4.15: Zinc adsorption onto goethite as a function of pH in 0.001, 0.01, 0.1 and 1.0 molal Na_2SO_4. The log K for $\equiv SOZnSO_4^-$ and $\equiv SOH_2ZnSO_4^0$ was fitted to all the experimental data from 0.001 – 1.0 molal Na_2SO_4. Log K for $\equiv SOHZn^{2+}$ = 7.37 and $\equiv SOZnOH^0$ = -11.76.

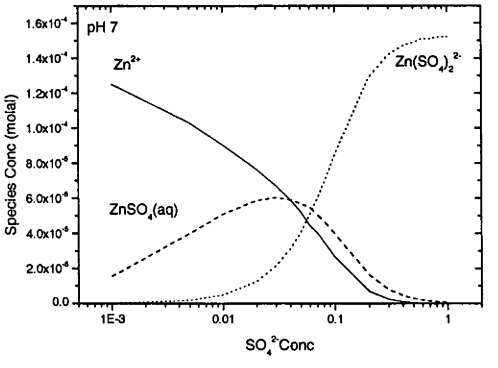

Figure 4.16: Predicted aqueous speciation of Zn^{II} as a function of sulfate concentration at pH 5 and 8 at 25°C and 1 atmosphere.

The surface speciation of zinc as a function of Na_2SO_4 for pH 7 is shown in Figure 4.16, where the dominant surface species changed as a function of the Na_2SO_4 concentration and pH. For example, in 0.001 molal Na_2SO_4, $\equiv SOHZn^{2+}$ is the dominant surface complex between pH 4 and 7, but in 0.01 molal Na_2SO_4, $\equiv SOH_2ZnSO_4$ is the dominant complex, reflecting the enhanced Zn adsorption. The decrease of zinc adsorption in solutions with greater than 0.01 Na_2SO_4 coincides with the formation of the $ZnSO_4(aq)$ and $Zn(SO_4)_2^{2-}$ complexes and suggests that Zn prefers to form zinc sulfate aqueous complexes which restrict zinc adsorption. The results of this study partly agree with those of Swedlund and Webster (1996) who proposed that the formation of the $ZnSO_4$ ternary surface complexes enhanced adsorption in acidic pH. However Swedlund and Webster do not describe a decrease of adsorption in higher concentrations of Na_2SO_4. Furthermore, the study of Swedlund and Webster used ferrihydrite as the adsorbing mineral and the different surface structure may result in the formation of other surface complexes. It is also possible that different experimental conditions (i.e. concentration of Na_2SO_4, concentration of Zn^{II}, and concentration of solid material) may change adsorption behaviour. Swedlund and Webster observed that in the presence of SO_4^{2-}, Zn adsorption increased by approximately 40% when the Zn/Fe ratio was low ($Zn/Fe = 3.17\times10^{-4}$). However, the measured increased was <5% when the Zn/Fe ratio was higher ($Zn/Fe = 7.57\times10^{-3}$). In our experiments, the Zn/Fe ratio was higher than those of Swedlund and Webster at 1.83×10^{-2}:1, which may explain why the experiments in this study showed a decrease in adsorption in higher Na_2SO_4 concentrations.

4.6 Summary and Conclusions

The results of this study indicated that zinc adsorption was enhanced by the presence of small concentrations of sulfate anions in acidic solutions (i.e. pH 4 – 6). The greatest enhancement was observed at pH 4 and 5 in solutions with 0.001 and 0.01 molal Na_2SO_4, where adsorption was increased by approximately 3 times. However, in neutral or more alkaline solutions no enhancement was observed. When the Na_2SO_4 concentration was greater than 0.01 molal less zinc was adsorbed onto goethite when the pH was constant, indicating that SO_4^{2-} suppressed adsorption. The initial enhancement of zinc adsorption is due to the formation of zinc sulfate surface ternary complexes such as $\equiv SOH_2ZnSO_4^0$ and $\equiv SOZnSO_4^-$, similar to those described by Swedlund and Webster (1996) for zinc adsorption onto schwertmannite and ferrihydrite. At higher Na_2SO_4 concentrations in acidic solutions, the formation of the aqueous species $ZnSO_4^0$ and $Zn(SO_4)_2^{2-}$ prevented the adsorption of zinc, although when the pH increased, adsorption occurred when $\equiv SOHZn^{2+}$ and $\equiv SOZnOH^0$ predominated. The results of experiments suggest that zinc sulfate ternary complexes adsorb onto goethite in solutions with low SO_4^{2-} (i.e less than 0.01 molal), but in solutions with greater than 0.01 molal zinc prefers to exist as aqueous zinc sulfate complexes.

Unlike zinc, no clear enhancement of copper adsorption in solutions with Na_2SO_4 was recorded. A small decrease in copper adsorption of approximately 10% was noted in experiments with 0.1 Na_2SO_4, between pH 4 and 6. Fitting the experimental data with only the $\equiv SOHCu^{2+}$ and $\equiv SOCu^+$ surface complexes resulted in a poor fit with the experimental data. The addition of the $\equiv SOHCuSO_4^0$ surface complex improved the fit, however, it was

unable to replicate the slope of the experimental data. The formation of aqueous copper sulfate complexes is predicted to predominate in solutions with greater than 0.01 molal SO_4^{2-}. Therefore the results of our experiments suggest that copper prefers to remain in solution as copper sulfate aqueous complexes which prevent adsorption. This is in contrast to the results of Swedlund and Webster (2001) who concluded that copper adsorption on schwertmannite and ferrihydrite was strongly enhanced in solutions with SO_4^{2-}. There are several possible explanations for the difference between our results and those of Swedlund and Webster (2001) such as different surface complexation properties between ferrihydrite, schwertmannite and goethite, while the SO_4^{2-} concentrations used by Swedlund and Webster (2001) were lower than those in this study.

The results of this study indicate that the mobility of zinc and potentially other metals may be restricted by the presence of sulfate, assuming that adsorption is a controlling factor. However, this trend may be reversed as sulfate concentrations increase and aqueous metal sulfate species predominate. For example, the interaction of solutions with high sulfate and or chloride concentrations with relatively fresh water may promote adsorption inhibit metal mobility, potentially concentrating metals in a confined area where the solutions mix. Further studies are still required to understand the role of metal adsorption in natural environments. This chapter has highlighted the importance of understanding the mineralogical component, and how oxidized copper and zinc mobility can be either enhanced or restricted with increasing sulfate concentrations. The behavior of natural groundwater conditions may influence adsorption as the geochemistry is likely to be more complex than the conditions used in our experiments (since chloride and sulfate anions are

likely to coexist in natural conditions). The potential effect combining chloride and sulfate anions in a single solution is addressed in the following chapter.

Chapter 5: Predicted Adsorption in a Multi Element Experiment and Measured Data from Lake Tyrrell, Victoria, Australia

5.1 Introduction

Previous chapters discuss the adsorption of metals, such as Cu^{II} and Zn onto mineral surfaces and how it may influence metal dispersion in natural, low temperature near surface environments, groundwater and soil contamination. Adsorption studies have only recently considered the wide range of mineralogical, geochemical and biochemical factors (i.e. Jong and Parry, 2004; Ikhsan et al., 2005; Düker et al. 1995; Balistrieri and Murray, 1982) that occur in natural environments, and understanding the effect of these factors is still limited.

This chapter aims to use the equilibrium constants derived from Chapters 2 – 4 and predict Cu^{II} and Zn adsorption in multi element conditions (i.e. solutions with Cu^{II}, Zn, NaCl and Na_2SO_4). The calculated thermodynamic properties are also applied to data from Lake Tyrrell in an attempt to predict the concentration of Cu^{II} and Zn adsorption in this natural system.

5.2 The Effect of Anion Competition on Copper and Zinc Adsorption

Previous studies have examined the effect of individual anions including sulfate (c.f. Ali and Dzombak, 1996; Persson and Lövgren, 1996) and chloride (i.e. Padmanabham 1980; Swallow et al., 1980; Barrow et al., 1982; Kanungo, 1994; Bargar et al., 1998; Kim et al., 2004) on metal adsorption. However, the study of Balistrieri and Murray (1982) is the only published study that examines the effect of coexisting anions on metal adsorption. This is surprising given that groundwater geochemistry often has significant chloride and sulfate coexisting in the same solution (e.g. Herczeg et al. 1991). To test this, an experiment with 1 molal NaCl and 0.1 molal Na_2SO_4 and 1.57×10^{-4} molal Cu^{II} and 1.50×10^{-4} molal Zn was conducted and compared to the results of Balistrieri and Murray (1982). Equilibrium constants for Cu^{II} and Zn surface complexes derived in Chapters 2-4 were used to model the same conditions used in the experiment and calculate adsorption over a range of NaCl and Na_2SO_4 concentrations.

Experiments contained 1.0 molal NaCl and 0.1 molal Na_2SO_4, a Cl^- to SO_4^{2-} ratio of 10:1 consistent with groundwater sampling data obtained in central NSW (Lenehan, pers comm. 2005). These concentrations were selected because they showed the largest changes of copper and zinc adsorption as a function of anion concentration described in Chapters 2 – 4. The ratio of Cl^- to SO_4^{2-} is in the mid-range for those found in natural environments. For example, Herczeg et al. (1991) measured groundwater from the Great Artesian Basin, Australia with Cl^- to SO_4^{2-} ratios ranging from 75:1 to 4.5:1.

The anion concentrations used by Balistrieri and Murray (1982) were selected to simulate seawater conditions, and were NaCl = 0.53 M and Na_2SO_4 = 0.028 M (with a

Cl^- to SO_4^{2-} ratio of 18:1). Although their selected anion concentrations were lower than those of this study any effect from anion competition should still be distinguishable.

5.2.1 Experiment Method

The method of goethite synthesis was according the method outlined by Schwertmann and Cornell (1991) and is described in the preceding chapters. Adsorption was measured as a series of 12 individual experiments. 0.075 g of goethite was added to a glass reaction vessel with 80 g of 0.1 molal Na_2SO_4, 1.0 molal NaCl, 1.50×10^{-4} Zn (prepared from $Zn(NO_3)_2.6H_2O$) and 1.57×10^{-4} Cu^{II} (prepared from $Cu(NO_3)_2.2^1/_2H_2O$). The pH of each experiment was adjusted using either 0.1 M HNO_3 or 0.1 M NaOH and measured using an Orion 290A+ pH Meter and Ross Sure Flow combination electrode calibrated with Sigma-Aldrich pH 4, 7 and 10 buffers with an uncertainty of ± 0.02 pH units. Each reaction vessel was sealed with a Dreschel head and placed in a water bath at 25°C ± 0.1. $N_2(g)$ was passed through a glass reaction vessel containing ultrapure water to minimise evaporation, and then into each reaction vessel to generate an inert atmosphere and minimise the effect of CO_2 adsorption and mix the solution.

Samples were left to equilibrate overnight for 16 hours, before being removed and the final pH measured. The goethite was filtered from each experiment using a 0.45 μm syringe filter, while the supernatant solution was preserved by adding several drops of 10% HNO_3. The solutions were analysed for copper, zinc and iron using a Varian Vista Pro Axial ICP-AES. The concentration of adsorbed copper and zinc was assumed to be the difference between the intial and final metal concentrations.

5.2.2 Results

Results for Cu^{II} and Zn adsorption onto goethite in solutions with 1.0 molal NaCl and 0.1 molal Na_2SO_4 are shown in Figure 5.1 and listed in Appendix D. These results are compared to the single end member experiments from Chapters 2 – 4 in Figure 5.1.

The adsorption of Cu^{II} and Zn in the combined NaCl and Na_2SO_4 was compared to the end member experiments with NaCl or Na_2SO_4 (Figure 5.1) and is summarised in Table 5.1. The adsorption of both copper and zinc onto goethite was lower in the combined 1.0 molal NaCl and 0.1 molal Na_2SO_4 at pH > 6 when compared to the results of the single element experiments. Zn adsorption was up to 50% lower in the combined NaCl and Na_2SO_4 experiment, compared to adsorption in 1.0 NaCl, and 30% lower than adsorption in 0.1 molal Na_2SO_4. Cu^{II} adsorption was up to 5 times greater (at pH 3.3) in 1 molal NaCl between pH 2.3 and 6.7, but adsorption was increased by approximately 20% in the combined NaCl and Na_2SO_4 when compared to the 0.1 molal Na_2SO_4 experiment.

Copper and zinc adsorption is dependent on the aqueous speciation of each metal, where adsorption decreased in solutions with > 1.0 molal NaCl and 0.01 molal Na_2SO_4. The aqueous speciation of copper and zinc in 0.1 molal Na_2SO_4 and 1.0 molal NaCl as function of pH (Figure 5.4) was calculated and the results are shown in Figure 5.2.

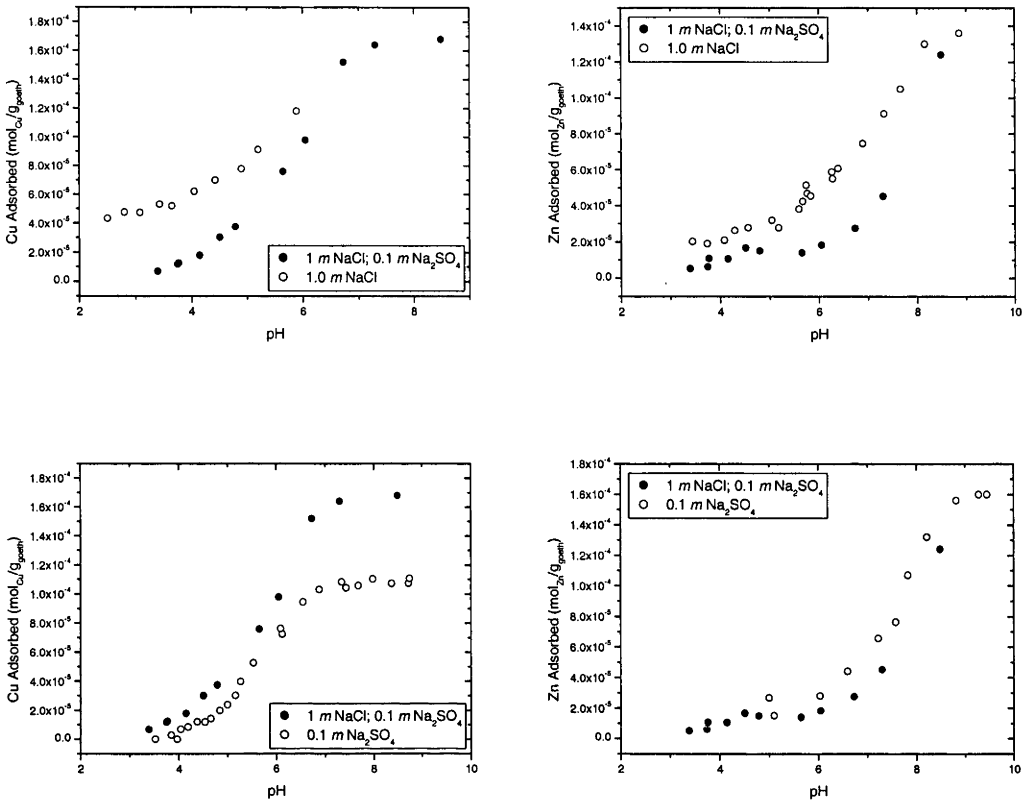

Figure 5.1: Adsorption of Cu^{II} and Zn onto goethite (0.9375 g/L) in 1.0 molal NaCl and 0.1 molal Na_2SO_4, compared to adsorption in 1.0 molal NaCl.

Table 5.1: Effect of anion concentration in combined Cu^{II} and Zn adsorption in combined Na_2SO_4 and NaCl solutions.

	Effect of SO_4 on Cl system	**Effect of Cl on SO_4 system**
Cu^{II}	Reduced adsorption at low pH	Increased adsorption at high pH
Zn	Reduced adsorption at pH 5-7	Slightly reduced adsorption at pH 5-7

The predominant aqueous copper species include Cu^{2+}, $CuCl^{+}$ and $CuSO_4(aq)$ at pH < 8.5, while $Cu(OH)_2(aq)$ predominates at pH > 8.5. Precipitation of the copper minerals brochantite ($Cu_4(OH)_6SO_4$), antlerite ($Cu_3(OH)_4SO_4$) and langite ($Cu_4(OH)_6SO_4.H_2O$) were predicted to occur at pH 6.5 when the dissolved Cu^{II} concentration was 1.57×10^{-4} molal. However, after the adsorbed component of Cu^{II} is removed approximately

1.4×10^{-5} molal of Cu^{II} is dissolved and precipitation of these minerals is unlikely. The aqueous zinc speciation in the same solution is dominated by Zn^{2+}, $ZnCl^{-}$ and $ZnCl_2(aq)$ and $ZnSO_4$ at pH < 8.5, and $Zn(OH)_2(aq)$ predominate at pH >8.5. Aqueous $Zn(SO_4)_2(aq)$ and $ZnOH^{+}$ were also included in the predicted speciation but were omitted from Figure 5.2 due to their low concentrations.

In Chapter 4, it was shown that copper sulfate aqueous complexes decreased Cu^{II} adsorption in solutions with >0.001 molal Na_2SO_4, due to the formation of $CuSO_4(aq)$ rather than being adsorbed. This was again inferred in the NaCl and Na_2SO_4 experiment where the concentration of Cu^{II} adsorbed in the 1.0 molal NaCl and 0.1 molal Na_2SO_4 experiment was lower than the 1.0 molal NaCl experiment. Zn adsorption exhibited a similar behaviour with less adsorption in the combined 1.0 molal NaCl and 0.1 molal Na_2SO_4 solution when compared to both the 1.0 molal NaCl experiment or the 0.1 molal Na_2SO_4 experiment. Again, this was explained by the preference for zinc aqueous complexes $ZnCl^{-}$, $ZnCl_2(aq)$ or $ZnSO_4(aq)$ rather than being adsorbed in onto goethite.

The Constant Capacitance Model in Visual MINTEQ was used to predict in Cu^{II} and Zn adsorption in 1.0 molal NaCl and 0.1 molal Na_2SO_4 (Figure 5.2). The Debye-Hückel "b-dot' equation was used to calculate activity coefficients for each experiment and concentrations of total Cu, Zn, Na, Cl, sulfate and nitrate. The transfer of equilibrium constants from FITEQL 4.0 to Visual MINTEQ was tested by calculating Cu^{II} adsorption onto goethite in 0.1 and 1.0 molal NaCl. The adsorption parameters used in FITEQL 4.0 were applied to Visual MINTEQ and the results showed that the predicted Cu^{II} adsorption from Visual MINTEQ was similar to the experimental results (Figure 5.3).

At pH > 6, the predicted Cu^{II} adsorption was similar to the experimental results, while at pH < 6, there is less agreement. The slope of the predicted adsorption curve was steeper than the slope of the experimental data and at low pH the predicted adsorption reached a minimum at 2.0×10^{-5} mol/g, while the experimental data approached zero. The surface species, plotted in Figure 5.2, show that $\equiv SOCu^{+}$ predominates at pH > 5, while at pH < 5 the formation of $\equiv SOHCuSO_4^{0}$ and $\equiv SOHCuCl^{+}$ account for the predicted adsorption.

The modelled Zn adsorption showed that the adsorption edge would be between pH 6 and 9, which was consistent with the experimental data. The slope of the predicted adsorption edge was steeper than the measured adsorption from the experiment between pH 6 and 7.5. At pH < 6, the model shows that adsorption is negligible, while the experimental data shows that approximately 1.5×10^{-5} mol/g Zn is adsorbed between pH 4 and 6. The $SOZnSO_4^{-}$ surface species is predicted to be the predominant surface complex between pH 5.5 and 7.5 despite Zn^{2+}, $ZnCl^{+}$ and $ZnCl_2(aq)$ occurring as the predominant aqueous species over the same pH range.

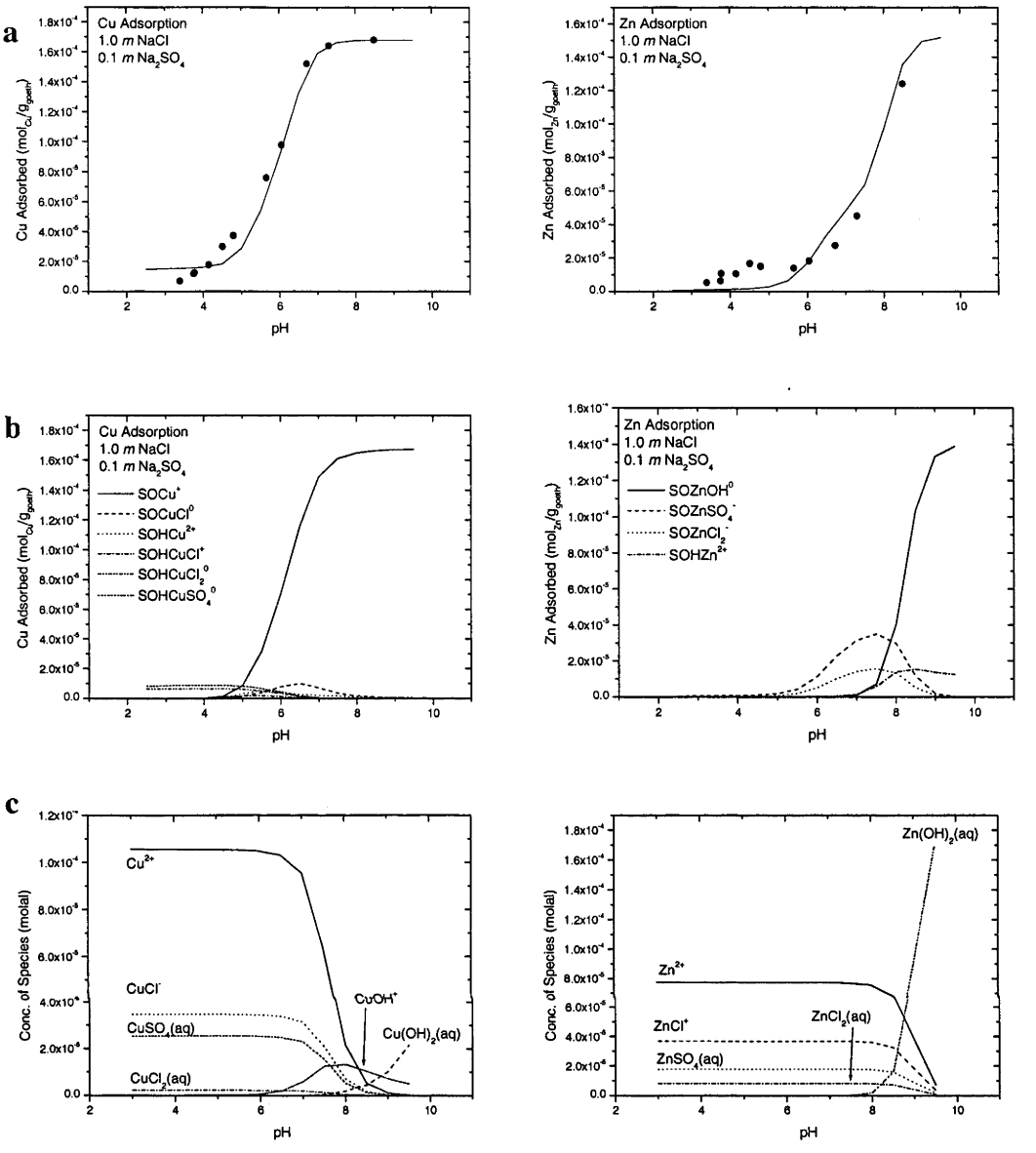

Figure 5.2: **(a)** Adsorption of Cu^{II} and Zn onto goethite (0.9375 g/L) in 1.0 molal NaCl and 0.1 molal Na_2SO_4, 10ppm Cu^{II} and 9ppm Zn^{II} at 25°C and 1 atmosphere. Solid lines show the predicted adsorption of copper and zinc calculated with the CCM. Equilibrium constants for the formation of Cu^{II} and Zn surface complexes are listed in Tables 2.4, Table 3.4 and Table 4.3. **(b)** Predicted Cu^{II} and Zn surface species on goethite in 1.0 molal NaCl and 0.1 molal Na_2SO_4. **(c)** Aqueous speciation of Cu^{II} and Zn in 1.0 molal NaCl and 0.1 molal Na_2SO_4 as a function of pH without the presence of goethite. Equilibrium constants are for formation reactions and are listed in Tables 2.3 and 3.3. Activity coefficients were calculated using the Debye-Hückel Equation.

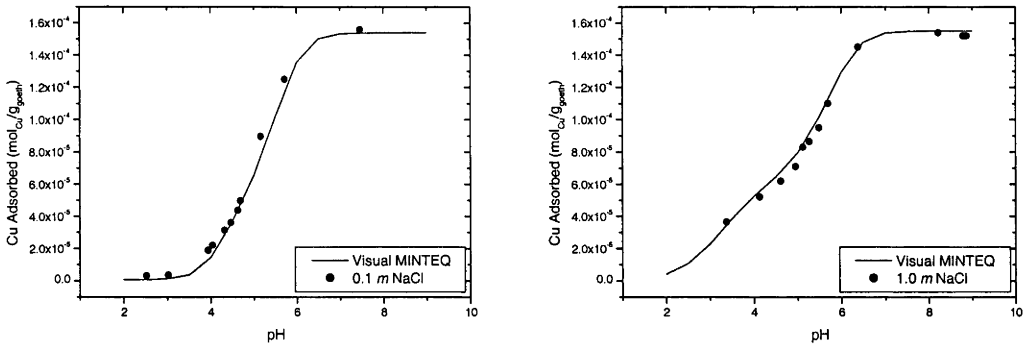

Figure 5.3: Predicted copper adsorption calculated with Visual MINTEQ compared to 0.1 and 1.0 molal NaCl experimental data showing that equilibrium constants fitted in FITEQL are transferable to Visual MINTEQ for NaCl data.

The close match between the predicted adsorption of Cu^{II} and Zn and the experimental data, especially at higher pH (i.e. pH > 6 for Cu^{II} and pH > 7 for Zn), shows that Cu^{II} and Zn adsorption can be predicted in complex solutions with the equilibrium constants calculated in Chapters 2 – 4. The small differences between experimental and model datasets in acidic conditions may be caused by one or more of the following reasons: (a) the concentration of adsorbed metal is incorrect due to analytical error associated with the experimental data; (b) incorrect identification of the surface species being present on goethite; or (c) possible ionic strength effects on pH, which shift the apparent pH for the data points.

Measuring small concentration changes in solutions with high concentrations of Cu^{II} or Zn is prone to error. The analytical error of the experiments was estimated conservatively at ±5% and because the experiments initially contain 1.57×10^{-4} molal Cu^{II} or 1.50×10^{-4} molal Zn, the error is $\pm7.85\times10^{-6}$ molal Cu^{II} or 7.65×10^{-6} molal Zn. This is similar to the concentration of adsorbed metal in acidic conditions, therefore the

difference between the experimental results and the predicted adsorption from the CCM at low pH may not be statistically significant.

The effect of ionic strength on pH was addressed in Chapter 2 where experiments aimed to determine how ionic strength influenced pH. Results from these experiments were inconclusive. The effect of ionic strength, if any, is unclear and requires further work. Until such time, it is assumed that the measured pH is correct.

The Cu^{II} and Zn surface complexes, and their associated equilibrium constants, used in the model were calculated in simple single anion systems. Iit is possible that both Cl^- and SO_4^{2-} in the same solution that additional aqueous and surface complexes containing both anions may exist (i.e. $CuClSO_4^-$) although no such complexes are reported in the literature. The amount of experimental data was insufficient to confirm the presence of such species with any confidence.

Results from the combined 1.0 molal NaCl and 0.1 molal Na_2SO_4 solution show that the concentration of sulfate decreases the influence of chloride ions and this effect is strongest for copper as shown in Figure 5.4. This finding agrees with that of Balistrieri and Murray (1982) and their conclusion regarding the independence of NaCl on adsorption. However, this is only true when both NaCl and Na_2SO_4 are present in the same solution. When chloride is the only anion in solution, copper and zinc adsorption increase with chloride, as shown in Chapters 2 and 3.

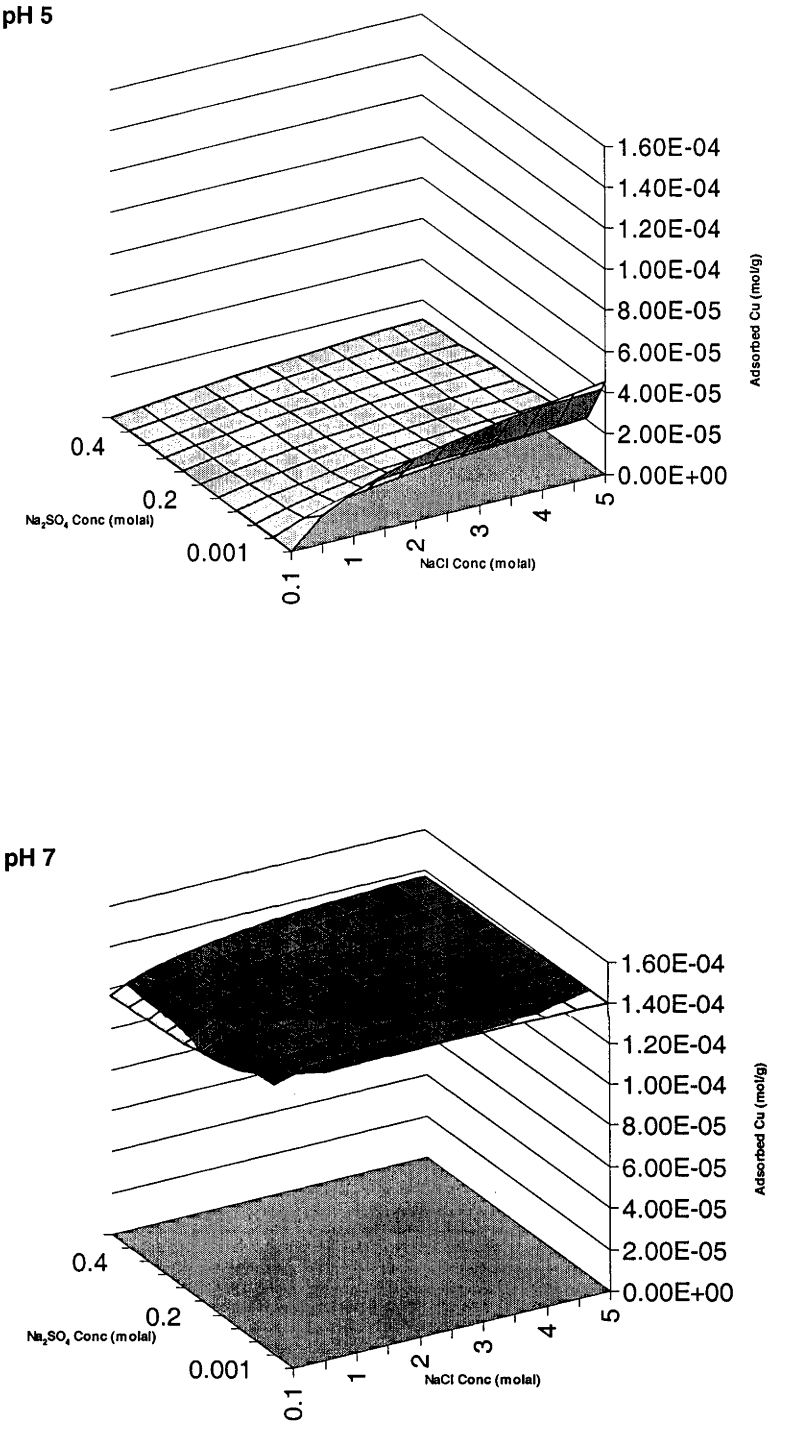

Figure 5.4: Predicted copper adsorption calculated with the CCM as a function of NaCl and Na_2SO_4 concentration at pH 5 and 7.

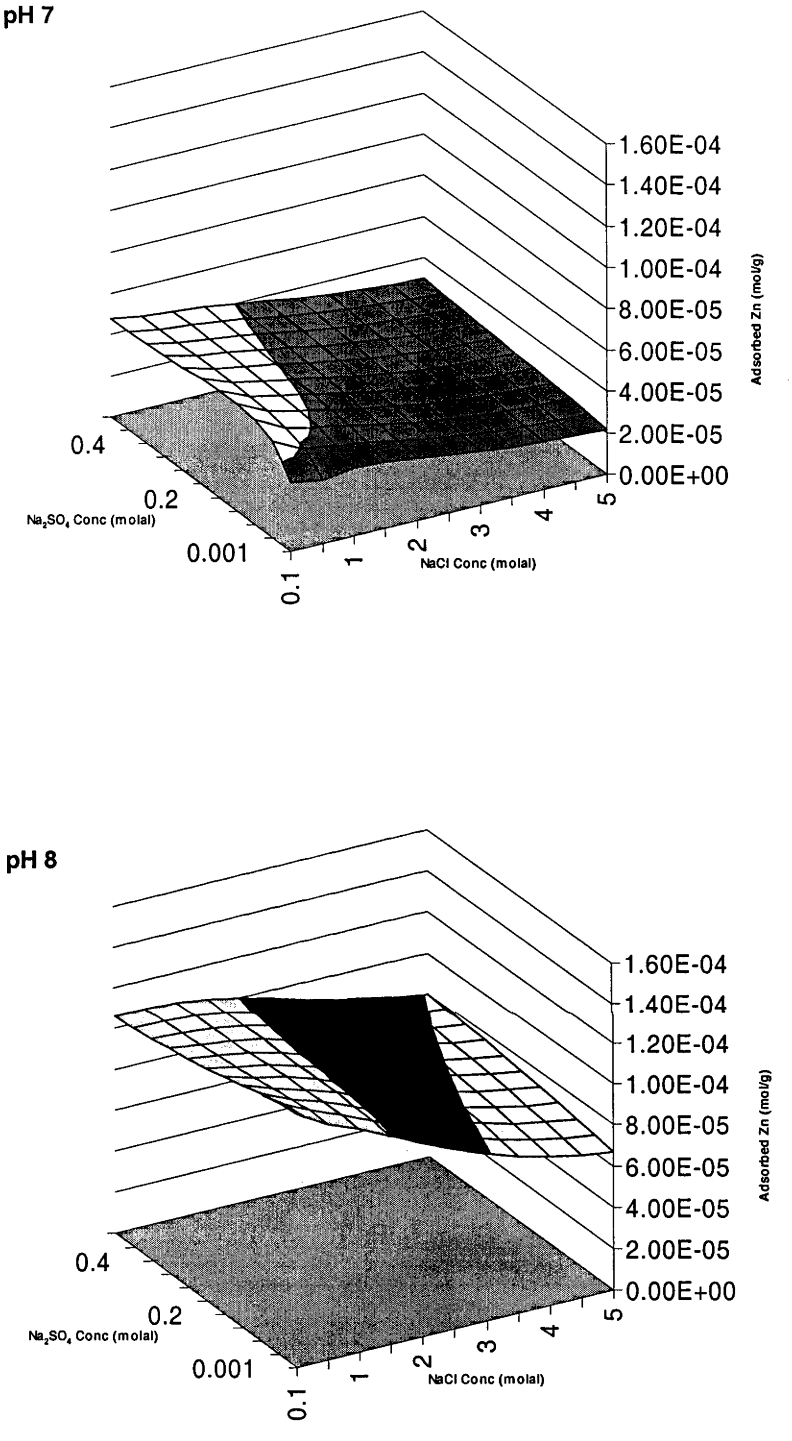

Figure 5.5: Predicted zinc adsorption calculated with the CCM as a function of NaCl and Na_2SO_4 concentration at pH 7 and 8.

The CCM was used to predict adsorption as a function of NaCl and Na_2SO_4 concentration between NaCl concentrations of 0.1 and 5 molal and Na_2SO_4 concentrations between 0.001 and 0.4 molal for pH 4 and 7 for copper and pH 7 and 8 for zinc. The predicted adsorption was calculated with the equilibrium constants calculated in Chapters 2-4 and the results are shown in Figure 5.4 and 5.5. Zn adsorption was shown to increase with rapidly between 0.001 and 0.1 molal Na_2SO_4, but when the concentration of NaCl increased Zn decreased over the entire range of sulfate concentrations. In contrast, Cu^{II} adsorption shows a stronger NaCl dependence with adsorption increasing with increasing copper when the Na_2SO_4 concentration was 0.001 molal. However, when the sulfate concentration increased, Cu^{II} adsorption decreased rapidly.

The decrease in Cu^{II} adsorption at NaCl > 2.0 molal as described in Chapter 2 is not reflected in Figure 4.7. Several possible causes for this have been identified. Firstly, the aqueous speciation of Cu^{II} in the combined NaCl and Na_2SO_4 solution is different to the speciation of solutions without Na_2SO_4. The total aqueous concentration of copper chloride species (i.e. $CuCl^+$, $CuCl_2(aq)$, $CuCl_3^-$) is approximately 10% lower in the solution with 0.4 molal Na_2SO_4. However, this still does not explain the cause of the continual increase in Cu^{II} adsorption at NaCl concentrations >3 molal. The equilibrium constants used to fit 0.1 – 3.0 molal experiments were used to predict Cu^{II} adsorption. In Chapter 2, the log K values for copper chloride surface complexes did not successfully describe adsorption for high NaCl concentrations, which may occur again in Figure 5.4.

The predicted adsorption for both Cu^{II} and Zn presented is a qualitative analysis of adsorption over a large range of NaCl and Na_2SO_4 concentrations. While the exact

concentrations of adsorbed metals may not be correct, the model provides enough detail to predict general adsorption behaviour as a function of sulfate and chloride concentrations and may be applied to natural environments. This is tested in the following section using measured data from Lake Tyrrell, Victoria, Australia.

5.3 Predicted Adsorption at Lake Tyrrell, Victoria, Australia

The thermodynamic properties derived in the earlier chapters can be used to predict adsorption in natural environments with geochemical modelling. Experimental results show that the species of aqueous Cu^{II} and/or Zn complex influence metal adsorption onto goethite. However, chemical changes such as pH, salinity, Eh etc. or physical changes such as temperature may alter the speciation of these metals and either enhance or suppress adsorption. Lake Tyrrell in Victoria, Australia (Lyons et al., 1995; Macumber, 1992) is an example where fresh surface water mixes with saline groundwater brines.

The concentrations of Cu^{II}, Zn, Cl and SO_4 measured at Lake Tyrrell were used in a model with the equilibrium constants calculated in previous chapters to predict the effect of adsorption in a natural environment. Groundwater concentrations of chloride at Lake Tyrrell range between those of freshwater and halite saturation, i.e., $2.8 < \log [Cl]$ (mg/L) < 5.3 (Long et al., 1992), which corresponds to approximately 0.02 to 5.6 molar NaCl, while sulfate concentrations range from $3.2 < \log [SO_4]$ (mg/L) < 4.8 (Long et al., 1992), which corresponds to a range of approximately 0.2 to 0.6 molar SO_4. The pH of groundwater mostly ranges between approximately 2.5 and 4.5, although some groundwater is near neutral (Lyons et al., 1992; Long et al., 1992). Cu^{II} concentrations

observed in groundwater at Lake Tyrrell range up to 3.5 mg/L and zinc concentrations range up to 1.3 mg/L (Giblin and Dickson, 1992). Goethite is the predominant iron oxyhydroxide at Lake Tyrrell (Fegan et al., 1992) and based on the observed iron concentrations (up to 15,000 ppm; Fegan et al., 1992), the goethite concentration could be up to 2 wt% of the sediment. Assuming a porosity of 0.5, this would correspond to approximately 60 g goethite/L water, although this is considered as a maximum as it is assumed that not all the goethite would be available for adsorption. Both Cu^{II} and Zn concentrations in the sediment of Lake Tyrrell range up to approximately 20 ppm, although the highest values were observed in reduced clay-rich layers (Fegan et al., 1992).

Cu^{II} and Zn adsorption onto goethite as a function of NaCl and sulfate was predicted for a range of conditions similar to those at Lake Tyrrell using Visual MINTEQ and the thermodynamic properties for surface reactions described in Chapters 2 – 4. Activity coefficients for aqueous species were calculated with the Debye-Hückel b-dot equation because of the large range of NaCl concentrations modelled. Both copper and zinc was modelled to coexist in the same solution, with a dissolved copper concentration of 4.72×10^{-5} molal (3 ppm) and 2.30×10^{-5} molal (1.5 ppm) zinc. The goethite concentration was set to 20 g/L in the model which is a conservative estimate of available goethite for adsorption. The specific surface area of goethite was taken to be 36.05 m^2/g. Cu^{II} and Zn adsorption was modelled for pH 4 and 6, and NaCl range from 0.1 to 5 molal and Na_2SO_4 range between 0.2 and 0.4 molal to cover typical conditions at Lake Tyrrell. Temperature and pressure were taken to be 25°C, 1 bar. The predicted copper adsorption is shown in Figure 5.6, and the predicted zinc adsorption is shown in Figure 5.7.

Adsorption decreased with increasing chloride and increasing sulfate. The predicted adsorption of Cu^{II} at Lake Tyrrell at pH 4 (Figure 5.6) ranged between 6.95×10^{-7} and 5.75×10^{-7} mol_{Cu}/g_{goeth}. Assuming that adsorption is the main geochemical process controlling the concentration of Cu^{II} on goethite and Cu^{II} incorporation into the mineral structure of goethite is not significant, the concentration of Cu^{II} adsorbed per litre (mol_{Cu}/L), is between 1.39×10^{-5} and 1.15×10^{-5} mol_{Cu}/L. The concentration of adsorbed Cu^{II} at pH 6 adsorption ranged between 3.63×10^{-4} mol_{Cu}/L (equivalent to 23.1 ppm_{Cu}/L) and 3.5×10^{-4} (22.2 ppm_{Cu}/L) and decreased with increasing chloride and sulfate. The range of adsorbed copper concentrations at pH 6 is consistent with the measured copper concentration of approximately 20 ppm in the clay rich sediments at Lake Tyrrell.

Zn adsorption at Lake Tyrrell at pH 5 (Figure 5.7) was predicted to be between 2.26×10^{-7} mol_{Zn}/L (equivalent to 0.02 ppm_{Zn}/L) and 3.84×10^{-7} mol_{Zn}/L (equivalent to 0.03 ppm_{Zn}/L), and increase with increasing NaCl up to 0.5 molal, and decrease when NaCl >0.5 molal. Adsorption was also predicted decrease slightly with increasing Na_2SO_4 concentrations. At pH 6, the range of adsorbed Zn was predicted to be between 2.68×10^{-6} (0.18 ppm) and 6.10×10^{-6} (0.40 ppm). The low concentration of adsorbed zinc predicted is due to the acidic conditions used in the model. The pH of the water where Zn concentrations were measured in clay rich sediments at Lake Tyrrell was not recorded, although the pH is expected to be >7.

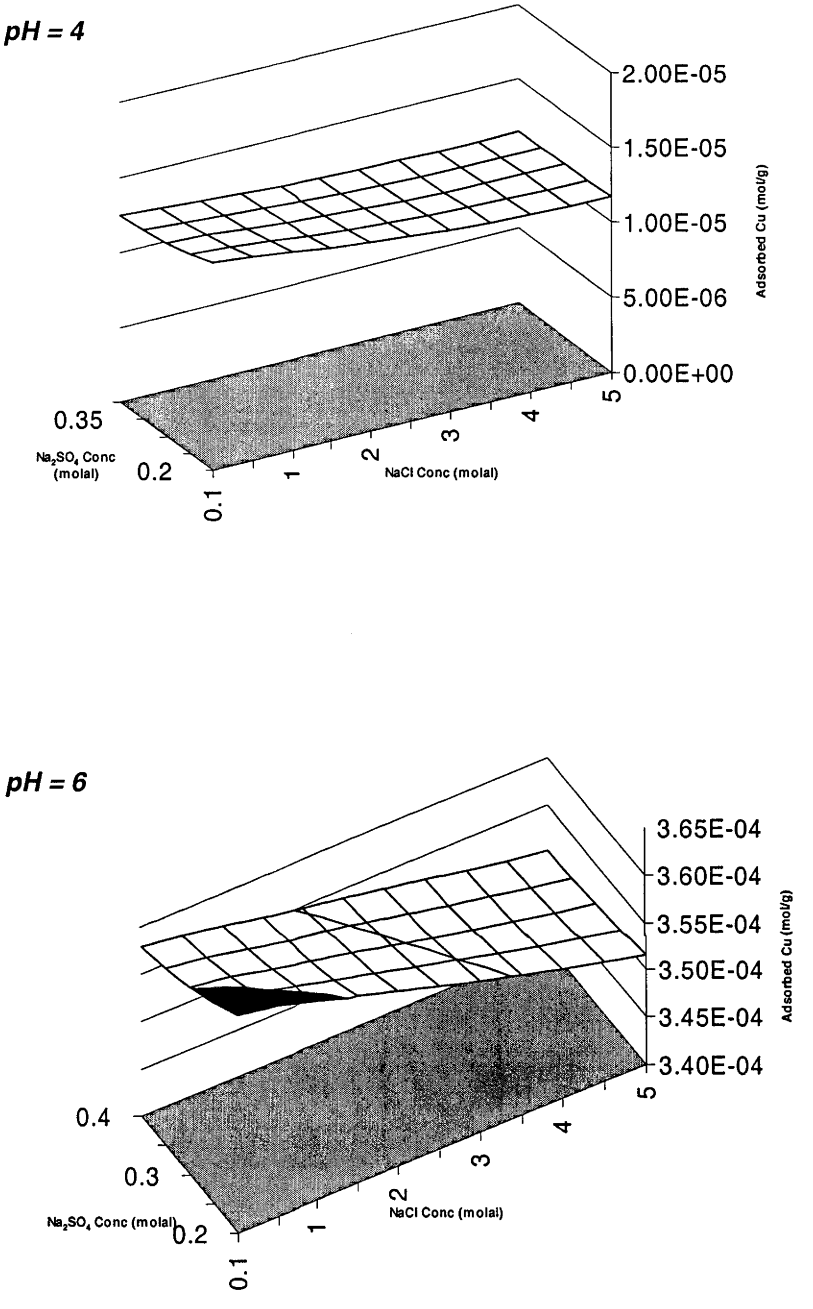

Figure 5.6: Predicted concentrations of adsorbed copper on goethite at Lake Tyrrel as a function of Cl^- and SO_4^{2-} concentration for pH 3.0 and 7.0 at 25°C and 1 bar. Total Cu^{II} concentration was 4.72×10^{-5} molal, goethite concentration of 1.0 g/L, goethite surface area of 36.05 m^2/g and surface site density of 16.4 sites/nm^2. The thermodynamic properties for adsorption reactions were determined from this study.

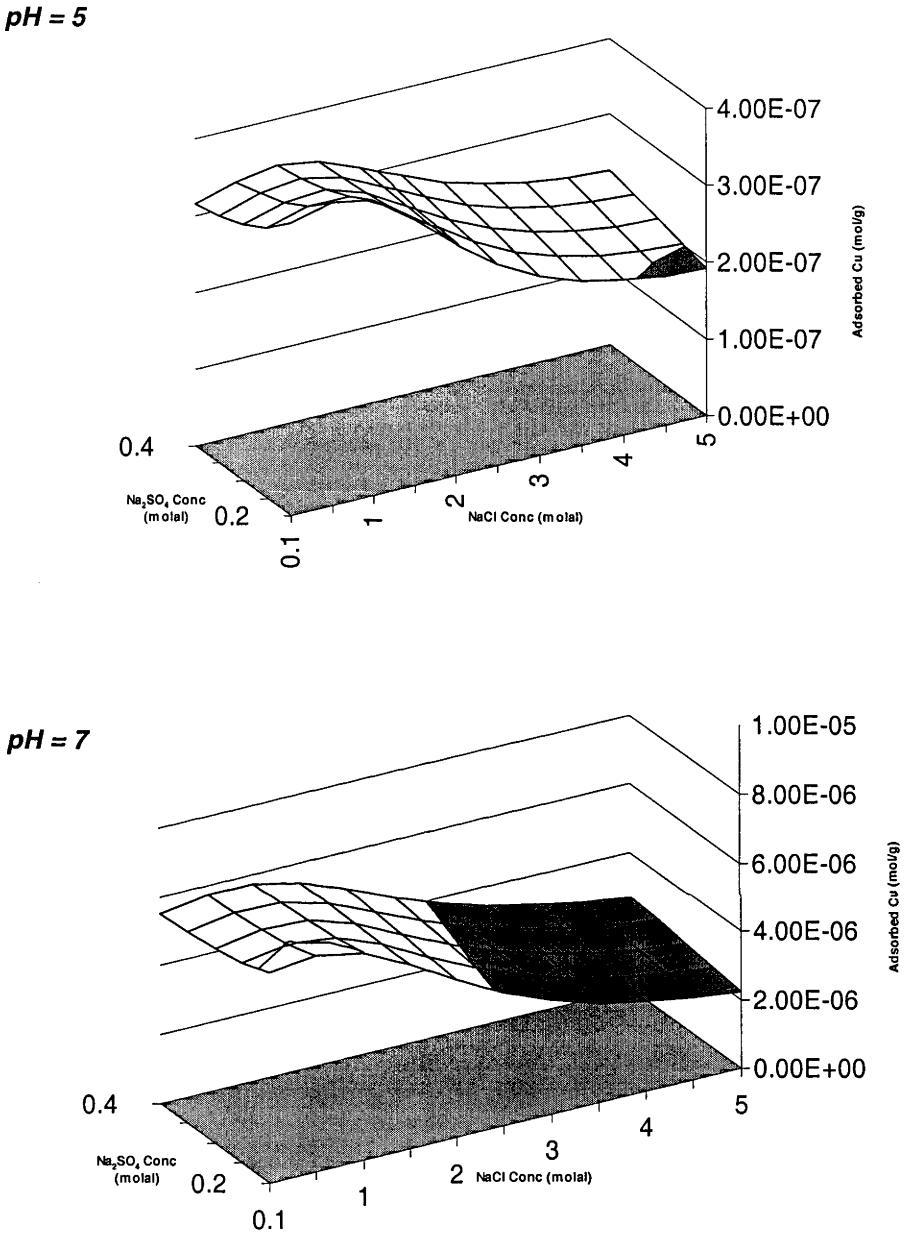

Figure 5.7: Predicted concentrations of adsorbed zinc on goethite at Lake Tyrrel as a function of Cl^- and SO_4^{2-} concentration for pH 5.0 and 7.0 at 25°C and 1 bar. Total Zn concentration was 2.30×10^{-5} molal, goethite concentration of 1.0 g/L, goethite surface area of 36.05 m^2/g and surface site density of 16.4 sites/nm^2. The thermodynamic properties for adsorption reactions were determined from this study.

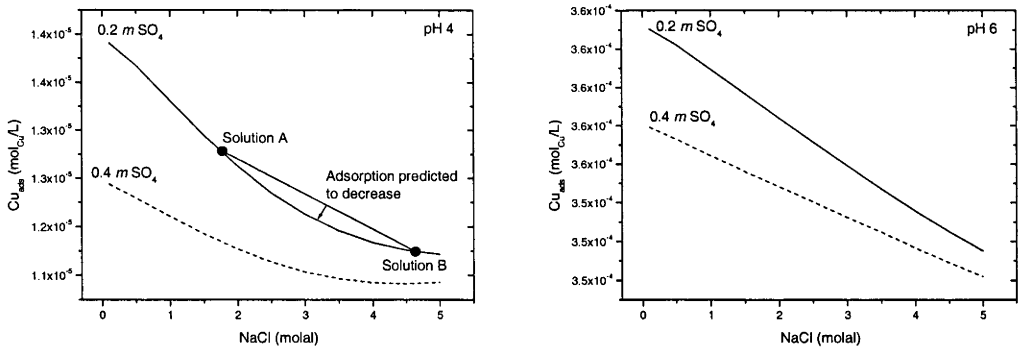

Figure 5.8: Predicted Cu^{II} adsorption at Lake Tyrrell as a function of NaCl concentration for 0.2 molal Na_2SO_4 at pH 4 and 6. Water mixing of solution A and solution B results in a decrease of Cu^{II} adsorption. At pH 6, solution mixing would decrease adsorption thereby increasing Cu^{II} mobility.

Figure 5.8 shows the predicted Cu^{II} adsorption at pH 4 and 6 for Na_2SO_4 concentrations of 0.2 and 0.4 molal. Solution mixing is considered at pH 4 (assuming that the pH of both solutions is 4) between a solution with 1 molal NaCl (Solution A) and solution with 4.5 molal NaCl (Solution B). The model predicts that mixing of these solutions will decrease Cu^{II} adsorption in acidic conditions, thereby increasing Cu^{II} mobility. At pH 6, Cu^{II} mobility is predicted to increase as metal adsorption decreases with increasing NaCl. If mixing solutions increased the pH of resulting water (i.e. mixing of an acidic solution with a near neutral pH solution), as indicated in Figure 2.8, Cu^{II} mobility will decrease as adsorption is promoted.

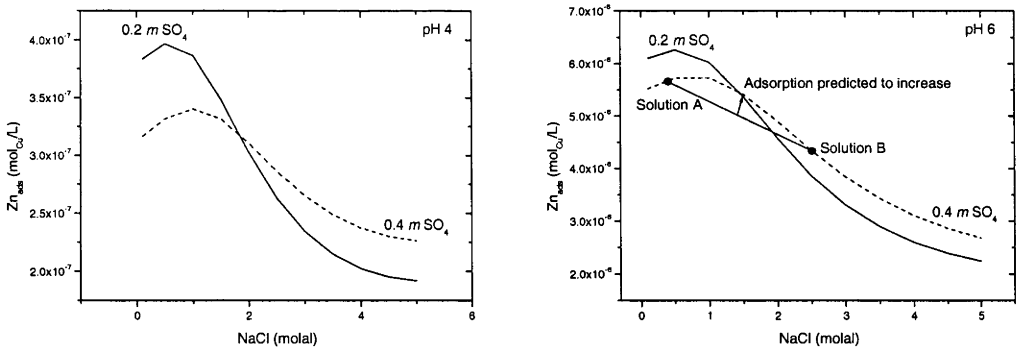

Figure 5.9: Predicted Zn adsorption at Lake Tyrrell as a function of NaCl concentration for 0.2 molal Na_2SO_4 at pH 4 and 6. Water mixing of solution A and solution B results in an increase of Zn adsorption.

Figure 5.9 shows the predicted Zn adsorption at pH 4 and 6 for Na_2SO_4 concentrations of 0.2 and 0.4 molal. Assuming that pH remains constant during mixing, a 0.5 molal NaCl solution (Solution A) and 2.5 molal solution (Solution B) is mixed. The model predicted that Zn adsorption would increase as a result of mixing at pH 6, thereby decreasing Zn mobility.

5.4 Conclusions

The result of experiments with both 1.0 molal NaCl and 0.1 molal Na_2SO_4 show that sulfate concentrations may over-ride the trends in Cu^{II} and Zn adsorption due to chloride. The concentration of adsorbed copper and zinc was lower in the combined NaCl and Na_2SO_4 solutions than observed in experiments with NaCl only. This is consistent with our earlier findings in Chapter 4 where zinc and copper adsorption was decreased in solutions with > 0.01 molal Na_2SO_4 due to the preference for these metals to remain in solution as aqueous copper and zinc sulfates. This finding is similar to that of Balistrieri and Murray (1982). Balistrieri and Murray's conclusion that the presence

of chloride does not influence copper or zinc adsorption is over simplistic, but because they did not isolate the effect of chloride in solution they were unable to see the effect of chloride as it was obscured by the effect of sulfate.

Natural environments are more complex than the conditions studied in our experiments. Despite this, thermodynamic properties derived in this study can be used in conjunction with previous research (such as that on the formation of aqueous copper chloride complexes; Brugger et al., 2002) in predictive tools such as reactive transport models and geochemical speciation models.

Chapter 6: Summary and Conclusions

6.1 Introduction

Adsorption data was presented and interpreted for Cu^{II} and Zn in a range of NaCl and Na_2SO_4 concentrations. The aim was to improve the understanding of how adsorption influences metal mobility in natural low-temperature, near-surface water and determine thermodynamic properties for use in predictive geochemical models. To achieve this, adsorption experiments were conducted with Cu^{II} and Zn in 0.1 – 5.0 molal NaCl and 0.001 – 1.0 molal Na_2SO_4 concentrations. The Constant Capacitance Model was used to interpret the experimental data, infer likely Cu^{II} and Zn surface complexes and fit the associated equilibrium constants. The key findings of this thesis are outlined below.

6.2 Key Findings

6.2.1 Copper Adsorption in NaCl Solutions

Cu^{II} adsorption in 0.1 molal $NaNO_3$ solutions showed systematic increases of adsorption with increasing pH between pH 4 and 6.5. These results were consistent with the findings of Peacock and Sherman (2004) Balistrieri and Murray (1982), Barrow et al. (1982), Padmanabham (1980) who described similar behaviour in the same experimental conditions. Surface complexation modelling with the Constant Capacitance Model implied

that the controlling copper surface complexes were $SOHCu^{2+}$ and $SOCu^{+}$. In 1.0 molal $NaNO_3$, Cu^{II} adsorption was suppressed by up to 30%. This was attributed to the formation of aqueous copper nitrate complexes, although the effect of ionic strength on adsorption was not eliminated as a possibility and will be discussed later.

The adsorption of Cu^{II} onto synthetic goethite increased with increasing NaCl concentration by 20 to 30 times between pH 2 and 5 up to 2 molal NaCl, but further increases of NaCl decreased Cu^{II} adsorption. No discernible change to Cu^{II} adsorption as a function of NaCl could be detected at pH >5. Fitting of the experimental data with the Constant Capacitance Model implied that the surface complexes $\equiv SOHCuCl^{+}$ and $\equiv SOHCuCl_2^{+}$ were the predominant surface species at pH >5 and were responsible for the increased Cu^{II} adsorption in solutions with pH <5. When the concentration of NaCl was >2.0, the predominance of stable copper chloride aqueous complexes inhibited the formation of Cu^{II} surface complexes. At pH >6, the predominant Cu^{II} surface complex was $\equiv SOCu^{+}$.

6.2.2 Zinc Adsorption in NaCl Solutions

Zinc adsorption onto goethite in $NaNO_3$ solutions did not change with increasing $NaNO_3$ concentrations from 0.1 molal and 1.0 molal, while surface complexation modelling with the CCM implied that surface reactions were controlled by $\equiv SOHZn^{2+}$ and $\equiv SOZnOH^{0}$ over a pH range of 3.5 to 9.5.

The presence of NaCl was shown to increase Zn adsorption onto synthetic goethite by up to 20 times in acidic solutions, which is in contrast to the findings of Balistrieri and Murray

(1982) and Kanungo (1990). However, adsorption decreased with increasing NaCl at NaCl concentrations >1.0 molal and pH >6. Surface complexation modelling with the CCM implied that the surface complex $\equiv SOHZnCl_2^0$ surface increased zinc adsorption when the NaCl concentration was < 1. At higher NaCl concentrations, the predominance of $ZnCl_3^-$ and $ZnCl_4^{2-}$ aqueous complexes coincided with decreasing adsorption, while the predominant zinc surface complex changed to $\equiv SOHZn^{2+}$. At pH >7.5 zinc adsorption was predicted to be controlled by the $\equiv SOHZn^{2+}$ and $\equiv SOZnOH^0$ surface complexes.

6.2.3 Copper and Zinc Adsorption in Na_2SO_4 Solutions

A 10% decrease in Cu^{II} adsorption onto synthetic goethite between 0.01 and 0.1 molal Na_2SO_4, between pH 4 and 6 was recorded in adsorption experiments. Surface complexation modelling with the CCM inferred that the $\equiv SOHCuSO_4^0$ surface complex occurred on the surface of goethite. However, aqueous $CuSO_4$ complexes predominated in solutions with >0.01 molal Na_2SO_4, which suppressed the adsorption of Cu^{II}. The suppressed adsorption was presumed to be caused by the preference of Cu^{II} to remain in solution as $CuSO_4(aq)$. This result apparently contradicted the findings of Swedlund and Webster (2001), who concluded that the presence of SO_4^{2-} increased Cu^{II} adsorption on schwertmannite and ferrihydrite. These differences may have been caused by different adsorption properties between goethite, schwertmannite and ferrihydrite, while the highest SO_4^{2-} concentration used by Swedlund and Webster was 0.0108 molal, which was close to the minimum concentration of this study.

Zn adsorption increased by up to 3 times between pH 4 – 5 in 0.001 and 0.01 molal Na_2SO_4. However, at Na_2SO_4 concentrations >0.01 molal zinc adsorption onto goethite decreased at a constant pH. Surface complexation modelling with the CCM inferred that increased zinc adsorption was caused by the formation of Zn surface ternary complexes such as $\equiv SOH_2ZnSO_4^0$ and $\equiv SOZnSO_4^-$. In greater than 0.01 molal Na_2SO_4, Zn preferred to exist as aqueous zinc sulfate complexes (i.e. $ZnSO_4^{2-}$ and $Zn(SO_4)_2^0$) and adsorption was suppressed. At pH >8.5 the Zn surface complexes $\equiv SOHZn^{2+}$ and $\equiv SOZnOH^0$ predominated.

6.3 Scope for future Work

Throughout this study, various issues were encountered that were beyond the scope of this study or were not investigated in detail due to time constraints. The following sections describe some of the more significant areas that may impact on metal adsorption in natural environments.

6.3.1 Ionic Strength Effects on pH

The effect of ionic strength on measured pH was identified as potential source of error for determining the pH range of adsorption in solutions with an ionic strength > 1. Highly saline solutions may have an effect either on the activity of H^+ in solution or modify the electrode surface. Further experiments designed to assess this effect were undertaken. No reproducible pattern was noted in these experiments. Further investigations into this effect are recommended with experiments aimed at identifying and quantifying pH variations as a

function of NaCl and Na_2SO_4 concentration. It is also recommended that future adsorption investigations in solutions with high ionic strength use pH meters calibrated with custom made saline buffers.

6.3.2 Investigation of Cu^{II} and Zn in mixed Anion Solutions

Further investigation of Cu^{II} and Zn adsorption in solutions containing both NaCl and Na_2SO_4 is also recommended. This study used a single experiment with Cu^{II}, Zn, NaCl and Na_2SO_4 coexisting in the same solution to test the predictive power of the thermodynamic properties calculated for Cu^{II} and Zn in single anion solutions. The result of this experiment suggested a complex competition between anions on metal adsorption. Time and resources did not permit further experiments examining single cation and multiple anion experiments although these experiments are recommended. Results of these experiments may assist with refining the speciation model for equilibrium constants and improve the accuracy of predictive models.

6.3.3 Effect of CO_2 on Metal Adsorption

The effect of dissolved CO_2 in solutions is expected to influence the adsorption behaviour of metals, especially in alkaline or near neutral solutions. However, this effect is normally minimised in adsorption experiments by atmospheric controls (i.e. reaction vessels purged with $N_2(g)$). Zeltner and Anderson (1988) used experiments to isolate CO_2 adsorption onto goethite and measure the pH where the goethite had a net charge of zero (zero point of

charge; ZPC). They concluded that the CO_2 decreased the ZPC from pH 9 ±0.3 to pH 8.1 ±0.1, which implies that CO_2 adsorbs to the goethite surface, thereby occupying adsorption sites. The effect of this on metal adsorption has not been tested, although it is expected that the presence of carbonate may reduce the adsorption capacity of goethite surface. The effect of CO_2 adsorption was excluded from this study, but may be important in natural low temperature near surface oxidised conditions, where the pH is expected to be near neutral and carbonate species are likely to be present. Hence a study of metal adsorption in elevated P_{CO2} is required.

6.3.4 Investigation of Ternary Surface Complexes

The enhancement of Cu^{II} and Zn adsorption in NaCl and Na_2SO_4 experiments relies on the assumption that ternary surface complexes (e.g. ≡SOHCuCl) form on the surface of goethite. This study was not able to determine if these complexes exist and if they did what the structure of the surface complex may be. Further investigation into the structure of possible ternary surface complexes using methods such as EXAFS is recommended to better understand the formation of these surface species. EXAFS spectroscopy has successfully been used to infer the molecular structure of Cu^{II} (e.g. Peacock and Sherman, 2004). However Peacock and Sherman did not investigate more complex solutions (i.e. solutions containing chloride and/or sulfate), therefore there is potential to further investigate the potential of ternary surface complexes with this type of analysis.

6.4 Conclusion

The effect of increasing chloride and increasing sulfate concentrations enhances Cu^{II} and Zn adsorption in acidic conditions, thereby decreasing the mobility of these and potentially other metals. This contradicts the generally accepted fact that chloride and sulfate ions increase metal mobility in acidic waters. An adsorption maximum for both metals in NaCl and Na_2SO_4 was identified and further increases to the anion concentration reduced the concentration of adsorbed Cu^{II} and Zn. This is due to Cu^{II} and Zn preferring to form stable aqueous metal complexes preventing adsorption under these conditions. Therefore, mixing of saline brines with freshwater is predicted to promote adsorption of Cu^{II} and Zn (and potentially other metals) onto goethite thereby decreasing their mobility.

Thermodynamic properties calculated by fitting equilibrium constants with the Constant Capacitance Model to the experimental data for solutions with NaCl or Na_2SO_4 were shown to successfully predict the adsorption behaviour of Cu^{II} and Zn in more complex solutions with both NaCl and Na_2SO_4 in the same solution.

The calculated thermodynamic properties were used to predicted the concentration of Cu^{II} and Zn, in simulated conditions similar to those measured at Lake Tyrrell. Results of the CCM showed that a goethite rich sediment would adsorb up to 22 ppm Cu^{II} and 0.4 ppm Zn adsorbed at pH 6. The predicted concentration of adsorbed Cu^{II} is similar to the measured concentration Cu^{II} in clay rich sediment (20 ppm) from Lake Tyrrell. Although the

predicted concentration of adsorbed Zn is lower than measured, this is most likely caused by the pH of Lake Tyrrell water being higher than 6 where sample was taken.

The experimental data collected in this study has shown a consistent, reproducible behaviour over a large range of $NaNO_3$, NaCl and Na_2SO_4 concentrations. The data could be used to fit thermodynamic properties which can predict the behaviour of cations and anions in conditions typical of natural near-surface oxidised environments. The findings of this study advance the knowledge of adsorption and its role in natural systems and even at this early stage, predicting adsorption and metal mobility in complex multi-component systems is possible.

References

Abate, G., Masini, J. C. (2005) Influence of pH, ionic strength and humic acid on adsorption of Cd(II) and Pb(II) onto vermiculite. *Colloids and Surfaces A: Physicochem. Eng. Aspects.* **262**, 33-39.

Agashe K. B. and Regalbuto J. R. (1997) A revised physical theory for adsorption of metal complexes at oxide surfaces. *J. Colloid Interface Sci.* **185**(1), 174-189.

Alcacio T. E., Hesterberg D., Chou J. W., Martin J. D., Beauchemin S., and Sayers D. E. (2001) Molecular scale characteristics of Cu^{2+} bonding in goethite-humate complexes. *Geochim. Cosmochim. Acta,* **65**(9), 1355-1366.

Ali M. A. and Dzombak D. A. (1996) Interactions of copper, organic acids, and sulfate in goethite suspensions. *Geochim. Cosmochim. Acta,* **60**(24), 5045-5053.

Allison J.D., Brown D.S. and Novo-Gradac K.J. (1991), MINTEQA2/PRODEFA2: A geochemical assessment model for environmental systems, Version 3.0 User's Manual, Environmental Research Laboratory, Office of Research and Development, U.S. Environmental Protection agency, EPA/600/3-91/021, Athens, Georgia, 30605, p. 92.

Anawar, H.M., Akai, J., Komaki, K., Terao, H., Yoshioka, T., Ishizuka, T., Safiullah, S., Kato, K. (2003) Geochemical occurrence of arsenic in groundwater of Bangladesh: sources and mobilization processes. *J. Geochem. Explor.*, **77**, 109-131.

Atkinson, R.J., Posner, A. M., Quirk, J.P. (1967) Adsorption of potential-determining ions at the ferric oxide-aqueous interface. *J. Phys. Chem.*, **71**, (3), 550-558.

Balistrieri L. S. and Murray J. W. (1982) The adsorption of Cu, Pb, Zn, and Cd on goethite from major ion seawater. *Geochim. Cosmochim. Acta,* **46**, 1253-1265.

Bampton K.F., Collins A.R., Glasson K.R. and Guy B.B. (1977) Geochemical indications of concealed copper mineralization in an area northwest of Mount Isa, Queensland, Australia. *J. Geochem. Explor.* **8**, 169-188.

Bargar J. R., Brown G. E., and Parks G. A. (1998) Surface complexation of Pb(II) at oxide-water interfaces: III. XAFS determination of Pb(II) and Pb(II)-chloro adsorption complexes on goethite and alumina. *Geochim. Cosmochim. Acta,* **62**(2), 193-207.

Barrow N. J., Bowden J. W., Posner A. M., and Quirk J. P. (1980) An objective method for fitting models of ion adsorption on variable charge surfaces. *Aust. J. Soil Res.* **18**, 37-47.

Barrow N. J., Bowden J. W., Posner A. M., and Quirk J. P. (1982) Describing the Adsorption of Copper, Zinc and Lead on a Variable Charge Mineral Surface. *Aust. J. Soil Res.* **21**, 309-320.

Benjamin M. M. and Leckie J. O. (1981) Conceptual-Model for Metal-Ligand-Surface Interactions During Adsorption. *Environ. Sci. Technol.* **15**(9), 1050-1057.

Bethke C. M. (2002) The Geochemists Workbench; A users guide to Rxn, Act2, Tact, React, and Gtplot. Release 4.0. *Hydrogeology Program, University of Illinois.*

Boily J. F., Persson P., and Sjoberg S. (2000) Benzenecarboxylate surface complexation at the goethite (α-FeOOH)/water interface - III. The influence of particle surface area and the significance of modeling parameters. *J. Colloid Interface Sci.* **227**(1), 132-140.

Bowden J. W., Posner A. M., and Quirk J. P. (1977) Ionic adsorption on variable charge mineral sufaces. Theoretical-charge development and titration curves. *Aust. J. Soil Res.* **15**, 121-136.

Bradl H.B. (2004) Adsorption of heavy metal ions on soils and soils constituents. *J. Colloid Interface Sci.* **277**(1), 1-18.

Brigatti, M. F., Colonna, S., Malferrari, D., Medici, L. (2004) Characterization of Cu-complexes in smectite with different layer charge location: Chemical, thermal and EXAFS studies. *Geochim. Cosmochim. Acta.* **68**, (4), 781-788.

Brugger J., McPhail D. C., Black J., and Spiccia L. (2001) Complexation of metal ions in brines: application of electronic spectroscopy in the study of the Cu^{2+}-LiCl-H2O system between 25 and 90 degrees C. *Geochim. Cosmochim. Acta,* **65**(16), 2691-2708.

Buck K.N. and Bruland K.W. Copper speciation in San Fransico Bay: A novel approach using multiple analytical windows. *Marine Chem.*, **96**(1-2) 185-198.

Cairns C. J., McQueen K. G., and Leah P. A. (2001) Mineralogical controls on element dispersion in regolith over two mineralised shear zones near the Peak, Cobar, New South Wales. *J. Geochem. Explor.* **72**(1), 1-21.

Catalano J.G., Brown Jr., G.E. (2005) Uranyl adsorption onto montmorillonite: Evaluation of binding sites and carbonate complexation. *Geochim. Cosmochim. Acta.* **69**, (12), 2995-3005.

Christl I. and Kretzschmar R. (1999) Competitive sorption of copper and lead at the oxide-water interface: Implications for surface site density. *Geochim. Cosmochim. Acta,* **63**(19-20), 2929-2938.

Collins, C.R., Ragnarsdottir, K. V., Sherman, D.M. (1999) Effect of inorganic and organic ligands on the mechanism of cadmium sorption to goethite. *Geochim. Cosmochim. Acta.* **63**, (19/20), 2989-3002.

Criscenti L. J. and Sverjensky D. A. (1999) The role of electrolyte anions (ClO_4^-, NO_3^-, and Cl^-) in divalent metal (M^{2+}) adsorption on oxide and hydroxide surfaces in salt solutions. *Am. J. Sci.* **299**(10), 828-899.

Criscenti L. J. and Sverjensky D. A. (2002) A single-site model for divalent transition and heavy metal adsorption over a range of metal concentrations. *J. Colloid Interface Sci.* **253**(2), 329-352.

Davies C. W. (1962) *Ion Association.* Butterworths.

Davis J. A. and Kent D. B. (1990) Surface Complexation Modeling in Aqueous Geochemistry. *Reviews in Mineralogy* **23**, 177-260.

Davis J.A. and Leckie J.O. (1978) Effect of adsorbed complexing ligands on trace metal uptake by hydrous oxides. *Environ. Sci. Technol.* **12,** 1309-1315.

De Caritat, P., Kirste, D., Carr, G., McCulloch, M. (2005) Groundwater in the Broken Hill region, Australia: recognising interaction with bedrock and mineralisation using S, Sr and Pb isotopes. *App. Geochem.*, **20**, 767-787.

Drever J. I. (1997) *The geochemistry of natural waters : surface and groundwater environments.* Prentice Hall.

Düker A., Ledin A., Karlsson S., Allard B. (1995) Adsorption of zinc on colloidal (hydr)oxides of Si, Al and Fe in the presence of fulvic acid. *App. Geochem.*, **10**, 197-205.

Dyer J.A., Trivedi P., Scrivner N.C., Sparks D.L. (2004) Surface complexation modelling of zinc sorption onto ferrihydrite. *J. Colloid Interface Sci.*. **270**, 56-65.

Dzombak D. A. and Morel F. (1990) *Surface complexation modeling : hydrous ferric oxide.* Wiley.

Edraki, M., Golding, S.D., Baublys, K.A., Lawrence, M.G. (2005) Hydrochemistry, mineralogy and sulfur isotope geochemistry of acid mine drainage at the Mt. Morgan mine environment, Queensland, Australia. *App. Geosci.* **20**, 789-805.

Elzinga, E.J., Peak, D., Sparks, D.L. (2001) Spectroscopic studies of Pb(II)-sulfate interactions at the goethite-water interface. *Geochim. Cosmochim. Acta.* **65**, (14), 2219-2230.

Fegan N. E., Long D.T., Lyons W.B., Hines M.E., Macumber P.G. (1992) Metal partitioning in acid hypersaline sediments: Lake Tyrrell, Victoria, Australia. *Chem. Geol.*, **96**, 167-181.

Forbes E. A., Posner A. M., and Quirk J. P. (1976) The specific adsorption of divalent Cd, Co, Cu, Pb and Zn on goethite. *J. Soil Sci.* **27**, 154-166.

Gaboriaud F. and Ehrhardt J. (2003) Effects of different crystal faces on the surface charge of colloidal goethite (α-FeOOH) particles: An experimental and modeling study. *Geochim. Cosmochim. Acta,* **67**(5), 967-983.

Gao Y. and Mucci A. (2001) Acid base reactions, phosphate and arsenate complexation, and their competitive adsorption at the surface of goethite in 0.7 M NaCl solution. *Geochim. Cosmochim. Acta,* **65**(14), 2361-2378.

Geelhoed, J.S., Hiemstra, T., van Riemsdijk, W.H. (1997) Phosphate and sulfate adsorption on goethite: Single anion and competitive adsorption. *Geochim. Cosmochim. Acta.* **61**, (12), 2389-2396.

Giblin A. (2001) Groundwaters chemical pathfinders to concealed ore deposits. *CSIRO Exploration and Mining, Sydney, Australia..*

Giblin A.M, Dickson B.L. (1992) Source, distribution and economic significance of trace elements in groundwaters from Lake Tyrrell, Victoria, Australia. *Chem. Geol.*, **96**, 133-149,

Gordon A.S., Donat J.R., Kango R.A., Dyer B.J. and Stuart L.M. (2000) Dissolved copper-complexing ligands in cultures of marine bacteria and estuarine water. *Marine Chem.* **70**, 149-160.

Gunneriusson L. (1994) Composition and Stability of Cd(II)-Chloro and Cd(II)-Hydroxo Complexes at the Goethite (Alpha-Feooh) Water Interface. *J. Colloid Interface Sci.* **163**(2), 484-492.

Gunneriusson L., Lövgren L., and Sjöberg S. (1994) Complexation of Pb(II) at the Geothite (Alpha-FeOOH) Water Interface - the Influence of Chloride. *Geochim. Cosmochim. Acta,* **58**(22), 4973-4983.

Gunneriusson L. and Sjöberg S. (1993) Surface Complexation in the H+-Goethite (Alpha-FeOOH)-Hg(II)-Chloride System. *J. Colloid Interface Sci.* **156**(1), 121-128.

Han N.Z. and Thompson M.L. (2003) Impact of dissolved organic matter on copper mobility in aquifer material. *J. Environ. Qual.* **32**(5), 1829-1836.

Heidmann, I., Christl, I., Kretzshmar, R. (2005) Sorption of Cu and Pb to kaolinite-fulvic acid colloids: Assessment of sorbent interactions. *Geochim. Cosmochim. Acta.* **69**, (7), 1675-1686.

Hem J.D. (1985) Study and interpretation of the chemical characteristics of natural water. *US Geological Survey Water Supply Paper 2254, Alexandria USA.*

Herbelin A. L. and Westall J. C. (1999) A computer program for determination of chemical equilibrium constants from experimental data. Version 4.0. *Report 99-01, Department of Chemistry, Oregon State University, Corvallis, Oregon, USA.*

Herczeg A.L., Torgerson T., Chivas A.R., Habermehl M.A. (1991) Geochemistry of Groundwaters from the Great Artesian Basin, Australia. *Journal of Hydrology*, **126**, 225-245.

Helgeson H. C. and Kirkham D. H. (1974a) Theoretical Prediction of Thermodynamic Behavior of Aqueous Electrolytes at High Pressures and Temperatures .1. Summary of Thermodynamic-Electrostatic Properties of Solvent. *Am. J. Sci.* **274**(10), 1089-&.

Helgeson H. C. and Kirkham D. H. (1974b) Theoretical Prediction of Thermodynamic Behavior of Aqueous Electrolytes at High Pressures and Temperatures .2. Debye-Hückel Parameters for Activity-Coefficients and Relative Partial Molal Properties. *Am. J. Sci.* **274**(10), 1199-&.

Helgeson H. C. and Kirkham D. H. (1976) Theoretical Prediction of Thermodynamic Properties of Aqueous Electrolytes at High-Pressures and Temperatures .3. Equation of State for Aqueous Species at Infinite Dilution. *Am. J. Sci.* **276**(2), 97-240.

Helgeson H. C., Kirkham D. H., and Flowers G. C. (1981) Theoretical Prediction of the Thermodynamic Behavior of Aqueous-Electrolytes at High-Pressures and Temperatures .4. Calculation of Activity-Coefficients, Osmotic Coefficients, and Apparent Molal and Standard and Relative Partial Molal Properties to 600-Degrees-C and 5 Kb. *Am. J. Sci.* **281**(10), 1249-1516.

Herbelin A. L. and Westall J. C. (1999) A computer program for determination of chemical equilibrium constants from experimental data. Version 4.0. *Report 99-01, Department of Chemistry, Oregon State University, Corvallis, Oregon, USA.*

Hiemstra, T and Van Riemsdijk, T.H. (1996) A surface structural approach to ion adsorption: The charge distribution (CD) model. *J. Colloid Interface Sci.*, **179**, 488-508.

Hochella M, F Jr., White A. F., *Mineral-water interface geochemistry; an overview.* Hochella M. F Jr., White A. F. (editors) In: Mineral-water interface geochemistry. Reviews in Mineralogy. 23; Pages 1-16. 1990.

Herczeg, A.L., Torgersen, T., Chivas, A.R., Habermehl, M.A. (1991) Geochemistry of graound waters from the Great Artesian Basin, Australia. *J. Hydrol.* **126**, 225-245.

Ikhsan J., Wells, J. D., Johnson, B.B., Angove, M.J. (2005) Surface complexation modelling of the sorption of Zn(II) by montmorillonite. *Colloids and Surfaces A: Physicochem. Eng. Aspects.* **252**, 33-41.

Johnson K. S. and Pytkowicz R. M. (1978) Ion Association of Cl^- with H^+, Na^+, K^+, Ca^{2+}, and Mg^{2+} in Aqueous-Solutions at 25-Degrees-C. *Am. J. Sci.* **278**(10), 1428-1447.

Jones B.F., Hanor J.F., Evans W.R. (1994) Source of dissolved salts in the central Murray Basin, Australia. *Chem. Geol.*, **111**, 135-154.

Jong, T., Parry, D.L. (2004) Adsorption of Pb(II), Cu(II), Cd(II), Zn(II), Ni(II), Fe(II), and As(V) on bacterially produced metal sulfides. *J. Colloid Interface Sci.* **275**, 61-71.

Juang, R., Wu, W. (2002) Adsorption of sulfate and copper (II) on goethite in relation to the changes of zeta potentials. *J. Colloid Interface Sci.* **249**, 22-29.

Kanungo S. B. (1994a) Adsorption of Cations on Hydrous Oxides of Iron .1. Interfacial Behavior of Amorphous FeOOH and Beta-FeOOH (Akaganeite) in Different Electrolyte-Solutions. *J. Colloid Interface Sci.* **162**(1), 86-92.

Kanungo S. B. (1994b) Adsorption of Cations on Hydrous Oxides of Iron .2. Adsorption of Mn, Co, Ni, and Zn onto Amorphous FeOOH from Simple Electrolyte-Solutions as Well as from a Complex Electrolyte Solution Resembling Seawater in Major Ion Content. *J. Colloid Interface Sci.* **162**(1), 93-102.

Kanungo S. B. (1994c) Adsorption of Cations on Hydrous Oxides of Iron .3. Adsorption of Mn, Co, Ni, and Zn on Beta-FeOOH from Simple Electrolyte-Solutions as Well as from a Complex Electrolyte Solution Resembling Seawater in Major Ion Content. *J. Colloid Interface Sci.* **162**(1), 103-109.

Kim, C. S., Rytuba, J.J., Brown Jr., G.E. (2004) EXAFS study of mercury (II) sorption to Fe- and Al-(hydr)oxides II. Effects of chloride and sulfate. *J. Colloid Interface Sci.* **270**, 9-20.

Kooner Z.S. (1992) Adsorption of copper onto goethite in aqueous systems. *Environ. Geol. Water Sci.,* **20**, 205-212.

Kooner Z.S. (1993) Comparative study of adsorption behaviour of copper, lead, and zinc onto goethite in aqueous systems. *Environ. Geol.,* **21**, 242-250.

Koretsky, C. (2000) The significance of surface complexation reactions in hydrologic systems: a geochemist's perspective. *J. Hydrology*, **230**, 127-121.

Kosmulski, M., Durand-Vidal, S., Mączka, E., Rosenholm, J.B. (2004) Morphology of synthetic goethite particles. *J. Colloid Interface Sci.*, **271**, 261-269.

Langmuir D. (1997) *Aqueous environmental geochemistry*. Prentice Hall.

Lee S.Y. and Gilkes R.J. (2005) Groundwater geochemistry and composition of hardpans in southwestern Australian Regolith. *Geoderma*, **126**, 59-84.

Long D.T., Fengan N.E., Lyons W.B., Hines M.E., Macumber P.G., Giblin A.M. (1992) Geochemistry of acid brines: Lake Tyrrell, Victoria, Australia. *Chem. Geol.*, **96**, 33-52.

Lövgren L., Sjöberg S., and Schindler P. W. (1990) Acid-Base Reactions and Al(III) Complexation at the Surface of Goethite. *Geochim. Cosmochim. Acta,* **54**(5), 1301-1306.

Lumsdon D. G. and Evans L. J. (1994) Surface Complexation Model Parameters for Goethite (Alpha-Feooh). *J. Colloid Interface Sci.* **164**(1), 119-125.

Lützenkirchen J., Boily J.-F., Lövgren L., and Sjöberg S. (2002) Limitations of the potentiometric titration technique in determining the proton active site density of goethite surfaces. *Geochim. Cosmochim. Acta,* **66**(19), 3389-3396.

Lyons W.B., Welch S., Long D.T., Hines M.E., Giblin A.E., Carey A.E., Macumber P.G., Lent R.M., Herczeg A.L. (1992) The trace-metal geochemistry of the Lake Tyrrell system brines (Victoria, Australia). *Chem. Geol.*, **96**, 115-132.

Macumber, P. G. (1992) Hydrological processes in the Tyrrell Basin, southeastern Australia. *Chem. Geol.* **96**, 1-18.

Manceau A., Schlegel M. L., Musso M., Sole V. A., Gauthier C., Petit P. E., and Trolard F. (2000) Crystal chemistry of trace elements in natural and synthetic goethite. *Geochim. Cosmochim. Acta,* **64**(21), 3643-3661.

Missana T., Garcia-Gutierrez M., and Maffiotte C. (2003) Experimental and modeling study of the uranium (VI) sorption on goethite. *J. Colloid Interface Sci.* **260**(2), 291-301.

Padmanabham M. (1983a) Adsorption-Desorption Behavior of Copper(II) at the Goethite-Solution Interface. *Aust. J. Soil Res.* **21**(3), 309-320.

Padmanabham M. (1983b) Comparative-Study of the Adsorption-Desorption Behavior of Copper(II), Zinc(II), Cobalt(II) and Lead(II) at the Goethite-Solution Interface. *Aust. J. Soil Res.* **21**(4), 515-525.

Palmqvist, U. Ahlberg, E. Lövgren, L. Sjöberg, S. (1997) In situ voltametric determinations of metal ions in goethite suspensions: Single metal ion systems. *J. Colloid Interface Sci.*, **196**, 254-266.

Peacock C. L. and Sherman D. M. (2004) Copper(II) sorption onto goethite, hematite and lepidocrocite: A surface complexation model based on ab initio molecular

geometries and EXAFS spectroscopy. *Geochim. Cosmochim. Acta,* **68**(12), 2623-2637.

Peacock C. L. and Sherman D. M. (2005) Surface complexation model for multisite adsorption of copper (II) onto kaolinite. *Geochim. Cosmochim. Acta,* **69**(15), 3733-3745.

Pena, M.E., Korfiatis, G.P., Patel, M., Lippincott, L., Meng, X., (2005) Adsorption of As(V) and As(III) by nanocrystalline titanium dioxide. *Water Res.*, **39**, 2327-2337.

Perkins, W. (1997) Mount Isa lead-zinc orebodies: Replacement lodes in a zined syndeformational copper-lead-zinc system? *Ore Geol. Review*, **12**, 61-110.

Persson P., Lövgren, L., (1996) Potentiometric and spectroscopic studies of sulfate complexation at the goethite-water interface. *Geochim. Cosmochim. Acta*, **60** (15) 2789-2799.

Pfeifer, H., Gueye-Girardet, A., Reymond, D., Schlegel, C., Temgoua, E., Hesterberg, D.L., Chou, J.W. (2004) Dispersion of natural arsenic in the Malcantone watershed, Southern Switzerland: field evidence for repeated sorption-desorption and oxidation-reduction processes. *Geoderma*, **122**, 205-234.

Pietrzak U. and McPhail D. C. (2004) Copper accumulation, distribution and fractionation in vineyard soils of Victoria, Australia. *Geoderma* **122**(2-4), 151-166.

Radford, N.W., Burton, P.E., (1999) The geochemistry of transported overburden: the time factor. An example from the Fender deposit, Big Bell, Western Australia. *J. Geochem. Explor.*, **66**, 71-83.

Reisman, D.J., Sundaram, V., Al-Abed, S.R., Allen, D. (2007) Statistical Validation of Sulfate Quantification Methods Used For Analysis of Acid Mine Drainage.*Talanta*, **71**, 303-311.

Richter, A., Brendler, V., Nebelung, C. (2005) Blind Prediction of Cu(II) sorption onto goethite: Current capabilities of diffuse double layer model, *Geochim. Cosmochim Acta*, **69** (11), 2725-2734.

Rietra, R.P.J.J., Hiemstra, T., van Riemsdijk, W.H. (1999) Sulfate adsorption on Goethite. *J. Colloid Interface Sci.* **218**, 511-521.

Rietra, R.P.J.J., Hiemstra, T., van Riemsdijk, W.H. (2000) Electrolyte anion affinity and its effect on oxyanion adsorption on goethite. *J. Colloid Interface Sci.* **229**, 199-206.

Robertson, A.P., Leckie, J.O. (1997) Cation binding predictions of surface complexation models: effects of pH, ionic strength, cation loading, surface complex, and model fit. *J. Colloid Interface Sci.*, **188**, 444-472.

Rodda D. P., Johnson B. B., and Wells J. D. (1993) The Effect of Temperature and pH on the Adsorption of Copper(II), Lead(II), and Zinc(II) onto Goethite. *J. Colloid Interface Sci.* **161**(1), 57-62.

Rodda D. P., Wells J. D. and Johnson B. B. (1996) Anomalous adsorption of copper(II) on goethite. *J. Colloid Interface Sci.* **184**, 564-569.

Rose A.W. and Bianchi-Mosquera G.C. (1993) Adsorption of Cu, Pb, Zn, Co, Ni and Ag on goethite and hematite: A control on metal mobilization from red beds into stratiform copper deposits, *Economic Geology*, **88**, 1226-1236.

Rustad J. R., Felmy, A.R., Hay, B.P. (1996) Molecular statics calculations of proton binding to goethite surfaces: A new approach to estimation of stability constants for multisite surface complexation models. *Geochim. Cosmochim. Acta,* **60**(9), 1563-1576.

Sahai N. and Sverjensky D. A. (1997a) Evaluation of internally consistent parameters for the triple-layer model by the systematic analysis of oxide surface titration data. *Geochim. Cosmochim. Acta,* **61**(14), 2801-2826.

Sahai N. and Sverjensky D. A. (1997b) Solvation and electrostatic model for specific electrolyte adsorption. *Geochim. Cosmochim. Acta,* **61**(14), 2827-2848.

Sammut, J. *An introduction to acid sulfate soils*. National Heritage Trust, Australian Government, 2000.

Schwertmann U. and Cornell R. M. (1991) *Iron oxides in the laboratory : preparation and characterization*. VCH.

Sen T.K. Mahajan S. P. and. Khilar K. C. (2000) Adsorption of Cu^{2+} and Ni^{2+} on iron oxide and kaolin and its importance on Ni^{2+} transport in porous media. *Colloids and Surfaces A: Physicochemical and Engineering Aspects* **211**(1), 91-102.

Smith R.W. and Martell A.E. (1997) *NIST - Critically Selected Stability Constants of Metal Complexes Database - Version 8.0*. Report, U.S. Department of Commerce.

Smith, J., Melville, M.D. (2004) Iron monosulfide formation and oxidation in drai-bottom sediments of an acid sulfate soil environment. *App. Geochem.* **19**, 1837-1853.

Sposito G. (1984) *The surface chemistry of soils*. Oxford University Press; Clarendon Press.

Stumm W. and Morgan J. J. (1981) *Aquatic chemistry : an introduction emphasizing chemical equilibria in natural waters*. Wiley.

Sverjensky D. A. (2001a) Comparison of surface complexation models for metal adsorption with spectroscopic studies. *Abstracts of Papers of the American Chemical Society* **221**, U527-U527.

Sverjensky D. A. (2001b) Interpretation and prediction of triple-layer model capacitances and the structure of the oxide-electrolyte-water interface. *Geochim. Cosmochim. Acta,* **65**(21), 3643-3655.

Sverjensky D. A. (2003) Standard states for the activities of mineral surface sites and species. *Geochim. Cosmochim. Acta,* **67**(1), 17-28.

Sverjensky D. A. and Sahai N. (1996) Theoretical prediction of single-site surface-protonation equilibrium constants for oxides and silicates in water. *Geochim. Cosmochim. Acta,* **60**(20), 3773-3797.

Swallow K.C., Hume D.N., Morel F.M.M. (1980) Sorption of copper and lead by hydrous ferric oxide. *Environ. Sci. Technol.* **14,** 1326-1331.

Swartz, C.H., Blute, N.K., Badruzzman, B., Ali, A., Brabander, D., Jay, J., Besancon, J., Islam, S., Hemond, H.F., Harvey, C.F. (2004) Mobility of arsenic in a Bangladesh aquifer: Inferences from geochemical profiles, leaching data, and mineralogical characterization. *Geochim. Cosmochim. Acta,* **68**(22), 4539-4557.

Swedlund P.J. and Webster J.G. (2001) Cu and Zn ternary surface complex formation with SO4 on ferrihydrite and schwertmannite. *App. Geochem.*. **16**. 503-511.

Trivedi P., Axe L., Tyson T.A. (2001) An analysis of zinc sorption to amorphous versus crystalline iron oxides using XAS. *J. Colloid Interface Sci.*. **244**, 230-238.

Uygur V. and Rimmer D.L. (2000) Reactions of zinc with iron-oxide coated calcite surfaces at alkaline pH. *J. Soil Sci.*, **51**, 511-516.

Van Geen A., Robertson A. P., and Leckie J. O. (1994) Complexation of Carbonate Species at the Goethite Surface - Implications for Adsorption of Metal-Ions in Natural-Waters. *Geochim. Cosmochim. Acta,* **58**(9), 2073-2086.

Venema P., Hiemstra T., Weidler P. G., and van Riemsdijk W. H. (1998) Intrinsic proton affinity of reactive surface groups of metal (hydr)oxides: Application to iron (hydr)oxides. *J. Colloid Interface Sci.* **198**(2), 282-295.

Vico, L.I. (2003) Acid-base behaviour and Cu^{2+} and Zn^{2+} complexation properties of the sepiolite/water interface. *Chem. Geol.*, **198**, 213-222.

Waychunas, G.A., Fuller, C.C., Davis, J.A. (2002) Surface complexation and precipitate geometry for aqueous Zn(II) sorption on ferrihydrite I: X-ray absorption extended fine structure spectroscopy analysis. *Geochim. Cosmochim. Acta*, **66**, (7), 1119-1137.

Waychunas, G.A., Fuller, C.C., Davis, J.A. (2002) Surface complexation and precipitate geometry for aqueous Zn(II) sorption on ferrihydrite II: XANES analysis and simulation. *Geochim. Cosmochim. Acta*, **67**, (5), 1031-1043.

Weisner, A.D., Katz, L.E., Chen, C. (2006) The impact of ionic strength and background electrolyte on pH measurements in metal ion adsorption experiments. *J. Colloid Interface Sci.,* **301**, 329-332.

Weng L.P., Fest E.P.M.J., Fillius J., Temminghoff E.J.M., Van Riemsdijk W.H. (2002) Transport of humic and fulvic acids in relation to metal mobility in a copper-contaminated acid sandy soil. *Environ. Sci. Technol.* **36**(8), 1699-1704.

Yates D. L. (1975) The structure of the oxide/aqueous electrolyte interface, University of Melbourne.

Yu, W., Harvey, C.M., Harvey, C.F. (2003) Arsenic in groundwater in Bangladesh: A geostatistical and epidemiological framework for evaluating health effects and potential remedies. *Water Resour. Res.*, **39**,1146.

Zeltner W. A. and Anderson M. A. (1988) Surface-Charge Development at the Goethite Aqueous-Solution Interface - Effects of CO_2 Adsorption. *Langmuir* **4**(2), 469-474.

Appendix A

Experimental data for copper adsorption onto goethite in 0.1 – 5.0 molal NaCl is listed below. Each table is an experimental series, while each row is a single experiment. Cu_{Tot} is the total dissolved copper at the start of each experiment before goethite is added. pH is the final pH of solution at the completion of each experiments, Cu_{Diss} is the total dissolved Cu^{II} in solution at completion while the Cu_{Ads} is the difference between Cu_{Tot} and Cu_{Diss}.

0.1 molal $NaNO_3$

Total Cu	pH	Cu_{Diss}	Cu_{Ads}
1.20×10^{-4}	3.2	1.05×10^{-4}	1.46×10^{-5}
	3.7	1.05×10^{-4}	1.49×10^{-5}
	4.12	1.04×10^{-4}	1.59×10^{-5}
	4.56	9.38×10^{-5}	2.62×10^{-5}
	4.96	7.86×10^{-5}	4.14×10^{-5}
	5.18	6.41×10^{-5}	5.59×10^{-5}
	5.62	3.83×10^{-5}	8.17×10^{-5}
	5.94	2.12×10^{-5}	9.88×10^{-5}
	6.79	4.58×10^{-6}	1.15×10^{-4}
	7.55	1.10×10^{-6}	1.19×10^{-4}
	9.26	3.59×10^{-6}	1.16×10^{-4}

1.0 molal $NaNO_3$

Total Cu	pH	Cu_{Diss}	Cu_{Ads}
9.10x10-5	3.12	8.62×10^{-5}	4.82×10^{-6}
	3.56	8.48×10^{-5}	6.16×10^{-6}
	3.96	8.20×10^{-5}	9.03×10^{-6}
	4.3	7.55×10^{-5}	1.55×10^{-5}
	4.76	6.05×10^{-5}	3.05×10^{-5}
	5.06	5.44×10^{-5}	3.66×10^{-5}
	5.22	4.96×10^{-5}	4.14×10^{-5}
	5.63	3.51×10^{-5}	5.59×10^{-5}
	6.3	8.97×10^{-6}	8.20×10^{-5}
	6.44	1.03×10^{-6}	9.00×10^{-5}

3.0 molal $NaNO_3$

Total Cu	pH	Cu_{Diss}	Cu_{Ads}
1.13x10-4	2.39	1.10×10^{-4}	2.56×10^{-6}
	2.74	1.11×10^{-4}	2.14×10^{-6}
	3.12	1.07×10^{-4}	6.09×10^{-6}
	3.52	1.11×10^{-4}	1.95×10^{-6}
	3.77	1.07×10^{-4}	6.39×10^{-6}
	4.36	9.36×10^{-5}	1.94×10^{-5}
	4.6	8.92×10^{-5}	2.38×10^{-5}
	4.72	8.80×10^{-5}	2.50×10^{-5}
	5.34	6.81×10^{-5}	4.49×10^{-5}
	5.88	4.70×10^{-5}	6.60×10^{-5}
	6.51	2.09×10^{-5}	9.21×10^{-5}
	7.91	6.07×10^{-7}	1.12×10^{-4}

0.1 molal NaCl

Cu_{Tot} (molal)	pH	Cu_{Diss} (molal)	Cu_{Ads} (molal)
1.57×10^{-4}	2.52	1.54×10^{-4}	3.15×10^{-6}
	3.02	1.53×10^{-4}	3.58×10^{-6}
	3.94	1.38×10^{-4}	1.89×10^{-5}
	4.04	1.35×10^{-4}	2.20×10^{-5}
	4.32	1.26×10^{-4}	3.14×10^{-5}
	4.47	1.21×10^{-4}	3.61×10^{-5}
	4.63	1.13×10^{-4}	4.37×10^{-5}
	4.69	1.07×10^{-4}	4.97×10^{-5}
	5.16	6.73×10^{-5}	8.97×10^{-5}
	5.72	3.19×10^{-5}	1.25×10^{-4}
	7.46	7.04×10^{-7}	1.56×10^{-4}

0.3 molal NaCl

Cu_{Tot} (molal)	pH	Cu_{Diss} (molal)	Cu_{Ads} (molal)
1.57×10^{-4}	2.63	1.39×10^{-4}	1.79×10^{-5}
	2.97	1.31×10^{-4}	2.55×10^{-5}
	3.11	1.30×10^{-4}	2.67×10^{-5}
	3.33	1.30×10^{-4}	2.65×10^{-5}
	3.96	1.18×10^{-4}	3.90×10^{-5}
	4.46	1.03×10^{-4}	5.40×10^{-5}
	4.87	8.37×10^{-5}	7.33×10^{-5}
	5.15	6.75×10^{-5}	8.95×10^{-5}
	5.38	5.81×10^{-5}	9.89×10^{-5}
	5.71	3.79×10^{-5}	1.19×10^{-4}
	6.13	1.29×10^{-5}	1.44×10^{-4}
	8.52	1.29×10^{-6}	1.56×10^{-4}

0.5 molal NaCl

Cu_{Tot} (molal)	pH	Cu_{Diss} (molal)	Cu_{Ads} (molal)
1.49×10^{-4}	2.88	1.16×10^{-4}	3.30×10^{-5}
	3.15	1.13×10^{-4}	3.63×10^{-5}
	3.26	1.13×10^{-4}	3.55×10^{-5}
	3.4	1.14×10^{-4}	3.53×10^{-5}
	4.33	9.23×10^{-5}	5.67×10^{-5}
	4.91	7.13×10^{-5}	7.77×10^{-5}
	5.16	6.39×10^{-5}	8.51×10^{-5}
	5.45	4.74×10^{-5}	1.02×10^{-4}
	5.77	3.36×10^{-5}	1.15×10^{-4}
	5.95	2.22×10^{-5}	1.27×10^{-4}
	6.06	1.41×10^{-5}	1.35×10^{-4}
	8.94	5.42×10^{-7}	1.48×10^{-4}

1.0 molal NaCl

Cu_{Tot} (molal)	pH	Cu_{Diss} (molal)	Cu_{Ads} (molal)
1.19×10^{-4}	2.5	7.57×10^{-5}	4.33×10^{-5}
	2.8	7.15×10^{-5}	4.75×10^{-5}
	3.08	7.18×10^{-5}	4.72×10^{-5}
	3.43	6.59×10^{-5}	5.31×10^{-5}
	3.65	6.70×10^{-5}	5.20×10^{-5}
	4.05	5.71×10^{-5}	6.19×10^{-5}
	4.43	4.93×10^{-5}	6.97×10^{-5}
	4.9	4.14×10^{-5}	7.76×10^{-5}
	5.2	2.79×10^{-5}	9.11×10^{-5}
	5.89	6.17×10^{-7}	1.18×10^{-4}
1.55×10^{-4}	3.38	1.18×10^{-4}	3.66×10^{-5}
	4.13	1.03×10^{-4}	5.21×10^{-5}
	4.61	9.30×10^{-5}	6.20×10^{-5}
	4.95	8.41×10^{-5}	7.09×10^{-5}
	5.12	7.20×10^{-5}	8.30×10^{-5}
	5.27	6.86×10^{-5}	8.64×10^{-5}
	5.49	6.00×10^{-5}	9.50×10^{-5}
	5.69	4.49×10^{-5}	1.10×10^{-4}
	6.38	9.74×10^{-6}	1.45×10^{-4}
	8.79	3.48×10^{-6}	1.52×10^{-4}
	8.87	2.53×10^{-6}	1.52×10^{-4}
	8.22	9.56×10^{-7}	1.54×10^{-4}

2.0 molal NaCl

Cu_{Tot} (molal)	pH	Cu_{Diss} (molal)	Cu_{Ads} (molal)
1.57×10^{-4}	2.2	1.23×10^{-4}	3.42×10^{-5}
	2.37	1.21×10^{-4}	3.58×10^{-5}
	2.8	1.10×10^{-4}	4.66×10^{-5}
	3.29	1.01×10^{-4}	5.61×10^{-5}
	4.02	8.01×10^{-5}	7.69×10^{-5}
	4.52	8.19×10^{-5}	7.51×10^{-5}
	4.79	5.81×10^{-5}	9.89×10^{-5}
	5.31	3.06×10^{-5}	1.26×10^{-4}
	5.54	2.06×10^{-5}	1.36×10^{-4}
	5.96	6.22×10^{-6}	1.51×10^{-4}
	6.88	5.61×10^{-7}	1.56×10^{-4}
	8.61	7.77×10^{-7}	1.56×10^{-4}
1.52×10^{-4}	2.52	1.23×10^{-4}	2.86×10^{-5}
	2.54	1.22×10^{-4}	3.02×10^{-5}
	2.76	1.15×10^{-4}	3.70×10^{-5}
	2.84	1.14×10^{-4}	3.82×10^{-5}
	3.17	1.04×10^{-4}	4.83×10^{-5}
	3.46	9.72×10^{-5}	5.48×10^{-5}
	4.22	8.15×10^{-5}	7.05×10^{-5}
	4.55	7.10×10^{-5}	8.10×10^{-5}
	4.97	4.65×10^{-5}	1.05×10^{-4}
	5.57	1.36×10^{-5}	1.38×10^{-4}
	6.46	1.19×10^{-6}	1.51×10^{-4}

3.0 molal NaCl

Cu_{Tot} (molal)	pH	Cu_{Diss} (molal)	Cu_{Ads} (molal)
1.58×10^{-4}	2.27	1.18×10^{-4}	4.04×10^{-5}
	2.57	1.10×10^{-4}	4.82×10^{-5}
	3.05	9.91×10^{-5}	5.89×10^{-5}
	4	7.28×10^{-5}	8.52×10^{-5}
	4.3	7.25×10^{-5}	8.55×10^{-5}
	4.47	6.48×10^{-5}	9.32×10^{-5}
	5.58	2.10×10^{-5}	1.37×10^{-4}
	5.64	2.67×10^{-5}	1.31×10^{-4}
	6.67	2.57×10^{-6}	1.55×10^{-4}
	7.13	9.50×10^{-7}	1.57×10^{-4}
	8.23	9.31×10^{-7}	1.57×10^{-4}
1.50×10^{-4}	2.31	1.14×10^{-4}	3.64×10^{-5}
	2.87	9.99×10^{-5}	5.01×10^{-5}
	2.99	9.49×10^{-5}	5.51×10^{-5}
	3.23	8.29×10^{-5}	6.71×10^{-5}
	3.54	8.51×10^{-5}	6.49×10^{-5}
	4.49	6.14×10^{-5}	8.86×10^{-5}
	4.53	5.49×10^{-5}	9.51×10^{-5}
	4.59	5.48×10^{-5}	9.52×10^{-5}
	4.65	6.03×10^{-5}	8.97×10^{-5}
	7.68	1.09×10^{-6}	1.49×10^{-4}

4.0 molal NaCl

Cu_{Tot} (molal)	pH	Cu_{Diss} (molal)	Cu_{Ads} (molal)
1.58×10^{-4}	2.35	1.30×10^{-4}	2.79×10^{-5}
	2.57	1.29×10^{-4}	2.92×10^{-5}
	2.75	1.24×10^{-4}	3.38×10^{-5}
	3.14	1.15×10^{-4}	4.33×10^{-5}
	3.86	1.02×10^{-4}	5.63×10^{-5}
	4.87	8.61×10^{-5}	7.19×10^{-5}
	5.35	6.65×10^{-5}	9.15×10^{-5}
	5.46	5.85×10^{-5}	9.95×10^{-5}
	5.62	4.67×10^{-5}	1.11×10^{-4}
	6.49	3.34×10^{-5}	1.25×10^{-4}
	7.75	3.09×10^{-5}	1.27×10^{-4}
	8.38	3.21×10^{-5}	1.26×10^{-4}
1.23×10^{-4}	2.39	9.53×10^{-5}	2.77×10^{-5}
	3.14	8.02×10^{-5}	4.28×10^{-5}
	3.54	7.34×10^{-5}	4.96×10^{-5}
	4.33	6.55×10^{-5}	5.75×10^{-5}
	4.92	5.52×10^{-5}	6.78×10^{-5}
	5.15	4.89×10^{-5}	7.41×10^{-5}
	5.15	4.91×10^{-5}	7.39×10^{-5}
	5.52	3.23×10^{-5}	9.07×10^{-5}
	6.69	4.92×10^{-6}	1.18×10^{-4}
	8.88	1.51×10^{-6}	1.21×10^{-4}
	10.8	9.66×10^{-7}	1.22×10^{-4}

5.0 molal NaCl

Cu_{Tot} (molal)	pH	Cu_{Diss} (molal)	Cu_{Ads} (molal)
1.57×10^{-4}	2.04	1.21×10^{-4}	3.59×10^{-5}
	2.36	1.17×10^{-4}	4.00×10^{-5}
	2.93	1.04×10^{-4}	5.26×10^{-5}
	3.42	9.61×10^{-5}	6.09×10^{-5}
	4.59	7.89×10^{-5}	7.81×10^{-5}
	4.91	8.03×10^{-5}	7.67×10^{-5}
	5.1	6.51×10^{-5}	9.19×10^{-5}
	5.14	6.57×10^{-5}	9.13×10^{-5}
	5.25	5.84×10^{-5}	9.86×10^{-5}
	5.82	2.11×10^{-5}	1.36×10^{-4}
	6.02	6.12×10^{-6}	1.51×10^{-4}
	6.6	8.49×10^{-7}	1.56x10-4
1.38×10^{-4}	2.27	1.08×10^{-4}	3.00×10^{-5}
	2.85	9.26×10^{-5}	4.54×10^{-5}
	3.32	8.52×10^{-5}	5.28×10^{-5}
	4.04	7.59×10^{-5}	6.21×10^{-5}
	4.74	6.60×10^{-5}	7.20×10^{-5}
	5.29	4.29×10^{-5}	9.51×10^{-5}
	5.6	2.55×10^{-5}	1.13×10^{-4}
	6.14	6.10×10^{-6}	1.32×10^{-4}
	7.37	1.99×10^{-6}	1.36×10^{-4}
	8.01	4.28×10^{-6}	1.34×10^{-4}
	8.49	3.40×10^{-6}	1.35×10^{-4}

Appendix B

Experimental data for zinc adsorption onto goethite in 0.1 – 5.0 molal NaCl is listed below. Each table is an experimental series, while each row is a single experiment. Zn_{Tot} is the total dissolved copper at the start of each experiment before goethite is added. pH is the final pH of solution at the completion of each experiments, Zn_{Diss} is the total dissolved Zn in solution at completion of each experiment while the Zn_{Ads} is the difference between Zn_{Tot} and Zn_{Diss}.

0.1 molal $NaNO_3$

Total Cu	pH	Cu_{Diss}	Cu_{Ads}
1.57×10^{-4}	5.44	1.39×10^{-4}	1.77×10^{-5}
	5.83	1.32×10^{-4}	2.49×10^{-5}
	6.55	1.11×10^{-4}	4.57×10^{-5}
	5.49	1.40×10^{-4}	1.74×10^{-5}
	7.29	7.36×10^{-5}	8.34×10^{-5}
	7.01	9.19×10^{-5}	6.51×10^{-5}
	3.54	1.44×10^{-4}	1.28×10^{-5}
	3.6	1.43×10^{-4}	1.41×10^{-5}
	3.09	1.44×10^{-4}	1.28×10^{-5}
	3.48	1.50×10^{-4}	7.32×10^{-6}
	3.07	1.44×10^{-4}	1.33×10^{-5}
	5.32	1.35×10^{-4}	2.24×10^{-5}
1.36×10^{-4}	3.74	1.53×10^{-4}	3.92×10^{-6}
	4	1.55×10^{-4}	1.98×10^{-6}
	5.4	1.46×10^{-4}	1.15×10^{-5}
	7.02	9.33×10^{-5}	6.37×10^{-5}
	7.32	7.53×10^{-5}	8.17×10^{-5}
	7.62	5.36×10^{-5}	1.03×10^{-4}
	8.02	3.31×10^{-5}	1.24×10^{-4}
	8.65	2.84×10^{-5}	1.29×10^{-4}
	8.8	2.63×10^{-5}	1.31×10^{-4}
	9.12	2.57×10^{-5}	1.31×10^{-4}
	9.09	2.19×10^{-5}	1.35×10^{-4}

0.01 molal NaCl

Zn_{Tot} (molal)	pH	Zn_{Diss} (molal)	Zn_{Ads} (molal)
1.58×10^{-4}	3.52	1.57×10^{-4}	1.33×10^{-6}
	4.13	1.54×10^{-4}	4.50×10^{-6}
	3.75	1.56×10^{-4}	1.73×10^{-6}
	4.52	1.53×10^{-4}	4.85×10^{-6}
	6.25	1.24×10^{-4}	3.37×10^{-5}
	3.77	1.57×10^{-4}	1.37×10^{-6}
	7.74	4.30×10^{-5}	1.15×10^{-4}
	7.88	2.41×10^{-5}	1.34×10^{-4}
	8.39	4.06×10^{-6}	1.54×10^{-4}
	9.16	6.29×10^{-8}	1.58×10^{-4}
	9.4	1.83×10^{-6}	1.56×10^{-4}
1.56×10^{-4}	4.08	1.55×10^{-4}	7.95×10^{-7}
	4.61	1.54×10^{-4}	2.10×10^{-6}
	4.9	1.49×10^{-4}	6.57×10^{-6}
	4.98	1.55×10^{-4}	9.94×10^{-7}
	5.53	1.43×10^{-4}	1.34×10^{-5}
	5.55	1.40×10^{-4}	1.56×10^{-5}
	6.09	1.32×10^{-4}	2.44×10^{-5}
	6.24	1.25×10^{-4}	3.05×10^{-5}
	7.45	5.59×10^{-5}	1.00×10^{-4}
	7.66	6.17×10^{-5}	9.43×10^{-5}

0.1 molal NaCl

Zn_{Tot} (molal)	pH	Zn_{Diss} (molal)	Zn_{Ads} (molal)
1.48×10^{-4}	3.79	1.32×10^{-4}	1.58×10^{-5}
	6.25	1.14×10^{-4}	3.37×10^{-5}
	7.34	7.45×10^{-5}	7.35×10^{-5}
	7.57	6.19×10^{-5}	8.61×10^{-5}
	7.76	4.92×10^{-5}	9.88×10^{-5}
	7.91	4.05×10^{-5}	1.07×10^{-4}
	7.94	3.91×10^{-5}	1.09×10^{-4}
	7.96	3.41×10^{-5}	1.14×10^{-4}
	8.04	2.74×10^{-5}	1.21×10^{-4}
	8.27	1.26×10^{-5}	1.35×10^{-4}
	8.54	4.22×10^{-6}	1.44×10^{-4}
	9.07	6.99×10^{-7}	1.47×10^{-4}
1.56×10^{-4}	4.67	1.33×10^{-4}	2.30×10^{-5}
	4.91	1.34×10^{-4}	2.20×10^{-5}
	5.61	1.26×10^{-4}	3.02×10^{-5}
	6.15	1.13×10^{-4}	4.30×10^{-5}
	6.42	9.91×10^{-5}	5.69×10^{-5}
	6.59	9.04×10^{-5}	6.56×10^{-5}
	7.06	8.20×10^{-5}	7.40×10^{-5}
	7.39	6.31×10^{-5}	9.29×10^{-5}
	7.7	4.43×10^{-5}	1.12×10^{-4}
	8	1.72×10^{-5}	1.39×10^{-4}
	8.7	7.65×10^{-7}	1.55×10^{-4}

0.3 molal NaCl

Zn_{Tot} (molal)	pH	Zn_{Diss} (molal)	Zn_{Ads} (molal)
1.34×10^{-4}	3.3	1.11×10^{-4}	2.28×10^{-5}
	3.42	1.10×10^{-4}	2.43×10^{-5}
	3.92	1.08×10^{-4}	2.56×10^{-5}
	5.16	1.00×10^{-4}	3.40×10^{-5}
	5.7	8.80×10^{-5}	4.60×10^{-5}
	2.95	1.07×10^{-4}	2.67×10^{-5}
	7.15	5.57×10^{-5}	7.83×10^{-5}
	7.54	2.86×10^{-5}	1.05×10^{-4}
	7.71	1.69×10^{-5}	1.17×10^{-4}
	7.97	6.79×10^{-6}	1.27×10^{-4}
	8.48	3.48×10^{-6}	1.31×10^{-4}
	8.46	6.48×10^{-7}	1.33×10^{-4}
1.56×10^{-4}	4.61	1.26×10^{-4}	3.01×10^{-5}
	5.07	1.19×10^{-4}	3.73×10^{-5}
	5.44	1.14×10^{-4}	4.15×10^{-5}
	5.96	1.05×10^{-4}	5.14×10^{-5}
	6.03	9.90×10^{-5}	5.70×10^{-5}
	6.57	7.70×10^{-5}	7.90×10^{-5}
	7.13	6.52×10^{-5}	9.08×10^{-5}
	7.65	3.97×10^{-5}	1.16×10^{-4}
	7.71	3.32×10^{-5}	1.23×10^{-4}
	8	2.50×10^{-5}	1.31×10^{-4}
	8.49	2.43×10^{-6}	1.54×10^{-4}
	8.99	2.01×10^{-6}	1.54×10^{-4}

0.5 molal NaCl

Zn_{Tot} (molal)	pH	Zn_{Diss} (molal)	Zn_{Ads} (molal)
1.38×10^{-4}	4.36	1.20×10^{-4}	1.75×10^{-5}
	5.14	1.17×10^{-4}	2.07×10^{-5}
	5.52	1.05×10^{-4}	3.26×10^{-5}
	5.92	9.37×10^{-5}	4.43×10^{-5}
	6.2	8.20×10^{-5}	5.60×10^{-5}
	6.64	6.96×10^{-5}	6.84×10^{-5}
	6.92	6.41×10^{-5}	7.39×10^{-5}
	7.75	3.92×10^{-5}	9.88×10^{-5}
	7.99	1.80×10^{-5}	1.20×10^{-4}
	8.5	1.90×10^{-6}	1.36×10^{-4}
	8.85	1.46×10^{-6}	1.37×10^{-4}
1.18×10^{-4}	3.45	1.15×10^{-4}	3.00×10^{-6}
	5.09	1.06×10^{-4}	1.20×10^{-5}
	6.04	8.57×10^{-5}	3.23×10^{-5}
	7.33	4.57×10^{-5}	7.23×10^{-5}
	7.72	2.30×10^{-5}	9.50×10^{-5}
	8.24	7.53×10^{-6}	1.10×10^{-4}
	8.31	9.22×10^{-6}	1.09×10^{-4}
	8.74	5.21×10^{-6}	1.13×10^{-4}
	8.65	5.67×10^{-6}	1.12×10^{-4}
	8.91	4.64×10^{-6}	1.13×10^{-4}
	8.75	4.74×10^{-6}	1.13×10^{-4}
	9.01	1.38×10^{-6}	1.17×10^{-4}
1.08×10^{-4}	3.5	1.03×10^{-4}	4.53×10^{-6}
	4.52	9.93×10^{-5}	8.74×10^{-6}
	5.53	9.32×10^{-5}	1.48×10^{-5}
	6.15	7.61×10^{-5}	3.19×10^{-5}
	6.9	5.65×10^{-5}	5.15×10^{-5}
	7.27	3.14×10^{-5}	7.66×10^{-5}
	7.67	2.72×10^{-5}	8.08×10^{-5}
	7.68	2.42×10^{-5}	8.38×10^{-5}
	7.86	1.61×10^{-5}	9.19×10^{-5}
	8.2	8.75×10^{-6}	9.93×10^{-5}
	8.57	5.20×10^{-6}	1.03×10^{-4}
	8.98	7.10×10^{-7}	1.07×10^{-4}

1.0 molal NaCl

Zn_{Tot} (molal)	pH	Zn_{Diss} (molal)	Zn_{Ads} (molal)
1.19×10^{-4}	3.44	9.89×10^{-5}	2.01×10^{-5}
	3.74	1.00×10^{-4}	1.90×10^{-5}
	4.08	9.82×10^{-5}	2.08×10^{-5}
	5.18	9.12×10^{-5}	2.78×10^{-5}
	5.83	7.36×10^{-5}	4.54×10^{-5}
	4.29	9.28×10^{-5}	2.62×10^{-5}
	6.28	6.40×10^{-5}	5.50×10^{-5}
	6.39	5.83×10^{-5}	6.07×10^{-5}
	6.89	4.44×10^{-5}	7.46×10^{-5}
	7.19	3.17×10^{-5}	8.73×10^{-5}
	7.85	8.49×10^{-6}	1.11×10^{-4}
	8.04	1.33×10^{-6}	1.18×10^{-4}
1.37×10^{-4}	4.56	1.09×10^{-4}	2.78×10^{-5}
	5.04	1.05×10^{-4}	3.19×10^{-5}
	5.76	9.03×10^{-5}	4.67×10^{-5}
	5.59	9.89×10^{-5}	3.81×10^{-5}
	5.67	9.46×10^{-5}	4.24×10^{-5}
	5.74	8.56×10^{-5}	5.14×10^{-5}
	6.26	7.83×10^{-5}	5.87×10^{-5}
	7.32	4.58×10^{-5}	9.12×10^{-5}
	7.66	3.19×10^{-5}	1.05×10^{-4}
	8.16	7.20×10^{-6}	1.30×10^{-4}
	8.86	9.74×10^{-7}	1.36×10^{-4}

2.0 molal NaCl

Zn_{Tot} (molal)	pH	Zn_{Diss} (molal)	Zn_{Ads} (molal)
1.22×10^{-4}	3.24	1.11×10^{-4}	1.11×10^{-5}
	3.54	1.07×10^{-4}	1.52×10^{-5}
	3.99	9.91×10^{-5}	2.29×10^{-5}
	5.32	8.99×10^{-5}	3.21×10^{-5}
	5.85	7.73×10^{-5}	4.47×10^{-5}
	6.12	7.07×10^{-5}	5.13×10^{-5}
	6.32	6.67×10^{-5}	5.53×10^{-5}
	6.51	6.11×10^{-5}	6.09×10^{-5}
	6.79	5.13×10^{-5}	7.07×10^{-5}
	7.22	3.85×10^{-5}	8.35×10^{-5}
	7.64	2.38×10^{-5}	9.82×10^{-5}
	8.26	1.11×10^{-6}	1.21×10^{-4}
1.65×10^{-4}	6.19	1.28×10^{-4}	3.67×10^{-5}
	6.51	1.21×10^{-4}	4.43×10^{-5}
	6.87	1.08×10^{-4}	5.68×10^{-5}
	7.33	7.53×10^{-5}	8.97×10^{-5}
	7.46	5.39×10^{-5}	1.11×10^{-4}
	7.34	7.14×10^{-5}	9.36×10^{-5}
	8.09	3.11×10^{-5}	1.34×10^{-4}
	8.46	9.91×10^{-6}	1.55×10^{-4}
	8.81	2.11×10^{-6}	1.63×10^{-4}
	8.92	1.02×10^{-6}	1.64×10^{-4}
1.35×10^{-4}	4.49	1.07×10^{-4}	2.81×10^{-5}
	5.56	9.63×10^{-5}	3.87×10^{-5}
	5.92	8.40×10^{-5}	5.10×10^{-5}
	6.49	7.57×10^{-5}	5.93×10^{-5}
	7.35	4.68×10^{-5}	8.82×10^{-5}
	7.55	3.34×10^{-5}	1.02×10^{-4}
	7.54	2.68×10^{-5}	1.08×10^{-4}
	7.37	4.66×10^{-5}	8.84×10^{-5}
	7.5	3.25×10^{-5}	1.02×10^{-4}
	7.59	2.62×10^{-5}	1.09×10^{-4}
	7.72	2.61×10^{-5}	1.09×10^{-4}
	7.84	2.23×10^{-7}	1.35×10^{-4}

3.0 molal NaCl

Zn_{Tot} (molal)	pH	Zn_{Diss} (molal)	Zn_{Ads} (molal)
1.57×10^{-4}	6.04	1.43×10^{-4}	1.39×10^{-5}
	6.68	9.64×10^{-5}	6.06×10^{-5}
	6.78	8.90×10^{-5}	6.80×10^{-5}
	7.24	8.20×10^{-5}	7.50×10^{-5}
	7.32	5.81×10^{-5}	9.89×10^{-5}
	7.46	4.60×10^{-5}	1.11×10^{-4}
	7.61	4.74×10^{-5}	1.10×10^{-4}
	8.07	3.20×10^{-5}	1.25×10^{-4}
	8.17	2.46×10^{-5}	1.32×10^{-4}
	8.27	8.17×10^{-6}	1.49×10^{-4}
	8.36	1.06×10^{-5}	1.46×10^{-4}
	8.81	7.66×10^{-7}	1.56×10^{-4}
1.43×10^{-4}	3.44	1.33×10^{-4}	1.00×10^{-5}
	4.31	1.24×10^{-4}	1.86×10^{-5}
	5.35	1.14×10^{-4}	2.90×10^{-5}
	6.63	9.06×10^{-5}	5.24×10^{-5}
	6.99	7.46×10^{-5}	6.84×10^{-5}
	7.06	7.59×10^{-5}	6.71×10^{-5}
	7.29	6.49×10^{-5}	7.81×10^{-5}
	7.61	4.55×10^{-5}	9.75×10^{-5}
	8.01	2.74×10^{-5}	1.16×10^{-4}
	8.27	1.36×10^{-5}	1.29×10^{-4}
	8.12	1.91×10^{-5}	1.24×10^{-4}
	9.46	5.23×10^{-7}	1.42×10^{-4}
1.04×10^{-4}	2.99	9.59×10^{-5}	8.08×10^{-6}
	5.45	9.12×10^{-5}	1.28×10^{-5}
	6.71	4.81×10^{-5}	5.59×10^{-5}
	7.03	4.51×10^{-5}	5.89×10^{-5}
	7.32	4.27×10^{-5}	6.13×10^{-5}
	7.57	1.81×10^{-5}	8.59×10^{-5}
	7.60	2.10×10^{-5}	8.30×10^{-5}
	7.85	9.96×10^{-6}	9.40×10^{-5}
	8.06	1.15×10^{-5}	9.25×10^{-5}
	8.19	8.34×10^{-6}	9.57×10^{-5}
	8.22	1.92×10^{-6}	1.02×10^{-4}
	8.35	8.19×10^{-7}	1.03×10^{-4}

4.0 molal NaCl

Zn_{Tot} (molal)	pH	Zn_{Diss} (molal)	Zn_{Ads} (molal)
1.43×10^{-4}	5.53	1.32×10^{-4}	1.06×10^{-5}
	6.12	1.09×10^{-4}	3.45×10^{-5}
	7.01	8.85×10^{-5}	5.45×10^{-5}
	7.25	8.08×10^{-5}	6.22×10^{-5}
	7.66	6.04×10^{-5}	8.26×10^{-5}
	7.87	4.98×10^{-5}	9.32×10^{-5}
	7.73	5.92×10^{-5}	8.38×10^{-5}
	8.05	3.45x10-5	1.09×10^{-4}
	8.16	3.51×10^{-5}	1.08×10^{-4}
	8.37	1.52×10^{-5}	1.28×10^{-4}
	8.74	1.31×10^{-6}	1.42×10^{-4}
1.23×10^{-4}	3.45	1.16×10^{-4}	7.41×10^{-6}
	4.93	1.15×10^{-4}	8.02×10^{-6}
	6.06	9.61×10^{-5}	2.69×10^{-5}
	6.89	7.00×10^{-5}	5.30×10^{-5}
	7.52	4.96×10^{-5}	7.34×10^{-5}
	7.56	5.03×10^{-5}	7.27×10^{-5}
	7.81	3.60×10^{-5}	8.70×10^{-5}
	8.08	2.31×10^{-5}	9.99×10^{-5}
	8.1	1.98×10^{-5}	1.03×10^{-4}
	8.48	6.95×10^{-7}	1.22×10^{-4}
	8.48	1.24×10^{-5}	1.11×10^{-4}

5.0 molal NaCl

Zn_{Tot} (molal)	pH	Zn_{Diss} (molal)	Zn_{Ads} (molal)
1.35×10^{-4}	2.88	1.28×10^{-4}	6.56×10^{-6}
	6.57	9.49×10^{-5}	4.01×10^{-5}
	7.05	7.76×10^{-5}	5.74×10^{-5}
	7.77	6.17×10^{-5}	7.33×10^{-5}
	7.91	5.05×10^{-5}	8.45×10^{-5}
	8.2	3.84×10^{-5}	9.66×10^{-5}
	8.52	2.17×10^{-5}	1.13×10^{-4}
	8.78	1.28×10^{-5}	1.22×10^{-4}
	9	5.31×10^{-6}	1.30×10^{-4}
	9.38	1.29×10^{-6}	1.34×10^{-4}
1.32×10^{-4}	6.04	1.07×10^{-4}	2.48×10^{-5}
	6.31	1.02×10^{-4}	3.04×10^{-5}
	6.66	9.25×10^{-5}	3.95×10^{-5}
	6.73	9.10×10^{-5}	4.10×10^{-5}
	6.87	8.70×10^{-5}	4.50×10^{-5}
	7.29	7.71×10^{-5}	5.49×10^{-5}
	7.33	7.09×10^{-5}	6.11×10^{-5}
	7.34	6.74×10^{-5}	6.46×10^{-5}
	8.31	3.90×10^{-5}	9.30×10^{-5}
	8.97	1.46×10^{-5}	1.17×10^{-4}
	9.78	4.17×10^{-7}	1.32×10^{-4}

Appendix C

Experimental data for the adsorption of copper and zinc onto goethite in 0.001 – 1 molal Na_2SO_4. Each table is an experimental series, while each row is a single experiment. Zn_{Tot} and Cu_{Tot} are the total dissolved copper and zinc concentrations at the start of each experiment before goethite is added. pH is the final pH of solution at the completion of each experiments, Zn_{Diss} and Cu_{Diss} are the total dissolved Zn and Cu in solution at completion of each experiment while the Zn_{Ads} and Cu_{Ads} are the differences between Zn_{Tot} and Zn_{Diss} and Cu_{Tot} and Cu_{Diss}.

0.001 molal Na_2SO_4

Zn_{Tot} (molal)	pH	Zn_{Diss} (molal)	Zn_{Ads} (molal)
1.62×10^{-4}	5.06	1.49×10^{-4}	1.28×10^{-5}
	5.61	1.38×10^{-4}	2.37×10^{-5}
	6.38	1.05×10^{-4}	5.67×10^{-5}
	6.7	9.55×10^{-5}	6.65×10^{-5}
	6.9	8.08×10^{-5}	8.12×10^{-5}
	7.51	4.77×10^{-5}	1.14×10^{-4}
	7.66	3.68×10^{-5}	1.25×10^{-4}
	8.26	3.74×10^{-6}	1.58×10^{-4}
	8.64	1.28×10^{-6}	1.61×10^{-4}
	8.76	1.28×10^{-6}	1.61×10^{-4}
	9.13	1.28×10^{-6}	1.61×10^{-4}
	9.25	1.28×10^{-6}	1.61×10^{-4}

0.01 molal Na_2SO_4

Zn_{Tot} (molal)	pH	Zn_{Diss} (molal)	Zn_{Ads} (molal)
1.62×10^{-4}	4.55	1.36×10^{-4}	2.62×10^{-5}
	5.16	1.36×10^{-4}	2.62×10^{-5}
	6.27	1.11×10^{-4}	5.10×10^{-5}
	6.85	9.73×10^{-5}	6.47×10^{-5}
	7.35	7.01×10^{-5}	9.19×10^{-5}
	7.65	3.11×10^{-5}	1.31×10^{-4}
	7.88	1.94×10^{-5}	1.43×10^{-4}
	8.79	1.05×10^{-6}	1.61×10^{-4}
	9	3.25×10^{-7}	1.62×10^{-4}
	9.23	3.25×10^{-7}	1.62×10^{-4}
	9.38	3.25×10^{-7}	1.62×10^{-4}

0.1 molal Na_2SO_4

Zn_{Tot} (molal)	pH	Zn_{Diss} (molal)	Zn_{Ads} (molal)
1.62×10^{-4}	5	1.35×10^{-4}	2.67×10^{-5}
	5.1	1.47×10^{-4}	1.51×10^{-5}
	6.04	1.34×10^{-4}	2.80×10^{-5}
	6.6	1.18×10^{-4}	4.41×10^{-5}
	7.22	9.63×10^{-5}	6.57×10^{-5}
	7.58	8.57×10^{-5}	7.63×10^{-5}
	7.83	5.50×10^{-5}	1.07×10^{-4}
	8.22	3.01×10^{-5}	1.32×10^{-4}
	8.82	6.33×10^{-6}	1.56×10^{-4}
	9.28	2.39×10^{-6}	1.60×10^{-4}
	9.45	2.44×10^{-6}	1.60×10^{-4}

1.0 molal Na_2SO_4

Zn_{Tot} (molal)	pH	Zn_{Diss} (molal)	Zn_{Ads} (molal)
9.40×10^{-5}	5.3	8.57×10^{-5}	8.27×10^{-6}
	5.45	8.42×10^{-5}	9.82×10^{-6}
	6.04	7.95×10^{-5}	1.45×10^{-5}
	6.73	6.29×10^{-5}	3.11×10^{-5}
	6.8	6.13×10^{-5}	3.27×10^{-5}
	7.13	4.83×10^{-5}	4.57×10^{-5}
	7.38	4.36×10^{-5}	5.04×10^{-5}
	7.54	2.53×10^{-5}	6.87×10^{-5}
	7.57	2.31×10^{-5}	7.09×10^{-5}
	7.74	1.35×10^{-5}	8.05×10^{-5}
	7.96	1.93×10^{-7}	9.38×10^{-5}

0.001 molal Na_2SO_4

Cu_{Tot} (molal)	pH	Cu_{Diss} (molal)	Cu_{Ads} (molal)
1.51×10^{-4}	3.57	1.42×10^{-4}	9.47×10^{-6}
	3.82	1.51×10^{-4}	1.14×10^{-5}
	3.96	1.42×10^{-4}	1.96×10^{-5}
	4.87	1.08×10^{-4}	5.36×10^{-5}
	5.06	9.71×10^{-5}	6.49×10^{-5}
	5.29	8.52×10^{-5}	7.68×10^{-5}
	5.44	7.49×10^{-5}	8.71×10^{-5}
	6.11	4.51×10^{-5}	1.17×10^{-4}
	6.92	1.81×10^{-5}	1.44×10^{-4}
	8.33	1.19×10^{-5}	1.50×10^{-4}
	9.43	1.19×10^{-5}	1.50×10^{-4}
	9.48	1.19×10^{-5}	1.50×10^{-4}

0.01 molal Na_2SO_4

Cu_{Tot} (molal)	pH	Cu_{Diss} (molal)	Cu_{Ads} (molal)
1.39×10^{-4}	3.84	1.23×10^{-4}	1.62×10^{-5}
	3.96	1.21×10^{-4}	1.80×10^{-5}
	4.24	1.16×10^{-4}	2.29×10^{-5}
	4.37	1.11×10^{-4}	2.76×10^{-5}
	5.15	7.40×10^{-5}	6.50×10^{-5}
	5.42	6.38×10^{-5}	7.52×10^{-5}
	6.03	3.44×10^{-5}	1.05×10^{-4}
	7.21	2.26×10^{-6}	1.37×10^{-4}
	8.15	1.07×10^{-6}	1.38×10^{-4}
	8.95	1.07×10^{-6}	1.38×10^{-4}
	9.04	1.07×10^{-6}	1.38×10^{-4}
	9.48	1.07×10^{-6}	1.38×10^{-4}

0.1 molal Na_2SO_4

Cu_{Tot} (molal)	pH	Cu_{Diss} (molal)	Cu_{Ads} (molal)
1.08×10^{-4}	3.97	1.07×10^{-4}	1.01×10^{-6}
	4.66	9.38×10^{-5}	1.42×10^{-5}
	4.54	9.61×10^{-5}	1.19×10^{-5}
	4.84	8.82×10^{-5}	1.98×10^{-5}
	5	8.42×10^{-5}	2.38×10^{-5}
	5.16	7.79×10^{-5}	3.01×10^{-5}
	5.53	5.55×10^{-5}	5.25×10^{-5}
	6.12	3.57×10^{-5}	7.23×10^{-5}
	7.43	3.73×10^{-6}	1.04×10^{-4}
	7.68	2.28×10^{-6}	1.06×10^{-4}
	8.37	8.04×10^{-7}	1.07×10^{-4}
	8.72	5.68×10^{-7}	1.07×10^{-4}
1.12×10^{-4}	3.52	1.12×10^{-4}	9.40×10^{-8}
	4.04	1.05×10^{-4}	6.94×10^{-6}
	4.19	1.03×10^{-4}	8.52×10^{-6}
	4.38	1.00×10^{-4}	1.20×10^{-5}
	3.85	1.09×10^{-4}	2.83×10^{-6}
	5.27	7.23×10^{-5}	3.97×10^{-5}
	6.09	3.58×10^{-5}	7.62×10^{-5}
	6.55	1.76×10^{-5}	9.44×10^{-5}
	7.34	3.83×10^{-6}	1.08×10^{-4}
	7.98	1.62×10^{-6}	1.10×10^{-4}
	6.88	8.94×10^{-6}	1.03×10^{-4}
	8.74	1.32×10^{-6}	1.11×10^{-4}

1.0 molal Na_2SO_4

Cu_{Tot} (molal)	pH	Cu_{Diss} (molal)	Cu_{Ads} (molal)
7.09×10^{-5}	3.81	6.73×10^{-5}	3.58×10^{-6}
	4.3	6.19×10^{-5}	9.00×10^{-6}
	4.45	6.43×10^{-5}	6.62×10^{-6}
	5.1	4.31×10^{-5}	2.78×10^{-5}
	5.84	3.38×10^{-5}	3.71×10^{-5}
	6.08	2.32×10^{-5}	4.77×10^{-5}
	6.94	1.07×10^{-5}	6.02×10^{-5}
	7.82	8.86×10^{-6}	6.20×10^{-5}
	8.34	7.39×10^{-6}	6.35×10^{-5}
	7.97	9.13×10^{-6}	6.18×10^{-5}
	8.58	8.16×10^{-6}	6.27×10^{-5}
	8.99	1.36×10^{-7}	7.08×10^{-5}

Appendix D

Experimental data for combined 1.0 molal NaCl, 0.1 molal Na_2SO_4 and 1.57×10^{-4} molal Cu^{II} and 1.54×10^{-4} molal Zn. Each table is an experimental series, while each row is a single experiment. Zn_{Tot} and Cu_{Tot} are the total dissolved copper and zinc concentrations at the start of each experiment before goethite is added. pH is the final pH of solution at the completion of each experiments, Zn_{Diss} and Cu_{Diss} are the total dissolved Zn and Cu in solution at completion of each experiment while the Zn_{Ads} and Cu_{Ads} are the differences between Zn_{Tot} and Zn_{Diss} and Cu_{Tot} and Cu_{Diss}.

1.0 molal NaCl + 0.1 molal Na_2SO_4

Cu_{Tot} (molal)	pH	Cu_{Diss} (molal)	Cu_{Ads} (molal)	Zn_{Diss} (molal)	Zn_{Ads} (molal)
7.09×10^{-5}	3.39	1.50×10^{-4}	6.54×10^{-6}	1.49×10^{-4}	4.92×10^{-6}
	3.77	1.45×10^{-4}	1.16×10^{-5}	1.44×10^{-4}	1.00×10^{-5}
	3.75	1.46×10^{-4}	1.10×10^{-5}	1.48×10^{-4}	5.87×10^{-6}
	4.15	1.40×10^{-4}	1.65×10^{-5}	1.44×10^{-4}	9.88×10^{-6}
	4.51	1.29×10^{-4}	2.82×10^{-5}	1.38×10^{-4}	1.57×10^{-5}
	4.79	1.22×10^{-4}	3.52×10^{-5}	1.39×10^{-4}	1.41×10^{-5}
	5.65	8.62×10^{-5}	7.08×10^{-5}	1.40×10^{-4}	1.30×10^{-5}
	6.05	6.47×10^{-5}	9.23×10^{-5}	1.36×10^{-4}	1.72×10^{-5}
	6.73	1.31×10^{-5}	1.43×10^{-4}	1.28×10^{-4}	2.59×10^{-5}
	7.3	4.14×10^{-6}	1.52×10^{-4}	1.12×10^{-4}	4.20×10^{-5}
	8.49	4.60×10^{-7}	1.56×10^{-4}	3.81×10^{-5}	1.15×10^{-4}

Appendix E

Example of FITEQL 4.0 input file with externally calculated Debye-Hückel "b-dot" activity coefficients.

```
': PROGRAM: FITEQL Version 4.0
': FILENAME: C:\FITEQL4\CUBDOT\FINAL\FIT-TEMP.DAT
': PATH: C:\FITEQL4\CUBDOT\FINAL\
': DESCRIPTION: Determination of Log K's for Cu species
   1
   1
   1
   1
   1
  40
   6    1   12   24    1    0
   1 SOH          0.000  8.935E-04
 160 PSI(o)      -1.000  0.000E+00
   3 Cu[2+]       0.000  1.570E-04
   5 Na[+]        0.000  1.000E-01
   6 NO3[-]       0.000  3.140E-04
   7 Cl[-]        0.000  1.000E-01
   4 Cu(ads)      0.000  0.000E+00
   2 H[+]         0.000  0.000E+00
  11 CuOHact      0.000  0.000E+00
  14 NaClact      0.000  0.000E+00
  10 CuClact      0.000  0.000E+00
  13 CuCl2act     0.000  0.000E+00
  12 CuCl3act     0.000  0.000E+00
   9 Cu2OH2act    0.000  0.000E+00
   8 CuOH2act     0.000  0.000E+00
  15 Cu_Act       0.000  0.000E+00
  16 H_Act        0.000  0.000E+00
  17 Cl_Act       0.000  0.000E+00
  18 OH_Act       0.000  0.000E+00

   2 H[+]         0.000   2   1  16   1
   5 OH[-]      -13.980   2  -1  18   1
   1 SOH          0.000   1   1
   6 Na[+]        0.000   5   1
   3 Cu[2+]       0.000   3   1  15   1
   7 NO3[-]       0.000   6   1
   4 Cl[-]        0.000   7   1  17   1
 100 CuOH[+]     -8.000   3   1   2  -1   8   1
 110 CuOH2      -13.680   3   1   2  -2  11   1
 120 Cu2OH2     -17.500   3   2   2  -2   9   1
```

```
130 CuNO3[+]     0.500   3   1  6   1
140 CuNO32[2]   -0.400   3   1  6   2
150 NaNO3       -0.550   5   1  6   1
160 CuCl[+]      0.300   3   1  7   1 10   1
170 CuCl2       -0.260   3   1  7   2 13   1
180 CuCl3[-]    -2.290   3   1  7   3 12   1
190 NaCl        -0.300   5   1  7   1 14   1
 10 SO[-]      -10.440   1   1 160  -1  2  -1
 20 SOH2[+]      6.360   1   1 160   1  2   1
 30 SOHCu[2+]    8.432   1   1 160   2  3   1  4   1
 40 SOCu[+]      0.849   1   1 160   1  3   1  4   1  2  -1
 60 SOHCuCl      5.584   1   1 160   1  3   1  7   1  4   1
 70 SOHCuCl2     3.246   1   1  3   1  7   2  4   1
 80 SOCuCl      -2.880   1   1  3   1  7   1  4   1  2  -1

  2 H[+]
  5 OH[-]
  1 SOH
  6 Na[+]
  3 Cu[2+]
  7 NO3[-]
  4 Cl[-]
100 CuOH[+]
110 CuOH2
120 Cu2OH2
130 CuNO3[+]
140 CuNO32[2]
150 NaNO3
160 CuCl[+]
170 CuCl2
180 CuCl3[-]
190 NaCl
 10 SO[-]
 20 SOH2[+]
 30 SOHCu[2+]
 40 SOCu[+]
 60 SOHCuCl
 70 SOHCuCl2
 80 SOCuCl

  1  36.050000   0.937500   0.870000

  0    0    0
  0   '* NDIS

  3   15
  logX     logX     logX     logX     logX
  2        11       14       10       13
'*  H[+]     CuOHact    NaClact    CuClact    CuCl2act
```

1	-2.500000	-0.435000	-0.215104	-0.423327	-0.645195
2	-3.000000	-0.431000	-0.213413	-0.420177	-0.640209
3	-3.500000	-0.430000	-0.212966	-0.419205	-0.638588
4	-4.000000	-0.430000	-0.212700	-0.418908	-0.638086
5	-4.500000	-0.430000	-0.212639	-0.418876	-0.638035
6	-5.000000	-0.430000	-0.212628	-0.418818	-0.637940
7	-5.500000	-0.430000	-0.212618	-0.418759	-0.637848
8	-6.000000	-0.429000	-0.212610	-0.418709	-0.637708
9	-6.500000	-0.429000	-0.212585	-0.418703	-0.637780
10	-7.000000	-0.429000	-0.212493	-0.418406	-0.637381
11	-7.500000	-0.429000	-0.212372	-0.418391	-0.637201
12	-8.000000	-0.429000	-0.212329	-0.418226	-0.636993
13	-8.500000	-0.429000	-0.212327	-0.418105	-0.636871
14	-9.000000	-0.429000	-0.212332	-0.418312	-0.637392
15	-9.500000	-0.429000	-0.212331	-0.418208	-0.637383

	logX 12	logX 9	logX 8	logX 15	logX 16
'*	CuCl3act	Cu2OH2act	CuOH2act	Cu_Act	H_Act
1	-0.638366	-0.449471	-0.669000	-0.430170	-0.107552
2	-0.633698	-0.447084	-0.661000	-0.426796	-0.106701
3	-0.632066	-0.447383	-0.660000	-0.425704	-0.106435
4	-0.631596	-0.448571	-0.660000	-0.425364	-0.106361
5	-0.631614	-0.448521	-0.660000	-0.425334	-0.106317
6	-0.631462	-0.448658	-0.659000	-0.425255	-0.106327
7	-0.631343	-0.448119	-0.659000	-0.425270	-0.106306
8	-0.631217	-0.448271	-0.659000	-0.425206	-0.106293
9	-0.631282	-0.448295	-0.659000	-0.425173	-0.106295
10	-0.630499	-0.448690	-0.658964	-0.424938	-0.106259
11	-0.630939	-0.448640	-0.658611	-0.424750	-0.106188
12	-0.630237	-0.448804	-0.658484	-0.424685	-0.106157
13	-0.630024	-0.448394	-0.658382	-0.424606	-0.106166
14	-0.630000	-0.448399	-0.658464	-0.424710	-0.106157
15	-0.630000	-0.448007	-0.658490	-0.424661	-0.106166

	logX 17	logX 18
'*	Cl_Act	OH_Act
1	-0.108000	-0.119261
2	-0.107000	-0.117124
3	-0.106000	-0.116770
4	-0.106000	-0.117161
5	-0.106000	-0.117113
6	-0.106000	-0.117095
7	-0.106301	-0.117102
8	-0.106279	-0.117095
9	-0.106294	-0.117081
10	-0.106228	-0.117029
11	-0.106228	-0.116925

```
 12 -0.106175 -0.116897
 13 -0.106144 -0.116904
 14 -0.106204 -0.116897
 15 -0.106178 -0.116904

  0  0  0  '* NST, NSX, KUWSOS

'* Graph Information
'* Type ID  RangeI RangeF Format  Axis Name     Format  Series Type
   4    0   1    12       '* X   Serial
   1    0   1    12   1   '* Y 1 None  Symbols  None
   1    0   1    12   1   '* Y 2 None  Symbols  None
   1    0   1    12   1   '* Y 3 None  Symbols  None
   1    0   1    12   1   '* Y 4 None  Symbols  None
   1    0   1    12   1   '* Y 5 None  Symbols  None
   1    0   1    12   1   '* Y 6 None  Symbols  None
   1    0            '* D   None         None

'* Max       Min       Step      Type
1 00.000E+00 00.000E+00 00.000E+00 '* linear
1 00.000E+00 00.000E+00 00.000E+00 '* linear
                                   '* Graph Title
                                   '* X - Axis Title
                                   '* Y - Axis Title
```

Appendix F

Summary of fitted log K values for Cu^{II} adsorption onto goethite in $NaNO_3$, NaCl and Na_2SO_4.

Species	Mass Balanace	Log K	
		Debye Huckel	*Davies*
$\equiv SOHCu^{2+}$	$\equiv SOH + Cu^{2+} = \equiv SOHCu^{2+}$	-	-1.85
$\equiv SOCu^{+}$	$\equiv SOH + Cu^{2+} = \equiv SOCu^{+} + H^{+}$	-	5.28
$\equiv SOCuCl^{0}$	$\equiv SOH + Cu^{2+} + Cl^{-} = \equiv SOCuCl^{0} + H^{+}$	-2.49	-1.96
$\equiv SOHCuCl^{+}$	$\equiv SOH + Cu^{2+} + Cl^{-} = \equiv SOHCuCl^{+}$	6.04	5.35
$\equiv SOHCuCl_2^{0}$	$\equiv SOH + Cu^{2+} + 2Cl^{-} = \equiv SOHCuCl_2^{0}$	2.82	3.37
$\equiv SOHZn^{2+}$	$\equiv SOH + Zn^{2+} = \equiv SOHZn^{2+}$	-	7.60
$\equiv SOZnOH$	$\equiv SOH + Zn^{2+} + H_2O = \equiv SOZnOH + 2H^{+}$	-	-11.63
$\equiv SOHZnCl_2^{0}$	$\equiv SOH + Zn^{2+} + 2Cl^{-} = \equiv SOHZnCl_2^{0}$	2.72	3.19
$\equiv SOZnCl_2^{-}$	$\equiv SOH + Zn^{2+} + 2Cl^{-} = \equiv SOZnCl_2^{-} + H^{+}$	-5.50	-4.17
$\equiv SOHCuSO40$	$\equiv SOH + Cu^{2+} + SO_4^{2-} = \equiv SOHCuSO_4^{0}$	-	6.00
$\equiv SOZnSO4-$	$\equiv SOH + Zn^{2+} + SO_4^{2-} = \equiv SOZnSO_4^{-} + H^{+}$	-	-2.88
$\equiv SOH2ZnSO4+$	$\equiv SOH + Zn^{2+}\ SO_4^{2-} + H^{+} = \equiv SOH_2ZnSO_4^{+}$	-	13.64